Asymptotic Performance of Multiuser Massive MIMO systems

By: Ismail Sh. Baqer Hburi

A Thesis Submitted in Fulfilment of the Requirements
for the Degree of Doctor of Philosophy (Ph.D.)
in
Communications

Department of Electronic and Computer Engineering,
College of Engineering, Design and Physical Sciences
Brunel University London
United Kingdom

Supervised By: Professor Hamed Al-Raweshidy

July 2017

In loving memory of my father

To my mother

With eternal love and appreciation

To my family . . .

Abstract

This thesis addresses and identifies outstanding challenges associated with the Multi user massive Multiple-Input Multiple-Output (MU massive MIMO) transmission, whereby various system scenarios have been considered to tackle these challenges.

First, for a single cell scenario, the uplink effective capacity under statistical exponent constraints, the asymptotic error and outage probabilities in a multi user massive MIMO system are provided. The proposed approach establishes closed form expressions for the aforementioned metrics under both perfect and imperfect channel state information (CSI) scenarios. In addition, expressions for the asymptotically high signal-to-interference ratio (SIR) regimes are established.

Second, the statistical queueing constraints, pilot contamination phenomenon and fractional power control in random or irregular cellular massive MIMO system are investigated, where base station locations are modelled based on the Poisson point process. Specifically, tractable analytical expressions are developed for the asymptotic SIR coverage, rate coverage and the effective capacity under the quality of service statistical exponent constraint. Laplace transform of interference is derived with the aid of mathematical tools from stochastic geometry. Simulation outcomes demonstrate that pilot reuse impairments can be alleviated by employing a cellular frequency reuse scheme. For example, with unity frequency reuse factor, we see that 40% of the total users have SIR above -10.5dB, whereas, with a reuse factor of 7, the same fraction of users have SIR above 20.5dB. In addition, for a certain parameters setting, the coverage probability in the lower 50^{th} percentile can be maximized by adjusting power compensation fraction between 0.2 and 0.5. Also, for SIR threshold of 0dB, allocating 0.25 fraction of uplink transmit power can achieve approximately 6% improvement in coverage probability in the cell edge area compared to constant power policy and about 14% improvement compared to the full channel-inversion policy.

Third and last, motivated by the powerful gains of incorporating small cells with macro cells, a massive MIMO aided heterogeneous cloud radio access network (H-CRAN) is investigated. More specific, based on Toeplitz matrix tool, tractable formulas for the link reliability and rate coverage of a typical user in H-CRAN are derived. Numerical outcomes confirm the powerful gain of the massive MIMO for enhancing the throughput of the H-CRAN while small remote radio heads (RRH cells) are capable of achieving higher energy efficiency.

Preface

The primary-results of this work have been presented in the following submitted for a publication, accepted or published manuscripts

- Chapter_3 of this thesis has been published as **Ismail H.** and Hamed Al-Raweshidy "Uplink Massive MIMO Systems Under Statistical-Queueing Constraints" in *Proceedings of the* 24^{th} *IEEE International Conference on Telecommunications (ICT)*, Nicosia, Cyprus, May 2017.
- Chapter_4 of this thesis has been published as **Ismail H.** and Hamed Al-Raweshidy "Outage and Average Error Probability for UL-Massive MIMO Systems: Asymptotic Analysis" in *Proceedings of the IEEE International Conference on Communications (ICC)*, Paris, France, May 2017.
- Chapter_5 of this thesis has been accepted for publication as **Ismail H.** and Hamed Al-Raweshidy "QoS-Constraints and Pilot-Contamination in the Uplink of Non-cooperative Cellular Massive-MIMO" *IEEE Global Communications Conference (GLOBECOM)*, Singapore, December 2017.
- Chapter_6 of this thesis has been accepted for publication as **Ismail H.** and Hamed Al-Raweshidy "Uplink Performance of Cellular Massive MIMO with Fractional Power Control: Asymptotic Analysis" *IEEE EUROCON 2017, International Conference on Information and Communication Technologies*, Ohrid, Macedonia, July 2017.
- Chapter_7 of this thesis is to be submitted for possible publication, as **Ismail H.** and Hamed Al-Raweshidy " Performance Analysis of Massive-MIMO Enabled Heterogeneous C-RAN " *IEEE Trans. Wireless Commun.*, 2017.

For each publication listed above, I carried out the problem_formulation, the system_model development, the mathematical_analysis, and computer_simulations under the supervision of Prof.,Hamed. While I was responsible for composition of the manuscript, Prof.,Hamed contributed to manuscript edits.

Acknowledgement

I would first like to express my gratefulness and appreciation to the Ministry of Higher Education and Scientific Research in Iraq for funding my Ph.D. project. My sincere appreciation and acknowledgement are extended to the University of Wasit for supporting my research over the past four years.
Special thanks and appreciation are for my supervisor Professor Hamed Al-Raweshidy for his helpful advice, guidance, constructive-feedback on my research and unlimited support for my work, I could not have accomplished this work without his support and encouragement.

I would also like to extend my deepest gratitude to my family for their encouragement and precious moral support throughout the years of the research. They always inspire me to pursue my study and encourage me to complete this work.
Finally, I would like to acknowledge all my colleagues and friends at Wireless Networks and Communications Centre (WNCC), Brunel University London, over the years for fruitful-collaborations and insightful-discussions, and I would like to present this humble work to all of them with a great appreciation.

London, July 2017
Ismail Sharhan Bager

Contents

List of Figures

List of Tables

Definition of Acronyms

Acronym	Definition
3GPP	Third Generation Partnership Project
4G	Fourth Generation
5G	Fifth Generation
ABEP	average bit error-rate probability
AWGN	additive white Gaussian noise
ASE	Area spectral efficiency
BS	base station
BPSK	binary phase shift keying
BER	bit error rate
BD	Block Diagonalisation
BS	Base Station
BF	Beamforming
BW	Bandwidth
CSI	channel state information
CoMP	coordinated multiple point
CDF	cumulative distribution function
CQI	Channel Quality Indicator
CSI	Channel State Information
CCDF	Complementary Cumulative Distribution Function
CDMA	Code Division Multiple Access
DoF	degrees of freedom
DL	Downlink
DPC	Dirty Paper Coding
EE	Energy Effciency
FDD	Frequency Division Duplex
FDMA	Frequency Division Multiple Access
FFR	Fractional Frequency Reuse
FRF	Frequency Reuse Factor
HetNet	Heterogeneous Network

ICI	Inter cell Interference
ICIC	Inter cell Interference Coordination
i.i.d	Independent and Identically Distributed
ISI	Inter symbol Interference
LSAS	large scale antenna systems
LTE	Long Term Evolution
LoS	Line of Sight
MIMO	Multiple-Input Multiple-Output
MISO	Multiple-Input Single-Output
MRC	Maximal Ratio Combining
MRT	Maximal Ratio Transmission
MU-MIMO	Multi User MIMO
NLoS	Non Line of Sight
OFDM	Orthogonal Frequency Division Multiplexing
OFDMA	Orthogonal Frequency Division Multiple Access
PF	Proportional Fairness
PDF	Probability Density Function
PPP	Point Poisson Process
PLE	path loss exponent
QAM	Quadrature Amplitude Modulation
QoS	Quality of Service
QPSK	Quadrature Phase Shift Keying
RAN	Radio Access Network
RB	Resource Block
RE	Resource Element
RV	Random Variable
RR	Round Robin
SDMA	Space Division Multiple Access
SINR	Signal to Interference plus Noise Ratio
SISO	Single Input Single Output
SIR	Signal to Interference Ratio
SNR	Signal to Noise Ratio
SFR	Soft Frequency Reuse

SU-MIMO	Single User MIMO
SVD	Singular Value Decomposition
TDMA	Time Division Multiple Access
TDD	Time-Division Duplex
UE	User Equipment
UL	Uplink
ZF	Zero Forcing

Definition of Notations

Notation	**Definition**
$f_X(x)$	probability density function of the r.v. X
$F_X(x)$	cumulative distribution function of the r.v. X
$\mathrm{erfc}(\cdot)$	complementary error function
$\Gamma(\cdot)$	Gamma function
$\Gamma(\cdot,\cdot)$	upper incomplete function
$\gamma(\cdot,\cdot)$	lower incomplete function
$\mathbb{E}\{\cdot\}$	expectation operator
$\mathcal{L}_I(s)$	Laplace transform of the r.v. I at s
$\mathbb{P}(X)$	probability of the r.v. X
$(A)^H$	Hermitian operation on matrix A
$(A)^*$	complex conjugate of matrix A
$(A)^\dagger$	pseudo inverse of a matrix A
$\|\cdot\|$	vector norm
$\mathrm{B}_x(\cdot,\cdot)$	the upper incomplete beta function
${}_2F_1(\cdot)$	Gauss hyper geometric function
${}_pF_q(\cdot)$	General hyper geometric function, where p and q are non-negative integers
$(x)_n$	the rising factorial or the Pochhammer polynomial

$U(\cdot)$	the Tricomi confluent hyper geometric function
$\mathcal{S}(\hat{\gamma})$	the success probability at SNR of $\hat{\gamma}$
$(.)!$	the factorial operation
$\overset{(a.s)}{=}$	almost surly the same
$\xrightarrow{a.s}$	almost surly converge to
$\overset{(d)}{=}$	statistical equivalence
$\mathbf{g}_k$	true value of channel gain
$\hat{\mathbf{g}}_k$	the estimated value of channel gain
$\bar{\mathbf{g}}_k$	the average value of channel gain
$\tilde{\mathbf{g}}_k$	error in the estimated value of channel gain
$\mathbf{I}_M$	identity matrix of dimension $M \times M$
θ_k	queueing delay constraint
$\mathbb{C}^{N_r \times K}$	the space of $N_r \times K$ complex matrix
$C_{eff}(\theta_k)$	the effective capacity at θ_k
$C_{IP}^{asy}(\cdot)$	the asymptotic effective capacity for imperfect channel information scenario
$C_{P}^{asy}(\cdot)$	the asymptotic effective capacity for perfect channel information scenario
$Q_b(\cdot, \cdot)$	the generalized Marcum-Q function
$\mathcal{P}_e^{(IP)}(\cdot)$	average bit error probability for imperfect channel information scenario
$\mathcal{P}_e^{(P)}(\cdot)$	average bit error probability for perfect channel information scenario
$\mathcal{P}_{out}^{(IP)}(\cdot)$	outage probability for imperfect channel information scenario
$\mathcal{P}_{out}^{(P)}(\cdot)$	outage probability for perfect channel information scenario
$\mathbb{R}$	set of real numbers
$\mathbb{R}^2$	the two dimensional Euclidean plane

Chapter 1

Introduction

This introductory chapter begins with the description of issues currently existing in the wireless transmission which needs to be addressed and it highlights the questions which this research aims to answer. First, section 1.1 identifies the problem that the thesis tries to address. Section 1.2 then, gives some details about Multiple-Input Multiple-Output (MIMO) transmission technologies. After that, section 1.3 highlights the motivation for employing large scale antenna arrays. Next, the major contributions of this research are highlighted in section 1.4. Finally, section 1.5 provides a description of the thesis outline.

1.1 The statement of the problem

Driven by the new applications and rapid growth in wireless communications, the demand for the radio frequency (RF) spectrum has been increased and market is demanding that next generation networks should support much higher system capacity (around 1000×) than current generation networks [1].*

This issue motivates the search for modern techniques that will utilise more efficiently the available resources (specifically the most expensive resource, i.e., radio spectrum). To this end, we need some alternative techniques to improve the spectral efficiency (SE), either by mitigating the interference or by providing more orthogonal channels within the same spectrum. In this aspect, a set of new-technologies is proposed which, according to the fifth generation evolution directions, can be categorized into three dimensions: (1) Heterogeneous network (HetNet) with dense Base stations (BSs) deployment [2]; (2) Cognitive radio techniques

* It's noteworthy that current wireless communication systems already are, in point to point (PTP) transmissions, close to the Shannon capacity limit [1].

(CR) with Spectrum extension; and (3) MIMO techniques via deployment of more antennas at the transceivers [3]. In order to utilise the available spectrum of radio frequency (RF) more efficiently, and consequently meet this rapidly increased traffic demand, different MIMO strategies have been proposed and identified for fifth generation networks [4]. The features for some of these proposed strategies are specified to enhance one of the most important metrics, i.e., spectral efficiency (SE), since RF spectrum is an expensive and limited resource. Consequently the throughput of the network can be improved according to the following definition $Throughput(bps) = Bandwidth(Hz) \times spectralefficiency(bps/Hz)$. Energy efficiency (EE), on the other hand, is another system crucial metric, where for a fixed bandwidth (BW), there is always an essential trade off between SE and EE. Since SE only grows up logarithmically with increasing signal to interference plus noise ratio (SINR), a large increase in signal power could result in only small gains in the channel SE, specially in high SINR regime. In addition, the SE enhancement for the network could be restricted due to high interference contribution to other channels when we transmit with higher power. In other words, for a multi-user MIMO transmission, in order to guarantee an acceptable quality of service (QoS), not only high throughput is required, but also a good SINR distribution or coverage performance is fundamental [4].

1.2 MIMO Transmission Mechanisms

There are distinct operating regimes or transmission strategies for MIMO systems. The main transmission strategies employed by MIMO technology to enhance spectral efficiency are by (1) Improving the signal power and link reliability via coherently processing of signals at multiple transceiver ports to achieve diversity gain [5], (2) Achieving spatial multiplexing gain via creating spatially separated links to transmit independent data-streams and providing more degrees of freedom (DoF) to the propagation channel, or (3) Interference nulling (IN) towards other cells users [6]. In contrast to multiplexing approach in which independent signals are sent, the main concept of diversity is to provide a channel diversity gain by transmitting redundant, i.e., same signals over multiple channel and the aim is to improve the reliability of the link in terms of bit error rate in fading environments (see Fig. 1.1).

The above mentioned strategies are complementary, where in general, it is not possible to utilise all of these MIMO technologies simultaneously due to the spatial

DoF conflicting nature. The optimal technique in the sense of maximising SE depends on multiple factors. In a cellular network scenario, where the base station (BS) serves a multitude of users over the same resource block (RB), a spacial division multiple access (SDMA) can be applied to serve different user terminals via spatially separated streams. This mechanism is termed multi user MIMO (MU-MIMO) (see Fig. 1.2) and the spectral efficiency of this approach can increase linearly with increasing spatial DoF and the number of simultaneously served users.

There are many relationships between spatial multiplexing (SM) regimes and multiuser (MU) communication regimes, where the basic concept is to adopt multiple access strategies to separate channels into individual layers. However, if perfect mutual channel orthogonality between all layers is required, then we have to scarify some of transmit antennas and make trades off between diversity and multiplexing [4]. For MU-MIMO approach to achieve multiplexing gain, an accurate knowledge of the channel-state-information (CSI) for each user terminal is required to be available at the BS. CSI is estimated over the coherence interval (limited frequency and time interval over which we can assume stationary channel gain) by sending predefined training symbols or pilot-sequence and observing the impact of the channel on this training sequence at the receiver.

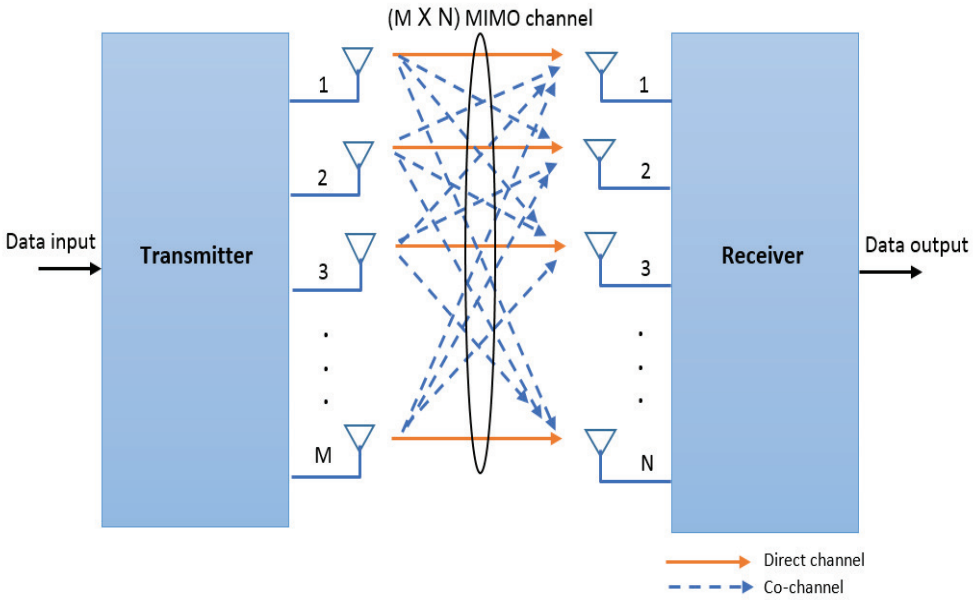

Figure 1.1: An illustration of single user multiple-input multiple-output (SU-MIMO) transmission channel.

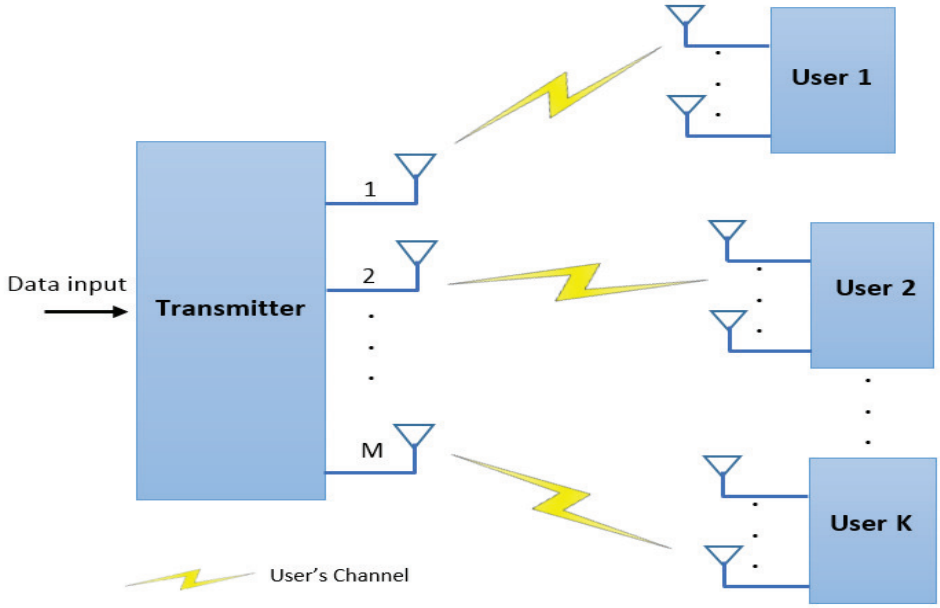

Figure 1.2: An illustration of multi user multiple-input multiple-output (MU-MIMO) transmission channel.

1.3 Motivation for Massive MIMO

It is found that for massive MIMO systems (when the number of antenna elements is allowed to grow without bound), energy efficiency (EE) and the system throughput grows dramatically. More specifically, massive MIMO, also referred to as large scale antenna systems (LSAS), is a multi user transmission mechanism designed to serve multi user equipment simultaneously in each time/frequency resource block (RB) where the number of supported (active) users is scalable with the number of antenna elements at the BS. Also, the effects of thermal noise and intra cell interference disappear with simple linear filtering [7], and the performance, theoretically, is only limited by the pilot contamination due to reuse of the same pilots across cells in channel estimation process. The aforementioned potential gains of deploying more antennas at the BS motivates the consideration and analysis of asymptotically infinite number of antennas at the BS in different system scenarios (a single cell, multi cell, and heterogeneous systems), and addressing of its impact on the key performance metrics. For multiuser massive MIMO systems under composed fading environment (Rayleigh fading and lognormal shadowing), the expressions for the signal-to-interference-plus-noise-ratio (SINR) characteristic do not exist in a closed form. Whereas SINR's closed form expressions are required to compute key performance metrics like the coverage probability and system capacity. This motivates

our study to consider an asymptotic model instead of the general model to analysis diverse massive MIMO scenarios. Accordingly, there are three main parts to this thesis.

The first part considers the benefit of employing massive MIMO or large scale MIMO (LS-MIMO) in the uplink (UL) of a single cell system by providing a statistical analysis of SIR asymptotic gain. The developed framework is useful in some scenarios, e.g., in hot spots environment such as train stations, entertainment centres and shopping malls. In addition, single cell analysis is very helpful to understand more complicated scenarios such as multi cell and heterogeneous networks.

The second part of this thesis quantifies the performance of LS-MIMO in cellular systems. Specifically, the second part tries to address the power control, pilot contamination and quality of service (QoS) constraints in the uplink of non cooperative cellular systems. The final part of this thesis tackles the performance issue in LS-MIMO enabled two-tier heterogeneous cloud-Radio access networks (H-CRANs) and explores approaches in which this scenario can bring key performance-gain.

1.4 Research Aim and Objectives

The main aim of the research presented in this thesis is to addresses and identifies outstanding challenges associated with the Multiuser massive Multiple-Input Multiple-Output (MU massive MIMO) transmission. The works have been carried out by developing physical and mathematical models for varies system topologies to meet the research objectives which are briefly explained and highlighted in the following points:

1. To Derive tractable (closed form or semi closed form) expressions for the performance metrics of massive antenna systems with different scenarios. These expressions will replace the need for long time system level simulations.

2. To Investigate and Analyse the behaviour of the massive MIMO for different topologies and channel scenarios.

3. To gain design insights about the impact of different setting of system parameters on the performance metrics of interest.

1.5 Contributions

This section highlights the key contributions of this thesis which are related to different massive MIMO scenarios and system architectures.

1.5.1 Multiuser massive MIMO in a single cell scenario

The uplink effective capacity is investigated in a multi user massive MIMO system over generalized composed fading channels considering the QoS statistical exponent constraints. In the proposed approach, a location dependent and a location independent (averaged out) closed form expressions are derived for the effective capacities in an asymptotically large receive antenna system with perfect and imperfect channel state information (CSI) scenarios. Moreover, expressions for the asymptotically high signal-to-noise ratio regimes are provided. Next, the asymptotic behaviour (error and outage probabilities) of a single cell multiple-input multiple-output (MIMO) system aided by a large scale antenna array is analysed. Specifically, the uplink transmission over composite fading channel with a power scaling scheme is considered. Two assumptions are addressed: perfect channel state information (perfect CSI) and imperfect channel state information (imperfect CSI). In both cases, closed form expressions for error and outage probabilities in asymptotically large receive antenna environments are derived. Moreover, users' location impact on the system performance is quantified for different channel information scenarios. The developed expressions are helpful to gain a deep insight into massive MIMO systems' design and the impact of different parameters on the aforementioned performance metrics.

1.5.2 Multiuser massive MIMO in a multiple cell scenario

The statistical queueing constraints and pilot contamination phenomenon are studied in a random or irregular cellular massive MIMO system where base stations are Poisson distributed. Particularly, tractable analytical expressions are provided for the asymptotic SIR-coverage, rate coverage and the effective capacity under the quality of service (QoS) statistical exponent constraint in uplink transmission when each base station deploys a large number of antennas. Laplace transform of the interference is derived with aid of mathematical tools from the stochastic geometry.

In addition, the spatial average analysis of uplink signal to interference ratio (SIR) and throughput in massive MIMO networks with maximum ratio combining

(MRC) are addressed. The analysis incorporates effects of fractional power control (FPC) and other cells interference (ICI) due to the estimation error in channel state information (CSI). Based on an asymptotic approach, tractable expressions are presented for SIR distributions, coverage probability and average rate in poisson topology model. Moreover, the considered approach is applicable both to random and deterministic network topologies. The impacts of key network features such as fractional power control, path-loss exponent and BS density are characterized.

1.5.3 Multiuser massive MIMO in a HetNet scenario

The multiple-input multiple-output (MIMO) aided heterogeneous cloud radio access networks (H-CRANs) is analysed. In the proposed model, massive MIMO enabled macro cells coexist with remote radio heads (RRHs) to potentially achieve high spectral and energy efficiencies(SE and EE). Employing a Toeplitz matrix tool from linear algebra, tractable formulas for the link reliability (signal-to-interference-ratio (SIR) distribution) and rate coverage of a typical user in H-CRAN are established. In this model, the macro base station tier (MBS) employs multi user MIMO policy via space division multiple access technique (zero forcing (ZF) beamforming with perfect channel state information (CSI)), whereas the second tier, i.e., RRH-tier employs single user transmission via single-input single-output (SISO) strategy.

1.6 Thesis Layout

The rest of this thesis is organized as follows, Chapter 2 gives an introductory background for this research work. First, it introduces a general overview of the importance of wireless communication and how, over the last years, the cellular-networks have developed in response to serious demands for high throughput technology. Next, it addresses techniques and issues of multi user MIMO wireless transmission and Time Division Duplex. Also, it discusses that enabling large scale antenna in MIMO systems is challenging and demands a rethinking of many of the models considered in the analysis and working assumptions which is the motivation behind this thesis. It then highlights some of the principle concepts that will guide the study of massive MIMO throughout this thesis such as channel estimation and asymptotic behaviour of the infinite antennas regime. This section is then followed by introducing an overview of linear precoding techniques for multi user MIMO. Finally, some mathematical challenges of cellular networks analysis are discussed briefly.

In Chapter 3, effective capacity for uplink of MU-massive MIMO system is investigated. The chapter starts with a simple background and literature review on the topic, then the system and channel model for the uplink massive MIMO system subject to a composite channel environment is described. Afterwards, the asymptotic effective capacity with the QoS statistical exponent is derived. Finally, an analysis of effective capacity is presented for zero forcing beam forming.

In Chapter 4, the asymptotic bit error and outage probability for the uplink of MU-massive MIMO in a single cell scenario is studied. The chapter starts with reviewing the literature related to the topic. Next, the system model and problem formulation are described. Afterword, closed form expressions for the asymptotic bit error and outage probability are derived as a function of several system parameters. Following that, a detailed analysis of the bit error and outage probabilities are provided.

Chapter 5, with aid of mathematical tools from stochastic geometry, addresses the statistical-queueing constraints and pilot contamination phenomenon in random or irregular cellular massive MIMO system where base stations are Poisson distributed. The chapter starts with a principle background and literature review on the topic. Then, it discusses the assumptions and provides system model. After that, it formulates the signal-to-interference ratio (SIR) model, presents the definition of the performance metrics, and presents some related aspects. Following this, an analysis for the asymptotic SIR coverage, rate coverage and the effective capacity under quality of service (QoS) statistical exponent constraint of a non cooperative cellular system is provided.

Chapter 6 then studies distance based uplink power control in cellular massive MIMO system with base stations are Poisson distributed. The chapter begins with the literature-review related to this issue. Then, the assumptions and system model are introduced. Next, channel estimation and the asymptotic SIR distribution are explained. Following that, using the spatial poisson model, tractable expressions for the coverage probability and average rate are derived for PPP Uniform and PPP Rayleigh network models and then, concerning coverage probability of edge area, the optimal policy for FPC is evaluated.

Chapter 7, with the help of stochastic geometry (SG) and triangular Toeplitz matrix, develops a framework for the analysis of two tiers massive-MIMO enabled heterogeneous CRAN (H-CRAN). The chapter starts with the literature review related to this issue. Then, the analysis and modeling for massive MIMO enabled

H-CRANs is provided using tools from linear algebra. Next, the proposed methodology to characterise the performance metrics of interest is presented. Following that, numerical studies are conducted for the sake of depicting system design guidelines. Finally, the thesis is concluded with significant discussion of potential future work in Chapter 8.

Chapter 2

Background

Since the introduction of the initial mobile systems in the 1950s, mobile communications have been developed orderly and so rapidly. The primitive-services, in the early days, restricted the number of simultaneously supportable users to the number of channels allocated to each particular base station. In addition, aside from mobile systems being bulky and power hungry, roaming between neighbouring BSs was impossible due to the lack of a commonly agreed standard. The 1st-generation (1G) of wireless networks is deployed in the early 1980's in Europe and USA [8], where a standardised voice traffic service over wide geographical areas was provided using analogue technology and allowing for the setting up of roaming between different-networks. In 1990, the first specifications of Groupe Spécial Mobile (GSM) standards were published by the European Telecommunications Standards-Institute (ETSI) to characterize the protocols for 2nd generation (2G) digital cellular networks. In addition to traditional voice-traffic, due to the digital-nature of these networks, additional services could be provided, including data services such as web browsing, email service and Short-Message System (SMS) [8]. Where, originally, the GSM-standard described as a circuit switched network (providing full duplex voice services at downlink rates of up to 14.4 kbps), then expanded to include data service by packet data transport in the later stages of the 1990s via 2.5G systems like General Packet Radio Services (GPRS). After the turn of the millennium (in 2001), based on code division multiple access (CDMA) technology, the third generation (3G) networks started deployment with the aims of supporting data rates up to 0.348 Mbps for mobile users and 2Mbps for stationary users. To this end, an internation association comprised of multiple international standardisation bodies based in U.S.A, Europe, and Asia, was created to be 3rd Generation Partnership Project

(3GPP) as the development group and standardisation for worldwide 3G-UMTS Terrestrial Radio Access (UTRA) systems. Then High-speed downlink packet access (HSDPA) is introduced to enhance the performance of existing 3G mobile telecommunication networks using the WCDMA protocols and support a speed of up to 21 Mbps. Then, a further enhanced 3GPP standard, Evolved High Speed Packet Access, a.k.a HSPA+, is released to support bit rates of up to 34/337 Mbps in the uplink/downlink transmission, respectively. After that, Long Term Evolution (LTE) is introduced by 3GPP to support data rate up to 160 Mbps for the 20MHz channel bandwidth.

This standard is based on orthogonal frequency division multiple access (OFDMA) technique for multiple-users resources sharing (multiple access), and incorporates some advanced technologies such as adaptive modulation, MIMO that employed up to 8-antennas at the BS, and link adaptation [9]. Following that, LTE Advanced (LTE-A) is adopted as the 3GPP initiative for the fourth generation (4G) communications systems to enhance system capacity and to keep-up with the increasing demands in the sense of user data-rate and Table 2.1 shows some requirements for LTE advanced standard [10]. The main features that make LTE-A outperforms LTE and 3G systems are OFDMA, carrier aggregation (CA), interference management via concept of Coordinated Multipoint (CoMP), and spectral efficiency/coverage enhancement through deploying heterogeneous-networks (HetNet) [10]. Furthermore, 4G systems impose the development of multi-mode user-terminals which are capable to operate in either time division duplex (TDD) or frequency-division duplex (FDD) mode.

On the other hand, to further enhance system-capacity, the coming generation, i.e., 5G is envisioned to employ some novel technologies, including massive-multiple-input multiple-output (MIMO) and millimeter wave (mmWave) communications with the legacy or traditional techniques such as cognitive radio and heterogeneous network [11].

2.1 MU-MIMO systems

In point to point wireless transmissions, the deployment of multiple antennas at both transmitter and receiver sides can considerably increase link reliability as well as link capacity compared to traditional single-input single-output (SISO) schemes. These advantages come from spatial diversity gains which are provided by the multiple

Table 2.1: Key technical requirements for LTE advanced cellular networks, given that spectrum efficiency is for 4×2 system of antennas at the base station and user terminal respectively [10].

Feature	Value
User plane latency	0.01 sec
Control Plane latency	0.05 sec
Uplink peak data rate	500 Mbps
Downlink peak data rate	1.0 Gbps
Spectrum Allocation	Up to 100 MHz
Uplink spectrum efficiency	Up to 15 bps/Hz
Downlink spectrum efficiency	Up to 30 bps/Hz
Cell edge Uplink spectrum efficiency	0.07 bps/Hz
Cell edge downlink spectrum efficiency	0.09 bps/Hz

antennas together with the scattering-environment surrounding both the transmitter and the receiver.* The number of independent sub-channels that can be provided by singular value decomposition (SVD) scheme is given as [12]

$$N_{min} = \min\{N_t, N_r, N_p\}, \tag{2.1}$$

where N_t N_r and N_p are, respectively, the number of transmitter antennas, receiver antennas and multipath created by the scatter.† With multi user MIMO (MU-MIMO) systems, the advantages are more attractive due to the capability to, simultaneously, transmit to several terminals over the same RB (more efficient in the sense of spectral resources), whereas in SU-MIMO systems the BS communicates with many terminals only through orthogonal resources (a separate time/frequency resources).

In 5G cellular systems, MIMO systems aided by massive antenna arrays are promising technology to further enhance cell throughput. These systems deploy an

* For a rich scattering environment, a system with BS of M antenna elements and $K-$scheduled single antenna users, such system can perform a multiplexing gain of $\min(M, K)$ and a spatial-diversity of order M.

† In poor propagation environments, when the channels of different terminals share some common scatterers, or when the numbers of the scatterers is small compared to the numbers of terminals, the channel is said to be not favourable. Favourable propagation-environments is required in Massive MIMO system, however, in such scenarios, distributed antenna system can be used to tackle this issue (e.g., see [13] and the citations therein).

order of magnitude more antenna elements at BS compared with the traditional MU-MIMO systems (64 antennas or more) to serve, simultaneously, a dozen of user equipment within their cells with high data rate [7].* In addition to the gain in cell throughout, theoretically, (with infinite antennas) the impacts of multi path fading vanish, as the SIR converges to a deterministic-equivalence (the random channel vectors between the BS and users become noiseless deterministic channel). Also, under i.i.d. Rayleigh fading channel, the useful signal channel becomes asymptotically orthogonal to inference and noise channels, i.e., the effects of thermal noise and intra cell interference become minor. As such, a simple linear signal processing, even with maximal ratio transmission (MRT) in the forward link or maximal ratio combining (MRC) in the reverse link, achieves near optimal performance. Moreover, in the sense of power efficiency, uplink (UL) and downlink (DL) transmit power scales down with the number of antenna elements by an order of magnitude, or even more (less energy to maintain certain SIR or QoS). For the UL, high array gain of coherent combining can allow for considerable reduction in the transmit power of each terminal. For the DL, the energy can be focused from the BS into the directions where the users are located via high resolution beamforming. Due to the aforementioned merits, the design aspect of massive MU-MIMO systems has attracted substantial interest in the recent literature.

The above discussion inspired this thesis to consider performance bounds of very-large MU-MIMO systems (especially the uplink transmission) under practical constraints such as imperfect channel-state information (Imp-CSI), inter cell interference, and different channel parameters. We proposed that the massive MIMO systems transmit signal using the Time-Division-Duplex (TDD) protocol to duplex communication-links.† An example of this protocol is displayed in the figure. 2.1, where Forward link is separated from Reverse link by the assigning of different symbols of time in the same frequency band [7, 14]. Such transmission mode allows a symmetric flow for downlink and uplink data transmission, and hence reciprocity between the downlink and uplink channels can be exploited to reduce channel training

* As an example, Marzetta in [7] proved that each user terminal can achieve a downlink link average throughput of 17Mbps in a multi cell massive MU-MIMO environment with a bandwidth of 20MHz and a frequency reuse factor (FRF) of 7.

† Since we need to acquire CSI between extreme numbers of service antennas and much smaller numbers of users, therefore we emphasise on Time-Division-Duplex (TDD) rather than Frequency-Division-Duplex (FDD). The time required for downlink pilots transmission is proportional to the antennas number, while the time required for uplink pilots transmission is independent of the antennas number, also UL/DL duality can be applied.

overhead. It is worth noting that in the channel training phase the system performs the acquisition of the channel state information (CSI) which in turn is required for precoding vectors.

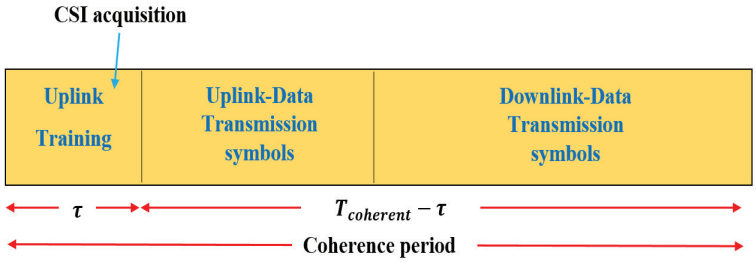

Figure 2.1: Example of TDD transmission protocol, where uplink channel training is exploited for the UL and DL transmission.

Figure 2.1 illustrates example for a simple training process in TDD scheme, in which uplink pilot sequences are utilised by both downlink and uplink data transmission. A total of τ OFDM symbols* are used entirely for pilots, i.e., all scheduled terminals in a given cell are allocated with orthogonal pilots each of length τ symbols and for massive antennas, the same set of pilot sequences is reused in adjacent cells. The remainder of the coherence interval is used for transmitting useful-data, either on the forward link or the reverse link or both. If we denote the symbol duration by T_s, then $T_{\text{pilot}} = \tau T_{\text{s}}$ is the time spent on sending reverse pilots. The simplest way to send reverse link pilots would be to assign each terminal one unique time-frequency index for its pilot (e.g., one sub-carrier within each smoothness interval and within one OFDM time slot). More generally, orthogonal sequences of time-frequency pilots can be assigned to the terminals.

2.2 The massive MIMO's basics

This section, first discusses the concept of massive MIMO systems, then introduces the asymptotic SIR of massive MIMO when the number of antenna-elements goes to infinity.

* It is worth noting that in the LTE standard, if a normal Cyclic Prefix (CP) is used, a Physical Resource Block (RB) is composed of seven symbols in time domain (with a duration of 0.5 ms) and twelve sub-carriers in the frequency domain (with a bandwidth of 180 KHz, i.e., 12×15 KHz), each cell of this (7×12) grid is called a resource element (RE).

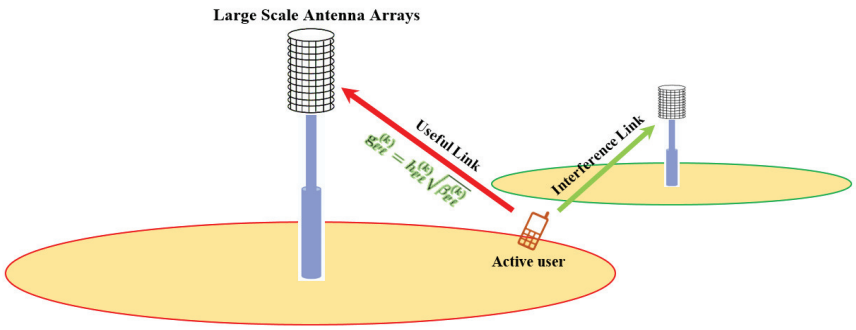

Figure 2.2: Example of an uplink transmission in two cells Massive MIMO network with $\mathbf{g}_k$ denotes the useful channel-gain from kth user to it's serving massive MIMO base station.

As shown in the figure.2.2, assuming the i.i.d. Rayleigh fading channel model, the complex propagation coefficient between the BS in the ℓth cell, and the kth user in the ℓ'th cell can be computed as [7]

$$\mathbf{g}_{\ell'\ell}^{(k)} = h_{\ell'\ell}^{(k)} \sqrt{\beta_{\ell'\ell}^{(k)}} \tag{2.2}$$

with $h_{\ell'\ell}^{(k)}$ is complex fast fading factor represents the kth column of all users' channel matrix $G_{\ell'\ell} \in \mathbb{C}^{M\times K}$ and $\beta_{\ell'\ell}$ is amplitude factor that accounts for both geometric attenuation and shadow fading, where it assumed to be constant over both frequency and the index of the BS-antenna since the geometric attenuation and shadow fading change very slowly with respect to spatial dimension, and can be given as [15]

$$\beta_{\ell'\ell}^{(k)} = \frac{\mu_{\ell'\ell}^{(k)}}{D_{\ell'\ell}^{(k)\nu}} \qquad k = 1, 2, ...K \tag{2.3}$$

The K terminals within each cell transmit, independently, data streams to their corresponding BS. Then the BS uses its channel information to perform a linear detection such as the maximum ratio combining (MRC).

2.3 SINR for the asymptotic regime

In this section, we consider an asymptotic scenario for a large antenna number $M \to \infty$ and a finite user number K, more specific, we analyse a simple scheme in which all the K scheduled users transmit the pilots to the BS simultaneously without time shift to estimate channel-gains. In this case, we assume that the same set of $\boldsymbol{\rho}$ orthogonal pilots of length τ is employed by every cell such that $\boldsymbol{\rho} = (\rho_1, \ldots, \rho_K)$ and $\boldsymbol{\rho}^H \boldsymbol{\rho} = \tau \mathbf{I}_K$.

2.3.1 Reverse Link Pilots

Assuming that pilots are, simultaneously, sent by all terminals in the system at the pilot transmission stage, then the ℓth BS receives the signal

$$\mathbf{y}_\ell = \sum_{\ell'=1}^{L} \sqrt{p_t}\mathbf{G}_{\ell\ell'}\boldsymbol{\rho}' + \mathbf{n}_\ell, \tag{2.4}$$

where $\mathbf{n}_\ell \in \mathbb{C}^{M\times K}$ is the additive noise and p_t is the transmit power for UL-channel training. Without loss of generality, we assume that the entries of $\mathbf{n}_\ell$ are i.i.d. follow the distribution $\sim \mathcal{CN}(0,1)$ r.v. and we scale all gains accordingly. Next, utilising matched filter detection, the BS correlates the signal $\mathbf{y}_\ell$ with the pilots $\boldsymbol{\rho}$ in order to obtain the channel gain observed by ℓth BS

$$\mathbf{z}_\ell = \underbrace{\sqrt{p_t}\mathbf{G}_{\ell\ell}}_{\substack{\text{useful channel}\\ \text{gain}}} + \underbrace{\sum_{\ell'\neq\ell}\sqrt{p_t}\mathbf{G}_{\ell\ell'}}_{\text{pilot contamination}} + \hat{\mathbf{n}}_\ell, \tag{2.5}$$

with $\hat{\mathbf{n}}_\ell = \frac{\mathbf{n}_\ell\boldsymbol{\rho}'}{\tau}$ and follows the distribution $\sim \mathcal{CN}(\mathbf{0}, \frac{1}{\tau}\mathbf{I}_M)$. Pilot contamination is due to other cell interference coming from users which reuse the same pilot. The kth vector of $\mathbf{z}_\ell$ can be given as

$$z_\ell^{(k)} = \sum_{\ell'=1}^{L}\sqrt{p_t}\mathbf{g}_{\ell\ell'}^{(k)} + \hat{n}_\ell^{(k)}, \tag{2.6}$$

and the channel estimate is computed as

$$\begin{aligned}\hat{\mathbf{g}}_{\ell\ell}^{(k)} &\overset{(a)}{=} p_t\beta_{\ell\ell}^{(k)}\mathbf{I}_M\left[\frac{1}{\tau}\mathbf{I}_M + \sum_{\ell'}\sqrt{p_t}\beta_{\ell\ell'}^{(k)}\mathbf{I}_M\right]^{-1} z_\ell^{(k)} \\ &\overset{(b)}{=} \frac{p_t\beta_{\ell\ell}^{(k)}}{\frac{1}{\tau} + p_t\sum_{\ell'}\beta_{\ell\ell'}^{(k)}} z_\ell^{(k)},\end{aligned} \tag{2.7}$$

wherein (a) we assume defined large scale path loss $\beta_{\ell\ell}$ by ℓth BS which in turn utilises an minimum mean square error (MMSE) estimator to evaluate the channel. Equation (b) shows that, for the i.i.d. Rayleigh fading scenario, the channel estimate $\hat{\mathbf{g}}_\ell^{(k)}$ is a scaled version of the vector $z_\ell^{(k)}$. The estimation error in channel gain can be expressed as $\tilde{\mathbf{g}}_{\ell\ell}^{(k)} = \mathbf{g}_{\ell\ell}^{(k)} - \hat{\mathbf{g}}_{\ell\ell}^{(k)}$.

2.3.2 Reverse Link data transmission

In the uplink data-transmission, the received signal at the ℓth BS is given as

$$y_\ell = \sqrt{p_u} \sum_{\ell'=1}^{L} \sum_{k=1}^{K} (\mathbf{g}_{\ell'\ell}^{(k)} \, x_{\ell'}^{(k)} + n_\ell^{(k)}), \tag{2.8}$$

where P_u is the uplink transmit-power, $x_{\ell'}$ is the message bearing-symbols vector from the users of the ℓ'th cell, n_ℓ is a vector of receiver-noise following the distribution $\sim \mathcal{CN}(0,1)$, i.e., distributed as zero_ mean and unit_ variance complex Gaussian independent random variables. For the sake of simplicity, we assume MRC receiver in which the BS employs the estimated channel $\hat{\mathbf{g}}_{\ell\ell}^{(k)}$ in detection process

$$\hat{x}_\ell = \underbrace{\sqrt{p_u} |\hat{\mathbf{g}}_{\ell\ell}^{(k)}|^2 \, x_\ell^{(k)}}_{\text{useful signal}} + \underbrace{\sqrt{p_u} \hat{\mathbf{g}}_{\ell\ell}^{(k)*} \tilde{\mathbf{g}}_{\ell\ell}^{(k)} \, x_\ell^{(k)}}_{\text{error in channel-estimation}} + \underbrace{\sqrt{p_u} \sum_{\ell' \neq \ell} \sum_{i \neq k} (\hat{\mathbf{g}}_{\ell\ell}^{(k)*} \mathbf{g}_{\ell\ell'}^{(i)} \, x_{\ell'}^{(i)} + \hat{\mathbf{g}}_{\ell\ell}^{(k)*} n_\ell}_{\text{enter-cell interference plus noise}} \tag{2.9}$$

and consequently, the uplink signal-to-interference plus noise SINR^{ul} is given as

$$\text{SINR}^{ul} = \frac{p_u \, |\hat{\mathbf{g}}_{\ell\ell}^{(k)*} \hat{\mathbf{g}}_{\ell\ell}^{(k)}|^2}{p_u \underset{\tilde{\mathbf{g}}_{\ell\ell}^{(k)}}{\mathbb{E}} \{|\hat{\mathbf{g}}_{\ell\ell}^{(k)*} \tilde{\mathbf{g}}_{\ell\ell}^{(k)}|^2\} + \underbrace{p_u \sum_{\ell \neq \ell} \sum_{i \neq k} |\hat{\mathbf{g}}_{\ell\ell}^{(i)*} \hat{\mathbf{g}}_{\ell\ell'}^{(k)}|^2}_{\text{channel-estimator error}} + |\hat{\mathbf{g}}_{\ell\ell}^{(k)}|^2} \tag{2.10}$$

2.3.3 Forward Link data transmission

The channel estimate is used by the BS to perform precoding towards users in the down-link transmission mode. Here we focus on the match-filter (MF) precoding, so the BS computes the beam-forming vector to its kth terminal as

$$\mathbf{w}_\ell^{(k)} = \frac{\hat{\mathbf{g}}_{\ell\ell}^{(k)}}{\|\hat{\mathbf{g}}_{\ell\ell}^{(k)}\|} \tag{2.11}$$

The received signal at the kth user is

$$\hat{x}_\ell = \underbrace{\sqrt{p_u} \mathbb{E}\{\mathbf{g}_{\ell\ell}^{(k)*} \mathbf{w}_\ell^{(k)}\} \, x_\ell^{(k)}}_{\text{average-effective channel-gain}} + \underbrace{\sqrt{p_d} (\mathbf{g}_{\ell\ell}^{(k)*} \mathbf{w}_\ell^{(k)} - \mathbb{E}\{\mathbf{g}_{\ell\ell'}^{(k)*} \mathbf{w}_{\ell'}^{(k)}\}) \, x_{\ell'}^{(k)}}_{\text{error in channel-estimation}}$$

$$+ \underbrace{\sqrt{p_d} \sum_{\ell'=1}^{L} \sum_{k=1}^{K} \mathbf{g}_{\ell'\ell}^{(i)*} \mathbf{w}_{\ell}^{(i)} \, x_{\ell'}^{(k)} + \hat{\mathbf{g}}_{\ell'\ell}^{(k)*} n_{\ell}}_{\text{enter-cell interference plus noise}} \tag{2.12}$$

where $x_{\ell}^{(k)}$ is the transmitted symbol. The downlink signal-to-interference plus noise SINR^{ul} is given as

$$\text{SINR}^{dl} = \frac{p_d \, |\mathbb{E}\{\mathbf{g}_{\ell\ell}^{(k)*} \mathbf{w}_{\ell}^{(k)}\}|^2}{p_d \, \text{Var}\{\mathbf{g}_{\ell\ell}^{(k)*} \mathbf{w}_{\ell}^{(k)}\} + \underbrace{p_d \sum_{\ell' \neq \ell} \sum_{i \neq k} |\mathbf{g}_{\ell'\ell}^{(i)*} \mathbf{w}_{\ell'}^{(i)}|^2}_{\text{channel-estimator error}} + 1} \tag{2.13}$$

2.4 Asymptotic behaviour

Now, we investigate some key features corresponding to massive MIMO, e.g., the asymptotic orthogonality for independent Gaussian channel vectors and the pilot contamination. The precoder equation in (2.11) is the normalized version of the gain $\hat{\mathbf{g}}_{\ell\ell}^{(k)}$ and can be rewritten as

$$\begin{aligned} \mathbf{w}_{\ell}^{(k)} &= \frac{\hat{\mathbf{g}}_{\ell\ell}^{(k)}}{\|\hat{\mathbf{g}}_{\ell\ell}^{(k)}\|} \\ &\overset{(a)}{=} \frac{\hat{\mathbf{g}}_{\ell\ell}^{(k)}}{a_{\ell}^{(k)} \sqrt{M}}, \end{aligned} \tag{2.14}$$

with $a_{\ell}^{(k)}$ is scalar represents the normalization-factor

$$a_{\ell}^{(k)} = \frac{\|\hat{\mathbf{g}}_{\ell\ell}^{(k)}\|}{\sqrt{M}} \tag{2.15}$$

For asymptotically large scale antennas system, i.e., when $M \to \infty$, the value of $a_{\ell}^{(k)}$ is computed in [7] using the following lemma which can be proofed directly with the aid of the strong law of large numbers (LLN).

Lemma 2.1. If $\mathbf{x}, \mathbf{y} \in \mathbb{C}^{M \times 1}$ are two independent random vectors with distribution $\sim \mathcal{CN}(\mathbf{0}, b\mathbf{I}_M)$, then in the limit of vector dimension, these vectors are asymptotic-orthogonal to each other and the square-norm of $\mathbf{x}$ converges to a finite value as [7]

$$\begin{aligned} \lim_{M \to \infty} \frac{\mathbf{x}^{\dagger} \mathbf{y}}{M} &\overset{\text{a.s.}}{=} 0 \\ \lim_{M \to \infty} \frac{\mathbf{x}^{\dagger} \mathbf{x}}{M} &\overset{\text{a.s.}}{=} b \end{aligned} \tag{2.16}$$

where (a.s) denotes that the equality holds almost surely and b is a constant. Accordingly, for independent Rayleigh fading massive MIMO channels, the useful-link becomes orthogonal to the vectors of both interfering-links and noise. Leverage Lemma 2.1, we can derive the SINR for reverse-link and forward link in the asymptotic-regime.

Lemma 2.2. If the number of BS antennas goes to infinity, the expressions in (2.10) and (2.13) converge to there asymptotic equivalence (the effective signal-to-interference ratio) as [7]

$$\lim_{M\to\infty} \mathrm{SINR}^{ul} = \frac{{\beta_{\ell\ell}^{(k)}}^2}{\sum_{\ell'\neq\ell} {\beta_{\ell\ell'}^{(k)}}^2} \tag{2.17}$$

$$\lim_{M\to\infty} \mathrm{SINR}^{dl} = \frac{p_d {\beta_{\ell\ell}^{(k)}}^2/\alpha_\ell^k}{p_d \sum_{\ell'\neq\ell} {\beta_{\ell'\ell}^{(k)}}^2/\alpha_{\ell'}^k}, \tag{2.18}$$

where the interference term in denominators is due to pilot contamination phenomena. Next, we discuss some key aspects regarding large scale MIMO systems.

2.5 Linear Precoding schemes

In our study, we focus on linear precoding techniques for massive-MIMO to cancel interference among sub-streams, as linear techniques has less complexity in implementing than the non linear techniques, such as dirty paper precoding (DPC), especially with a large number of antennas. Numerical simulations shows that the achievable rate of linear precoding approaches the channel capacity upper bound (suboptimal performance) when the number of antennas is very large. In this context, this section briefly discusses three different techniques, namely maximum ratio transmission (MRT), Zero forcing (ZF) and Signal-to-Leakage plus Noise Ratio maximising Beamforming (SLNR_Max).* Fig.2.3 shows the beamforming directions with ZF, MRT, and SLNR-MAX beamforming, where ZF is orthogonal to the channel of non-intended users, MRT-direction follows the channel of the intended

* The counterparts to these precoding techniques are three combining techniques, namely maximum ratio combining (MRC), zero forcing filter (ZF), and signal-to-leakage-and-noise-ratio maximising (SLNR-MAX) filter (also known as Wiener or linear MMSE-filter).

user, and SLNR-MAX achieve a balance between these extremes according to the SNR [16].

- **MRT beamforming**: This beamforming scheme is applied to provide the spatial diversity gain of multiple antennas. Recall that in equation (2.11), BS computes matched filtering or the maximum-ratio-transmission (MRT) beamforming vector that maximises the desired channel gain of the kth terminal as $\mathbf{w}_\ell^{(k)} = \frac{\hat{\mathbf{g}}_{\ell\ell}^{(k)}}{\|\hat{\mathbf{g}}_{\ell\ell}^{(k)}\|}$. As illustrated in Fig. 2.3, MRT chooses the vector that spans the desired channel direction, therefore the two vectors inner product is maximised.

- **ZF beamforming**: (Also known as channel inversion) In order to cancel out multiple user interference, a ZF precoding vector $\mathbf{w}_k$ for a user k is designed to lie in the null space of all other co_users channels. Thereby, $\mathbf{w}_k$ should be orthogonal to all other co users channels and the null space dimension should be non-empty space, which means that antennas number should be greater than non-intended users $M \geq K$. The ZF precoding vectors represents the column vectors of the Moore Penrose pseudo inverse of matrix $\mathbf{G}$ which can be given as [16]

$$\mathbf{W} = \mathbf{G}^{\dagger} = \mathbf{G}^H(\mathbf{G}\mathbf{G}^H)^{-1} \tag{2.19}$$

  While ZF technology being heuristic or suboptimal beamforming, it is proven, in the high SNR regime when the number of users gets very large, to be optimal solution and approach, asymptotically, the performance of DPC. Where multiuser diversity can be increased with the increase of active users, hence plentiful channel directions will be available with good quality. Consequently, offers an opportunity for the BS to schedule a set of terminals with better conditions in terms of spatial-separation and channel gain.

- **SLNR-Max-beamforming**: This filtering terminology is equivalent to MRT in noise-limited scenarios (i.e., when the noise is very strong compared with the interference) and equivalent to zero-forcing in interference limited scenarios (i.e., when the interference is very strong). SLNR for the kth user represents the signal-to-leakage interference produced by this user to the received signal

of other users in the same system and can be expressed as [17]

$$\mathrm{SLNR}_k = \frac{\|\mathbf{g}_k \mathbf{w}_k\|}{\sigma_k^2 + \sum\limits_{i \neq k} \|\mathbf{g}_i \mathbf{w}_k\|} \tag{2.20}$$

where the second term in the denominator is the leakage interference contributed by user k to other users. Thereby, the beamforming $\mathbf{w}_k$ can be evaluated by maximising the SLNR to make a balance between maximising signal power and suppressing interference. Accordingly, operation region of SLNR-Max lies, from a geometric perspective, between the two extremes of MRT and ZF,

$$\mathbf{w}_k = \frac{\left(\mathbf{I}_M + \sum\limits_{i=1}^{K} \frac{P}{K\sigma^2} \mathbf{g}_i \mathbf{g}_i^H\right)^{-1} \mathbf{g}_k}{\left\|\left(\mathbf{I}_M + \sum\limits_{i=1}^{K} \frac{P}{K\sigma^2} \mathbf{g}_i \mathbf{g}_i^H\right)^{-1} \mathbf{g}_k\right\|} \tag{2.21}$$

where $\frac{P}{K}$ is the average transmit power and σ^2 is the noise-power.

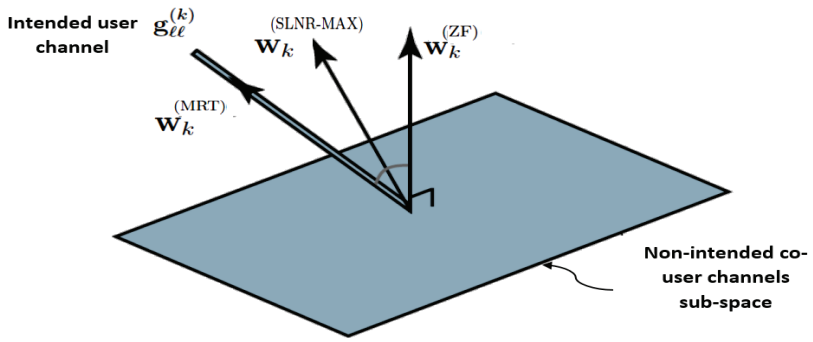

Figure 2.3: The geometric interpretation of maximum signal (ZF) versus minimum inter user interference trade off [16], where operation region of the suboptimal scheme lies in between these two extremes.

To display the performance of the aforementioned linear beamforming technologies we investigate an interference channel environment of $K = 4$ users and $M = \{4, 64\}$ antenna elements at the BS. Specifically, figures 2.4 and 2.5 show the average per user information rate for transmit antennas of $M = 4$ and $M = 64$ respectively. Here we assume full interference coordination and users channel vectors are generated as i.i.d. Rayleigh fading distribution. The performance metric is the average, per user, downlink information rate,

$$\mathbf{R}^{dl} = \mathbb{E}\{\log_2\left[1 + \mathrm{SINR}^{dl}\right]\}, \qquad \text{bps/Hz}, \tag{2.22}$$

with the expectation operation $\mathbb{E}\{\cdot\}$ is taken over different channels and noise realisations. Results depict that MRT is optimal in low SNR case, while ZF performs better in high SNR case. Where in high SNR regime (multi user interference dominates over thermal noise), for the sake of interference elimination by ZF, a user can afford to lose some of its signal quality. By the contrary, in low SNR regime (thermal noise dominates over multi user interference), it is more beneficial to enhance the strength of desired signal than to eliminate the interference. More significant, obtained results in Fig.2.5 reveal the importance of performance analysis for another asymptotic-regime, i.e., the use of large antenna arrays (when M goes to infinity).

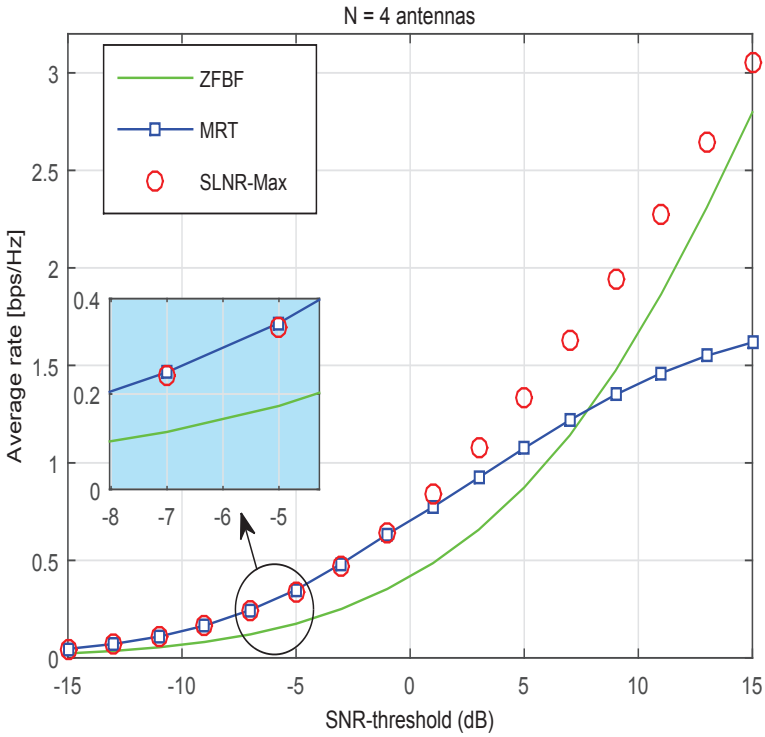

Figure 2.4: The average achievable user information rate as a function of the total per BS transmit power for traditional MIMO system ($M = 4$ antenna elements and $K = 4$ users).

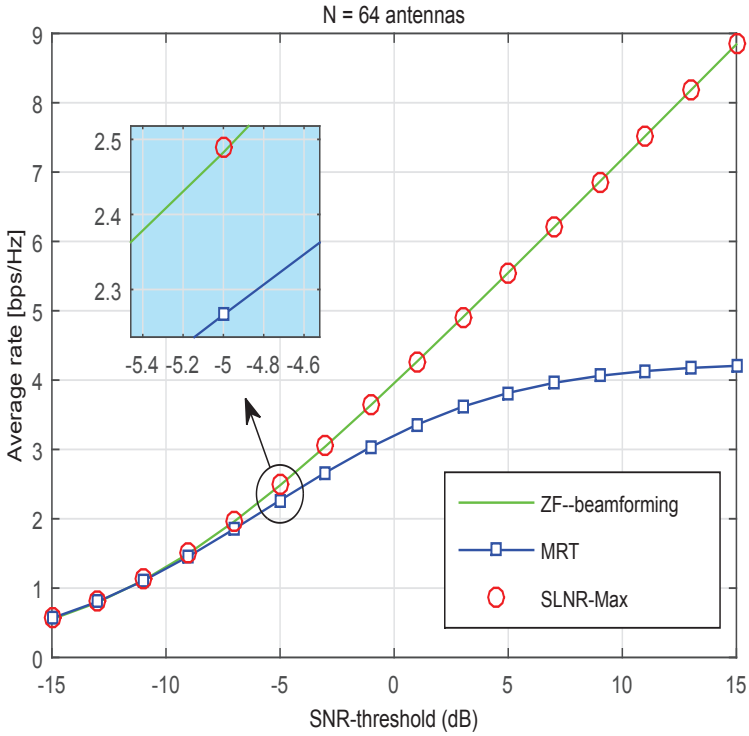

Figure 2.5: The average achievable user information rate as a function of the total per BS transmit power for massive MIMO environment ($M = 64$ antenna elements and $K = 4$ users).

2.6 Cellular Networks analysis challenges

The mathematical modelling of wireless cellular-networks is often carried out through simplified spatial models for the locations of the base stations where common strategies for these models include the Wyner, the single cell interfering and the hexagonal grid models. However, these models are either require time exhaustive numerical computations or they are inaccurate for many operating-scenarios.

- **Wyner Model**: This model was supposed for uplink transmission, however, it was applied to analyse the ideal performance of downlink transmission in multi cell systems. The idea is proposed by A. Wyner [18], where users are assumed to only receive signals from their own BS and the immediate adjacent BSs. Figure 2.6 displays the linear or one dimensional version of the model, where all BSs are located on the boundary of a large circle and it is usually proposed that all terminals in the ℓth cell are served, jointly, by $\mathrm{BS}_{\ell+1}$, BS_{ℓ} and $\mathrm{BS}_{\ell-1}$. Users in this model assumed to have deterministic average SINR regardless of their location and because of its analytical tractability and simplicity, it has been extensively employed in the literature. However, this abstraction and

related mean value approaches are proven to be inaccurate in most cases like the uplink of CDMA systems with heavily loaded scenarios [19], unless there is a very large amount of, spatial, interference averaging.

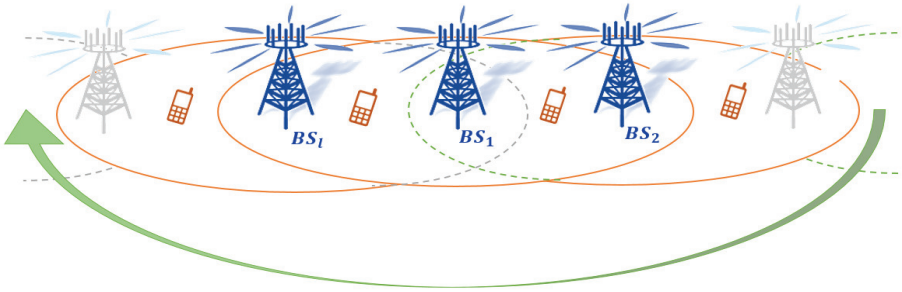

Figure 2.6: An illustration of the linear Wyner Model of multi cell scenario (one-dimensional). Terminals are served, jointly, by the closest BS and its two neighbours, whereas only experience interference from these three BSs.

- **Grid Models**: Hexagonal (figure 2.7) and other grid architectures have been widely considered to analyse and evaluate the performance of multi-cell networks. In this approach, locations of BSs follow deterministic grid (e.g., square or hexagonal grid) where all cells have the same regular shape and size. In addition, these models approximate, closely, practical cellular system topology and they are quite easy to numerically simulate the cellular systems [20]. The hexagonal model yields the lowest perimeter-to-area ratio of any other regular tessellation of the 2D plane. Hence, the edge effects are minimised when applying the hexagonal model in network analysis. However, researchers are resorted to more simplified topology to analyse multi-cell networks (e,g, widely known Wyner Model) because of analytical complexity inherent in grid architectures.

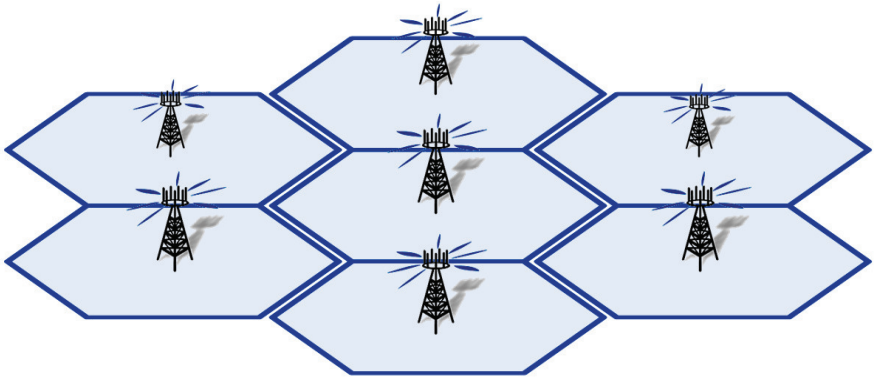

Figure 2.7: An example of grid architecture (Hexagonal grid) of multi cell scenario. Obtained results for analysis of such model represent the optimistic upper bound on system performance, whereas random model provides the lower bound.

- **Stochastic Models**: Although cellular systems are usually modelled on a regular hexagonal (or a bit more simply square) lattice, these grid models have key limitations as well. First, these abstraction models are inaccurate for today's heterogeneous network elements deployment, in which the size of a cell, considerably, varies. Where such deployments in modern networks leads to a more irregular and flexible network layout and complicates the inter cell interference distribution. Also, time consuming and complicated Monte Carlo simulations are required for grid-model analysis while they rarely give insights in network designs since the obtained SINR is still a random-variable.

  Therefore, mathematical modelling is a needed task to address the challenge of irregular-layout and to better characterise the interference distribution. Recently, an alternative model is adopted to deal with the architectures of cellular networks where BSs are positioned randomly, especially in modern heterogeneous networks [21]. Intuitively, such approach provides accurate expressions for SINR-distributions and analytical tractability. A Powerful tool from Stochastic Geometry (SG) can be efficiently employed to Mathematical analyse these random models of cellular networks [22].* Stochastic geometric models, in general, consist of introducing network structural components as realisations of stochastic processes. Cell sizes, BS positioning, traffic demand, mobility and other characteristics of the network are, solely, dependent on distributions and parameters of these processes.

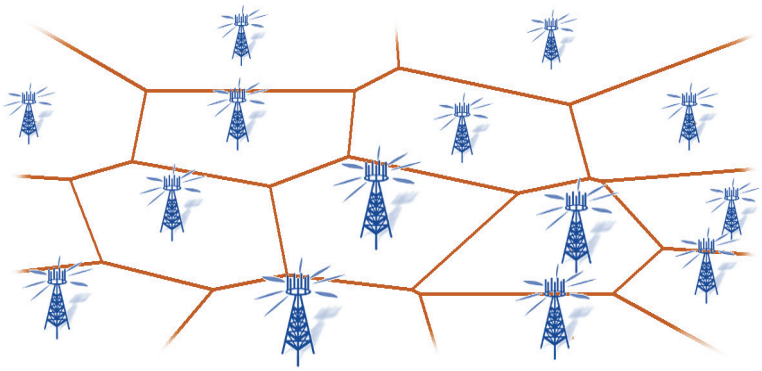

Figure 2.8: An example of single tier multi cell network with a random or irregular model of base stations deployment. Such scenario yields analytical tractability, and develops almost accurate formulas for the distributions of the SINR via stochastic geometry (SG) tools.

* While regular models gives an optimistic upper bound of the performance, irregular-models determine the lower bound e (e.g., see [21] and the references therein).

Chapter 3

Statistical Queueing Constraints in the Uplink of a Single Cell Massive-MIMO

Cross-layer design is a suitable approach that can address some of the throughput challenges for future multimedia applications. In this regard, the effective capacity concept offers a suitable metric to assess the implications that physical layer design may have on link layer performance. However, most reported studies in this aspect consider the case of downlink scenario for convenience multiple input multiple output (MIMO) systems. This chapter analyses the uplink effective capacity in a multi user massive MIMO system over generalised composed fading channels considering the QoS statistical exponent constraints. In the proposed approach, a location dependent and a location independent (averaged out) closed form expressions are derived for the effective capacities in asymptotically large receive antenna system with perfect and imperfect channel state information (CSI) scenarios. In addition, the analytical analysis considers the perfect and imperfect channel information CSI effects. Moreover, expressions for the asymptotically high signal-to-noise ratio regimes are provided. Obtained results show that the effective capacity performance is a monotonically increasing function of the base station receive antennas (N_r) and the large scale shadowing parameter. Moreover, increasing N_r by almost 74 antennas for imperfect CSI, can compensate for system capacity degradation due to queueing delay constraint of $\theta = 1.9 \times 10^{-4}$ per bit.

3.1 Introduction

Most of the emerging real time applications imposed stringent constraints on queue lengths or queuing delays of transmit buffer. As such, besides the signal-to-interference plus noise ratio (SINR) metric in *physical layer*, there was a need of new metric to deal with quality-of-service delay constraints, i.e., queueing behaviour in the *link layer* of the wireless networks. Motivated by the theory of effective bandwidth, the authors in [23], Wu and Negi introduced a concept of effective capacity as a novel metric to bridge the gap and characterise system performance with different quality of service (QoS) limitations, e.g., data rate and the probability delay violation. Accordingly, this metric quantifies the maximum arrival rate that can be achieved with respect to a given service demands for the steady-state flow of data at a buffer input.

The effective capacity for single antenna communication systems is analysed in [24]. Reference [25] considers the effective capacity of Gaussian block-fading MIMO systems. Moreover, [26], examined in detail, high and low SNR asymptotic behaviour of MIMO and shown the relationship between the buffer-queuing constraints and MIMO spatial-dimensions over the entire range of SNR values. Authors in [27] investigated energy efficient uplink communications for battery constrained mobile terminals, where a heterogeneous wireless medium is considered. In [28] the effective throughput of MIMO systems is investigated over both independent identically distributed and independent non-identically distributed $\kappa - \mu$ fading channels under QoS delay constraints.

It is well known that the use of massive antenna arrays can significantly increase the energy and spectral efficiency of wireless systems [29]. Motivated by this fact, we seek in this chapter to address the potential benefits of massive-MIMO configuration on the uplink effective capacity of a wireless system. Different from the existing works on effective capacity, in our analysis, we exploit the asymptotic results of random matrix theory (RMT) introduced in [29] to further analyses the uplink channel performance of large system focusing on QoS statistical constraints. We resort to the asymptotic formulas since the analysis of the massive MIMO system becomes extremely difficult with the exact SINR's expression. In addition, the analysis considers the shadowing effect when zero forcing receiver is employed. Such analysis could play a key role in 5G systems designing, in particular, vulnerable to shadowing and path loss attenuation, mm-Wave frequencies. The specific contributions of this

chapter can be summarised as follows,

1) We derive, in closed form expression, the uplink's asymptotic effective capacity when the base station (BS) deploys a large antenna-array, as well as when the system is in high power regime for perfect and imperfect channel information. (unique to the best of our knowledge). The derived expressions are helpful to gain a deep insight into the system design and the impact of different parameters on the performance.

2) The implications of user location, channel and system parameters on the uplink performance are evaluated via numerical analysis with remarkable comments. The provided precise approximation results can replace the need for lengthy Monte Carlo simulations to take spatial average over different user distributions. Moreover, obtained results are of particular interest for the cross layer design of massive MIMO systems and to characterise the effects of large scale shadowing in next generation wireless systems (e.g. vulnerability to shadowing mm-Wave systems).

The remainder of the chapter is organised as follows, In Section 3.2, a system and channel model for uplink of massive MIMO system are described. Afterwards, the asymptotic effective capacity with the QoS-statistical exponent is derived. Numerical results are presented in section 3.3. Finally, section 3.4 concludes the chapter.

3.2 System and Channel Model

We consider the uplink channel of a single cell massive antenna system, assuming that users are equipped with a single transmitting antenna. The output of the channel can be written as [30] $y = \sqrt{p_u}\mathbf{G}x + n$, where $\mathbf{G} \in \mathbb{C}^{N_r \times K}$ is the complex channel matrix between the users and the BS. N_r is the number of receiver antennas at the BS, p_u is the average power transmitted by each user, x denotes the data signal and $n \sim \mathcal{CN}(0,1)$ denotes the AWGN noise. For individual user k, the column vector of G will be [29], [30, eq.(2)]

$$g_k = h_k\sqrt{\beta_k}\,, \tag{3.1}$$

with h_k is the fast fading component of g_k and β_k is the large scale component which in turn can be expressed as follows [29], [31, eq.(2)]

$$\beta_k = \frac{\mu_k}{D_k^{\nu}} \quad k = 1, 2, ...K \ , \tag{3.2}$$

with μ_k is the large scale shadowing and D_k is the distance between the BS and the k-th user and ν is the path-loss exponent, where real measurements in wireless channels have shown the distance dependence of the average received power.* It is noteworthy to mention that in case of generalized-K composite fading channel g_k, the fast fading component h_k can be characterised using Nakagami-m distribution and Log-normal distribution can be used for the large-scale component μ_k [32].

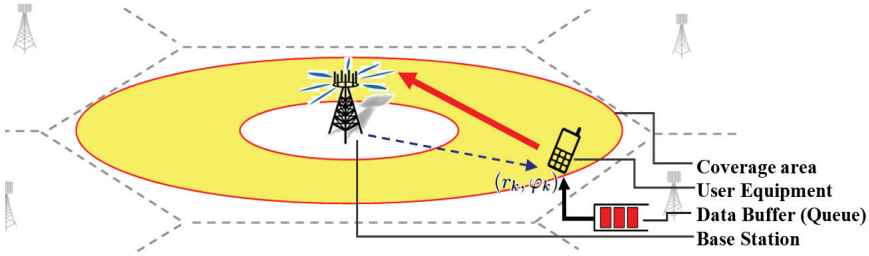

Figure 3.1: System model employed in the analysis, where the scheduled users (with locations expressed in polar coordinates as (r_k, φ_k)) are uniform, independently, distributed in a circular cell having an inner radius of R_i and outer radius of R_o, while the BS is located at the centre (0,0) of the circle [33].

Since, in large scale MIMO systems, zero-forcing (ZF) detector† tends to be optimal [29], thus in our work ZF is adopted and all results are derived based on this requisite. Moreover, in massive antenna environments, just small scale fading corresponding to micro diversity can be averaged out, while large scale fading corresponding to macro diversity environment stays active and affects system performance.

Lemma 3.1. (Large-system regime Ergodic information rate approximation); The upper bound on the uplink ergodic rate of k-th user $\mathbb{E}\{R_k\}$ can be characterised applying RMT based large system analysis.

*This fact led to the well-known path loss law, where the typical values of ν ranging from 2 to 6 in urban areas. It is interesting to note that, in order to cope with the singularity issue of the path loss model when the distance is zero, one can use the function $f(D, \nu) = min(1, D_k^{-\nu})$ in the path-loss model [35].

† It is worth mentioning here that for massive MIMO systems, antenna dimensions render the ZF-matrix inversion, in the beamforming or detection formula, computationally expensive, however, according to [36], a truncated polynomial expansion formula can be applied with nearly similar outcome.

Capitalising on the outcomes of [29], assuming ZF detector and perfect CSI, the asymptotic rate of the k-th user can be written as [29, eq.(21)], [34]

$$R_k^{asy} \overset{N_r \to \infty}{=} \log_2(1 + \beta_k p_u N_r), \qquad \texttt{bits/s/Hz} \tag{3.3}$$

Next, the approximation of the ergodic sum rate is derived as follows

$$\begin{aligned} R_k^{asy}(\mu_k, D_k) &= \mathbb{E}_{\mu_k, D_k}\left\{\log_2(1 + \beta_k p_u N_r)\right\} \\ &\overset{(a)}{\leqslant} \log_2(1 + \mathbb{E}_{\mu_k, D_k}\left\{\beta_k p_u N_r\right\}) \\ &\overset{(b)}{=} \log_2(1 + \mathbb{E}_{\mu_k, D_k}\left\{\frac{\mu_k\, p_u}{D_k^{\nu}} N_r\right\}), \end{aligned} \tag{3.4}$$

where inequality (a) follows from Jensen's inequality since $\log_2(\cdot)$ is a concave function and (b) stems from eq.(3.2). In our analysis, for practical considerations, we assumed that μ_k and D_k are two random variables with distributions given in eq.(3.5) and eq.(3.6) respectively. Furthermore, for analytical tractability, the spatial correlation of large scale fading μ_k due to common obstacles is not considered here. Hence, shadowing from different users are assumed to be i.i.d r.vs.* In this regard, gamma distribution has shown a good fit to real or practical measurements and also it is analytically more tractable than the log-normal distribution. The probability density function (PDF) of gamma r.vs can be given by the following equation [29, eq.(26)]

$$f(x) = \frac{x_k^{m-1}}{\Gamma(m_k)\Omega_k^{m_k}} e^{-x/\Omega_k} U(0), \quad x, m_k, \Omega_k > 0 \tag{3.5}$$

here, $U(0)$ is the unit step function to ensure that the probability is defined over the range $0 \leq x < \infty$ and $\Gamma(\cdot)$ represents the gamma function, see e.g., [39, eq.(06.05.03.0001.01)]. Parameters $m_k \geq 0$ and $\Omega_k \geq 0$ are the fading figure (shape) and the average power (scale parameter) respectively, which depend on the channel conditions. Assuming that the fading figure, m_k and the average power, Ω_k are the same for all the users within the cell, henceforth, in our analysis, we are going to drop user's index from these parameters. Moreover, we assume the common circular-cell system model, where there is an independent and uniform distribution of UEs in a circular area of radius R_o and excluded from the guard-zone with a radius of R_i as shown in Fig.3.1. So, the corresponding probability density function (PDF) of the

*This assumption is sufficiently reasonable for distributed-antenna systems. Nevertheless, it was recently proved, through real measurements [38], that shadowing can be i.i.d across the array even for co-located antenna arrays.

distance r_k between users terminals and the serving base station (at the centre) can be modelled as follows [40]*

$$f_R(r) = \begin{cases} \dfrac{2r}{(R_o^2 - R_i^2)}, & \text{for } r \in (R_i, R_o] \\ 0, & \text{others} \end{cases} \tag{3.6}$$

Additionally, the probability density function (PDF) of the angle of the UEs locations w.r.t horizontal axis, φ is uniformly distributed on the range $[0, 2\,\pi]$ and is given by

$$f_\phi(\varphi) = \frac{1}{2\,\pi}, \tag{3.7}$$

while the cumulative distribution functions (CDFs) of r and φ are, respectively, given by

$$F_R(r) = \begin{cases} \dfrac{(r^2 - R_i^2)}{(R_o^2 - R_i^2)}, & \text{for } r \in (R_i, R_o] \\ 0, & \text{others,} \end{cases} \tag{3.8}$$

and

$$F_\phi(\varphi) = \frac{\varphi}{2\,\pi}, \tag{3.9}$$

It is worth emphasising that the well known Shannon's capacity formula used in eq.(3.4), cannot account for the quality of service demands. So, in the following section, a significant figure of merit, namely, effective capacity is introduced to incorporate statistical delay QoS into the capacity formula of wireless applications.

3.2.1 Effective Capacity

In order to incorporate the status of the user buffer to our model, a new parameter θ_k, relates to the asymptotic decay rate of the buffer occupancy is described as follows [23]†

$$\theta_k = -\lim_{x \to \infty} \frac{ln(Pr\{L > x\})}{x} \tag{3.10}$$

here, L is the queue length at steady state of the transmitter buffer and x is the delay bound. The effective capacity as a function of QoS exponent can be expressed

*For ease of notation, user index, i.e., the subscript k is omitted hereafter.

† It should be noted that θ_k characterises the equilibrium state delay violation probability of the k-th user, where a smaller θ_k indicates a looser QoS constraint, while a larger θ_k imposes more stringent constraints.

accordingly by defining the asymptotic logarithmic moment generating function of the service process [24]

$$C_{eff}(\theta_k) = -\lim_{n\to\infty} \frac{1}{n\,T\theta_k B} \log_2 \mathbb{E}_{R_k}\left\{ e^{-T\theta_k B \sum_{i=1}^{n} R_k[i]} \right\} \tag{3.11}$$

where, $R_k[i]$ is the transmission rate in time slot i, T is the block length or the total number of data symbols in one time frame* and B is system bandwidth.

3.2.2 Perfect CSI Performance

Assuming uncorrelated (independent and identically distributed) stochastic service process, C_{eff} in (3.11) can be simplified to [23], [24]

$$C_{eff}(\theta_k) = -\frac{1}{T\theta_k B} \log_2 \mathbb{E}_{R_k}\{e^{-T\theta_k B R_k}\} \tag{3.12}$$

where T is the block length, B is system bandwidth and the expectation is taken w.r.t the random variable R_k. Obviously, the effective capacity coincides with the traditional Shannon's ergodic capacity in case there is no delay constraint i.e. $\theta_k \to 0$. Analytically, with the assumption of steady state of the buffer input (stationary and ergodic process), and after substituting for rate R_k from eq.(3.3), the asymptotic effective capacity normalised by the bandwidth, will be as follows,

$$C_{P,k}^{asy}(A, D_k, p_u, \Omega, m) = -\frac{1}{A} \log_2 \mathbb{E}\Big\{(1 + \beta_k p_u N_r)^{-A}\Big\} \tag{3.13}$$

where $A \triangleq \theta_k TB/ln2$ the subscript P refers to perfect-CSI and the expectation is taken over all realisations of the channel (assumed to be ergodic). Using the PDF which is given in eq.(3.5), the averaging over the SIR distribution is given by

$$C_{P,k}^{asy}(A, D_k, p_u, \Omega, m) = -\frac{1}{A} \log_2 \int_0^\infty \underbrace{(1 + \beta_k p_u N_r)^{-A} f(x) dx}_{\mathcal{I}} \tag{3.14}$$

Theorem 3.1 (Perfect CSI)**.** *The asymptotic effective capacity of k-th user in uplink of massive MIMO systems in generalised-k channels with perfect CSI is given by the following compact form*

*In the Resource grid designing, block length must be less than or equal to the length of the channel coherence-interval in which the channels are assumed to be invariant.

$$C_{P,k}^{asy}(A, D_k, p_u, \Omega, m) = -\frac{1}{A}\log_2\left\{{}_2F_0\left[\begin{matrix} m, A \\ \cdots \end{matrix}\middle| \frac{-p_u N_r \Omega}{r_k^{\nu}}\right]\right\} \tag{3.15}$$

where r_k is the distance between the k-th user and the BS, ${}_pF_q(\cdot)$ stands for the generalized hyper geometric function [46, eq.(9.14.1)] and $(\cdots)$ denotes coefficients absence.

$${}_pF_q\left[\begin{matrix} a_1, \cdots, a_p \\ b_1, \cdots, b_q \end{matrix}\middle| z\right] = \sum_{n=0}^{\infty} \frac{(a_1)_n, \cdots, (a_p)_n}{(b_1)_n, \cdots, (b_q)_n} \frac{z_n}{n!}, \tag{3.16}$$

with, $(x)_n$ is the rising factorial or the Pochhammer polynomial, $(x)_n = \prod_{i=1}^{\infty}(x+i)$, p and q are non-negative integers.

Proof: A detailed proof is given in appendix A.1. □

Practically, users are randomly located within cell area, such that path loss for different users are different.* The following corollary corresponds to this significant fact by using distance marginal distribution function PDF given by eq.(3.6) to evaluate the average effective capacity over users of the entire cell area.

Corollary 3.1.1 (Spatial Average)**.** The average asymptotic effective capacity over all the users in the uplink of massive MIMO systems over generalised-k channels can be parametrised as

$$C_P^{asy}(A, D_k, p_u, \Omega, m) = -\frac{1}{A}\log_2\left\{\frac{R_o^2}{(R_o^2 - R_i^2)}\,{}_3F_1\left[\begin{matrix} \frac{-2}{\nu}, m, A \\ \frac{(\nu-2)}{\nu} \end{matrix}\middle| \frac{-p_u N_r \Omega}{R_o^{\nu}}\right] - \frac{R_i^2}{(R_o^2 - R_i^2)}\,{}_3F_1\left[\begin{matrix} \frac{-2}{\nu}, m, A \\ \frac{\nu-2}{\nu} \end{matrix}\middle| \frac{-p_u N_r \Omega}{R_i^{\nu}}\right]\right\} \tag{3.17}$$

Proof: see appendix A.2 □

The estimation of channel state information (CSI) is very important for multi user MIMO systems to achieve the required performance. However, in practical scenarios, the performance is limited as the knowledge of channel state information (CSI) is fundamentally made employing limited number of orthogonal uplink pilot sequences (a predefined reference or training sequences). As shown in Fig.2.1, increasing the

* It is worth to note that in literature, analysis corresponding to path loss attenuation and interference from random spatial distributed users usually gets benefits of a significant approach, namely, stochastic geometric models because of their tractability.

number of pilots could results in more signalling overhead as we restricted to the channel coherence time. Therefore, in the following subsection, our efforts will be devoted to considering the limited channel information scenario, i.e. when we have a limited number of pilot sequences.

3.2.3 Imperfect CSI Performance

As mentioned above, in realistic wireless systems, training pilots or sequences of limited length say e.g. τ symbols, usually used in acquiring CSI. Because of limited length of training pilots and the time varying characteristic of the fading channels, estimation errors are unavoidable. Hence imperfect-CSI performance is of key point in real systems analysis. For simplicity, and without loss of generality, we assume no power control policy, i.e., an equal power transmitted by all users [44], according to power-scaling law, $p_u = E_u/\sqrt{N_r}$, where E_u is the total available power.

Lemma 3.2. (Uplink Rate in Infinite Antenna Regime with imperfect CSI); The large system asymptotic uplink rate can be written as [29, eq.(37)]

$$\begin{aligned} R_k^{asy} &\overset{N_r\to\infty}{\approx} \frac{T-\tau}{T}\log_2(1+\tau\beta_k^2E_u^2), \\ &\overset{N_r\to\infty}{\approx} \log_2(1+\tau\beta_k^2E_u^2), \qquad \text{for} \quad T\gg\tau \end{aligned} \tag{3.18}$$

where the multiplying factor $\frac{T-\tau}{T}$ is the ratio of time required for sending data-to-the total time frame which accounts for the effect of the time required for channel estimation, i.e., the overhead imposed by pilot training.

Consequently, the asymptotic uplink effective capacity for imperfect CSI can be evaluated as follows. First, from the definition of effective capacity we have

$$C_{IP,k}^{asy}(A, D_k, p_u, \Omega, m) = -\frac{1}{A}\log_2 \underbrace{\int_0^\infty (1+\tau\beta_k^2E_u^2)^{-A} f(x)\,dx}_{\mathcal{I}_{IP}} \tag{3.19}$$

where the subscript IP refers to imperfect-CSI. Next, we arrive at the following statements for the metric.

Theorem 3.2 (Imperfect CSI)**.** *The asymptotic effective capacity of k-th user in uplink of massive MIMO systems over generalised-k channels with imperfect CSI is given by*

$$C_{IP,k}^{asy}(A, D_k, p_u, \Omega, m) = -\frac{1}{A}\log_2\left\{ {}_3F_0\left[\begin{matrix}\frac{m}{2}, \frac{m+1}{2}, A \\ -- \end{matrix}\middle| \frac{-4\tau p_u^2 N_r\Omega^2}{r_k^{2\nu}}\right]\right\} \tag{3.20}$$

Proof: see appendix A.3 □

Now we can take the effect of distance distribution into account by averaging over all the users, assuming they are independently normalised distributed.

Corollary 3.2.1 (Spacial Average)**.** The average asymptotic effective capacity over all the users in the uplink of massive MIMO systems over generalised-k channels is given by the following formula

$$C_{IP}^{asy}(A, D_k, p_u, \Omega, m) = -\frac{1}{A}\log_2\left\{\frac{R_o^2}{(R_o^2-R_i^2)}\,{}_4F_1\left[\begin{matrix}\frac{-1}{\nu}, \frac{m}{2}, \frac{m+1}{2}, A \\ \frac{(\nu-1)}{\nu}\end{matrix}\middle| \frac{-4\tau p_u^2 N_r \Omega^2}{R_o^{2\nu}}\right]\right. \\ \left. - \frac{R_i^2}{(R_o^2-R_i^2)}\,{}_4F_1\left[\begin{matrix}\frac{-1}{\nu}, \frac{m}{2}, \frac{m+1}{2}, A \\ \frac{(\nu-1)}{\nu}\end{matrix}\middle| \frac{-4\tau p_u^2 N_r \Omega^2}{R_i^{2\nu}}\right]\right\} \quad (3.21)$$

Proof: see appendix A.4 □

3.2.4 High SNR Regime Characterisation

In order to get more insights into the implications of system and channel parameters on the effective capacity, we investigate the asymptotic effective capacity of uplink MU-MIMO systems in the high SIR regime, i.e., when $SIR \to \infty$.

Corollary 3.2.2. The high SIR asymptotic behaviour of the effective capacity for perfect CSI can be parametrised as

$$C_P^{\infty}(A, D_k, p_u, \Omega, m) = \log_2(\Omega\, p_u N_r) \\ - \frac{1}{A}\log_2\left\{\frac{\Gamma(m-A)}{\Gamma(m)}\frac{2(R_o^{2+A\nu}-R_i^{2+A\nu})}{(2+A\,\nu)(R_o^2-R_i^2)}\right\} \quad (3.22)$$

Proof: Keeping only the dominant term in eq.(3.14), the effective capacity goes asymptotically to the following expression,

$$C_P^{\infty}(A, D_k, p_u, \Omega, m) = \lim_{p_u\to\infty} -\frac{1}{A}\log_2\int_0^{\infty}(1+\beta_k p_u N_r)^{-A} f(x)dx \\ \approx -\frac{1}{A}\log_2\int_0^{\infty}(\beta_k p_u N_r)^{-A} f(x)dx \quad (3.23)$$

Taking into account user location effect, then we have

$$C_P^{\infty}(A, D_k, p_u, \Omega, m) = -\frac{1}{A}\log_2\left\{\frac{2}{(R_o^2 - R_i^2)} \times \int_{R_i}^{R_o}\int_0^{\infty} r \left(\frac{\Omega p_u N_r}{r_k^{\nu}}\right)^{-A} \frac{x^{m-1}}{\Gamma(m)\Omega} e^{-x/\Omega} dx\, dr\right\} \tag{3.24}$$

Next, with the aid of integral identity [46, eq.(3.351.3)], eq.(3.22) follows immediately. □

The statement in the next corollary is a consequence of Theorem 3.2.

Corollary 3.2.3. The high SIR asymptotic behaviour of the effective capacity for imperfect CSI is given by

$$C_{IP}^{\infty}(A, D_k, p_u, \Omega, m) = \log_2(\tau\Omega^2 p_u^2 N_r) - \frac{1}{A}\log_2\left\{\frac{\Gamma(m-2A)}{\Gamma(m)}\frac{2(R_o^{2+2A\nu} - R_i^{2+2A\nu})}{(2+2A\,\nu)(R_o^2 - R_i^2)}\right\} \tag{3.25}$$

Proof: One can pursue a similar analysis for the approximated effective capacity of perfect CSI case in corollary 3.2.2. □

3.3 Numerical Results

This section investigates the utility function of interest, i.e., the effective capacity in [bps/Hz] as a function of the number of the receive antenna, transmit power, shadowing parameter m and QoS exponent. Our simulation model is based on the uplink of a single cell with the following parameters, unless otherwise specified, the minimum or guard radius is $R_i = 0.1$ Km, the maximum or cell coverage radius' is $R_o = 1$ Km, system bandwidth is 1×10^6 Hz, block length is $T = 1 \times 10^{-3}$ sec, total number of symbols of data and pilots per block is 20 symbols and length of pilot symbols is $\tau = 3$. Gamma distribution is used for large scale fading channel with scale parameter $\Omega = 1/m$ to ensure unity mean value i.e. $\mathbb{E}\{\gamma\} = \Omega \cdot m = 1$. Path loss attenuation exponent is set to $\nu = 4.0$ unless otherwise specified in figure captions.

a) Impact of Transmit Power: Fig.3.2, demonstrates the effective capacity versus transmit power via Monte Carlo simulations, high SNR approximation eq.(3.22) and

Table 3.1: Numerical parameters used in the simulation.

PARAMETERS	VALUES
BS coverage radius R_o	1000 m
Number of users per resource block	$K = 3$ users
Long term fading (Shadowing)	Gamma distribution
User locations	Uniform distribution
Shadowing parameter	$m \in [0.5, 3.5]$
Path loss exponent	$\nu \in [3.3, 4.0]$
Channel bandwidth	1.0 MHz
Total Monte Carlo trials	10^5 system geometric realizations
OFDM frame duration	$T_{slot} = 1$ ms, LTE standard [7]
Pilot length	$\tau = K$ symbols
Pilot training overhead T_{ov}	$(T_{slot} - \tau\, T_{symbol}/T_{slot}) = 3/7$, [7]

analytical expression provided in eq.(3.17). The analysis is carried out for perfect CSI with fixed shadowing parameter m and different values of the QoS exponents θ_k. The outputs of a Monte Carlo is obtained through the generation of 10^4 gamma random realisations for the large scale fading matrix. The validation of the derived closed form expressions can be observed where the simulation results agree very well with the analytical results. Moreover, the high SNR approximations become sufficiently tight when SNR is high around 20 dB for $\theta_k = 10^{-5}$. As expected, the effective capacity increases with the delay constraint θ_k decreasing.

b) Impact of Queueing Constraints: Fig.3.3 and Fig.3.4 investigate, more deeply, the impact of delay QoS constraints on the effective capacity with fixed number of the receive antenna, fixed shadowing parameter and different values of transmitting power. Clearly, effective capacity approach Shannon capacity as θ_k goes toward zero,i.e., the case when no constraints are imposed by the application on the queueing delay, on the other hand, effective capacity is almost zero when θ_k approach infinity, i.e., the case of highly delay constraint. We observe that more stringent delay QoS requirements can be supported with higher transmit power. As expected, imperfect CSI decays the performance of the system while perfect CSI scenario experiences a superior capacity performance.

c) Impact of Adding more Receive Antenna: Fig.3.5, considers the implications of increasing the number of receive antenna on the effective capacity with fixed

transmit power p_u, fixed shadowing parameter m and different QoS exponent θ_k, i.e., different delay QoS constraints using (3.17) and (3.21). It is shown that the effective rate, logarithmically, improves with increasing N_r for both cases, perfect CSI (solid curves) and imperfect CSI (dashed curves) due to the large array-gain of the system. This fact indicates that large antenna arrays carry more data traffic. The relative difference between the curves gets steadily larger, see eq.(3.18).

d) Impact of Large-scale Shadowing: Fig.3.6 introduces the asymptotic performance provided by very large MIMO for different shadowing parameters. As expected, higher values of large-fading shape parameter $m > 2$, usually correspond to rural-scenario, tend to result in a higher effective capacity due to a weaker shadowing condition, while lower values of shape parameter $m < 2$, usually correspond to urban-scenario (heavy-shadowing), tend to result in a lower effective capacity for both perfect and imperfect CSI scenarios. Moreover, the effective_capacity decreases monotonically with the exponent θ_k increasing.

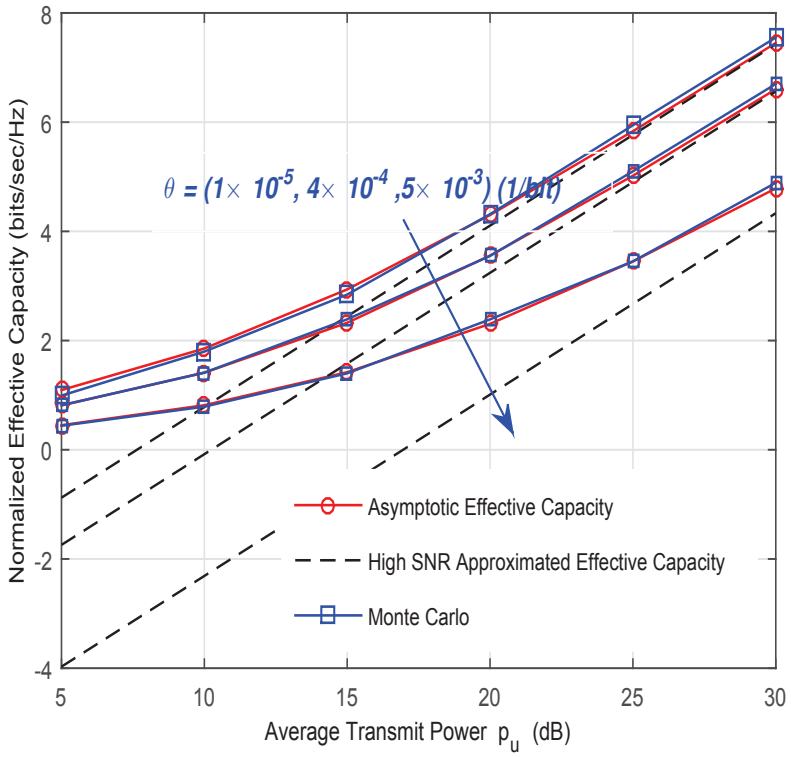

Figure 3.2: Monte Carlo Simulated, Analytical, and high-SNR approximated effective capacity with perfect CSI, different values of delay QoS constraints, antenna elements $Nr = 300$, path loss $\nu = 4.0$, and sadowing parameter $m = 3.5$.

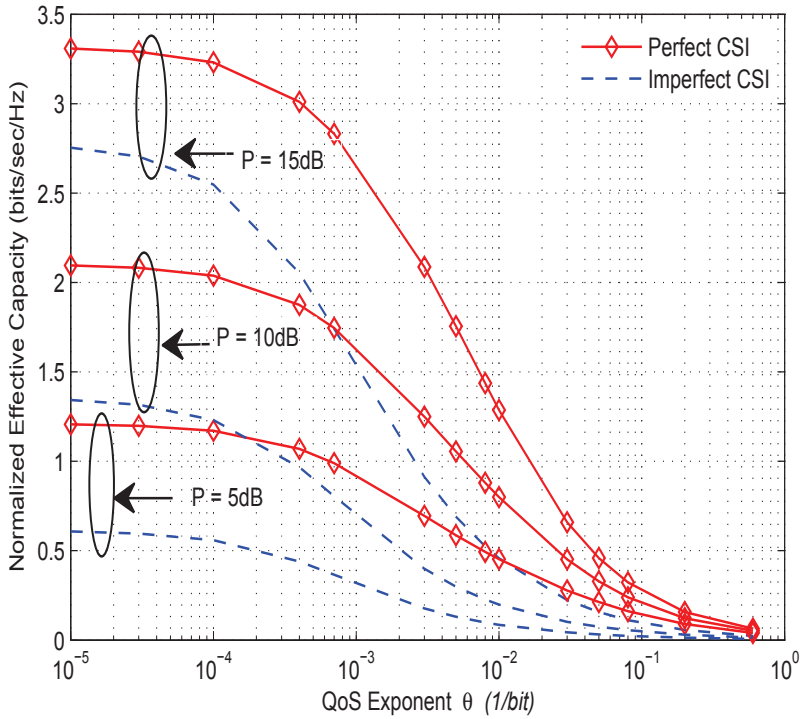

Figure 3.3: Effective Capacity performance for perfect/imperfect CSI with different values of transmit power, antenna elements $Nr = 128$, path loss $\nu = 3.3$, sadowing parameter $m = 2.5$, and pilots $\tau = 6$.

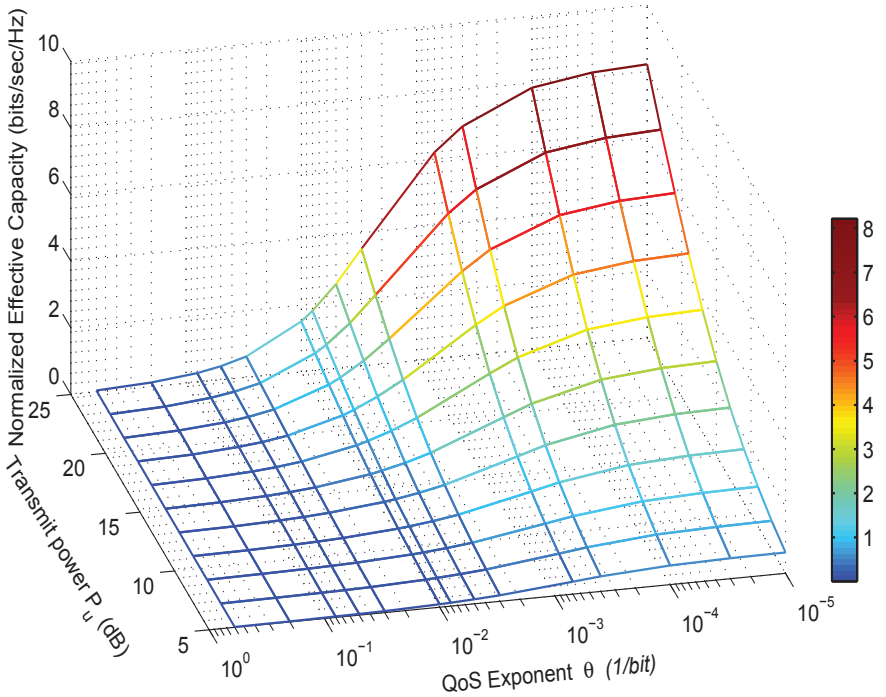

Figure 3.4: Effective Capacity performance for imperfect CSI, different values of transmit power, different values of delay QoS constraints, antenna elements $Nr = 128$, path loss $\nu = 3.3$, sadowing parameter $m = 2.5$, and pilots $\tau = 6$.

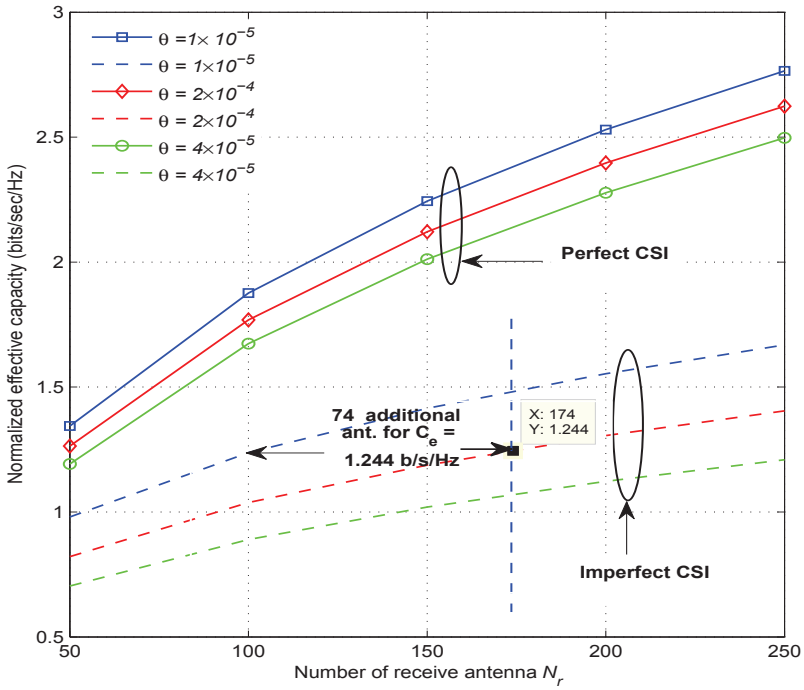

Figure 3.5: Normalized effective capacity with different QoS exponent θ i.e. different delay QoS constraints, path loss $\nu = 3.3$, transmit power $P = 10\,dB$, shadowing parameter $m = 2.5$, and pilots $\tau = 6$.

3.4 Conclusion

This chapter quantifies the implications of channel and system parameters (e.g. shadowing parameter m, the number of receive antennas N_r and delay constraints θ_k) on the effective capacity in uplink transmission of asymptotically large receive antennas system. Closed form analytical expressions are obtained for a single user. These expressions are subsequently used to get the average effective capacity over the entire cell users. Furthermore, closed form expressions for the high SNR regime for both perfect and imperfect channel information are derived.

The conclusions from the obtained results are twofold. First, the proposed approach is a valid analysis approximation and the tractable analytical results of effective capacity can eliminate the need for time intensive Monte Carlo simulations. Second, random shadowing degrades the QoS and stringent delay constraints can affect considerably the achieved effective capacity as θ_k gets larger. Importantly, user location impacts on the effective capacity can be extended to different channel models. Here, the study focuses on the uplink multiple access channel for simplicity. However, as future work, we aim to address these challenges in more general channel models like the interference channels in large-scale systems.

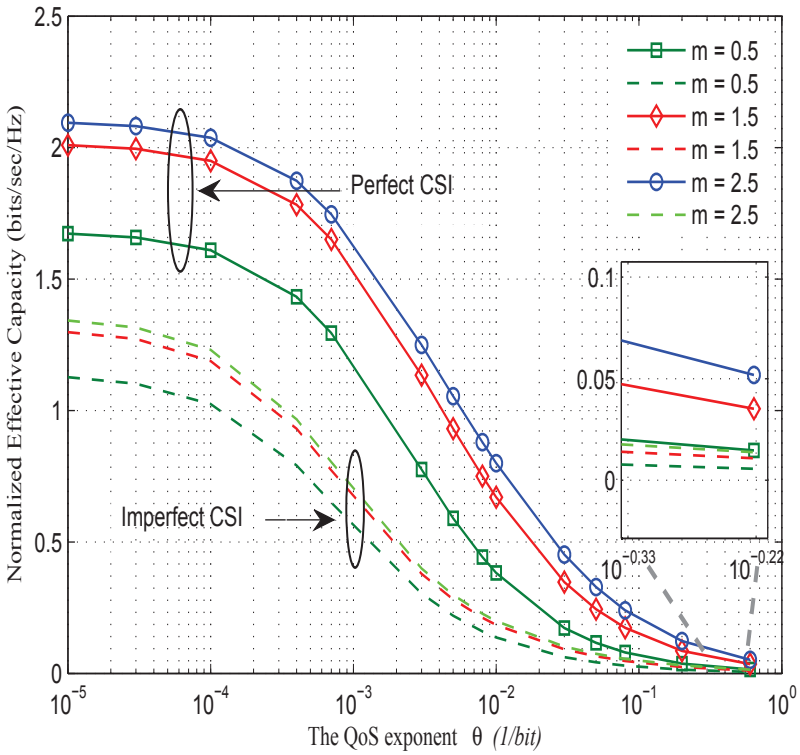

Figure 3.6: Normalized effective capacity with different values of shadowing shape parameter m, antenna elements $Nr = 128$, path loss $\nu = 3.3$, transmit power $P = 10\,dB$, and pilots $\tau = 6$.

Chapter 4

Average Error and Outage Probabilities in the Uplink of a Single Cell Massive MIMO

This chapter investigates the asymptotic behaviour (error and outage probabilities) of a single cell multiple-input multiple-output (MIMO) system aided by a large scale antenna array. Specifically, the uplink transmission over composite fading channel with a power scaling scheme is considered. Where most reported studies in this respect discuss the case of downlink scenario for convenience MIMO systems. Two assumptions are addressed: perfect channel information (CSI) and imperfect-CSI. In both cases, closed form expressions for error and outage probabilities in asymptotically large receive antenna environments are derived.

Moreover, users' location impact on the system performance is investigated for different channel information scenarios. Numerical outcomes, validated by Monte Carlo simulations, shed light on how different parameters and conditions can affect the aforementioned performance metrics. Numerical results, for some cases, indicate that bit error probability (BEP) decreases from about 10^{-3} to 10^{-5} when shadowing shape parameter increases from 2.5 to 4.5. Interestingly, increasing the number of receiving antennas by 200 elements (i.e., from 50 to 250) achieves approximately 87% (i.e., from 0.9 to 0.12) improvement in outage probability for rate threshold of $5\,bps/Hz$ and certain system parameters. Finally, these findings reveal that the performance improvements achieved by large scale antenna arrays over the convenience MIMO (non-massive MIMO with less than 64 antenna elements [29]) can be considered to tackle some channel and system impairments.

4.1 Introduction

Fading and shadowing are great challenges for reliable transmission in wireless environment [45]. In particular, the challenges are obvious for real time applications, over slow fading environment, when the desired transmission delay constraint is on the order of the channel coherent time. Two important metrics have been proposed in the literature to characterise system performance with different quality of service (QoS) and data rate limitations. These metrics are the average error and the outage probabilities. Where outage event occurs if instantaneous signal-to-noise-ratio (SNR) drops below the minimal desired threshold value.

The uplink error and outage analysis for MIMO channels have been addressed over multiple studies. The uplink of a multi cell multi user single-input multiple-output system (MU-SIMO) has been considered in [7]. In their work, authors derived exact analytical expressions for the symbol error rate, the uplink rate, and the outage probability per user for linear zero forcing receiver and perfect channel state information. In [53], authors investigated the uplink and downlink of multi cellular massive MIMO systems. Their adopted system model accounts for error in channel-estimation, pilot_contamination, antenna correlation and path-loss for each link. The work in [54], addresses the uplink of a multicell MU-SIMO system when the channel experiences small and large-scale fading. The detection is done by using linear ZF scheme and the base station has perfect CSI of all users in its own cell. L. Zhao *et al.* in [55], derived both the outage probability and bit error rate expressions corresponding to the degrees of freedom (the difference between the number of the user terminal and BS antennas) in downlink transmission of massive-MIMO.

Power scaling law for uplink massive MIMO systems with different rank channel has been considered in [15]. Delayed CSI due to user mobility has been addressed in [56], where authors considered an uplink model and each BS employs zero forcing decoder. The implications of channel aging on the performance of uplink massive MIMO systems have been investigated by the authors in [57]. In [58], the authors introduced tight closed form lower bounds for the rate performance of maximal ratio combining and zero forcing detectors over aged CSI. Recently, the authors in [59] introduced approximate closed-form formulas for the uplink outage probability of a user with maximal ratio combining (MRC) at the BS.

It is well known that the use of massive antenna arrays can significantly alleviate the effect of small scale fading (through micro diversity) and intra cell interference,

and consequently, increase the energy and spectral efficiencies of wireless systems [29]. Motivated by this fact, this chapter seeks to address the potential benefits of massive MIMO configuration on the uplink error and outage performance of wireless systems. Different from the existing studies, this work exploits the asymptotic results of random matrix theory introduced in [29] to further analysis the impacts of user location and shadowing parameter on the performance of large antenna system with different modulation schemes. Such analysis could play a key role in 5G systems designing, in particular, vulnerable to shadowing and path-loss, mm-Wave frequencies. The specific contributions of this chapter can be summarised as follows,

1) Closed form expressions are derived for the uplink's asymptotic error and outage probabilities when the BS deploys a large antenna array with power scaling policy (unique to the best of our knowledge). The results enable us to explicitly study the impacts of the shadowing parameter, number of BS receive antennas and the transmit power on the system performance.

2) The implications of channel and system parameters on the uplink performance are investigated via analytical analysis with numerical validation. The provided precise approximation results can replace the need for lengthy or time exhausting Monte Carlo simulations.

The remainder of the chapter is organised as follows, In Section 4.2, the system-model and problem-formulation are described. Afterwards, in section 4.4, closed form expressions for the asymptotic bit error and outage probability are derived as a function of several system parameters. Numerical results are presented in section 4.5. followed by Section 4.6 where the work is concluded.

4.2 System and Channel Model

The system under study considers the uplink of single cell scenario consisting of a massive antenna base station as shown in Fig.(4.1). Assuming that users are equipped with a single transmitting antenna, as previously stated, the output of the uplink channel can be given as [30] $y = \sqrt{p_u}Gx+n$, where $G \in \mathbb{C}^{N_r \times K}$ is the complex channel matrix between the base station and its associated user terminals. N_r is the number of receive antennas at the BS, p_u is the average power transmitted by each user, x denotes the data signal and $n \sim \mathcal{CN}(0,1)$ is the AWGN noise. For the generalized-K composite fading channel model, the fast fading component can be characterised by Nakagami-m distribution, while the large scale component can be characterised using Log-normal distribution [45]. For individual *user k*, the column vector of G will be [29], [30, eq. 2] $g_k = h_k\sqrt{\beta_k}$, given that h_k is the fast fading component of g_k and β_k is the large scale component which can be given as [15] $\beta_k = \mu_k\, D_k^{-\nu}$, where μ_k is the log-normal distributed shadowing, D_k is the distance between the BS and the *k-th* user and ν is the path loss exponent.*

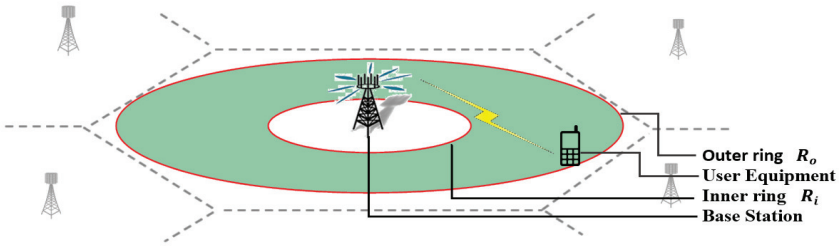

Figure 4.1: MU-MIMO system model, where users are assumed to be deployed uniformly within the area of shaded region and multiplexed via the zero forcing linear detector.

As previously mentioned in chapter 3, in large scale MIMO systems zero-forcing (ZF) linear detector tends to be sub-optimal and strikes a balance between system's complexity and performance [29]. Thus, in our work ZF is adopted and all results are derived based on this requisite. It is worth mentioning that in massive antenna environments, just small scale fading corresponding to micro diversity can be averaged out, while large scale fading corresponding to macro diversity environment stays active and affects system performance. As such, with ZF detector and perfect CSI, capitalising on the outcomes of [29], asymptotic power scaling data-rate of the

*The typical values of ν ranging from 2 to 6 in urban areas, however, in high density small coverage cells analysis (interference is dominated) it is required that $\nu > 2$ to ensure that the aggregate interference is finite [60].

k-th user can be written as [29, [eq. 21)], [34] $R_k^{asy}(\mu_k, D_k) \approx \log_2(1 + \beta_k p_u N_r)$. According to lemma (3.1), the upper bound on the uplink ergodic rate of k-th user follows from Jensen's inequality and can be expressed as follows

$$R_k^{asy}(\mu_k, D_k) \approx \log_2 \left[1 + \mathbb{E}\left\{ \frac{\mu_k \, p_u}{D_k^{\nu}} N_r \right\}\right] \qquad \texttt{bits/s/Hz} \tag{4.1}$$

where the expectation operation $\mathbb{E}\{\cdot\}$ is over two random variables, i.e., channel realisations and terminal locations. In our analysis, μ_k and D_k distributions are, respectively, Gamma, $\sim \Gamma(m, \Omega)$ and Uniform, $\sim \mathcal{U}(R_i, R_o)$ as shown on the next page. It's noteworthy that gamma distribution has shown a good fit to real channel measurements and also it is analytically more tractable than the log-normal distribution. The probability density function (PDF) of gamma distributed r.vs can be written as [29, eq.26], $f(x) = \frac{x^{m_k - 1} \, e^{-x/\Omega_k}}{\Gamma(m_k)\Omega_k^{m_k}}, \quad x, m_k, \Omega_k > 0$, where the parameters $0 \leq m_k$ and $0 \leq \Omega_k$ are the fading figure (or shape) and the average power (or scale) parameters of the gamma distribution, respectively. $\Gamma(\cdot)$ denotes the gamma function. The values of these parameters are affected by the communication environments and the expectation $\Omega_k = \mathbb{E}\{\gamma_k\}/m_k$, is usually chosen to be one. Moreover, we assume an independent and uniform distribution of users on disc formed by two rings R_i and R_o in the cell coverage area as shown in Fig.4.1. So, the corresponding PDF of the distance between users terminals and base station can be modelled as, [40], [55, eq.9], $f_d(x) = \frac{1}{(R_o^2 - R_i^2)} \, 2x$.

4.3 Error and Outage probability

In this section, first, a closed-form expression is derived for the error probability as a function of several important system parameters for a general k-th user. After this, the behaviour of user with a spatial averaging is addressed. Next a closed form expression for the outage probability is provided for both full and limited knowledge of the channel information.

4.3.1 Average error probability

A. Perfect CSI

For binary signals in AWGN environments, the bit error probability (BEP) of coherent, differentially coherent, and non-coherent detection is given by the generic

expression [45, eq.(8.100)]

$$\mathcal{P}_e(a,b,\gamma_k) = \frac{\Gamma(b,a\gamma_k)}{2\Gamma(b)} = \frac{1}{2}Q_b(0,\sqrt{2a\gamma_k}), \tag{4.2}$$

where the parameters a and b are given in Table 4.1 for different (orthogonal/non-orthogonal) modulation/ (coherent-non-coherent) detection combinations and the generalized Marcum-Q function $Q_b(\cdot,\cdot)$ is defined as [45, eq.(4.33)]

$$Q_b(q_1,q_2) = \int_{q_2}^{\infty} \frac{x^b}{a^{b-1}} \exp\left[-\frac{q_1^2+x^2}{2}\right] \mathrm{I}_{b-1}(q_1x)\,\mathrm{d}x \tag{4.3}$$

where $q_1 > 0$ and $q_2 \geq 0$, are real parameters and $\mathrm{I}_{b-1}(\cdot)$ is the *m-th* order modified-Bessel function of the first kind. The order-index b is an integer and typically $b \geq 0$. Employing scale law for the transmit power [29], then the approximated uplink SNR γ_k in eq.(4.1) for the k-th user at the receiver end (BS serving a finite number of users K) with perfect CSI will achieve the following

$$\gamma_k - \frac{p_u N_r}{D^\nu} \xrightarrow[N_r \to \infty]{a.s} 0 \tag{4.4}$$

where a.s. means almost sure convergence. Equation (4.2) can be written in term of lower incomplete gamma function using the identity [133, eq.(6.5.2)],
$\gamma(b,x) = \Gamma(b) - \Gamma(b,x)$. Consequently, the error probability is immediate, and can be given as

$$\mathcal{P}_e(\gamma_k) = \frac{1}{2}\left\{1 - \frac{\gamma(b,a\gamma_k)}{\Gamma(b)}\right\} \tag{4.5}$$

Table 4.1: Values of the parameters a and b for different combinations of Modulation/Detection schemes.

Modulation or Detection type	**Parameters values**	
	a	b
Orthogonal-coherent BFSK	1/2	1/2
Antipodal coherent BPSK	1	1/2
Differentially coherent DPSK	1	1
Orthogonal noncoherent BFSK	1/2	1

Proposition 4.1 (Perfect CSI)**.** In the regime of large N_r with linear ZF receiver, the asymptotic uplink average bit error probability of the k-th user under generalised-k channels, with full channel information, can be expressed in the following compact form

$$\mathcal{P}_{e_k}^{(P)}(D, N_r, p_u, m) = \frac{1}{2} - \frac{(ap_u N_r \Omega / D^{\nu})^b \Gamma(m+b)}{2\Gamma(b+1)\Gamma(m)} \; {}_2F_1\left[\begin{matrix} b, b+m \\ b+1 \end{matrix}\middle| -\frac{ap_u N_r \Omega}{D^{\nu}}\right], \tag{4.6}$$

where ${}_2F_1(\cdot)$ stands for qauss hyper geometric function [46, eq.(9.14.2)], ${}_pF_q\left[\begin{matrix} a_1, \cdots, a_p \\ b_1, \cdots, b_q \end{matrix}\middle| z\right] = \sum_{n=0}^{\infty} \frac{(a_1)_n, \cdots, (a_p)_n}{(b_1)_n, \cdots, (b_q)_n} \frac{z_n}{n!}$, given that, $(x)_n$ is the rising factorial or the Pochhammer polynomial, $(x)_n = \prod_{i=1}^{\infty}(x+i)$, p and q are non-negative integers.

Proof: A detailed proof is given in Appendix B.1 □

Remark 4.1. The asymptotic uplink average bit error probability can be expressed in term of the upper incomplete beta function, $\mathrm{B}_x(a,b) = \int_0^x t^{a-1}(1-t)^{b-1}dt$, which, in many cases, can be calculated more efficiently than the gauss hyper geometric function (using e.g., MATLAB® software). Then, with aid of the identity $\mathrm{B}_x(a,b) = \frac{x^a}{a} {}_2F_1(a, 1-b; a+1; x)$, eq.(4.6) can be rewritten as follows

$$\mathcal{P}_{e_k}^{(P)}(D, N_r, p_u, m) = \frac{1}{2} - \frac{(-1)^b \, b \, \Gamma(m+b)}{2\Gamma(b+1)\Gamma(m)} \; \mathrm{B}_{\frac{-ap_u N_r \Omega}{D^{\nu}}}(b, 1-b-m)\,, \tag{4.7}$$

Spatial Average Analysis Under Imperfect CSI

Next, error probability analysis derived in the previous proposition is pursued for more practical case where users are randomly located within cell area, and consequently experiencing a different path loss. The following theorem corresponds to this significant fact by using the aforementioned distance marginal distribution-function PDF to evaluate the average error probability over users of the entire cell area.

Theorem 4.1 (Perfect CSI Spatial Average)**.** *The asymptotic average error probability over all the users in the uplink of large N_r regimes for generalised-k channels is given by eq.(4.8)*

$$\mathcal{P}_{e}^{(P)}(D, N_r, p_u, m) = \frac{1}{2} - \frac{\Gamma(m+b)}{(2-b\nu)\Gamma(b+1)\Gamma(m)} \left\{ \frac{a^b R_o^2 (p_u N_r \Omega / R_o^{\nu})^b}{(R_o^2 - R_i^2)} \; {}_3F_2\left[\begin{matrix} b, b+m, b-\frac{2}{\nu} \\ b+1, b-\frac{2}{\nu}+1 \end{matrix}\middle| \frac{-p_u N_r \Omega}{R_o^{\nu}}\right] \right.$$

$$- \frac{a^b R_i^2 (p_u N_r \Omega / R_i^\nu)^b}{(R_o^2 - R_i^2)} \, {}_3F_2 \left[\begin{matrix} b, b+m, b-\frac{2}{\nu} \\ b+1, b-\frac{2}{\nu}+1 \end{matrix} \Big| - \frac{a p_u N_r \Omega}{R_i^\nu} \right] \Bigg\} \tag{4.8}$$

Proof: The proof of this theorem is shown in appendix B.2 □

B. Imperfect CSI

In realistic wireless systems, training pilots or sequences of limited length say e.g. τ symbols, usually used in acquiring CSI. Because of limited length of training pilots and the time varying characteristic of the fading channels, estimation errors are unavoidable and this effect is termed as channel information imperfection. Hence imperfect CSI performance is of a key point in real systems analysis. For simplicity, we assume no power control policy or equal power scale transmitting for all users [44], $p_u = E_u/\sqrt{M}$, where E_u is the total available power. In this case, invoking the law of large numbers, the large system asymptotic uplink rate can be written as [29, eq.37]

$$\begin{aligned} R^{asy} \approx \; & \frac{T-\tau}{T} \log_2(1+\tau\beta_k^2 E_u^2), \quad \texttt{for } N_r \longrightarrow \infty \texttt{ and } \tau \gg K \\ \approx \; & \log_2(1+\tau\beta_k^2 E_u^2), \qquad \texttt{for} \quad T \gg \tau \end{aligned} \tag{4.9}$$

where T is the total number of symbols in one time frame and K is the total number of users. Consequently, the approximated uplink SNR γ_k for the k-th user at the receiver end (BS) for imperfect CSI with the power scaling law [29], will satisfy the following

$$\gamma_k - \frac{\tau p_u^2 N_r}{D^{2\nu}} \xrightarrow[N_r \to \infty]{a.s} 0 \qquad \texttt{for fixed} \quad K \tag{4.10}$$

Proposition 4.2 (Imperfect CSI)**.** For large scale MIMO systems with linear ZF receiver, the asymptotic uplink average bit error probability of the k-th user under generalised-k channels with perfect CSI can be expressed by the following equation

$$\begin{aligned} & \mathcal{P}_{e_k}^{(IP)}(D, N_r, p_u, m) = \\ & \qquad \frac{1}{2} - \frac{(a\rho)^b \Gamma(b+\frac{m}{2}) \Gamma(b+\frac{(m+1)}{2})}{2^{2-m}\sqrt{\pi}\Gamma(b+1)\Gamma(m)} \; {}_3F_1 \left[\begin{matrix} b, b+\frac{m}{2}, b+\frac{m+1}{2} \\ b+1 \end{matrix} \Big| - a\rho \right] \end{aligned} \tag{4.11}$$

with $\rho = 4\tau p_u^2 N_r \Omega / D^{2\nu}$

Proof: A detailed proof is given in Appendix B.3 □

Spatial Average Analysis Under Imperfect CSI

Now, we pursue an error probability analysis, which is limited by the performance of the worst user, by taking into account the impacts of randomness of users' location as well as the imperfect CSI. To this end, we invoking the aforementioned user distance distribution function PDF once more in the following theorem.

Theorem 4.2 (Spatial Average)**.** *The average asymptotic error probability over all the users in the uplink of massive MIMO systems over generalised-k channels and an imperfect channel information is given by eq.(4.12)*

$$\mathcal{P}_e^{(IP)}(D, N_r, p_u, m) = \frac{1}{2} - \frac{\Gamma(b+\frac{m}{2})\Gamma(b+\frac{(m+1)}{2})}{2^{2-m}\sqrt{\pi}\Gamma(b+1)\Gamma(m)(b-1/\nu)} \times \left\{ \frac{a^b R_o^2 (4\tau p_u^2 N_r \Omega^2 / R_o^{2\nu})^b}{(R_o^2 - R_i^2)} \; {}_3F_2\left[\begin{matrix} b, b+\frac{m}{2}, b+\frac{m+1}{2}, b-\frac{1}{\nu} \\ b+1, b+1-\frac{1}{\nu} \end{matrix} \Big| -\frac{4a\tau p_u^2 N_r \Omega^2}{R_o^{2\nu}} \right] - \frac{a^b R_i^2 (4\tau p_u^2 N_r \Omega^2 / R_i^{2\nu})^b}{(R_o^2 - R_i^2)} \; {}_3F_2\left[\begin{matrix} b, b+\frac{m}{2}, b+\frac{m+1}{2}, b-\frac{1}{\nu} \\ b+1, b+1-\frac{1}{\nu} \end{matrix} \Big| -\frac{4a\tau p_u^2 N_r \Omega^2}{R_i^{2\nu}} \right] \right\} \tag{4.12}$$

Proof: Using the same methodology used in appendix B.2, the theorem can be easily proofed. □

Intuitively, error probability ($\mathcal{P}_e$) increases when it's averaged over entire cell area, due to the worst case corresponding to cell edge users.

4.3.2 Rate outage probability

The rate outage probability can be defined as the probability that the user rate R_k (as a random variable) drops under a particular rate threshold R_{th} which is the achievable or desired transmission data rate for the specific k-th user. Hence the outage probability is given by

$$\mathcal{P}_{out_k} \triangleq Pr\Big[R_k < R_{th}\Big] = Pr\Big[\gamma_k < (2^{R_{th}} - 1)\Big], \tag{4.13}$$

where the second line follows from Shannon capacity definition i.e. the tight upper bound on information rate of the channel.

Proposition 4.3 (Perfect CSI)**.** For large scale MIMO systems with linear ZF receiver, the asymptotic uplink rate outage probability of the k-th user under generalised-k channels with perfect CSI can be expressed in the following compact form

$$\mathcal{P}_{out_k}^{(P)}(D, N_r, p_u, m) = \frac{\left(D^{\nu}\left(2^{R_{th}}-1\right)/p_u N_r \Omega\right)^m}{m\,\Gamma(m)} \times {}_1F_1\left[\begin{matrix} m \\ m+1 \end{matrix}\middle| -\frac{D^{\nu}\left(2^{R_{th}}-1\right)}{p_u N_r \Omega}\right] \tag{4.14}$$

Proof: see appendix B.4 □

Next, we pursue an outage analysis for the case with limited knowledge of the CSI.

Proposition 4.4 (Imperfect CSI)**.** For large scale MIMO systems with linear ZF receiver, the asymptotic uplink rate outage probability of the k-th user under generalised-k channels with imperfect CSI can be expressed as follows

$$\mathcal{P}_{out_k}^{(IP)}(D, N_r, p_u, m) = \frac{\left(D^{2\nu}\left(2^{R_{th}}-1\right)/\tau p_u^2 N_r \Omega\right)^{(m+2)}}{(m+2)\,\Gamma(m+2)} \quad {}_1F_1\left[\begin{matrix} m+2 \\ m+3 \end{matrix}\middle| -\frac{D^{2\nu}\left(2^{R_{th}}-1\right)}{\tau p_u^2 N_r \Omega}\right] \tag{4.15}$$

Proof: see appendix B.5 □

4.4 Numerical results

In this section, we present simulated performance results, corresponding to the uplink of a single cell with a coverage area ranges between two rings of radii $R_i = 100$ m and $R_o = 1$ Km from the BS. In our simulation, power is normalised to the distance of R_i for all scenarios. Gamma distribution is used for large scale fading channel with a scale value of $\Omega = 1/m$. We used some specific parameters, e.g. the path loss exponent is set to $\nu = 2.0$ and the length of pilot symbols are set to $\tau = 4$ unless otherwise specified.

a) Impact of Transmit Power: In Fig.4.2, two popular modulation schemes, namely, Binary Phase Shift King (BPSK) and Binary deferential Phase Shift Keying (BDPSK) are considered. For both techniques, bit error probability versus transmitting power (via Monte Carlo simulations and analytical expression) are provided

using equations (4.20), (4.22) for a single user and spatial averaging, respectively. The analysis is carried out for perfect and imperfect CSI with a fixed shadowing parameter m. The outputs of the Monte Carlo is obtained through generation of 10^4 gamma random realizations for the large scale fading matrix. The validation of the derived closed form expressions can be observed where the simulation results agrees very well with the analytical results. As expected, the channel imperfection increases error probability compared to the case of the full channel knowledge. Also, the figure shows the impact of user location on the uplink bit error probability. It can be seen that a spatial averaging (red curves) causes in performance degradation compared to a single user at distance of $600m$ i.e., cell interior user (blue curves). Where the spatial averaging takes into account the worst-case i.e., cell-edge users.

b) Impact of Pilot Length: Fig.4.3, demonstrates the impact of the pilot length used in the channel estimation on the rate outage probability of a user located at distance of $R = 600m$ from the base station with two values of the channel shape parameter and two modulation schemes. It is seen that the performance gets better with a high shadowing parameter m as well as with the increasing number of symbols used for channel estimation τ.

c) Impact of Adding more Receiver Antenna: Fig.4.4, reveals the interesting implications of increasing the number of receive antenna on the error performance with a fixed and normalised transmit power p_u. In addition, the figure compares results for two shadowing parameter values m and two modulation techniques (dashed curves for BPSK and solid curves for BDPSK). Note that any increase in the number of antennas N_r tends to increase the performance logarithmically, for both cases, perfect and imperfect CSI. The relative difference between the curves gets steadily larger because of the squaring effect, see (eq. 4.9) and this can quantify the total information loss due to imperfect CSI.

d) Impact of large scale Fading: Fig.4.5, jointly compares the functionality among error probability, the shadowing shape parameter m and the size of the receive antenna array. Here, we recall that lower shadow fading parameter means more severity channel and this is why bit error performance gets worse as we move from suburban scenario ($m = 4.5$) into nearly urban scenario ($m = 2.5$).

e) Rate-Profile: Fig.4.6, considers the uplink outage performance. It is interesting to observe the effect of adding more receive antennas on rate CDF, where almost 87% outage advantage can be achieved for $R_{th} = 5$ bps/Hz as N_r is increased from 50 to 250 elements. Also, for perfect channel information and QoS constraint of 4 bps/Hz,

almost 50% of the users are satisfied with their service in case of $N_t = 50$, while more than 98% of the users are covered when the deployed antennas are $N_t = 250$ for the same rate constraint. Moreover, the figure depicts the impact of channel imperfection, especially at the high outage probability regime, on the achievable user data rate threshold.

f) Impact of User Distance: Finally, Fig.4.7, clearly shows the impact of user distance on the rate outage probability for different values of the shadowing parameter m and path loss exponent ν at a rate threshold of $R_{th} = 2.5$ bit/s/Hz. As expected, increasing ν causes curves divergence with distance increasing. On the other hand, decreasing m causes constant outage increasing for all user radii.

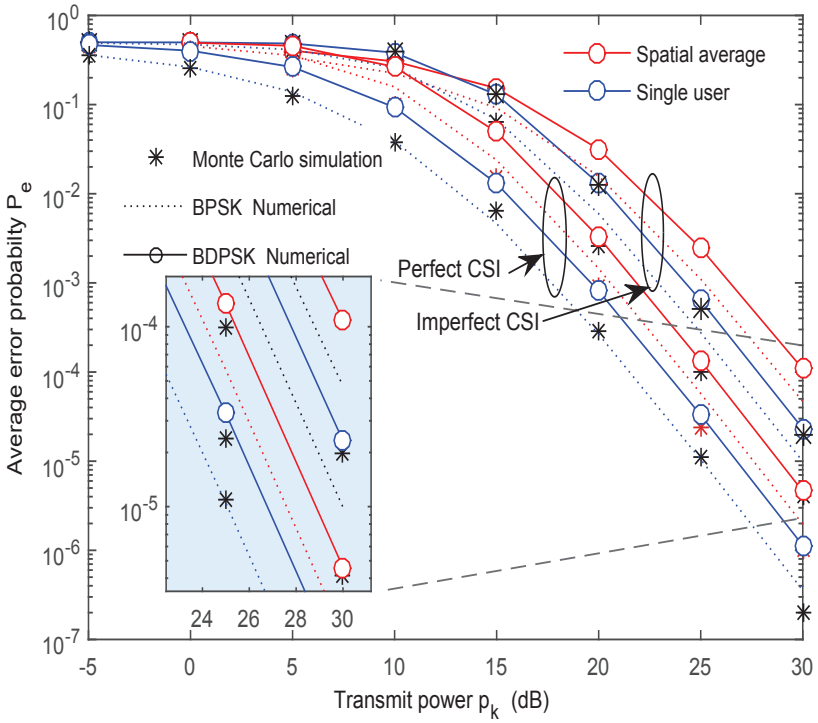

Figure 4.2: Average bit error probability for a single user located at $R_k = 600m$ compared with a spatial averaged user (entire cell) with perfect/imperfect CSI, different modulation, path loss $\nu = 3.3$, sadowing parameter $m = 3.0$, pilots $\tau = 4$, and antenna elements $N_r = 250$.

4.5 Conclusion

This chapter studies the asymptotic power-scaling performance (average error probability and rate outage) of the uplink transmission in large antennas regime. Specifically, closed-form formulas are derived for the aforementioned performance metrics when BS uses linear ZF detector. In addition, impact of user location on the average

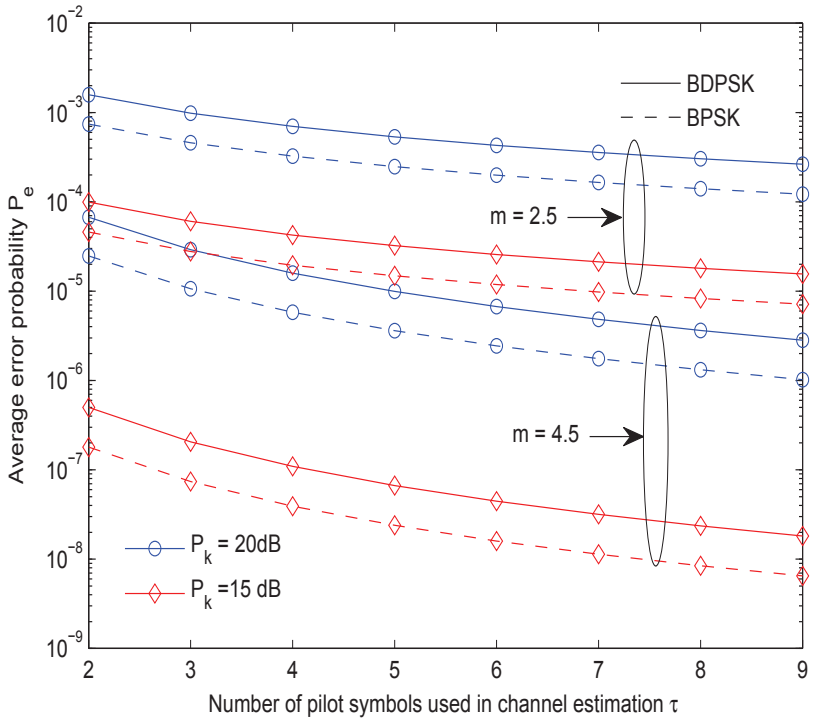

Figure 4.3: Average bit error probability for a single user-terminal located at $R_k = 600m$ versus the number of symbols used in training sequence of channel estimation for antenna elements $Nr = 150$, path loss $\nu = 2.0$, and shadowing parameter of $m = \{2.5, 4.5\}$.

error probability is characterised, where the derived formulas take into consideration the inevitable statistical-spatial-randomness of users distribution. The findings of this chapter point out that imperfect CSI degrades both the corresponding error probability and rate outage. However, results reveal that increasing the number of received antennas at the base station can significantly compensate for this deterioration and improve error and outage probabilities performance. For instance, increasing the number of BS-antennas by 200 elements gives about 87% improvement in outage_probability for rate threshold of 5 bps/Hz at certain system parameters.

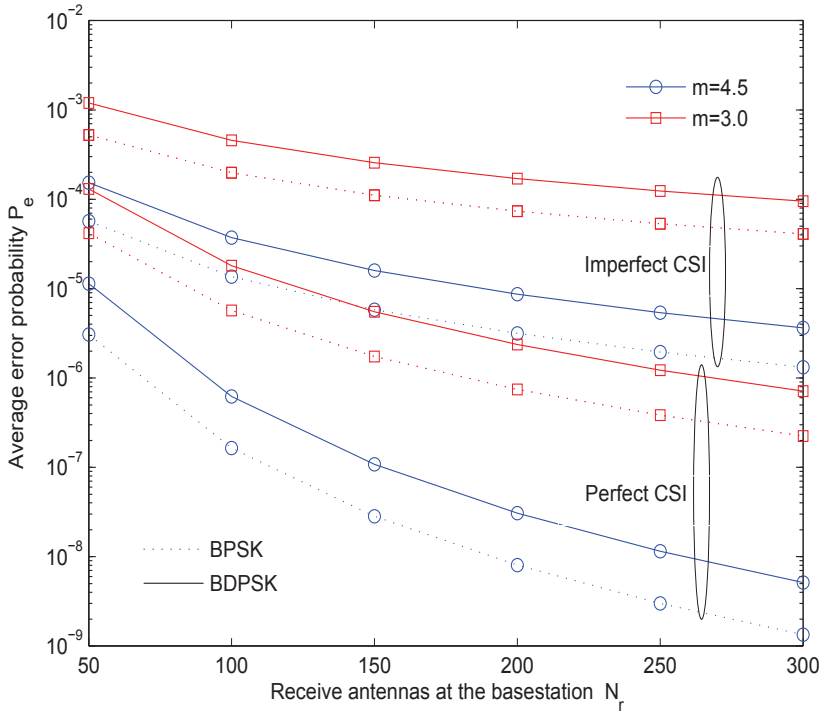

Figure 4.4: Average bit error rate performance for perfect/imperfect CSI with different values of channel parameter m and two modulation schemes for a single user located at $R_k = 600m$, $P = 15dB$, antenna elements $Nr = 128$, path loss $\nu = 2.0$, shadowing parameter $m = 2.5$, and pilots $\tau = 4$.

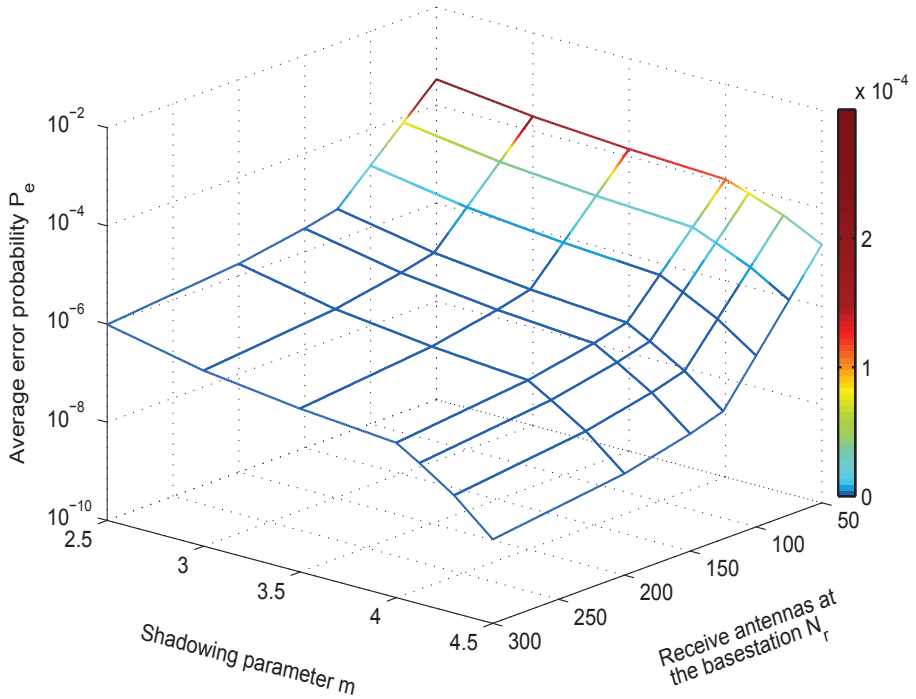

Figure 4.5: The functional comparison among average bit error rate performance, channel parameter m and number of receive antennas for perfect CSI, differentially coherent DPSK detection, user distance $R_k = 600m$, transmit power $P = 15dB$, path loss $\nu = 2.0$, detection scheme parameters $a = 1$, and $b = 1$.

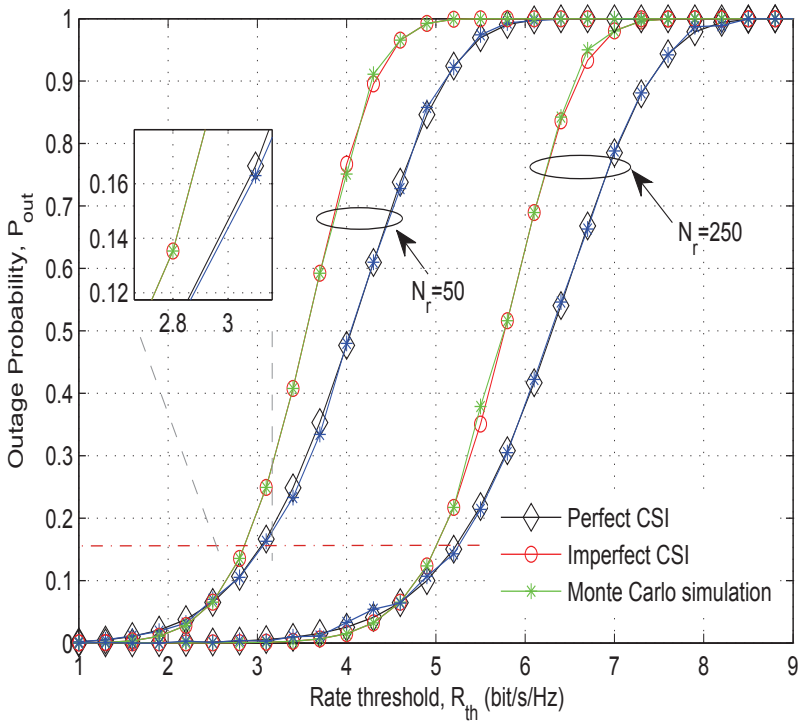

Figure 4.6: Monte Carlo Simulation and Analytical outage prbabilties for a single user located at $R_k = 600m$ from the base station with perfect/imperfect CSI, different number of base station antennas, transmit power $P = 15dB$, path loss $\nu = 2.5$, shadowing parameter $m = 2.5$, and pilots $\tau = 1$.

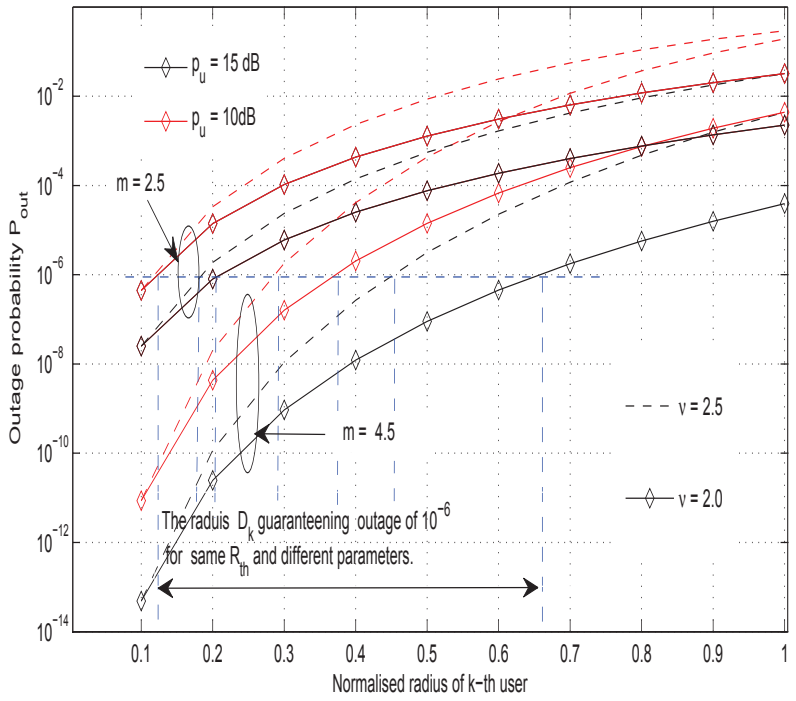

Figure 4.7: Outage prbabilties versus normalised user locatitions with perfect CSI, antenna elements $N_r = 250$, and rate threshold of $R_{th} = 2.5$ b/s/Hz.

Chapter 5

QoS-Constraints in the Uplink of Cellular Massive-MIMO

While large scale multiple input multiple output (MIMO) cellular system is a promising strategy to enhance energy and spectral efficiencies of the next generation wireless networks, pilot sequences reusing in adjacent cells causes inter cell interference due to pilot contamination. Therefore, this chapter investigates the statistical queueing constraints and pilot contamination phenomenon in random or irregular cellular massive MIMO system where base stations are Poisson distributed. Specifically, tractable analytical expressions are provided for the asymptotic SIR coverage, rate coverage and the effective capacity under quality of service (QoS) statistical exponent constraint in uplink transmission when each base station deploys a large number of antennas. Laplace transform of interference is derived with aid of mathematical tools from stochastic geometry. We show that the QoS constrained capacity is proportional to the path loss exponent and inversely proportional to the pilot reusing probability which in turn is a function of cell load.

Our simulation results prove that pilot reuse impairments can be alleviated by employing a cellular frequency reuse scheme. For example, with unity frequency reuse factor, we see that 40% of the total users have signal to interference ratio (SIR) above -10.5 dB, whereas, with frequency reuse factor of $\Omega = 7$, the same fraction of users has SIR above 20.5 dB. However, this can reduce the effective bandwidth of the overall system, e.g., for 15% level, the rate drop is almost $10Mbps$ due to using reuse factor of $\Omega = 7$.

5.1 Introduction

The large scale multi user MIMO technique is introduced as a promising technique for the fifth generation (5G) radio systems [61]. Where recent researches validate that BSs, deploy an order of magnitude more antennas than scheduled users, have great capability to enhance the spectral efficiency (SE) in cellular systems and consequently, meet the fast growth in wireless-traffic of various multimedia-applications [62]. It is worth noting that, feedback burden of channel state reporting can be avoided by exploiting the channel reciprocity in time division duplex (TDD) transmission mode [63]. Moreover, in order to minimise training overhead in channel estimation, massive MIMO system exploits the reuse of pilot sequences. However, the major challenge is the contamination of channel-estimate due to reusing the same pilots in nearby cells and this impairment is termed as pilot-contamination.

5.1.1 Related works

Quality of Service (QoS): Most of the emerging real time applications imposed stringent constraints on queue lengths or queuing delays of transmit buffer. The effective capacity quantifies the maximum arrival rate that can be achieved w.r.t a given service demands with a steady state flow of data at buffer input. In this concern, authors in [24] analysed the effective capacity in single antenna communication systems. In [25], the effective capacity of Gaussian block fading MIMO systems is investigated. Moreover, [26] examined in detail, high and low SNR asymptotic behaviour of MIMO and illustrated the relationship between the buffer queuing constraints and MIMO spatial dimensions over the entire range of SNR values. M. Ismail *et al.* in [27] investigated energy efficient uplink communications for heterogeneous wireless medium. In [28] the effective throughput of MIMO systems is investigated over both independent identically distributed and independent non-identically distributed $\kappa - \mu$ fading channels under the quality of service (QoS) delay constraints.

Pilot contamination: In the planning and performance evaluation of a wireless network, one of the crucial aspects is the statistics of the co-channel interference. Many studies have been conducted to address the impact of pilot contamination on statistical distribution of signal to interference ratio (SIR) in forward and reverse radio links. The authors in [64], studied the impact of pilot contamination on the asymptotic distribution of SIR. M. Debbah et al, in [53], characterized the minimum mean squared error (MMSE) channel estimation in wireless systems. Thomas

L. Marzetta, in [7] considered regular hexagonal cell topology and uniformly distributed users. He addressed the performance limitations of the non-cooperative cellular multi user MIMO system due to the phenomenon of pilot contamination. Furthermore, he demonstrated that in massive regimes, the effects of uncorrelated noise and fast fading vanish, spectral efficiency(SE) is independent of bandwidth and the desired per bit transmitted energy vanishes. Inter cellular interference (ICI), is the only remaining impairment due to reuse of the pilot sequences in other cells which is known as pilot contamination and does not vanish with large number of BS antennas.

W. Heath et al, in [65], analyzed the performance of massive MIMO cellular networks with random topology. They provided analytical expressions for rate and the asymptotic coverage probability for downlink and uplink transmissions when BSs have Poisson distributions. They proved that, though bounded by pilot contamination, large scale MIMO systems can provide significantly higher performance than the systems with single antenna. In reference [66], the authors investigated the uplink of a multi cell multi user single input multiple output (MU-SIMO) system with zero forcing detection technique and perfect channel information(CSI). They derived user outage probability in exact analytical form. Moreover, they demonstrated that, while maintaining a required quality of service in massive antenna arrays, user transmit-power can be made proportional to the reciprocal of the number of BS-antennas.

The authors in [67], focused on the uplink of multi cell massive MIMO systems with linear detection. They proposed a novel pilot allocation scheme to mitigate the effect of Pilot contamination known as fractional pilot reuse (FPR) scheme. The key-idea is to improve cell spectral efficiency, where cell center users in neighbouring cells are allowed to reuse the same pilot sequences. Yuehao Zhou et al, in [68], considered the uplink of massive MIMO systems with dual-antenna users. Where closed form expressions have been derived for the achievable sum rate of several transmission schemes with power scaling law.

In [69], the authors examined different pilot reuse factors and different interference scenarios in large antenna regimes. P. Herath et al, in [70], employed stochastic geometry tools to derive an expression for the coverage probability of uplink mode in a massive-MIMO cellular network over path-loss and log-normal shadowing.

5.1.2 Contributions

Uplink SIR analysis is of primary concern compared to the downlink analysis, since signals in the downlink scenario all come from the centre of the cells, whereas in uplink scenario signals may come from the boundaries of the cells [71]. Moreover, due to the irregular deployment of modern networks, and with non-orthogonal pilots, uplink interference from other users (UEs) can be stronger than the useful signal at the serving base station although highest SIR is depended in users schedule. Motivated by these reasons, and the fact that Pilot-contamination is the main limiting factor in large antenna regimes [29], we seek in this chapter to address these challenges as well as the statistical queueing constraints in uplink massive-MIMO wireless systems and investigate some key metrics such as SIR outage, rate-outage and effective capacity. Unlike the regular topology considered in prior work [7], we examine irregular topology of cellular massive MIMO which is known to be closer to the practical demand-based deployment of BSs [72]. Moreover, different from [65], we consider the QoS constraints and the effective capacity performance which offers a suitable metric to assess the implications that physical layer design may have on link layer performance. Such cross layer analysis could play a key role in 5G systems designing. The specific contributions of this work can be summarised as follows,

1) We characterise the uplink's asymptotic SIR coverage probability, rate coverage and effective capacity of a large antenna-array regime when the BSs are deployed according to poison point process (PPP) distribution. Crucial expressions are obtained (closed form or analytical formula) in the sense of benchmarking the performance of a randomly selected user (typical user)in the cellular network.

2) We evaluate the implications of channel and system parameters on the uplink performance via numerical analysis with remarkable comments. The provided precise approximation results can replace the need for lengthy Monte Carlo simulations in designing of large scale MIMO systems.

5.1.3 Notations and Paper Organization

The notation $\mathbb{E}_x\{\cdot\}$ represents the expectation operator over the random variable x, $\mathbb{P}\{X\}$ stands for the probability of event X [73], $\Gamma(x)$ denotes the gamma function $\int_0^\infty t^{x-1}e^{-t}dt$ [43], $\mathscr{L}_x(s)$ is Laplace transform (L.T) of x at specific value s, $f_x(\cdot)$ is

probability density function of random variable x PDF, CCDF is the complementary cumulative distribution function, $\|\cdot\|$ is the Euclidean-norm. The remainder of the chapter is structured as follows, Section 5.2 discusses the assumptions and provides system model. Afterwards, section 5.3 formulates the signal-to-interference ratio (SIR) model, presents the definition of the performance metrics, and presents some related aspects. Section 5.4 shows our numerical results. Finally, section 5.5 concludes the work.

5.2 Assumptions and System Model

We consider the uplink of a non-cooperative cellular multi-user massive-MIMO system. In our mathematical-formulation, we leverage the following assumptions,

1) Time division-duplex (TDD) protocol is assumed with channel reciprocity. Where the BSs exploit the UL orthogonal-pilot-sequences to estimate the DL-channel of the served UEs.

2) For the BSs layout or deployment model, we assume homogeneous Poisson Point Process (PPP) Φ_b of density λ_b on the plane which provides further tractability from stochastic geometry tools (homogeneity of Φ_b, imposes symmetric traits and a constant BS density λ_b over all the plane $\mathbb{R}^2$). Hence, Cell boundaries will form a Voronoi-tessellation* as shown in Fig.5.1 which depicts a sample of user deployment snapshot in the cellular network. Each BS is equipped with M antennas and randomly allocated (with equal probability) one of Ω different frequency bands.

3) The number of, one antenna, UEs associated with a BS follow a homogeneous PPP Φ_u with an intensity of λ_u. The UEs' locations are assumed to follow uniform distribution in a disc of radius R_o and uncorrelated with the distribution of other cells users.

*Consequently, concentric-circles around the BSs will no longer describe the constant SIR contours and the geographical interpretation of users classification (interior or edge users) may defers from cell to another. Thus, performance analysis corresponds to spatial PPP model provides lower-bound compared to the deterministic models that reflect upper-bound of system performance. Consult [74] for further details.

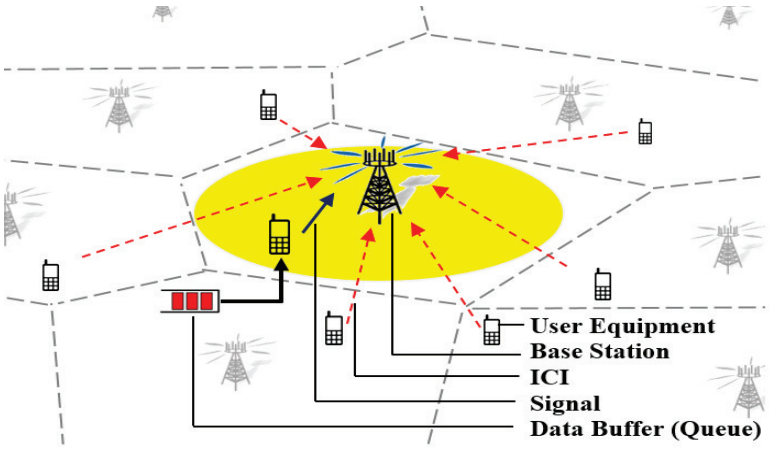

Figure 5.1: Illustration of a PPP model for the BS-locations and the corresponding Voronoi tessellation cell boundaries. Dashed lines are the ICI for case of unity frequency reuse factor(FRF), when all BSs use the same frequency bands with full load assumption i.e., there is at least one user in each cell share the same pilot sequence with the typical user.

5.2.1 Estimating Uplink-Channel

For acquiring channel state information (CSI), we consider pilot based channel estimation in which all the users send pre-assigned training sequences (from orthonormal pilot set $\{\Phi_p\}_{p=1}^{P}$) each of length τ to their BSs as shown in Fig.5.2. The pilot set is assumed to be reused among all cells. Leveraging channel estimates, BSs apply a maximum ratio combining (MRC) to recover received uplink data. The received pilot signals at the serving base station ($\mathrm{BS_b}$) can be written as

$$\mathbf{Y}_b = \sqrt{p_u}\sum_{l=1}^{\infty}\sum_{p=1}^{P}\alpha_{bl}\mathbf{G}_{blp}\mathbf{S}_l^H\chi_{lp} + \mathbf{n}_b \tag{5.1}$$

where, M is the number of BS antennas, b is the typical or serving BS index, l is the cell index, p is the pilot index, p_u is signal to noise ratio (SNR) of the pilot, $\mathbf{G}_{blp} = h_{blp}\sqrt{\beta_{blp}/r_{blp}^{\nu}}$, $\mathbf{G}_{blp} \in \mathbb{C}^{M\times 1}$ is the channel vector from interfering user ($\mathrm{UE_{lp}}$) to $\mathrm{BS_b}$ $h_{blp} \in \mathbb{C}^{M\times 1}$ models the small scale fading vector with i.i.d. zero mean and unit-variance entries, r_{blp} denotes the distance between $\mathrm{UE_{lp}}$ and $\mathrm{BS_b}$, ν is the path-loss-exponent, $\beta_{blp} \sim LogNormal(0, \sigma_{dB}^2)$ is the long term shadow fading coefficients, $\mathbf{S}_l$ is the pilot symbol transmitted by $\mathrm{UE_{lp}}$, the superscript H denotes conjugate-transpose and $\mathbf{n}_b \sim \mathcal{CN}(0,1)$ denotes the AWGN-noise received at $\mathrm{BS_b}$'s antennas. The factor α_{bl} accounts for the frequency reuse probability between the typical and interfering BSs

$$\alpha_{bl} = \begin{cases} 1 & \text{if } \mathrm{BS_b} \text{ and } \mathrm{BS_l} \text{ employ the same frequency band.} \\ 0 & \text{Otherwise .} \end{cases} \tag{5.2}$$

The factor χ_{lp} in 5.1 accounts for pilot reuse probability by a particular interfering $\mathrm{BS_l}$,

$$\chi_{lp} = \begin{cases} 1 & \text{if } \mathrm{BS_l} \text{ uses the p-th pilot sequence.} \\ 0 & \text{Otherwise .} \end{cases} \tag{5.3}$$

According to the received signal (5.1), $\mathrm{BS_b}$ estimates the channel gain of the terminal transmitting the p-th pilot sequence as follows

$$\begin{aligned} \hat{\mathbf{G}}_{bbp} =& \frac{1}{\sqrt{p_u}} \mathbf{Y}_b \mathbf{S}_b \\ \overset{(a)}{=}& \mathbf{G}_{bbp} \mathbf{S}_b^H \mathbf{S}_b + \sum_{l=1}^{\infty} \sum_{p=1}^{P} \alpha_{bl} \mathbf{G}_{blp} \mathbf{S}_b^H \mathbf{S}_b \chi_{lp} + \frac{\mathbf{n}_b \mathbf{S}_b}{\sqrt{p_u}} \\ \overset{(b)}{=}& \mathbf{G}_{bbp} + \sum_{l=1}^{\infty} \sum_{p=1}^{P} \alpha_{bl} \mathbf{G}_{blp} \chi_{lp} + \frac{\mathbf{n}_b \mathbf{S}_b}{\sqrt{p_u}}, \end{aligned} \tag{5.4}$$

where $\mathbf{G}_{bbp}$ is the required or desired channel, (a) follows by substituting for $\mathbf{Y}_b$ from (5.1), (b) follows due to employing orthogonal pilot sequences. The second term in (b) is the contamination due to pilot reusing by the users associated with other cells* and the last term represents the background noise.

5.2.2 Reverse link Signal

The estimation phase is followed by uplink data transmission phase, where all the UEs transmit useful data_symbols to their BSs. The reverse-link baseband signal at $\mathrm{BS_b}$ can be expressed as

$$\mathbf{y}_b = \sqrt{p_b} \sum_{l=1}^{\infty} \sum_{p=1}^{P} \alpha_{bl} \mathbf{G}_{blp} \mathbf{u}_l^H \chi_{lp} + \mathbf{n}_b', \tag{5.5}$$

where, p_b is the signal SNR, $\mathbf{u}_l$ represents uplink data symbols of cell-l and $\mathbf{n}_b' \sim \mathcal{CN}(0, 1)$ denotes the AWGN-noise. Uplink data can be recovered by left multiplying the received signal (5.5) by the conjugate transpose of the channel-estimate (5.4) of

*Kindly note that since the same set of pilot sequences are reused among all the BSs, so index subscript can be dropped from the symbol $\mathbf{S}_b$.

the required terminal, i.e., passing through MRC-detector yields

$$\begin{aligned}\hat{\mathbf{u}}_{lb} &= \lim_{M\to\infty} \frac{\hat{\mathbf{G}}_{bbp}^{H}\,\mathbf{y}_b}{M\sqrt{p_b}} \\ &\overset{(a)}{=} \lim_{M\to\infty} \frac{1}{M\sqrt{p_b}} \left[\mathbf{G}_{bbp} + \sum_{l=1}^{\infty}\sum_{p=1}^{P} \alpha_{bl}\mathbf{G}_{blp}\chi_{lp} + \frac{\mathbf{n}_b\mathbf{S}_b}{\sqrt{p_u}}\right]^H \\ &\qquad \cdot \left[\sqrt{p_b}\sum_{m=1}^{\infty}\sum_{n=1}^{P}\alpha_{bl}\mathbf{G}_{bmn}\mathbf{u}_l^H\chi_{mn} + \mathbf{n}_b'\right], \end{aligned} \tag{5.6}$$

where (a) follows due to substituting for $\hat{\mathbf{G}}_{bbp}$ and $\mathbf{y}_b$, from (5.4) and (5.5) respectively. Now, we can simplify the expression in (5.6), leveraging the fact that entries of $\mathbf{n}_b$ and h_{blp} are i.i.d. random variables with zero-mean and unit-variance. Hence, exploiting the strong law of large-numbers (SLLN), only the products of identical-quantities in (5.6) remain significant, e.g see [7], [65], [75]. So, for identical-quantities we have

$$\begin{aligned}\lim_{M\to\infty} \frac{\mathbf{G}_{blp}^H\,\mathbf{G}_{bmn}}{M\sqrt{p_u}} &= \frac{(\beta_{blp}\beta_{bmn})^{1/2}}{(r_{blp}r_{bmn})^{\nu/2}} \lim_{M\to\infty} \frac{h_{blp}^H\,h_{bmn}}{M\sqrt{p_u}} \\ &= \frac{\alpha_{bl}\,\beta_{blp}}{r_{blp}^{\nu}}\,\delta(lm), \end{aligned} \tag{5.7}$$

where $\delta(x)$ is the Dirac-delta function. On the other hand, for non-identical-quantities we have*

$$\begin{aligned}\lim_{M\to\infty} \frac{\mathbf{n}_b^H\,h_{bmn}}{M\sqrt{p_u}} &= \lim_{M\to\infty} \frac{\mathbf{n}_b^H\,\mathbf{n}_b'}{M\sqrt{p_u}} \\ &= \lim_{M\to\infty} \frac{h_{blp}^H\,\mathbf{n}_b'}{M\sqrt{p_u}} = 0 \end{aligned} \tag{5.8}$$

Using (5.7) and (5.8), we can express (5.6) as

$$\hat{\mathbf{u}}_{bp} = \frac{\beta_{bbp}}{r_{bbp}^{\nu}}\,\mathbf{u}_{bp} + \sum_{\substack{l=1\\ l\neq b}}^{\infty}\sum_{p=1}^{P} \frac{\alpha_{bl}\,\beta_{blp}\,\chi_{lp}}{r_{blp}^{\nu}}\,\mathbf{u}_{lp} \tag{5.9}$$

The simplified expression in (5.9) compared with (5.6) reveals the typical and appealing traits of massive-MIMO systems.

*Thermal noise in most urban wireless networks is negligible compared to the background interference from the adjacent base stations and such networks are termed as interference limited networks. The corresponding uplink performance metric is the signal to interference ratio (SIR) at the required BS, which defined as the ratio of the received *signal-power* from the serving UE to the *aggregated powers* from all interfering UEs.

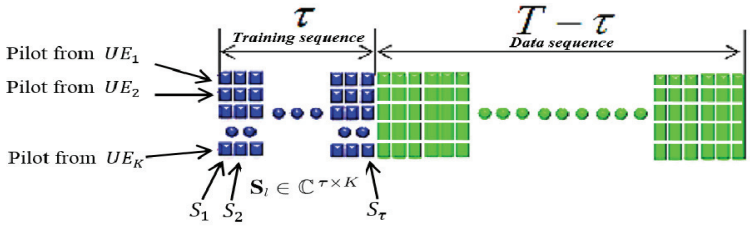

Figure 5.2: Uplink Training sequence allocation, each user assigned a specific pilot, each pilot sequence is a τ length normalised-vector, orthogonal to all sequences within the same cell. T represents the number of symbols or duration over which the channel is constant.

5.3 Asymptotic interference distribution

The significant step in analysing the performance of the system is to characterise the interference statistical distribution. With no loss of generality, and since we have a homogeneous PPP, the typical $\mathrm{BS_b}$ in consideration is assumed to be at the origin of the plane, i.e., the centre of $\mathbb{R}^2$ [76] as shown in Fig.5.3. UEs are uniformly distributed in each cell and the locations of all the interfering users sharing the same pilot sequence are assumed to form an independent poison point process on the two-dimensional Euclidean space $\mathbb{R}^2$.

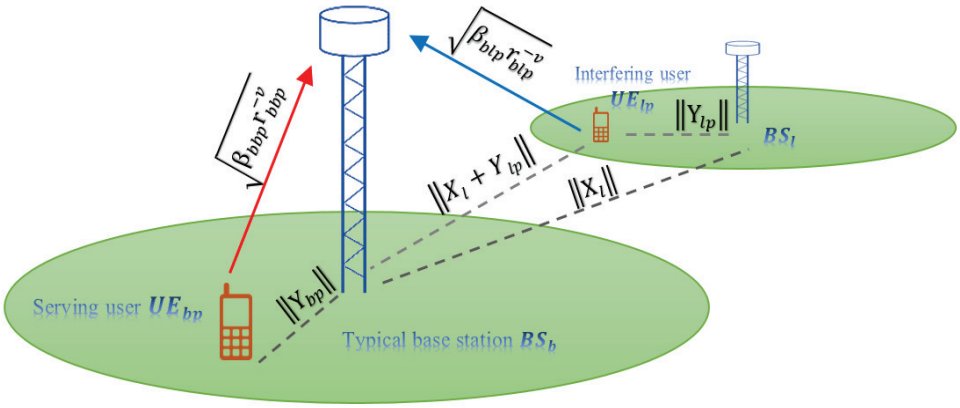

Figure 5.3: System parameters of the adopted reverse link model. Where $Y_{lp} \in \mathbb{R}^2$ are the cartesian coordinates location of the interfering user UE_{lp} w.r.t its basestation BS_{lp}, $X_l \in \mathbb{R}^2$ are the cartesian coordinates location of basestation BS_{lp} w.r.t BS_{bp}, r_{lbp} is the polar coordinates representation of the distance $\|X_l + Y_{lp}\|$.

Assuming that all BSs perform channel information acquiring at the same instant*(almost the worst scenario), then Laplace transform (L.T) of the interference

*It's worthwhile to remark that the pilot decontamination can be performed using a time shift of the training phase in adjacent cells, see, e.g., [77] or [75, and references therein] for more details about the mechanism.

contributions of all the users employ p$^{\text{th}}$ pilot sequence into BS$_{\text{b}}$ can be obtained as follows.

Lemma 5.1. (Interference Characteristic); Invoking the basic formula of L.T [76], the uplink interference at the typical BS can be characterised as follows

$$\begin{aligned}
\mathscr{L}_{I_{bp}}(s) &= \mathbb{E}_{I_{bp}}\{e^{-sI_{bp}}\} \\
&\overset{(a)}{=} \mathbb{E}_{\beta_{blp},r_{blp}}\left\{ \exp\left[-s \sum_{l\in\mathcal{B}\setminus\{b\}} \frac{\alpha_{bl}\,\beta_{blp}^2\,\chi_{lp}}{r_{blp}^{2\nu}}\right]\right\} \\
&\overset{(b)}{=} \mathbb{E}_{\beta_{blp},r_{blp}}\left\{ \prod_{l\in\mathcal{B}\setminus\{b\}} \exp\left[-s \frac{\alpha_{bl}\,\beta_{blp}^2\,\chi_{lp}}{r_{blp}^{2\nu}}\right]\right\} \\
&\overset{(c)}{=} \exp\left[\frac{-2\pi\lambda_b\,\bar{\chi}}{\Omega}\,\mathbb{E}_{\beta_{blp}}\left\{\int_{r\in\mathbb{R}^+} r\left(1-e^{-s\,\beta_{blp}^2 r^{-2\nu}}\right)dr\right\}\right] \\
&\overset{(d)}{=} \exp\left[\frac{-\pi\lambda_b\,\mathbb{E}\{\chi_{lp}\}\;s^{\frac{1}{\nu}}}{\Omega}\right. \\
&\qquad\qquad \left.\times\;\mathbb{E}\left\{\beta_{blp}^{\frac{2}{\nu}}\right\}\int_{x\in\mathbb{R}^+}\underbrace{\left(e^{-x^{-\nu}}-1\right)dx}_{I_1}\right]
\end{aligned} \tag{5.10}$$

where, (a) is obtained by substituting for I_{bp} which is the inter cell interference ICI, i.e., the sum of powers from all interfering users of other cells except cell-b (orthogonal pilot sequences assumption implies no intra-cell interference), $\alpha_{bl} \in \{0,1\}$ is a Bernoulli random variable with mean $1/\Omega$, i.e., $\alpha_{bl} \sim$ *Bernoulli*$(\frac{1}{\Omega})$ [78]. Which implies that α_{bl} takes a value of one if the serving BS$_{\text{b}}$ and interfering BS$_{\text{l}}$ share the specified frequency sub-band* and $\mathcal{B}$ is the set of all the cells in the cellular system. (b) follows since exponential of a sum is a product of exponential. (c) follows from probability generating functional of the Poisson point process (PGFL) [76], given that $\mathbb{E}\{\prod_{x\in\Phi} v(x)\} = \exp\Big[-\lambda_b \int_{\mathbb{R}^2}\Big(1-v(x)\Big)dx\Big]$, converting into polar coordinates gives $\mathbb{E}\{\prod_{x\in\Phi} v(x)\} = \exp\Big[-2\pi\lambda_b \int_{\mathbb{R}^+}\Big(1-v(r)\Big)dr\Big]$ and then averaging out the Bernoulli r.v. α_{bl}, where each cell is randomly-allocated one of the Ω sub-bands (frequency reuse factor), hence the interference is thinned with a reuse-factor of Ω. Finally, (d) is obtained by setting $x = s^{-1/\nu}\beta_b^{-2/\nu}\,r^2$, evaluating the expectation over β_{blp}, assuming $\{\beta_i\}_{i=0}^{\infty}$ is a set of i.i.d. unit mean exponential random variables with moment of $\mathbb{E}[\beta_{blp}^{2/\nu}] < \infty$ [80], and the expectation over the random variable, χ_{lp} can

*It's noteworthy that incorporating frequency-reuse to the model introduces correlation among the BSs using the same sub_bands, however, authors in [74] claim that employing frequency reuse is equivalent to employing independent-thinning to the entire set of interfering base stations.

be performed using the same approach used in [81]

Remark 5.1. (Pilot Reuse Probability): The expectation over the probability of pilot reusing χ_{lp} can be obtained as follows

$$\mathbb{E}\{\chi_{lp}\} = \frac{\mathbb{E}_{k \geq P}[k]}{P}\,\mathbb{P}\{k < P\} + \mathbb{P}\{k \geq P\} \tag{5.11}$$

where, k is the number of active users associated with base station BS_l. The first term accounts for the case when $\{k < P\}$ hence, there exists a probability that the interfering base station BS_l doesn't use the kth pilot-sequence. The second term stands for the case when $\{k \geq P\}$, i.e., all the available pilot sequences will be used by the interfering base station. It's worthwhile to note that k is a r.v. associated with the size-distribution of Voronoi cell corresponding to BS_l which has no known accurate distributions. However, the distribution has been approximated in [82] using gamma distribution $\sim \Gamma(m, \mu)$ with pdf of $f(x) = \frac{1}{\mu^m\,(m-1)!}\,x^{m-1}\,e^{-x/\mu}$, where m, μ are, respectively, the shape and scale parameters. Accordingly, (5.11) can be re-written as follows

$$\mathbb{E}\{\chi_{lp}\} = \sum_{k=1}^{P-1} \frac{1}{P}\,\frac{(\lambda_u \pi R_o^2)^k}{(k-1)!}\,e^{-\lambda_u \pi R_o^2} + \sum_{k=P}^{\infty} \frac{(\lambda_u \pi R_o^2)^k}{(k)!}\,e^{-\lambda_u \pi R_o^2} \tag{5.12}$$

Next, we evaluate the integration I_1 in (5.10-d) with the help of the following identities, $\{\,\Gamma(1+z) = z\,\Gamma(z)\}$, $\{\Gamma(1-z) = 1/\Gamma(1+z)\,\mathrm{sinc}(\pi z)\}$ and $\{\int_0^\infty x^{\nu-1}(1 - e^{-\mu x^p})\,\mathrm{dx} = -\frac{1}{|p|}\,\mu^{-\nu/p}\,\Gamma(\frac{\nu}{p})\}$ (eq. 3.478) [46], which results in

$$I_1 = \int_{\mathbb{R}^+} \left(e^{-x^{-\nu}} - 1\right) dx = \frac{1}{\Gamma(1+\frac{1}{\nu})\,\mathrm{sinc}(\frac{\pi}{\nu})} \quad , \tag{5.13}$$

plugging again into (5.10-d) yields

$$\mathscr{L}_{I_{bp}}(s) = \exp\left[-\frac{\pi\,\lambda_b\,\mathbb{E}[\beta_{blp}^{2/\nu}]\,\bar{\chi}\,s^{1/\nu}}{\Omega\,\Gamma(1+\frac{1}{\nu})\,\mathrm{sinc}(\frac{\pi}{\nu})}\right] \tag{5.14}$$

where, $\bar{\chi} = \mathbb{E}\{\chi_{lp}\}$ is the 1^{st} moment or mean of the r.v χ which can be set to one if we consider a scenario of interfering UEs with a full buffer such that all the interferers are always active. In our approach of interference analysis, arbitrary distribution for large scale shadowing β_{blp} can be handled as long as $\mathbb{E}[\beta_{blp}^{2/\nu}] < \infty$, in the same manner as [83], [72].

Remark 5.2. (Displacement Theorem [83]): According to the displacement Theorem, for some constant ν, the propagation effects (shadow fading in this case) can be represented as independent random transformation of a given homogeneous-PPP (Φ) of density λ, where the resulting point-process is also a PPP (thinned-PPP Φ_e) with equivalent density $\lambda_e = \lambda\,\mathbb{E}[\beta^{2/\nu}]$.

The common assumption for the distribution of shadowing is the log-normal one, in which $\beta_{blp} = 10^{X_{blp}/10}$, given that $X_{blp} \sim \mathcal{N}(\mu_{blp}, \sigma^2_{blp})$ and $\mu_{blp}, \sigma^2_{blp}$ are, respectively, the "mean" and "standard deviation" of the large scale channel gain. In this case, the $2/\nu^{th}$ moment can be found, employing the moment-generating function (MGF) of Gaussian distribution, which is [83] $\mathbb{E}[\beta^{2/\nu}_{blp}] = \exp[\frac{\ln(10)}{5}\frac{\mu_{blp}}{\nu} + \frac{1}{2}(\frac{\ln(10)}{5}\frac{\sigma_{blp}}{\nu})^2]$ and it is finite for $\{\mu_{blp}, \sigma_{blp}\} < \infty$. For exponential-distribution approximation, $\beta^2_{blp} \sim \exp(\mu_{blp})$ we have from table I in [72], $\mathbb{E}[\beta^{2/\nu}_{blp}] = \mu^{-2/\nu}_{blp}\,\Gamma(\frac{2}{\nu}+1)$ and $\Gamma(\frac{2}{\nu}+1)$ is the $2/\nu^{th}$ moment of unit-mean exponential random variables. Plugging in (5.14) we obtain L.T of the interference for exponential approximation shadowing as an immediate consequence of applying independent-thinning on Φ_b (Remark 5.2), and yields

$$\mathscr{L}_{I_{bp}}(s) = \exp\left[-\frac{\pi\,\lambda_b\,\bar{\chi}\,s^{1/\nu}}{\Omega\,\mathrm{sinc}(\frac{\pi}{\nu})}\right] \tag{5.15}$$

This expression can be used for further system analysis in the next section.

5.4 Performance metrics

In this section, we are going to derive the mathematical expression for some key metrics that characterised system performance.

5.4.1 Probability of coverage

This subsection considers the link reliability or the coverage probability of uplink massive MIMO systems. This metric is a significant performance metric to analyse since it can have a big effect on the quality of service of cell edge user and hence can give an overall picture of the system capacity when incorporated into resource efficiency. According to [83], the probability of coverage can be thought as being the average area or the average fraction of users in coverage. It can also be formally defined as the complementary cumulative distribution function (CCDF) of SIR, i.e.,

the probability that the uplink $\mathrm{SIR}_{\mathrm{b}}^{\mathrm{UL}}$ at the tagged base station BS_{b} is greater than the threshold (or target) $\mathrm{SIR}_{\mathrm{th}}^{\mathrm{UL}}$, $\mathbb{P}\Big\{SIR_b^{UL} > SIR_{th}^{UL}\Big\}$.

Theorem 5.1 (Coverage Probability)**.** *For massive antenna BS's with a homogeneous ppp distribution of density λ_b and unit mean exponential shadowing, the tail probability of uplink SIR of a typical user UE for SIR threshold of T_1 can be mathematically expressed as*

$$\mathbf{P}_{cov}(T_1, \lambda_b, \nu) = \frac{1}{C_1(T_1, \lambda_b, \nu)\, R_o^2}\left[1 - \exp(-C_1(T_1, \lambda_b, \nu)\, R_o^2)\right], \tag{5.16}$$

with

$$C_1(T_1, \lambda, \nu) = \frac{\pi\, \lambda_b\, \bar{\chi}\, T_1^{1/\nu}}{\Omega\, \mathrm{sinc}(\frac{\pi}{\nu})}, \tag{5.17}$$

and T_1 is the target or level that the SIR must exceed in order to establish a connection. *Proof*: see appendix C.1 □

5.4.2 Rate coverage probability

Rate coverage ($\mathrm{R}_{\mathrm{cov}}$) for a typical user UE can be defined as the probability that the data rate of this user is larger than a predefined threshold value (lowest rate) required for a given application. This metric is useful for applications with QoS constraint requirements, e.g., video services. It completely characterizes the rate distribution since it represents the complementary cumulative distribution function of the rate (e.g., see [83] and the references therein).

Theorem 5.2 (Rate Coverage Probability)**.** *For massive antenna BS's with a homogeneous ppp distribution of density λ_b and unit mean exponential shadowing, the tail probability of the uplink-rate of a typical user, UE for rate threshold of T_2 can be given by the following expression*

$$R_{cov}^{UL}(T_2, \lambda_b, \nu) = \frac{1}{C_2(T_2, \lambda_b, \nu)\, R_o^2}\left[1 - \exp\left(-C_2(T_2, \lambda_b, \nu)\, R_o^2\right)\right] \tag{5.18}$$

with

$$C_2(T_2, \lambda_b, \nu) = \frac{\pi\, \lambda_b\, \bar{\chi}\, (e^{\frac{\ln(2)\, \Omega\, T_2}{\vartheta\, B}} - 1)^{1/\nu}}{\Omega\, \mathrm{sinc}(\frac{\pi}{\nu})}, \tag{5.19}$$

and the factor ϑ stands for the pilot and cyclic prefix (CP) overheads [7].

Proof: see appendix C.2. □

5.4.3 Effective Capacity

It is easy to notice that the well known Shannon's capacity formula for wireless transmission, cannot account for the quality of service demands. So, a significant figure of merit, namely, effective capacity is introduced to incorporate statistical delay QoS into capacity formula of wireless applications [23]. In this regard, as previously mentioned, a new parameter θ, relates to the asymptotic decay rate of the buffer-occupancy is introduced, $\theta = -\lim_{x\to\infty} \frac{\ln(Pr\{L>x\}}{x}$, with L is the queue length at a steady-state flow of the transmitter buffer, x is the delay bound, and Φ is determined by the arrival state and service processes [42]. According to this equation, θ_k quantities the equilibrium state delay violation probability of the k-th user. It should be noted that a smaller θ indicates a looser QoS constraint whereas a larger θ imposes a more stringent constraints. And here we recall the effective capacity formula given by eq.(3.11) $C_{eff}(\theta) = -\lim_{n\to\infty} \frac{1}{nT\theta B} \log_2 \mathbb{E}_R\Big\{e^{-T\theta B \sum_{i=1}^{n} R[i]}\Big\}$, where T is frame duration and $R_k[i]$ is the information rate for the ith time slot. With no loss of generality, we assume that the fading process over wireless channels is independent of each other and holds invariant within a block length T and the service process is uncorrelated stochastic process (independent and identically distributed). Therefore, C_{eff} can be simplified to [23], [24] $C_{eff}(\theta) = -\frac{1}{T\theta B} \log_2 \mathbb{E}_R\{e^{-T\theta BR}\}$, with B is system bandwidth and the expectation is taken w.r.t the random variable R_k. Obviously, the effective capacity coincides with the traditional Shannon's ergodic capacity in case there is no delay constraint i.e. $\theta \to 0$. Analytically, with the assumption of steady state of the buffer input (stationary and ergodic process), and after substituting for rate R from Shannon's formula, the effective capacity normalised by the bandwidth will be as follows, $C_{eff}^{UL}(t, \lambda_b, \nu, \theta) = -\frac{1}{A} \log_2 \mathbb{E}\Big\{(1 + SIR)^{-A}\Big\}$, with $A \triangleq \frac{\theta TB}{\Omega \ln(2)}$ and the expectation is taken over the distribution of SIR.

Theorem 5.3 (Effective Capacity)**.** *For massive antenna BS's with a homogeneous ppp distribution of density λ_b and unit mean exponential shadowing, the asymptotic uplink effective capacity of a typical user UE for a threshold of t and QoS exponent*

θ, can be found as

$$C_{eff}^{UL}(t, \lambda_b, \nu, \theta) = -\frac{1}{A} \log_2 \left[1 - \sum_{i=1}^{N} \omega_i \, V(x_i) \right] + \mathcal{O}_N, \tag{5.20}$$

where, $V(x_i)$ is the coverage probability (5.16) replacing T_1 by $\left(t^{-1/A} - 1\right)$, the factor N is an integer, represents the number of terms used in the approximation and determines the accuracy of integration. ω_i, x_i are respectively, the weights and abscissas which are determined by Hermite polynomial according to the selected value of N. A simple MATLAB® code can be used to compute the weights and abscissas or by a specific using lookup table (LUT) [51]. The symbol $\mathcal{O}_N$ is a remainder term, which decreases to zero as terms number N increases.

Proof: see appendix C.3 □

5.5 Numerical Results and Discussion

This section presents the details of numerical validation for the derived analytical results of section (5.4) and gives insights into how the various parameters impact the distribution of the performance metrics in the cellular system. Theoretical results ,using the proposed analytical framework, and simulation results are respectively depicted by solid/markers and dashed/markers lines. Table-5.1 summarises the specific parameters used in the simulations unless otherwise specified.

a) Impact of Ω *on SIR Profile:* First, Fig.5.4-(a) compares the log-normal Monte Carlo simulated uplink coverage (Flowchart of simulation platform in fig 5.11 indicates the steps used in the simulation study) with the corresponding exponential-analytical formula given in (5.16) under various frequency reuse factor Ω. We can see that the analytical results almost matches the simulation ones, particularly at large threshold SIR. Average interferer distance in the wireless cellular system increases as Ω increases, this helps establish an intuition of why a higher frequency reuse factor has a better SIR tail probability than lower ones. For instance, we see that 40% of the users have SIR above -10.5 dB with unity frequency reuse factor, whereas the same fraction of users has SIR above 20.5 dB with frequency reuse factor of $\Omega = 7$. The SIR gain drops when we consider lower or higher SIR users but is again significant. It is noteworthy that low percentile levels are for cell-edge users

while high percentile levels are for cell center users.

b) Impact of Cell Load: Fig.5.4-(b) analyses different scenarios based on cells load. It is noticeable that the complementary cumulative distributions of the uplink SIR degrade in the case of fully loaded cells when each BS serving its maximum capacity of users, $\bar{\chi} = 1$ for $K = P$ (high contamination scenario). This is consistent with simple intuition, since increasing the number of served users K means increasing in the pilot reuse probability between the typical and interfering BSs according to the formula in (5.11). Consequently, this will decrease the average interferer distance, i.e., increases aggregated interference power. In contrast, best coverage performance is for $\bar{\chi} = 0.25$ (low contamination scenario). On the other hand, the marginal-gain in coverage performance increases with decreasing in cell load.

c) Pilot-reusing Probability: Fig.5.5 considers the impact of pilot number P used in channel training phase on the probability of reusing the same sequence between the serving and interfering BSs for different cell coverage radius R_o. The figure shows that for fixed user density λ_u, the probability of pilot reusing is relatively large for less number of pilot sequences or larger cell coverage radius, e.g., when $P = 8$ pilots, coverage radius extension from 0.5 km to 1.0 km leads to nearly 50% increment in pilot-reuse probability $\bar{\chi}$.

d) Impact of Ω on Rate Profile: The effect of Ω on the uplink rate coverage is investigated in Fig.5.6-(a). Unlike the SIR tail probability, here the story is different, where the average achievable rate doesn't definitely increase with Ω increasing. Table 5.2 gives some insight into the rate profile and the implications of reuse factor. In the high reliability regime*, when the rate outage probability goes to zero, the rate coverage gains increase with Ω increasing. In contrast, in the high spectral efficiency regime, when the rate threshold goes to infinity, increasing Ω will decrease the rate coverage gains. Although, larger Ω means less average interference power, but also it means smaller cell effective bandwidth, hence, for $R_{th} > 7$ Mbps increasing Ω has a negative effect on the rate performance, e.g., we see that, for 15% level the rate drop is roughly 10 Mbps due to using reuse factor of 7.

e) Impact of $\bar{\chi}$ on Rate Profile: Fig.5.6-(b), depicts the effect of the pilot reuse probability on the rate tail probability, which is nearly the same effect as for the

*It is noteworthy that the high reliability regime refers to the limit where the typical UE is, almost surely, covered.

Table 5.1: Numerical parameters used in the simulation.

PARAMETERS	SETTING
BS coverage-radius R_o	1,500 m
Cellular area radius R	40 Km
Density of BSs λ_b	$1/\pi\, R_o^2$
Frequency reuse factors Ω	1, 3 and 7
Path-loss-exponent ν	4.0
Large scale shadowing β_{blp}	$\sim$ Log-normal(μ, σ^2) for simulation
	$\sim$ exp(1) for analytical analysis
Log-normal shadowing μ, σ_{dB}^2	0, 7 dB respectively
Channel bandwidth	20 MHz
Monte Carlo trials	10^5 system realizations.
OFDM symbol duration T_s	$500/7 \approx 71.4$ us, LTE standard [7]
Pilot training overhead T_{ov}	$(T_{slot} - \tau\, T_s)/T_{slot} = 3/7$, [7].
Useful symbol duration T_u	$1/\Delta_f = 1/15$ kHz$\approx$ 66.7 us, LTE standard [7]

SIR coverage performance. As an example, for the 20^{th} percentile users, the rate performance drops by almost 75% for pilot reuse probability of $\bar{\chi} = 1.0$ as compared to the $\bar{\chi} = 0.25$ scenario. Similar to the SIR coverage performance, the marginal gain in average rate increases with decreasing in cell load. The impact of path loss exponent (PLE), ν is investigated in more detail in Fig.5.7 for SIR and rate coverages. As ν decreases, the UEs farther away from the typical BS have a greater contribution to the aggregated interference power at the BS, and this leads to a less uplink SIR and consequently a smaller SIR and rate-tail probability.

f) Effective Capacity: Fig.5.8-(a) simulates the normalised effective capacity w.r.t different pilot reuse probability, as expected, C_{eff} decreases with $\bar{\chi}$ increasing. Fig.5.8-(b), according to the analysis of *Theorem 3*, compares the effective capacities for various path-loss-exponent ν, where a better C_{eff} performance is for larger values of ν for the same reasons mentioned before. Moreover, fig.5.9 demonstrates the functional-relationship among uplink normalised effective capacity C_{eff}^{UL}, path-loss exponent ν and the QoS exponent θ.

g) Shannon Capacity: Finally, the comparison of the effective capacity with Shannon capacity, $\theta \longrightarrow 0$ is illustrated in Fig.5.10 for various PLE values. As expected, for all cases, the effective capacity decreases monotonically with the in-

crease of the QoS statistical exponent θ (more stringent delay QoS requirements), while the curves tend to flatten and saturate to the Shannon capacity C_{SH} when θ becomes small enough.

Table 5.2: Rate-profile for different frequency reuse factor Ω

$\mathbf{Rate_{threshold}}$ (b/s/Hz)	$\mathbf{Rate_{cov}}$ %	
	$\mathbf{\Omega = 1}$	$\mathbf{\Omega = 7}$
30.0	11.41	00.22
1.00	61.91	88.39
0.01	76.11	93.47

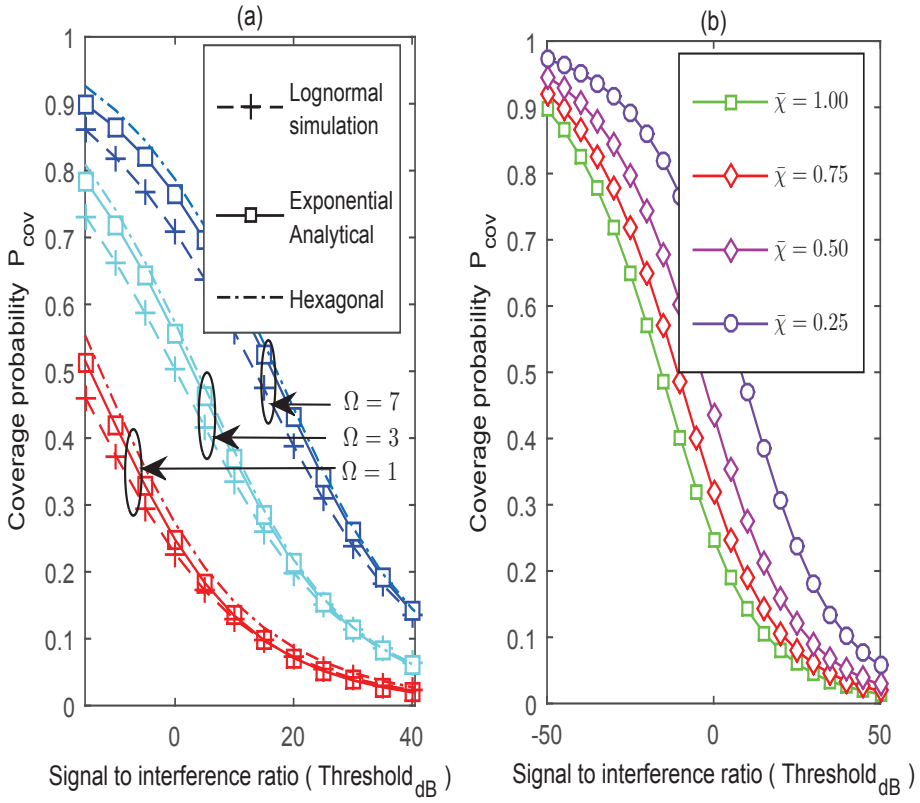

Figure 5.4: Uplink Coverage performance of a typical UE for, (a) Different frequency band reuse factor. (b) Different pilot reuse probability. For the sake of benchmarking, this figure also shows the performance of traditional hexagonal BSs topology [7], which can be cosidered as a system performance upper bound.

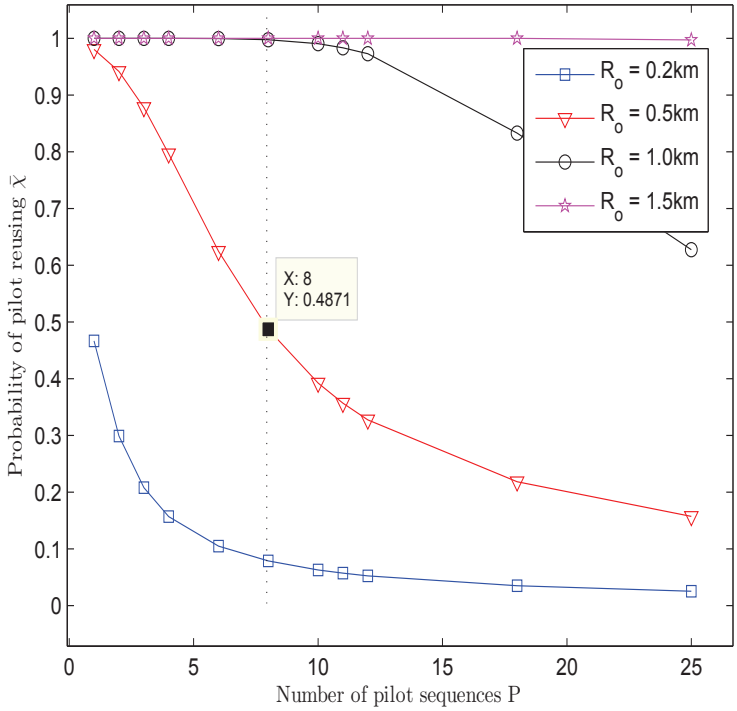

Figure 5.5: Pilot reuse probability versus the number of available pilot sequences P for user density λ_u of $5/km^2$ and various cell coverage radius R_o.

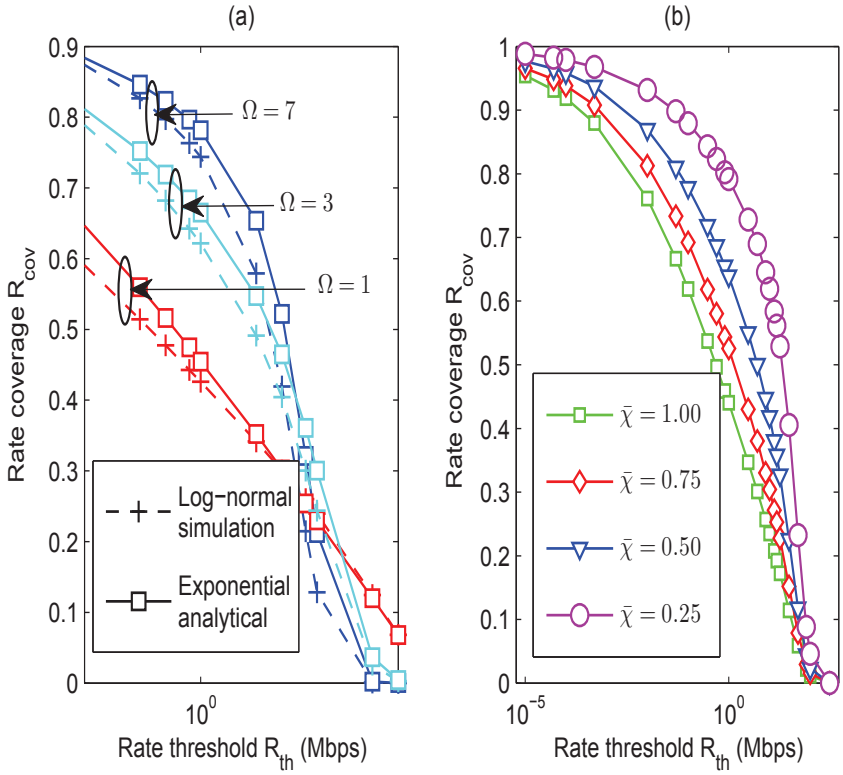

Figure 5.6: Uplink Rate coverage performance of a typical UE with, (a) Different frequency band reuse factor. (b) Different pilot reuse probability.

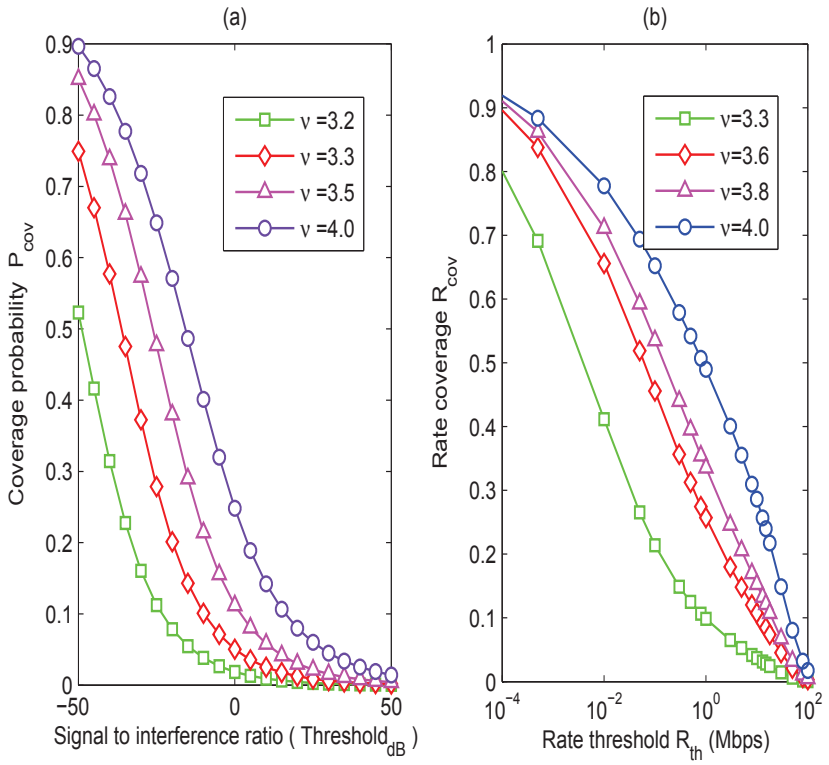

Figure 5.7: Path loss exponent impact, (a) Uplink Coverage probability. (b) Uplink Rate coverage probability.

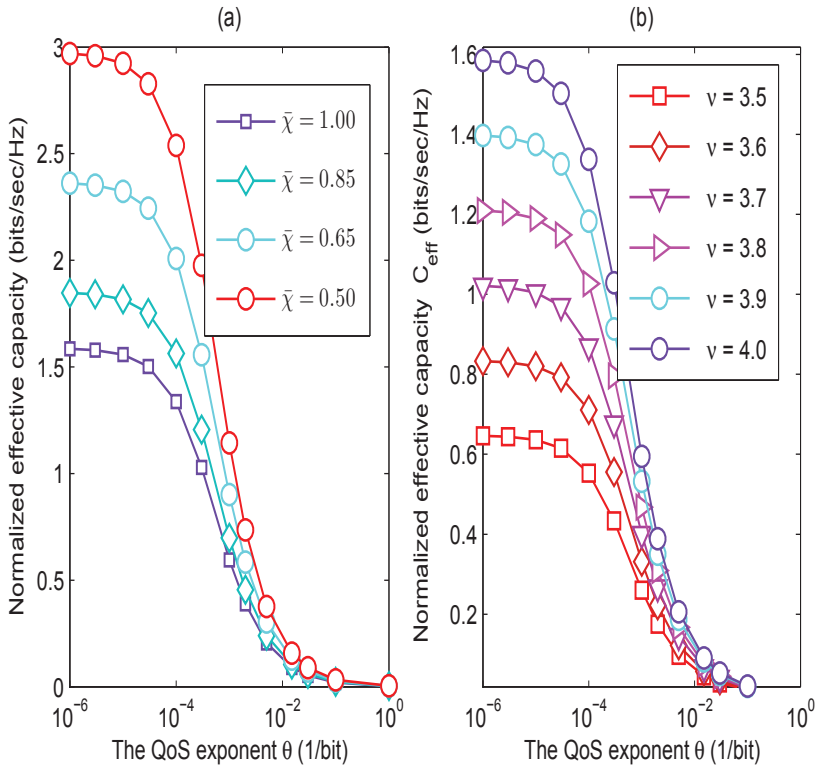

Figure 5.8: Uplink normalised effective capacity of a typical UE, (a) Different pilot reuse probability. (b) Different path-loss exponent, (System bandwidth is BW = 0.3 MHz, block length is T = 2 ms).

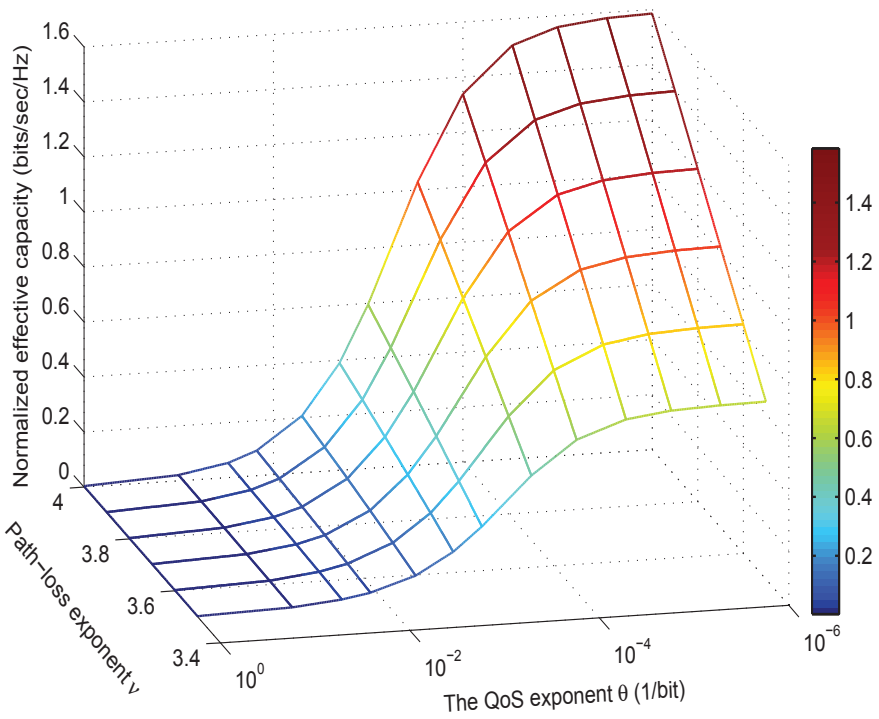

Figure 5.9: The functional relationship among uplink normalised effective capacity C_{eff}^{UL}, path-loss exponent ν and the QoS exponent θ of a typical UE (System bandwidth is BW = 0.3 MHz, block length is T = 2 ms).

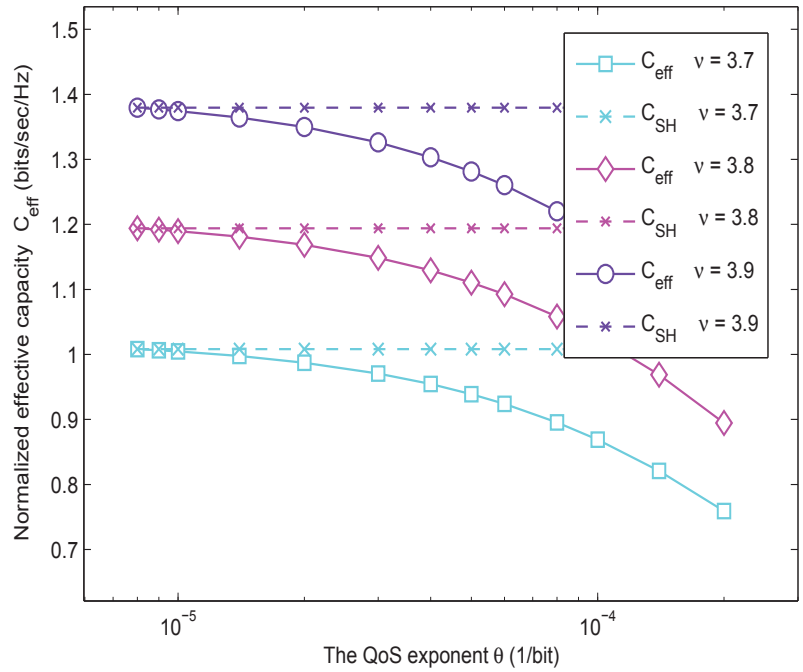

Figure 5.10: The behaviour of the normalised effective capacity C_{eff} compared with the Shannon capacity C_{SH}, (System bandwidth is BW = 0.3 MHz, block length is T = 2 ms).

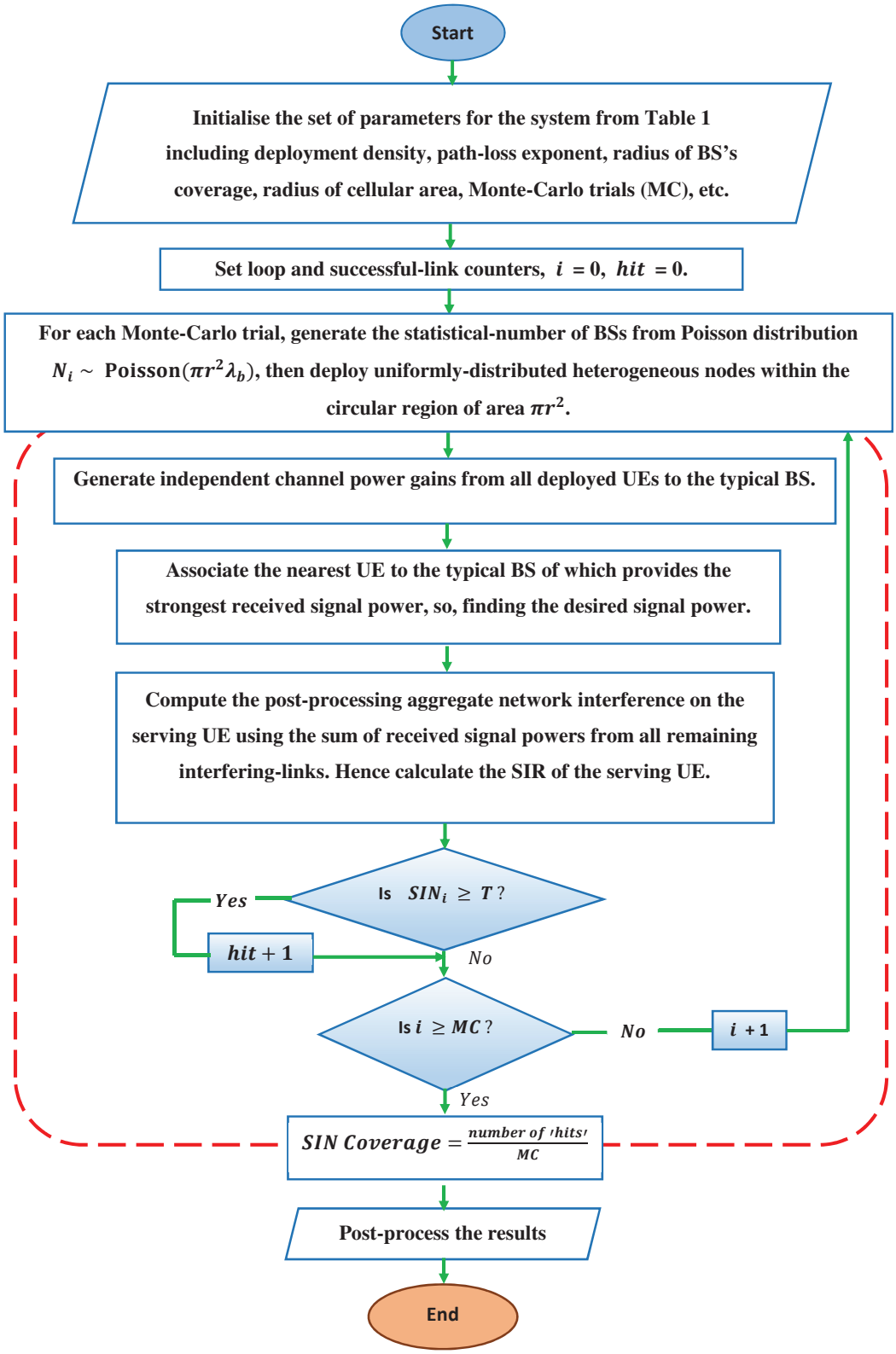

Figure 5.11: Flowchart describes Monte Carlo simulation platform for evaluating the SIR coverage probability of a typical UE in massive MIMO cellular networks. In our case, the trials were conducted for 100k times (geometric drops) over a cellular radius of 40 km in order to obtain typical simulation curves.

5.6 Conclusion

In this chapter, we provided tractable expressions for the asymptotic SIR coverage, rate coverage and effective capacity in the uplink of the interference limited cellular massive MIMO. The expressions are based on a Poisson point process topology using stochastic geometry tools. The presented results provide valuable insight into the impacts of key system features such as path loss attenuation, shadowing and pilot contamination on the statistical distributions of various system metrics. Simulations clearly illustrate that the SIR coverage performance improves as frequency reuse factor Ω increases due to the increases of distances between the typical and interfering UEs.

However, a trade off is required in Ω selection when a guaranteed minimum-rate is required since increasing Ω will decrease the effective bandwidth. Furthermore, we investigated the impacts of path loss exponent and the pilot reusing probability, which is a function of the cell load, on the effective capacity at a typical BS. In this aspect, results show that path loss in the cellular system plays a key role in mitigating the system overall interference and the effective capacity is in proportion to the path loss attenuation. More practical issues, like uplink power control and dynamic frequency reuse scheme, are expected to be addressed in the future analysis.

Chapter 6

Fractional Power Control in the Uplink of a Cellular Massive-MIMO

This chapter addresses the spatial average analysis of the uplink signal to interference ratio (SIR) and throughput in massive MIMO networks with maximum ratio combining (MRC). The analysis incorporates effects of fractional power control (also known as channel inversion policy) and other cells interference (ICI) due to estimation error in channel state information (CSI). Fractional Power Control (FPC) is an open loop uplink power control in cellular networks and it is so called because it allows the user terminal to partially compensate for the attenuation or the geometric path loss. So, far away edge users will transmit with full power, while interior users transmit with low power.

Based on an asymptotic approach, tractable expressions are presented for SIR distributions and specific performance metrics (coverage probability and average rate) in poisson topology model. Moreover, the considered approach is applicable both to random and deterministic network topologies. The impacts of key network features such as fractional power control, path loss exponent and BS density are characterised. Numerical results validate the model and show that the coverage probability in the lower 50^{th} percentile can be maximised by adjusting FPC compensation fraction between 0.2 and 0.5 depending on the system parameters. Also, for SIR threshold of $0\,dB$, allocating $\epsilon = 0.25$ of uplink transmit power can achieve approximately 6% improvement in coverage probability in cell edge area compared to constant power policy ($\epsilon = 0$) and about 14% improvement compared to full channel

inversion policy ($\epsilon = 1$). The provided approximation results can replace the need for lengthy Monte Carlo simulations in designing of large scale MIMO systems and quantify the trade off between improved cell edge SIR for low and moderate values of FPC.

6.1 Introduction

Massive multiple-input multiple-output (massive MIMO) technology achieves a key breakthroughs in the multiple access domain and brings benefits to the efficient-usage of both energy and spectrum in wireless communication [84].* By deploying arrays with large scale antenna elements, BSs can use the available degree of freedom in the spatial domain to serve simultaneously a large number of user equipments (UEs). This chapter addresses the effect of fractional power control (FPC) and inter cell interference on the uplink transmission (UL) of massive MIMO in time division duplex (TDD) systems. Where pilot aided channel estimation is executed in the uplink, and pilots are reused across different cells to reduce the training-overhead.†

It is worth mentioning that in cellular uplink, the basic motivations for FPC are to introduce beneficial coverage improvements for the cell edge users (lowest percentile), also to maintain energy in battery powered mobile equipments (reduce battery draining speed). Most prior work in this concern considered the performance of down link mode of massive MIMO systems using a simplified regular topology, e.g. studying only a few base stations (BSs) in a hexagonal grid [7], [53]. For cellular networks with a large number of BSs (dense networks), it is of interest to consider irregular topologies, where BSs are randomly located. J. G. Andrews et al in [74] introduced a simple expressions for the signal to interference ratio (SIR) and the throughput in dense networks based on stochastic geometry (SG) using poisson point process (PPP).

Authors in [65] applied SG to analyse the asymptotic SIR and rate in a massive MIMO systems. In [70], Herath *et al.* considered power control for uplink-transmission in a random topology network operating over path loss and Rayleigh/log-normal composite channel. They observed that at low SINR thresholds, complete

*It is worth emphasising that improving spectral efficiency (SE) and energy efficiency (EE) is the fundamental-requirement for 5G wireless networks.

†However, in general, pilot contamination is the key factor that limits the performance of systems that rely on pilot reuse schemes to acquire CSI at BSs (e.g., see [7] and the references therein for more details).

channel inversion improves uplink coverage, while at high SINR thresholds inverting only the impact of shadowing gives a higher uplink coverage.

In reference [85], the authors investigated the uplink SIR distribution (exact and asymptotic) in a large scale MIMO system using maximum ratio combining (MRC) receiver. The proposed model accounts for exponential correlated multipath fading and FPC which compensates for a fraction of the path loss. Additionally, they obtained a scaling law between the BS antennas and scheduled users per cell required to keep the same SIR distribution for uplink and downlink.

6.1.1 Contributions

Uplink SIR analysis is of primary concern compared to the downlink analysis, since signals in the downlink scenario all come from the centre of the cells, whereas in uplink scenario signals may come from the boundaries of the cells [71]. Moreover, due to the irregular deployment of modern networks, and with non-orthogonal pilots, uplink interference from other user equipments can be stronger than the useful signal at the serving base station. So, for scenarios wherein the UE may be able to connect and decode the downlink transmission, but unable to establish the uplink connection will effect hand-off algorithms between adjacent BSs.

Inspired by the analytical tractability of the pioneering work on Poisson model [74], we seek in this chapter to tackle the potential benefits of massive MIMO configuration in wireless systems in the sense of uplink SIR and related metrics such as SIR coverage and average rate using FPC policy. Unlike the regular topology considered in [7], we examine irregular topology of cellular massive MIMO which is known to be closer to the practical demand-based deployment of BSs [72].

Besides, different from [85], this work considers a general framework that can be applied to networks where BSs are distributed according to irregular as well as regular topologies. This work has presented tractable expressions for the coverage probability and average rate in the cellular uplink, which are applicable both to deterministic and random networks.

First, we derive an analytical formula for the uplink's asymptotic SIR* coverage probability and the average rate of a large antenna array regime based on poisson

* It is not always easy to evaluate the main performance metrics such as coverage probability and user rate in closed form when general models is adopted, Hence, to facilitate analysis, we consider an asymptotic model for the system that results in simple analytical expressions for the metrics of interest (upper-bound on the coverage probability).

model. The transmit power of a user depends on the distance to its associated BS, i.e., using fractional path loss compensation as a power control policy.

Next, we evaluate the implications of channel and system parameters on the uplink performance via numerical analysis with remarkable comments. Obtained results confirm that the coverage probability in the 50^{th} percentile can be maximised by adjusting the compensation-fraction in the FPC between 0.2 and 0.5 depending on the system parameters.

Additionally, applying a fraction of full transmit power of $\epsilon = 0.25$ can achieve approximately 6% improvement in coverage probability in the cell edge area for $0\,dB$ SIR threshold compared to constant power policy ($\epsilon = 0$) and 14% improvement compared to full channel inversion policy ($\epsilon = 1$). The provided approximation results can replace the need for lengthy Monte Carlo simulations in designing of the large scale MIMO systems and quantify the trade off between improved cell edge SIR for low and moderate values of the FPC.

6.1.2 Notations and Chapter Organization

Throughout this work we use the following notation, $\mathbb{E}_x\{\cdot\}$ refers to the expectation operator over the random variable x, $\mathbb{P}\{X\}$ stands for the probability of event X [73], $\Gamma(x)$ denotes the gamma function, i.e., the integration $\int_0^\infty t^{x-1}e^{-t}dt$ [43], $\mathscr{L}_x(s)$ is Laplace transform (L.T) of x at specific value s, $f_x(\cdot)$ is probability density function (PDF) of random variable x, CCDF is the complementary cumulative distribution function. The remainder of the chapter is structured as follows, Section 6.2 discusses the assumptions and provides system model. Afterwards, section 6.3 formulates the signal-to-interference ratio (SIR) model, presents the definition of the performance metrics, and presents some related aspects. Section 6.4 shows our numerical results. Finally, section 6.5 concludes the work.

6.2 Assumptions and System Model

The proposed network topology considers a simple uplink massive MIMO system, where the SIR expression can be analysed using tools from stochastic geometry. The BSs are assumed to have a PPP distribution with density λ_b. A user equipment (UE) is assumed to be associated with the BS that provides the signal with minimum path loss. Also, UEs are independent identically distributed (i.i.d) of uniform profile

in two-dimensional Euclidean plane $\mathbb{R}^2$ with sufficiently high density in their cells enough for potential scheduling.

For simplicity's sake, we assume that each base station has a single active uplink-UE scheduled for a given resource block (RB) which is randomly chosen from all the UEs deployed in its cell area. Hence, the UE PPP deployment density λ_u can be *thinned* in order to obtain a point process which describes the spatial locations of the active UEs (λ_a). Since only one UE per base station can be selected among all UEs situated in that BS's cell area, the *thinning* process is not independent causes main complications for the uplink analysis. So for tractability's sake, we assume that the active UEs also form a poisson point process even after associating only one UE per each BS*. Without loss of generality, a typical base station $\mathrm{BS_o}$ is located at the origin and will be used as a probe to investigate the SIR-distribution and rate-performance. It is worth noting that allocating of the unique pilots within a cell results in correlations in the scheduled UEs' locations even though the UEs are located as a PPP on the plane $\mathbb{R}^2$. Which in turn makes the analysis intractable unless using some approximations and assumptions. Thus, we assume that the distribution of the scheduled UEs to be i.i.d.

6.2.1 Estimating Uplink-Channel

For acquiring channel state information (CSI), we consider pilot based channel estimation in which all the users send pre assigned training sequences. The pilot set is assumed to be reused among all cells. Leveraging channel estimates, BSs then applies a maximum ratio combining (MRC) to recover received uplink data by correlating the received training signal with the corresponding pilot. Similar to that used in long term evolution (LTE) systems [86], in both the uplink-training and uplink-data stages, FPC policy is assumed in order to compensate for a fraction of the channel path loss.

For notational simplicity, let $\mathcal{Z}$ denote the set of all interfering users. As shown in Fig.6.1, D_z, ($z \in \mathcal{Z}$) denotes the distance of an interfering user ($\mathrm{UE_z}$) to the serving base station ($\mathrm{BS_o}$), D_o is the distance between serving user ($\mathrm{UE_o}$) and $\mathrm{BS_o}$ and R_z indicates the distance of $\mathrm{UE_z}$ to its associated base station ($\mathrm{BS_z}$). In the

*Simulations show that this approximation does not affect the coverage probability result too much. Since there is just one active UE per cell, the thinned points density of active UEs λ_a should be set equal to the density of BSs λ_b [79].

channel estimation stage*, BS_o estimates the channel gain of the terminal UE_o using a specific pilot sequence as follows

$$\hat{g}_o = D_0^{-\epsilon/2}\, g_o + \sum_{z\in\mathcal{Z}} R_z^{-\epsilon/2}\, g_z \tag{6.1}$$

where, $g_o = h_o\sqrt{\beta_o/D_o^{\nu}}$ is the channel-gain from scheduled user UE_o to BS_o (desired link), $g_z = h_z\sqrt{\beta_z\, D_z^{\nu\epsilon}/R_z^{\nu}}$ is the channel gain from interfering user UE_z to BS_o, (h_o, h_z) model the small-scale fading vectors with i.i.d. zero mean and unit variance entries, ν is the path loss exponent and (β_o, β_z) are the long-term shadow fading coefficients. The second term in (6.1) is the contamination due to the pilot reusing by the UEs associated with the other cells (estimation error). Additionally, thermal noise is ignored, as massive MIMO cellular networks are generally interference limited, and the effect of noise vanishes [7]. Assuming M-antenna BSs and one antenna UEs, then channel gain vectors are of dimension $\{g_o,\, g_z,\, h_o,\, h_z\} \in \mathbb{C}^{M\times 1}$. In the uplink stage, to decode the uplink data, the serving BS is assumed to use the estimated channel $\hat{g}_o$ to perform MRC. Therefore, the uplink SIR for a typical UE with FPC can be written as follows

$$SIR = \frac{D_o^{\epsilon}\, ||\hat{g}_o^*\, g_o||^2}{\sum_{z\in\mathcal{Z}}\; R_z^{\epsilon}\, ||\hat{g}_o^*\, g_z||^2} \tag{6.2}$$

Lemma 6.1 (Asymptotic Behaviour)**.** The expression in (6.2) can be simplified leveraging the fact that entries of h_o and h_z are i.i.d. random variables with zero mean and unit variance. Hence, exploiting the strong law of large numbers (SLLN), only the products of identical quantities in (6.2) remain significant, e.g see [7], [65] or [75] for more details.

Consequently, the SIR distribution can equivalently be represented by a simple massive MIMO model [85]

$$SIR \xrightarrow{d} \frac{\beta_o^2/D_o^{2\nu\,(1-\epsilon)}}{\sum_{z\in\mathcal{Z}}\; \beta_z^2\, R_z^{2\nu\epsilon}/D_z^{2\nu}}, \tag{6.3}$$

*A time division duplex (TDD) protocol is assumed with channel reciprocity. Where the BSs exploit the UL orthogonal pilot sequences (no intra cell interference) to estimate the DL channel of the served UEs.

where $\xrightarrow{d}$ denotes a distribution equivalence. The following sections, study the uplink SIR-distribution using tools from stochastic-geometry.

6.3 Asymptotic Performance with an Uplink FPC Mechanism

6.3.1 Fractional Power Control

In this subsection we consider a cellular network utilising FPC policy and focus on the uplink received SIR at a randomly chosen BS. It is worth emphasising that the random variables $\{R_z\}_{z\in\mathcal{Z}}$ are, in general, identically distributed but not independent* [76]. However, the weak dependence motivates a helpful independence assumption, that is the random variables $\{R_z\}_{z\in\mathcal{Z}}$ are assumed to be i.i.d. Fig.6.1 gives a relationship between system parameters and provides a visual representation of the model.

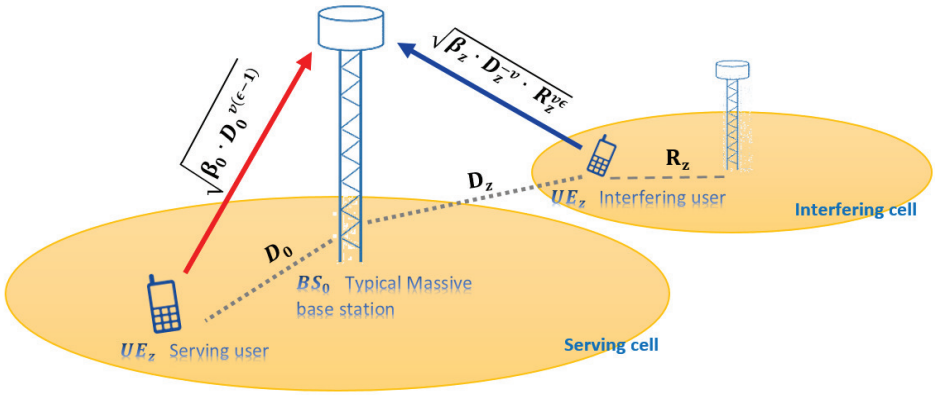

Figure 6.1: System model of the adopted UL cellular system. ϵ is the FPC, accordingly, the received signal-power at the target BS (located at the centre of the plane $\mathbb{R}^2$.) from serving user at distance R_0 is given by $\beta_0\, R_0^{\nu(\epsilon-1)}$. The received interference-power from UE at distance R_z is given by $\beta_z\, D_z^{\nu\epsilon}\, R_z^{-\nu}$, where D_z is the distance from one interfering UE to its serving-BS.

6.3.2 User Distribution D_o

The locations of UE are assumed to form a realisation of a homogeneous spatial-PPP in $\mathbb{R}^2$ [76]. The baseline assumption is that the spatial-PPP corresponds to a uniform-distribution of UEs in the cellular system and that a user is connected to

*Kindly note that this dependence is caused by the restriction that only one BS can lie in each Poisson Voronoi cell.

the closest BS.* Consequently, we can consider that each BS is uniformly-distributed in the Voronoi cell of its interesting UE.† In this case, Rayleigh distribution can be used to characterise the random variable D_o which follows from Lemma 6.2,

Lemma 6.2 (Null-probability of a PPP in $\mathbb{R}^2$ [76])**.** The probability that no user in a circle of area $\pi\lambda_b r_z^2$ can be expressed as

$$\mathbb{P}\{D_o > r\} = e^{-\pi\lambda_b r_z^2}$$

From which the probability density function (PDF) of D_o follows

$$f_{D_o}(d_o) = 2\pi\lambda_b d_o e^{-\pi\lambda_b d_o^2}, \quad d_o \geq 0. \tag{6.4}$$

Lemma 6.3 (Interference Characteristic)**.** Based on the basic formula of Laplace Transform (L.T) [74], the uplink interference at a probe or a typical BS can be characterised as follows

$$\begin{aligned}
\mathscr{L}_{I_z}(s) &= \mathbb{E}_{I_z}\{e^{-sI_z}\} \\
&\overset{(a)}{=} \mathbb{E}_{\beta_z, D_z}\left\{ \exp\left[-s \sum_{z\in\mathcal{Z}} \frac{\beta_z^2 R_z^{2\nu\epsilon}}{D_z^{2\nu}}\right]\right\} \\
&\overset{(b)}{=} \mathbb{E}_{\beta_z, D_z}\left\{ \prod_{z\in\mathcal{Z}} \exp\left[-s \frac{\beta_z^2 R_z^{2\nu\epsilon}}{D_z^{2\nu}}\right]\right\} \\
&\overset{(c)}{=} \exp[\,-2\pi\lambda_b \int_{y=r}^{\infty} y \left(1 - \mathbb{E}_{\beta_z, R_z}\{e^{-s\,\beta_z^2 y^{-2\nu} R_z^{2\nu\epsilon}}\}\right) dy\,] \\
&\overset{(d)}{=} \exp[\,-2\pi\lambda_b\, \mathbb{E}_{\beta_z, R_z}\left\{ \tfrac{s^{1/\nu} R_z^{2\epsilon}\, \beta_z^{2/\nu}}{\nu} \int_0^{t_o} t^{-1/\nu\, -1} (1 - e^{-t}) \right\} dt\,] \\
&\overset{(e)}{=} \exp\left[\,\pi\lambda_b\, r^2 (1 \,-\, \mathbb{E}_{\beta_z, R_z}\{ \tfrac{s^{1/\nu} R_z^{2\epsilon} r^{-2} \beta_z^{2/\nu}}{\nu}\, \gamma(\tfrac{-1}{\nu},\, s R_z^{2\epsilon\nu} r^{-2\nu} \beta_z^2)\})\,\right] \\
&\overset{(f)}{=} \exp\left[\pi\lambda_b\, r^2 (1 - \mathbb{E}_{R_z}\{ \tfrac{s R_z^{\nu\epsilon}}{r^{-\nu(2-\epsilon)}}\, {}_2F_1\left[\begin{matrix} 1, 1 + 2/\nu \\ 2 + 2/\nu \end{matrix}\middle| \frac{-s R_z^{\nu\epsilon} r^{-\nu(2-\epsilon)}}{\nu + 2}\right]\})\right]
\end{aligned} \tag{6.5}$$

where, (a) is obtained by substituting for I_z which is the inter cell interference ICI, i.e., the sum of powers from all interfering users, (b) follows since exponential of a sum is a product of exponential, (c) follows from probability generating functional of the Poisson point process (PGFL), given that $\mathbb{E}\{\prod_{x\in\Phi} v(x)\} = \exp\big[-\lambda_b \int_{\mathbb{R}^2} \big(1 -$

*We assumed that each BS has always an active uplink UE scheduled according to the association metric of max-average SIR

†One BS is assumed to fall in the Voronoi cell of each user which is a point uniformly chosen on $\mathbb{R}^2$ i.e. just one active user is assumed per cell per resource block, so thinning density of active users is equal to λ_b.

$v(x)\Big)dx\Big]$, converting into polar coordinates gives $\mathbb{E}\{\prod_{x\in\Phi} v(x)\} = \exp\Big[-2\pi\lambda_b \int_{\mathbb{R}^+}\Big(1-v(r)\Big)dr\Big]$, (d) follows by variable changing $t = s\,y^{-2\nu}\,R_z^{2\nu\,\epsilon}\beta_z^2$, $t_o = s\,r^{-2\nu}\,R_z^{2\nu\,\epsilon}\beta_z^2$, (e) follows using the definition of $\gamma(a,z)$ which is the lower incomplete Gamma-function identity $\gamma(a,z) = \int_0^z t^{a-1}e^{-t}dt = \Gamma(a) - \Gamma(a,z)$ [43] and (f) follows using the integration formula [46, eq.(6.455.2)],

$$\int_0^\infty x^{\mu-1}\,e^{-\beta\,x}\gamma(\nu,\,\alpha x)\,dx = \frac{\alpha^\nu\,\Gamma(\mu+\nu)}{\mu(\alpha+\beta)^{\mu+\nu}}\;\;{}_2F_1\left[\begin{matrix}1,\mu+\nu\\1+\mu\end{matrix}\middle|\frac{\beta}{\alpha+\beta}\right]$$

with the identity [39, eq.(07.23.17.0055.01)],

$${}_2F_1\left[\begin{matrix}a,\;b\\c\end{matrix}\middle|z\right] = (1-z)^{-a}\,{}_2F_1\left[\begin{matrix}a,c-b\\c\end{matrix}\middle|\frac{z}{1-z}\right]$$

to average out the large scale fading $\beta_z^2 \sim exp(1)$, where ${}_pF_q(\cdot)$ stands for the generalised hyper geometric function [46, eq.(9.14.1)], ${}_pF_q\left[\begin{matrix}a_1,\cdots,a_p\\b_1,\cdots,b_q\end{matrix}\middle|z\right] = \sum_{n=0}^\infty \frac{(a_1)_n,\,\cdots,\,(a_p)_n}{(b_1)_n,\,\cdots,\,(b_q)_n}\frac{z_n}{n!}$, $(x)_n$ is the rising factorial or the Pochhammer polynomial, $(x)_n = \prod_{i=1}^\infty (x+i)$, p and q are non-negative integers.

6.3.3 Interferers Distribution R_z

Two approximation approaches can be used to model the random variable R_z in (6.5) corresponding to deterministic and random topologies.

A. Regular BS Deployment Model: Uniformly distributed over a circle of fixed radius from its centre when we approximate hexagon cells as circles with area of $1/\lambda_b$ (regular deployment of BSs), in this case, R_z can be described as

$$f_{R_z}(r_z) = 2\pi\lambda_b\,r_z, \quad r_z \in \Big[0,\,\frac{1}{\sqrt{\pi\lambda_b}}\Big] \tag{6.6}$$

B. Irregular BS Deployment Model: For non-uniform coverage regions, R_z can be approximated as the distance of a randomly chosen point on two dimension plane to its closest BS which is Rayleigh distribution (motivated by the same null probability discussed in Lemma 6.2), and the probability density function is

$$f_{R_z}(r_z) = 2\pi\lambda_b r_z e^{-\pi\lambda_b r_z^2}, \quad r_z \geq 0 \tag{6.7}$$

Next, these probability distribution functions can be used to characterise the performance of the system.

6.3.4 Probability of Coverage

The coverage formulas for deterministic and random models are derived in theorems 6.1 and 6.2 respectively.

Theorem 6.1 (Regular Topology)**.** *The asymptotic uplink coverage probability of a typical UE with i.i.d. Uniform distributed interfering users R_z (PPP-Uniform model under FPC policy) can be approximated as follows*

$$P_{cov}(T_1, \lambda_b, \nu, \epsilon) = 2\pi\lambda_b \int_0^{\infty} r\, e^{-2\pi\lambda_b r^2\, \Upsilon_1(T_1,\lambda_b,\nu,\epsilon)} dr \tag{6.8}$$

where

$$\Upsilon_1(T_1, \lambda_b, \nu, \epsilon) = \int_{x=0}^{1/\sqrt{\pi\lambda_b}} \frac{2\pi\lambda_b x\, C_1}{\nu+2}\, {}_2F_1\left[\begin{matrix}1, 1+2/\nu \\ 2+2/\nu\end{matrix}\middle| -C_1\right] dx$$
$$C_1 = T_1\, r^{-\nu\epsilon} x^{\nu\epsilon} \tag{6.9}$$

Proof: First, we are going to characterise the statistical distribution of SIR conditioned on user location $\mathrm{D_o}$

$$\begin{aligned}
\mathbb{P}\Big\{SIR > T_1\Big\} &\overset{(a)}{=} \mathbb{P}\left\{\beta_o^2 > T_1\, D_o^{2\nu(1-\epsilon)} \sum_{z\in\mathcal{Z}} \frac{\beta_z^2\, R_z^{\nu\epsilon}}{D_z^{2\nu}}\right\} \\
&\overset{(b)}{=} \mathbb{E}_{I_z,\beta_z}\left\{ \exp\left[-T_1\, D_o^{2\nu(1-\epsilon)} \sum_{z\in\mathcal{Z}} \frac{\beta_z^2\, R_z^{\nu\epsilon}}{D_z^{2\nu}}\right]\right\} \\
&\overset{(c)}{=} \mathbb{E}_{I_z,\beta_z,D_o}\left\{ e^{-T_1\, D_o^{2\nu(1-\epsilon)}\, I_z}\right\} \\
&\overset{(d)}{=} \mathbb{E}_{I_z,\beta_z}\left\{ e^{-s\, I_z}\right\} \\
&\overset{(e)}{=} \mathscr{L}_{I_z}(s)\,,
\end{aligned} \tag{6.10}$$

where, (a) is obtained by substituting for the signal-to-interference ratio and rearrange the inequality variables, (b) follows since $\{\beta_i^2\}_{i=0}^{\infty}$ is assumed to be a set of i.i.d. unit-mean exponential random variables ($\sim exp(1)$), (c) is obtained by denoting the inter cell interference as I_z which is the sum of the powers from all the interfering UEs placed farther than D_o (no intra-cell interference with orthogonal pilot sequences assumption), (d) follows assuming $s = T_1\, D_o^{2\nu(1-\epsilon)}$ as a constant in Laplace equation and (e) is, by definition, the Laplacian of interference w.r.t the

constant s. Next, substitute for $\mathscr{L}_{I_z}(s)$ from (6.5-f) yields

$$\mathbb{P}\Big\{SIR > T_1\Big\} = \exp\Big[\pi\lambda_b\, r^2(1 - \mathbb{E}_{R_z}\{\tfrac{T_1\, r^{-\nu\epsilon} R_z^{\nu\epsilon}}{\nu+2}\, {}_2F_1\left[\begin{matrix}1, 1+2/\nu\\ 2+2/\nu\end{matrix}\Big| \frac{-T_1\, R_z^{\nu\epsilon}}{r^{\nu\epsilon}}\right])\Big] \quad (6.11)$$

Based on (6.11), the coverage probability is calculated as

$$\begin{aligned} P_{cov}(T_1, \lambda_b, \nu, \epsilon) =& \mathbb{E}_r\Big[\mathbb{P}\Big\{SIR > T_1\Big\}\Big] \\ &\overset{(a)}{=} \int_0^\infty \mathbb{P}\Big\{SIR > T_1\Big\} f_{D_o}(r) dr \\ &\overset{(b)}{=} 2\pi\lambda_b \int_0^\infty r\, e^{-\pi\,\lambda_b\, r^2} \exp\Big[\pi\lambda_b\, r^2 \\ &\times (1 - \int_{x=0}^{1/\sqrt{\pi\lambda_b}} \tfrac{2\pi\lambda_b x\, C_1}{\nu+2}\, {}_2F_1\left[\begin{matrix}1, 1+2/\nu\\ 2+2/\nu\end{matrix}\Big| - C_1\right] dx)\Big]\, dr \end{aligned} \quad (6.12)$$

where (b) follows by using (6.4) and averaging out the random variable R_z employing (6.6). Then, one deduces the proof after simple algebraic manipulations. □

It is worthwhile to mention that the inner integral in (6.12-b) can be evaluated using change of variables $t = s\beta_z^2 r^{-2\nu} x^{2\nu\epsilon}$ and the identity [132, eq.(1.15.1.1)], while the outer one can be easily evaluated by recalling Gauss Laguerre quadrature, $\int_0^\infty e^{-x} f(x)\, dx = \sum_{j=1}^n \omega_i f(x_i)$, with n is the number of terms used in the approximation, x_i, ω_i are, respectively, the corresponding abscissas and weights. Now we state the coverage for the case of a random model as Theorem 6.2.

Theorem 6.2 (Irregular Topology)**.** *The asymptotic uplink coverage for a typical random located user with i.i.d. Rayleigh distributed interfering users R_z (PPP-Rayleigh model under FPC policy) is given by*

$$P_{cov}(T_1, \lambda_b, \nu, \epsilon) = 2\pi\lambda_b \int_0^\infty r\, e^{-2\pi\lambda_b r^2\, \Upsilon_2(T_1, \lambda_b, \nu, \epsilon)} dr \quad (6.13)$$

where

$$\begin{aligned} \Upsilon_2(T_1, \lambda_b, \nu, \epsilon) &= \int_{x=0}^\infty \tfrac{2\pi\lambda_b x\, C_1}{\nu+2}\, {}_2F_1\left[\begin{matrix}1, 1+2/\nu\\ 2+2/\nu\end{matrix}\Big| - C_1\right] e^{-\pi\lambda_b\, x^2}\, dx \\ C_1 &= T_1\, r^{-\nu\epsilon} x^{\nu\epsilon} \end{aligned} \quad (6.14)$$

Proof: The same approach used in the previous theorem can be used here. However, in this case, the PDF given in (6.7) can be used to average out R_z. □

In short, (6.8) and (6.13) give, with fairly easy to compute integrals, general results for the coverage probability.

6.3.5 Optimal Fractional Power Control

One advantage of having a coverage framework for the uplink transmission is the ability to optimise the performance as a function of the relevant network parameters. Also, to investigate trade offs between user coverage enhancements and BS spectral efficiency. The value of FPC that achieves optimal coverage for a given system parameters can be obtained according to

$$\epsilon^*(T_1, \lambda_b, \nu) = \underset{\epsilon\in[0,1]}{\arg\max}\ 2\pi\lambda_b \int_0^\infty r\, e^{-\pi\lambda_b r^2} \left[\mathscr{L}_{I_z}(T_1 r^{2\nu(1-\epsilon)})\right] dr \tag{6.15}$$

which reveals that the system parameters, e.g., deployment density λ_b and path-loss exponent ν, impact optimal FPC value.

6.3.6 Average Rate

In the modern cellular network, link-adaptive algorithms are very useful in improving the overall performance. Where the average SIR is directly associated to users average data-rate [76]. The obtained analytical expressions for Laplace transform is useful in the analysis of user-rate under different stochastic power control strategies and gain insight into the system uplink design, something previously very difficult with deterministic deployment models. Here, we focus on the PPP Rayleigh scenario (non-uniform topology), where the BS is located uniformly in the Voronoi cell of its corresponding UE and the distance to the nearest BS is Rayleigh distributed. However, a similar analysis could be performed for regular topology networks.

Theorem 6.3 (Average Rate for Irregular Topology)**.** *The asymptotic uplink average rate of a randomly chosen user for i.i.d. Rayleigh distributed interfering users Rz, is given by*

$$R_{avg}(\lambda_b, \nu, \epsilon) = 2\pi\lambda \int_0^\infty r\, e^{-\pi\lambda r^2} \int_0^\infty \left[\mathscr{L}_{I_z}(\frac{e^{\ln(2)\, t} - 1}{r^{2\nu(\epsilon-1)}})\right] dt\, dr \tag{6.16}$$

where $\mathscr{L}_{I_z}(s)$ is given by (6.5-e).

Proof: Starting from the definition of R_{avg},

$$R_{avg}(\lambda_b, \nu, \epsilon) = \mathbb{E}\Big\{\ \log_2(1 + SIR)\Big\}$$

$$\overset{(a)}{=} \int_0^\infty f_R(r) \int_0^\infty \mathbb{P}\Big\{ \Big[\log_2(1+SIR) \; > \; t | r \Big] dt \Big\} dr$$
$$\overset{(b)}{=} \int_0^\infty f_R(r) \int_0^\infty \mathbb{P}\Big\{ \underbrace{\Big[SIR \; > \; \Big(e^{\ln(2)\, t} \; - \; 1 \Big) | r \Big]}_{\text{SIR-ccdf}} \, dt \Big\} dr$$
$$\overset{(c)}{=} \int_0^\infty f_R(r) \int_0^\infty \Big[\mathscr{L}_{I_z}(s) \Big] \, dt \, dr \; , \tag{6.17}$$

the first line in (6.17) follows from the definition of the average data rate based upon the Shannon capacity expression, (a) follows by integrating over the distribution of SIR and employing the identity $\mathbb{E}[X] = \int_{t>0} \mathbb{P}(X > t)\, dt$ since power is non negative, (b) is obtained after re-arrange the inequality variables and (c) follows by substituting for Laplace transform from (6.10) given that $s = \dfrac{e^{\ln(2)\, t} - 1}{r^{2\nu(\epsilon-1)}}$, which in turn concludes the proof. □

6.4 Numerical-Results and Discussions

This section presents the details of numerical and analytical results for the design parameters given in Table-6.1. Results give insights into how the various parameters impact the performance metrics in the system.

a) Model Validation: First, Fig.(6.2) plots the uplink coverage probability using different expressions of the Laplace transform (6.8), (6.13) and compares them with the simulated hexagonal topology (Hex grid) under actual power control which can be used as a baseline model (upper performance bound).* Note that the analytical result derived under the PPP-Uniform assumption closely approximates the true power control results for the simulation of the hex grid model with regular deployment of BSs for the entire range of SIR-threshold values.

Additionally, significant performance gap can be observed between PPP Uniform and PPP Rayleigh cases over the SIR entire range and slightly larger for full channel inversion policy $\epsilon = 1.0$, where the disparity becomes more noticeable. This confirms the fact that the PPP topology represents the worst case of BSs deployment (Lower performance bound). Also at the high SIR threshold values, the use of larger ϵ values,

* Irregular or random layout of BSs gives a lower bound on the coverage performance. This is due to the fact that in PPP topology the distances between BSs are random, no constraints on minimum distance, and therefore users associated with nearby BSs may contribute to high uplink interference levels at the typical BS. On the other hand, hex grid layout obviously is more optimistic and provides the upper bound on coverage performance. The reason is that regular or deterministic topologies have optimal geometric structure, resulting in constraints on minimum distance between adjacent BSs.

for both topologies, negatively impacts the probability of coverage since users closest to their corresponding BSs (interior users) greatly reduce their transmitting power compared to the users at the cell edge (exterior users). In the following plot, the effect of FPC, ϵ is addressed in further detail.

b) SIR Profile: Now, the discussion is concentrated on the effect of power control techniques on coverage performance in both regular and irregular schemes. Constant power or no-power control with $\epsilon = 0$ is considered as the reference or baseline of comparison. Fig.(6.3) displays the uplink coverage performance for a PPP Rayleigh network versus a range of SIR threshold values under stochastic fractional power control. It can be clearly observed that the constant power allocation almost shows comparable coverage performance in low SIR threshold regimes, whereas, in high SIR values, outperforming all other power control policies. The largest coverage probability in the lower 50^{th} percentile is provided by $\epsilon = 0.25$ power control policy before crossing below $\epsilon = 0$ cases at $12\,dB$. In the low SIR-thresholds, the coverage difference for $\epsilon = 0.5$ and $\epsilon = 0.25$ is almost negligible.

As ϵ increases towards unity, i.e., full channel inversion, the coverage decreases accordingly. Where, across the entire range of SIR thresholds, full channel inversion experiences the lowest coverage performance. FPC impact can be fully interpreted by focusing on the trade off between the performance of cell center and cell edge users. Constant power is the optimal power policy for cell interior users due to the fact that users in cell center enjoy , usually, good environment and are not experiencing too strong interference (noise limited scenario). So reducing their transmit power definitely reduces their SIR. Cell exterior users (users with large path loss), on the other hand, are more vulnerable to high interference from users in neighbouring cells (interference limited scenario). Therefore, using high power control factors absolutely leads to an increase in their SIR, whereas relatively reducing the interference power transmitted by adjacent cell center users. Accordingly, there is a subtle trade off between reducing interference contributed by adjacent cell centre users and increasing interference experienced by cell edge users. This fact leads to employ fractional values of ϵ (less than one) in order to improve the overall coverage probabilities for the majority of users.

c) Optimal Fractional Power Control: Fig.(6.4) plots the value of the optimal FPC ϵ^* at a given SIR threshold for different ν using (6.15). The plot gives insight into the chosen of FPC that maximise coverage probability. Here, two distinct regions can be observed (dual regime behaviour), for low SIR users a moderate

value of FPC ($\epsilon = 0.2$ to 0.5) provides the greatest gains while for high SIR users, the coverage is maximised by transmitting with no power control ($\epsilon = 0$, i.e. all users transmit with the same constant power). Noticeable that for the different path loss exponent ν, the transition from one region to another occurs on steep slopes, with less than $5\,dB$ range.

d) Average Rate Profile: In Fig.(6.5), using the Rayleigh distribution assumption for interferers (PPP Rayleigh model), we plot the normalised average data rate versus fractional power control ϵ and path loss exponent ν. It is shown that the average rate increases with path-loss exponent over all values of fractional power control.

Additionally, as ϵ increases, the average rate decreases as a result of the loss in the rate of some users (interior users) whose transmitted power is reduced by FPC, which is not compensated on average by the interference lowering and rate increasing for other users (cell edge users). Where the impacts of fractional power control on the throughput of different users (in low, medium and high SIR regimes) is lumped into a single value since the calculated average rates are for a user chosen randomly through the entire network.

6.5 Conclusion

This chapter studied the coverage performance and the average rate in massive MIMO uplink cellular networks applying distance based power control. Employing the spatial poisson model, the coverage probability and the average rate are established via tractable expressions for PPP Uniform and PPP Rayleigh network models and then, concerning coverage of edge area, the optimal policy for FPC is evaluated. Simulation result validates the PPP approximation model of ICI in hexagonal cellular networks. Hence, the framework eliminates the necessity of system level Monte Carlo realisations, which are time intensive simulations.

Besides, numerical and analytical results draw several key network-design insights regarding the SIR-coverage and the average rate in uplink massive MIMO systems. First, depending on network features, the coverage probability in lower 50^{th} percentile can be maximized by setting FPC compensation fraction between 0.2 and 0.5. Second, for SIR threshold of $0\,dB$, applying $\epsilon = 0.25$ of maximum uplink transmit power can achieve approximately 6% (from 0.78 to 0.84) improve-

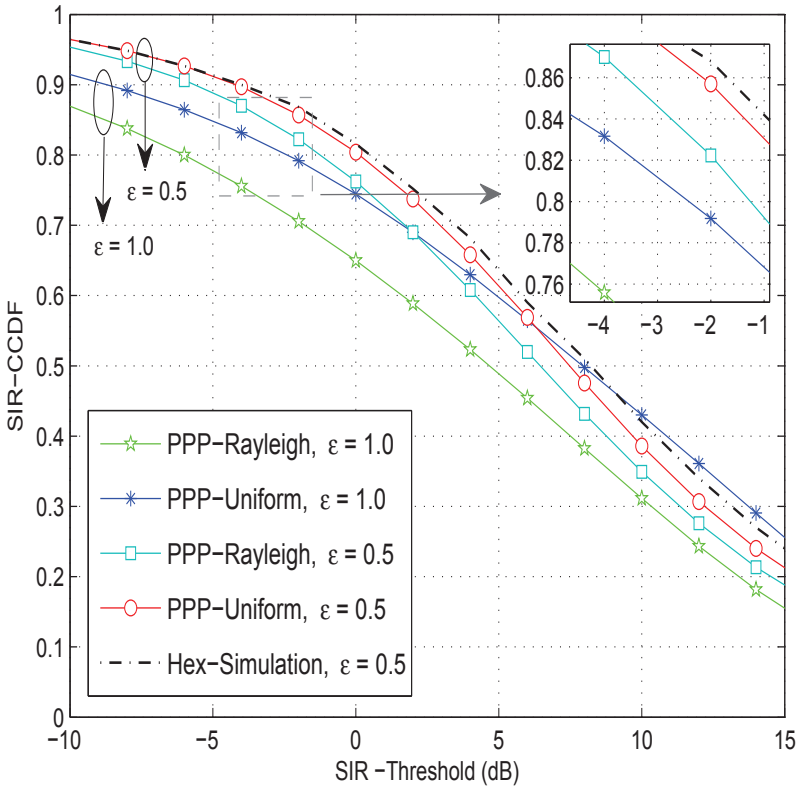

Figure 6.2: A comparison of the complementary cumulative distribution function (CCDF) of the asymptotic uplink SIR for the proposed model with simulation of the hexagonal grid and the PPP models (Rayleigh and Uniform) for different power control strategies $\epsilon = \{0.5, 1.0\}$, path loss $\nu = 3.3$ and cell density $\lambda_b = 0.24$ per km^2.

ment in coverage probability in cell edge area compared to constant-power policy, i.e., $\epsilon = 0$ and about 14% (from 0.70 to 0.84) improvement compared to full channel inversion policy, i.e., $\epsilon = 1$. For future work, the framework can be extended to address the performance of further advanced detection schemes, e.g. zero forcing detectors. Also, to incorporate some system issues such as antennas' spatial correlation into the analysis.

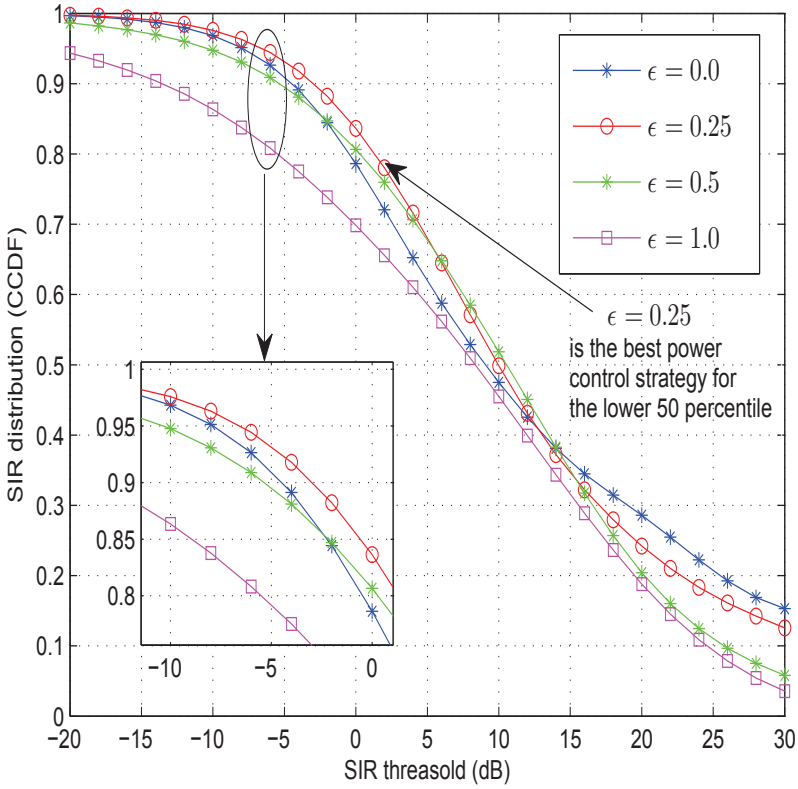

Figure 6.3: A comparision of the complementary cumulative distribution function (CCDF) for the asymptotic uplink SIR with different strategies of power control $\epsilon = \{0, 0.25, 0.5, 1.0\}$, path loss $\nu = 3.3$ and cell density $\lambda = 0.24$ per km^2.

Table 6.1: Numerical parameters used in the simulation, otherwise specified in figures caption.

PARAMETERS	SETTING
Density of BSs λ_b	0.24 per square Km
BS coverage_radius	$1/\sqrt{\pi\,\lambda_b} = 1.1519$ Km
Fractional power control ϵ	0.25, 0.5 and 1.0
Path-loss (dB)	37 $\log(r)$, r is distance in meter
Large scale shadowing	$\beta_z \sim \exp(1)$
User distribution	uniform
Hex grid simulation	25 regularly deployed BSs
Channel bandwidth	20 MHz
Monte Carlo realizations	10^5 geometry drops

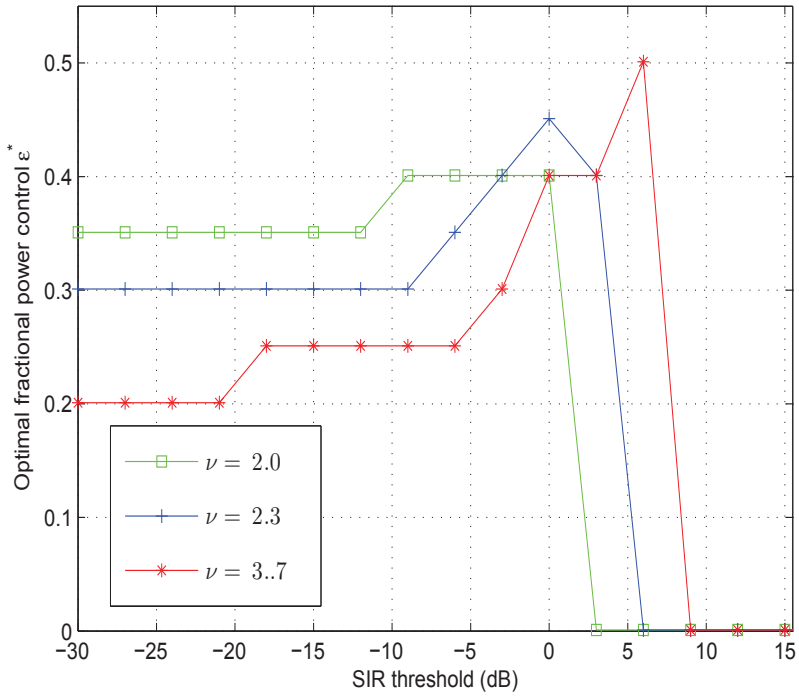

Figure 6.4: The coverage maximising plot versus SIR threshold values (optimal fractional power control values) for poisson point process deployed BSs, cell density of $\lambda_b = 0.24$ per Km^2 and different path loss exponent values $\nu = \{2.0, 2.3, 3.7\}$.

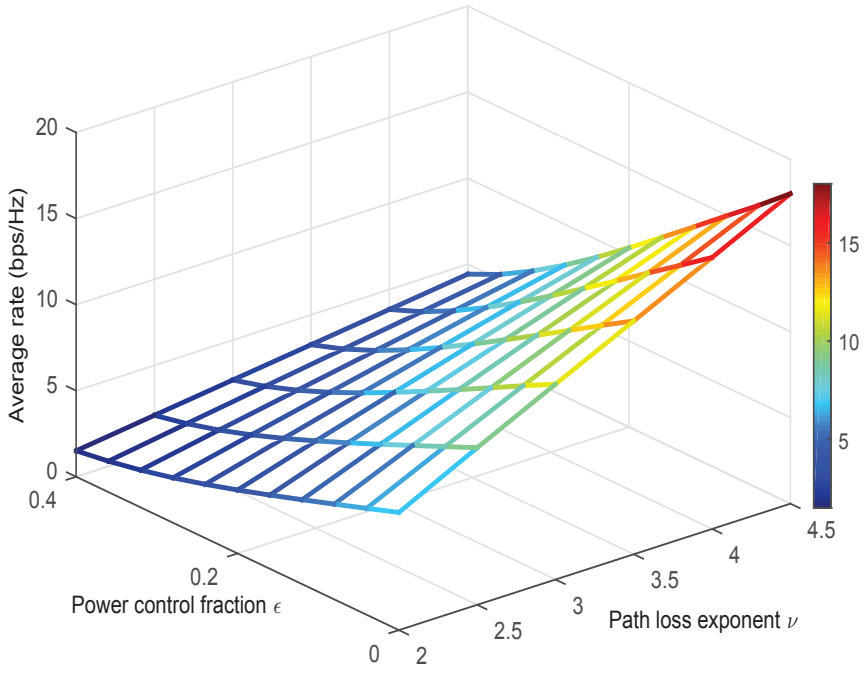

Figure 6.5: Normalised average user rate versus fractional power control ϵ and path loss exponents ν for poisson point process deployed BSs and cell density of $\lambda_b = 0.24$ per Km^2.

Chapter 7

Performance Analysis of Massive-MIMO Enabled Heterogeneous C-RANs

This chapter addresses the multiple-input multiple-output (MIMO) aided heterogeneous cloud radio access networks (H-CRANs), where massive MIMO enabled macro cells coexist with remote radio heads (RRHs) to potentially achieve high spectral and energy efficiencies. We derive tractable formulas for the link_reliability (or signal-to-interference-ratio distribution) and rate coverage of a typical user in H-CRANs by employing a Toeplitz matrix tool from linear algebra. Macro base station tier (MBS) is proposed to apply multi user MIMO policy via space division multiple access technique (zeroforcing beamforming (ZF) with perfect channel state information). The second tier, i.e., RRH-tier employs single user transmission via single-input single-output (SISO) strategy. Our obtained findings confirm the powerful gain of the massive MIMO for enhancing the throughput of the H-CRAN while small RRH-cells are capable of achieving higher energy efficiency. In addition, the number of users served, simultaneously, with ZF-precoding by an MBS can significantly affect the link reliability of the different tier.

7.1 Introduction

It is widely accepted that fifth generation (5G) systems should achieve a 1000× capacity increase and a 10× energy/spectrum efficiencies increase compared to fourth generation systems (see, e.g., [105] and the references therein for more details). To

fulfil the aforementioned requirements, a new promising paradigm has been proposed as an integration of emerging-techniques from the information technology and the wireless industries, where this new architecture known as cloud radio access networks (C-RANs) [88]. C-RAN networks can deal, efficiently, with large-scale processing for both data and control signals, where baseband processing is centralised and coordinated among remote radio heads (RRHs) in a centralised pool (cloud server), which in turn, provides flexible management of the spectrum and reduces the capital/operating expenditures of the networks. Further, the distributed remote radio heads (RRHs) are installed in C-RAN networks to provide seamless coverage and support high capacity in hot spots [89].

Besides, massive multiple-input multiple-output (massive MIMO) and heterogeneous networks are another key enablers for 5G [90] and, recently, incorporation of multiple antenna techniques into traditional HetNets, has received enormous momentum in academic research with the introduction of the large scale-MIMO concept [91–94].* In this context, the cost effective method, of BSs' dense deployment, is to install a low power BSs (RRHs-tier) within the coverage areas of high power macro-tier [112]. Driven by their large degrees of freedom (DoF) in the spatial domain and high array gain, massive MIMO can be used in allowing multiple users to be served simultaneously on the same time/frequency resource block (RB) [113]. Motivated by these merits, a considerable attention has been paid in literature on the massive MIMO [97] and numerous studies have emphasised the significance of massive MIMO enabled heterogeneous network (HetNet) [98–100]. However, deploying a large number of antennas at the macro base stations (BSs) complicates the analysis and will be difficult to gain insight into impacts of system design parameters on the overall performance.

7.1.1 Related Works

In reference [101], Poor *et al.* considered the outage probability in a cluster of single antenna RRHs (a distributed antenna array) with two transmission techniques namely distributed beamforming and best RRH selection. In [102], C-RAN downlink transmission with multiple antenna RRHs is examined. Both tiers, the RRHs and the MBSs are proposed to apply maximal ratio transmission or transmit antenna selection. The outage performance of different schemes is addressed. In the

* In this work, the terms 'massive MIMO', 'large scale MIMO' and 'large scale antenna array' are interchangeable.

first transmission scheme, the RRH or the MBS with the best-channel is chosen for signal transmission, whereas in the second scheme, all the RRHs take part in serving the target user and, in the third scheme, a minimal number of RRHs, to achieve a required information rate, take part in signal transmission. Imran *et al.* [103] proposed a multiple tiers C-RAN with user centric selection for the RRH with the highest signal to noise ratio (SNR) to serve the typical user. References [104] and [105] addressed heterogeneous networks which are integrated with cloud computing to form heterogeneous C-RAN (H-CRAN). The work of [105] proposed a heterogeneous CRAN to integrating traditional heterogeneous networks (HetNets) with cloud computing. Where, the challenges, the opportunities and the appropriate MBSs/RRHs densities for massive MIMO enabled H-CRAN are addressed. In [104] soft fractional frequency reuse in the H-CRAN is considered, where Lagrange dual decomposition is employed to allocate the transmit power and resource block (RB). The work of [106] employed soft fractional frequency reuse to mitigate the inter-tier interference in the H-CRAN, where a tractable-approach is developed to calculate the throughput and energy efficiency of the network.

In [107], using stochastic orders tools, the performance of single-input single-output scheme, space division multiple access (SDMA) and single user beamforming (SUBF) in HetNets are considered. Specifically, addressing interference-limited scenario, bounded closed-form formulas for the area spectral efficiency (ASE) for these different transmission strategies are derived. In [108], the interference statistic distribution was characterised for MU-MISO HetNet systems with a hybrid network-topology, where simplified expressions for the ergodic-rate and coverage probability are provided using moment matching of the interference-statistics with the Gamma distribution. On the other hand, in [109], the performance of the SDMA-scheme with multiple antennas users and single tier cellular MIMO networks for minimum mean square estimation (MMSE) and linear ZF receivers is evaluated. An equivalent in distribution (EiD) based technique is utilised in [110] for the performance evaluation of single tier cellular networks in different MIMO structures.

It's worth to mention that in multiple-user multiple-antennas transmission environment the main analysis difficulty arises from the gamma distributed of the serving and interfering links (instead of exponential one in SISO system) where higher order derivations for the Laplace transform are needed. To deal with such derivations, e.g., in [95] the Faà di Bruno formula is employed. However, in this approach, the complexity of the derived equations make it very difficult to get any important in-

sight for the design parameters. With the aid of the equivalent in distribution (EiD) approach, the Gil-Pelaez inversion theorem is employed to deal with coverage and rate analyses of multiple antennas scheme of the homogeneous network in [119]. Also, the work in [118] addressed coverage and rate in the homogeneous network with Gamma distributed channel-gains using the theorem of Gil-Pelaez. On the other hand, in [96], the problem of multi-antenna in a single tier cellular system has been solved via a more tractable technique using triangular Toeplitz matrix. A new and simple expression of the SINR distribution is established, which is particularly helpful with multiple antenna transmissions and is, analytically, tractable. The new expression is then used to drive the system throughput and energy efficiency. In addition, it is proved, analytically, that deploying more base stations or more antenna elements at the BS can significantly improve the system_throughput, however this performance gain depends, critically, on the ratio of the base station to the user density and the number of antenna elements at the BS.

In this chapter, motivated by the afore mentioned merits of combining HetNet and MIMO techniques, we extend the analysis applied in [96] into two-tier heterogeneous CRAN (H-CRAN). Accordingly, we characterise SIR and rate distribution for the entire network employing tools from stochastic geometry (SG) and triangular Toeplitz matrix. Different from [106], in this work we leverage tools from linear algebra in our approach and we consider the impacts of RRHs' density and number of users served by macro-BSs per each block of resource elements (REs) of the time /frequency grid. The developed framework helps to get a better understanding of the effects of key parameters on the performance behaviour of the system.

7.1.2 Contributions and Outcomes

We can summarise the main contributions of this chapter as follows

1. A tractable framework to analyse the Success Probability (SIR distribution profile) for the downlink of MU massive MIMO two-tier HetNets is developed using tools from stochastic geometry. Consequently, based on the SIR distribution, Rate distribution is characterised.

2. Leverage the obtained semi closed form expressions, we investigate the impacts of the RRH tier density, number of deployed antennas and number of served users on the rate and link reliability. We prove that increasing RRHs deployment density provides better user rate coverage for some system parameters setting. In addition,

the coverage probability is a function of the different tier densities and the number of users multiplexed by the system, i.e., transmission strategy employed in the MIMO scheme of the macro BSs tier.

3. Our findings provide several useful insights about system design. First, obtained results show that there is an inherent trade off between signal power enhancement (small users number S in each resource block) and achieving more multiplexing gain (large users number S in each resource block). Also, massive MIMO aided macro cells can significantly enhance the performance of the entire H-CRAN network while SISO scheme adopted in RRH-cells provides higher gain in term of energy efficiency.

The rest of this chapter is organised as follows. The analysis and modelling for massive MIMO enabled H-CRAN is provided in Section 7.2. The proposed methodology to characterise the Performance Metrics of interest are presented in Section 7.3 , first we establish the per-tier formulas and then we introduce the overall expression for the HetNet system. In Section 7.4, comprehensive theoretical and numerical studies are conducted for the sake of depicting system design guidelines. Finally, Section 7.5 summarises the chapter.

7.2 System Model

First, we will describe a stochastic model for the position of base stations and then we introduce the channel model, cell association strategy and the key performance metrics that adopted in this work. We consider a downlink transmission in a heterogeneous cloud radio access network (H-CRAN) with two classes of base stations, as illustrated in Fig.7.1. The first-class, without loss of generality, represents the tier of macro-base stations (MBSs) with a massive antenna array. Owing to its high number of antennas, each MBS employs linear-zero forcing beamforming (ZFBF) to serve multiple-users simultaneously over each resource block (RB). This tier is overlaid with a second class of small-cell tier with single antenna remote radio heads (RRHs), each head serves one user per RB. Both tiers are, independently, distributed on the $\mathbb{R}^2$ plane as a homogeneous spatial Poisson point process (HPPP) such that the Euclidean-plane is divided into cells of a Poisson Voronoi tessellation.

In our analysis, we adopt an open access scenario, perfect downlink channel-information and universal frequency reuse (MBS and RRH tiers share the same

Table 7.1: Summery of symbols and Notations.

Notation	Description
$j = \{m, r\}$	indices of the macro and RRH tiers, respectively
ϕ_m, ϕ_r	a PPP modelling of massive BSs and RRHs locations, respectively
P_m, Pr	MBS and RHH total transmission power, respectively
ϕ_j	a point process modeling the locations of j-th tier BSs
N_t, S, Δ_m	number of MBS transmit antennas, number of users served over each resource-block by a MBS and available spatial DoF at a MBS, respectively
$g_{x_j x}$	channel power of the interfering link from a jth tier BS located at y to a typical user, $g_{x_j x} \sim \Gamma(1,1)$
$h_{x_j x}$	channel power of the direct link from a j-th tier BS located at x to a typical user, $h_{x_j x} \sim \Gamma(\Delta_j, 1)$ with $\Delta_j = N_t - S + 1$
$\mathcal{A}_j$, B_j	cell association probability and tier biasing, respectively
$\mathcal{B}(o, x_j)$	an exclusion region around the typical user represents a ball with radius x_j centred at the origin of the $\mathbb{R}^2$ plane
$\hat{\gamma}$, $\mathcal{S}_j$, $\mathcal{R}_j$	threshold SIR, coverage probability and rate coverage probability, respectively
$\boldsymbol{G}$, $\boldsymbol{W}$	the channel and beamforming matrices, respectively
λ_m, λ_r	density of macro BSs and density of RRHs, respectively
R	BS coverage radius
ϵ, α	fractional frequency control and path-loss (dB), respectively
$\mathbf{Q}_\Delta$	a $\Delta \times \Delta$ Toeplitz matrix
$\mathbf{\Phi}_u^m$, $\mathbf{\Phi}_u^r$	the set of users associated with the MBS and RRH tiers, respectively
η_m, η_r	the macro BS's and RRH's power amplifier efficiencies, respectively
P_m^o, P_r^o	the macro BS's and RRH's static hardware power consumption, respectively
$\mathcal{Q}_m$, $\mathcal{Q}_r$	the rate coverage probability for the macro BS's and RRH's tiers, respectively
$\mathcal{Q}_{het}$	the rate coverage probability for the overall H-CRAN network

spectrum). The analysis, without loss of generality, is performed at a typical user, i.e., a user located at the origin. We indicate it's jth tier corresponded BS, located at x_j , as the serving BS or tagged BS. Hence, the geometric propagation loss is $\|x_j\|^{-\alpha_j}$ where $\alpha_j > 2$ represents the path loss exponent. All the multi path fading channel is assumed to be independent and identically distributed (i.i.d.) Rayleigh fading channels. In addition, we assume that for the macro tier zero forcing beamforming (ZFBF) with perfect channel state information (CSI) is employed, i.e., intra cell interference mitigation scheme.* The ZFBF matrix at an MBS is $\boldsymbol{W} = \boldsymbol{G}(\boldsymbol{G}^{\boldsymbol{H}}\boldsymbol{G})^{-1}$ with the channel matrix $\mathbf{G}$, where $(.)^H$ denotes the Hermitian transpose. Therefore, as demonstrated in [126], power gain distribution of the effective channel between the typical user and the serving BS and the interferer BS, i.e., the direct and interfering links follow the Gamma distribution (see Table 7.1). In the following sub-section, we introduce the criterion of cell selection in H-CRAN.

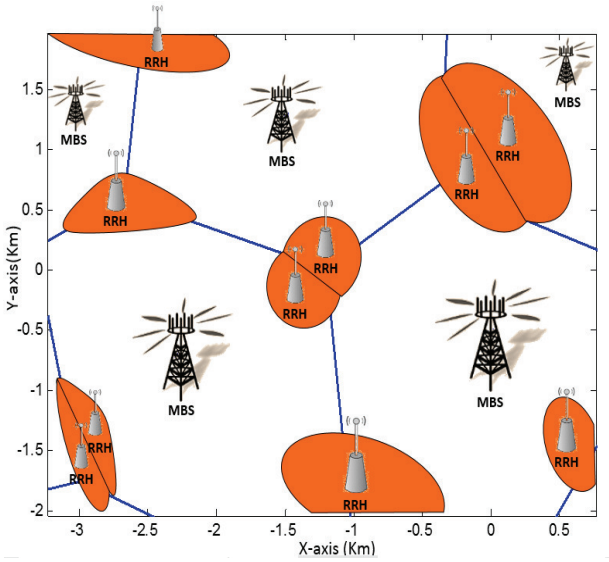

Figure 7.1: Poisson's spatial realisation of the 2-tier massive MIMO enabled H-CRAN system.

7.2.1 Tier Association Probability

We assume an open access scenario with the cell selection policy is based on the largest average-power, i.e, a user corresponds to the BS that ensures the maximum average-power. Owning to it's large array gains, an MBS in the macro cell has a higher coverage probability and consequently, has an impact on the user-association.

* It's worth noting that HetNets are diverse in the sense of BSs coordination degree, however, we assumed the worst case, i.e., there is no across tiers or across cell interference coordination and the system utilise an aggressive frequency reuse policy where different BSs can access the same system resources.

Beside, the higher power of the macro BSs can result in problem of load imbalance if cell selection is carried out just depending on the received power. Therefore, to offload users from the heavily loaded macro tier to the lightly loaded RRH-tier, cell selection bias term $B_j,\ j \in \{m, r\}$ is adopted* and according to the ratio between B_m and B_r, a typical user selects the nearest BS of jth tier if

$$j = \arg \max_{j \in \{m,r\}} B_j P_j \Delta_j \|x_j\|^{-\alpha} \tag{7.1}$$

where x_j is the distance between the typical-user and its nearest-BS in the jth tier. The introducing of the biasing B_j results in exclusion-regions around the typical user and all the interfering-BSs lie outside of this region. The values of biasing can be optimised depending on the metric that is being maximised. The normalised biasing factor w.r.t the MBS serving tier is $\hat{B} = \frac{B_r}{B_m}$. It is noteworthy that the array gain for zero forcing beam-forming (ZFBF), i.e., the available DoF per stream can be given as $\Delta_m = N_t - S_m + 1$ and transmitting power is scaled down by S_m which is the number of MBS users. The following lemma introduces asymptotic-analysis of association probability when employing Large-Antenna Arrays.

Lemma 7.1 (Massive antenna analysis)**.** For large antenna system with power scaling law and in the case of equal path-loss exponents, the association probabilities for MBS and RRH tiers can be given, respectively, as

$$\mathcal{A}_m \ = \ \frac{\lambda_m \ - \ \lambda_r \, (\rho \, \hat{B})^{\frac{2}{\alpha}}}{\lambda_m}, \qquad \mathcal{A}_r \ = \ \frac{\lambda_r}{\lambda_r \ + \ \lambda_m \, \rho^{\frac{2}{\alpha}}}, \tag{7.2}$$

given that $\hat{P}_j \triangleq \frac{P_j}{P_k}, \hat{B}_j \triangleq \frac{B_j}{B_k}, \hat{\alpha}_j \triangleq \frac{\alpha_j}{\alpha_k}$, and $\rho = (\frac{P_r B_r}{P_m B_m})^{-1/\alpha}$.

Proof: see appendix D.1. □

7.2.2 Channel Model and Precoding Vectors

For multi antenna systems, the distribution of useful and interference channel gains for a typical user with single antenna depends upon the transmission strategy employed at the BSs. For each MBS, we adopt MU-MIMO transmission strategy to

* The policy of long term average biased received power cell association is commonly employed in the existing relevant literature [126] since it is practical and very simple offloading strategy.

transmit S data streams under equal power allocation. If we consider that macro and RRH BS tiers are indexed, respectively, by $\{m, r\}$, the channel power for the useful link from a serving BS located at x_o in $\mathbb{R}^2$ to a typical user located at origin is denoted by $g_{x_o,j},\ j \in \{m, r\}$ and for the interfering link from an interferer BS located at x_j in $\mathbb{R}^2$ is denoted by $g_{x_j,j},\ j \in \{m, r\}$.

For Rayleigh fading assumption*, it can be claimed that the distributions of channel gain for the interfering and the direct links follow the Gamma distribution [117]. Therefore, for zero-forcing (ZF) precoding with perfect CSI, we have $g_{x_o,j} \sim \Gamma(\Delta_j, 1),\ j \in \{m, r\}$ and $g_{x_j,j} \sim \Gamma(S_j, 1),\ j \in \{m, r\}$, where $\Delta_j = N_j - S_j + 1,\ j \in \{m, r\}$. On the other hand, for RRH tier there is no precoding (SISO transmission technique) and therefore we have the same channel gains h_{x_jj} and g_{x_jj} from any RRH to a typical user and under Rayleigh fading assumption both are exponential distribution† exp(1), i.e., $g_{x_r,j} \sim \Gamma(1, 1)$.

Now, we can describe the received-signal and the aggregated interference for the typical-user $u_0 \in \mathcal{U}_j,\ j \in \{m, r\}$. In this context, the received power at a typical-user located at origin from the BS located at $x_j \in \boldsymbol{\phi}_j$ as $P_j g_{x_jj} \|x_j\|^{-\alpha},\ j \in \{m, r\}$ where $\|x_j\|^{-\alpha}$ is a standard power-law path-loss with exponent α. With universal-frequency reuse assumption, the user suffer interference from all the other BSs except home BS, so the resulting signal-to-interference ratio‡ (SIR) of the typical user, served by a home BS in the j-th tier is given by

$$\mathrm{SIR}_j = \frac{\frac{P_j B_j}{S_j} g_{x_0,j} \left\|x_j\right\|^{-\alpha}}{\sum_{j\in\{m,r\}} I_j} \tag{7.3}$$

with the aggregate interference from jth tier is

$$I_j = \sum_{x\in\Psi_j\setminus\{x_0\}} \frac{P_j B_j}{S_j} g_{x,j} \left\|x_j\right\|^{-\alpha}, \tag{7.4}$$

given that the factor $\frac{1}{S_j}$ is due to the equal power allocation for all the users over the Rayleigh fading channel, and α is the geometric attenuation constant. All the aggregate-interference from j-th tier are due to the interfering BSs located outside

* It is noticeable that this analysis can be used for other distributions of fading links, rather than Rayleigh, that follows Gamma profile after precoding, e.g., Nakagami-m, and reference [116] provide some approaches that can be used to obtain the shape and the scale parameters for the Gamma random variables corresponding to the gains of the interfering and desired channels.

†Other precoding techniques, such as minimum mean square error (MMSE), are left for future work.

‡ We hereby assume interference limited network for simplicity of notation, however, thermal noise can be included in the analysis with some extra work.

of an exclusion region around the typical user denoted by the ball $\mathcal{B}(o, x_j)$ with radius x_j. In this model, although we don't adopt shadow fading, but it can be easily considered by employing BSs' density scaling with a constant according to proposed distribution of the shadow effect.

7.2.3 Distance Distribution

Since MBSs and RRHs are deployed as a poisson point process(PPP), the distances between the serving BS and a typical user Z_j, $j \in \{m, r\}$ is a Rayleigh random variable [125], and the following lemma characterises it's corresponding PDF.

Lemma 7.2 (Distance Distribution)**.** The PDF f_{Z_m} of the distance Z_m between the serving macro BS and a typical user u when $u \in \mathbf{\Phi}_u^m$ is given by

$$f_{Z_m}(z) = \frac{2\pi\lambda_m}{\mathcal{A}_m} z \exp(-\pi(\lambda_m + \lambda_r/\rho^2)z^2), \tag{7.5}$$

and the PDF $f_{Z_r}(z)$ of the distance Z_r between the serving RRH and a typical user u when $u \in \mathbf{\Phi}_u^r$ is given by

$$f_{Z_r}(z) = \frac{2\pi\lambda_r}{\mathcal{A}_r} z \exp(-\pi(\lambda_m\rho^2 + \lambda_r)z^2), \tag{7.6}$$

with $\rho = (\frac{P_r B_r}{P_m B_m})^{-1/\alpha}$, and $\mathcal{A}_m$, $\mathcal{A}_r$ are access probability for MBS and RRH tiers, respectively.

Proof:

Given that $u \in \mathbf{\Phi}_u^j$ is the target user, Z_m is the distance to the nearest macro BS from u, then the cumulative distribution function (CDF), $F_{Z_m}(z) = \mathbb{P}(Z_m \leq z)$, can be expressed as

$$\begin{aligned} F_{Z_m}(z) = \mathbb{P}(Z_m \leq z | u \in \mathbf{\Phi}_u^m) &= \frac{\mathbb{P}(Z_m \leq z, u \in \mathbf{\Phi}_u^m)}{\mathbb{P}(u \in \mathbf{\Phi}_u^m)} \\ &= \frac{1}{\mathcal{A}_m} \int_0^{Z_m} \mathbb{P}\left(Z_m > \frac{y}{\rho}\right) f_{Y_m}(y) dy, \end{aligned} \tag{7.7}$$

where $f_{Y_m}(y) = 2\pi\lambda_m y e^{-\pi\lambda_m y^2}$. The PDF $f_{Z_m}(z)$ in (7.5) is obtained by differentiating (7.7) with respect to z and then applying the probability distributions of Rayleigh r.v.s Z_m for the null probability in the serving area i.e. the ball $\mathcal{B}(o, y/\rho)$, $\mathbb{P}\left(Z_m > \frac{y}{\rho}\right) = e^{-\pi y Z_m^2/\rho}$. □

For the derivation of the PDF $f_{Z_r}(z)$, as the approach is similar, the proof is omitted.

7.3 Performance Metrics

In this section, we introduce key-metrics to measure H-CRAN performance such as the link_connectivity, the rate coverage and the area spectral_efficiency.

7.3.1 The SIR Coverage Analysis

Coverage or link success probability $\mathcal{S}_j$, $j \in \{m, r\}$ is the probability that a serving BS provides a typical-user with downlink SIR_j above a certain threshold $\hat{\gamma}$. The mathematical expression for the overall network coverage can be given as [114], [115], [127]

$$\begin{aligned}\mathcal{S}_{H-CRAN}(\hat{\gamma}) &= \sum_{j\in\{m,r\}} \mathbb{P}[\text{SIR}_j > \hat{\gamma} | j = \text{ associated tier}] \\ &\overset{(a)}{=} \sum_{j\in\{m,r\}} \mathcal{A}_j \, \mathbb{P}[\text{SIR}_j > \hat{\gamma}] \end{aligned} \tag{7.8}$$

with $\mathcal{A}_j$ in (a), is the j-th tier access probability and the term of probability represents CCDF of the SIR_j which depends on the transmission policy employed in the jth tier. As we mentioned before, in the multiple user multiple-antennas transmission scheme the main difficulty of dealing with the SIR expression is the gamma distribution of the direct and interfering channels which require higher order Laplace transform (LT) derivations beside evaluation of LT of the aggregated interference. The following theorems compute the CCDF of the SIR term (eq.7.8) for the MBS and RRH tiers, respectively, using triangular Toeplitz matrix from a linear algebra for the macro BSs tier analysis. First, for the multiple antennas environment in the macro tier the following theorem gives the equation for the coverage probability.

Theorem 7.1 (Macro tier SIR coverage)**.** *The success probability of a typical user served by a MBS cell, assuming an interference limited scenario, is given by*

$$\mathcal{S}_M(\hat{\gamma}) = \kappa \left\| [(k_0 + \kappa)\mathbf{I} + \mathbf{Q}_\Delta]^{-1} \right\|_1, \tag{7.9}$$

wherein, $\kappa = \sum_{j\in\{m,r\}} \lambda_j (P_j B_j)^{-2/\alpha}$, $\|\cdot\|_1$ is the L_1 induced matrix norm (i.e., $\|\mathbf{a}\|_1 = \max_{1\le j\le n} \sum_{i=1}^{m} |\mathsf{a}_{ij}|$ for $\mathbf{a} \in \mathbb{R}^{m\times n}$, $\mathbf{I}$ is a $\Delta \times \Delta$ identity matrix, $\mathbf{Q}_\Delta$ is a

$\Delta \times \Delta$ Toeplitz matrix which can be given as

$$\mathbf{Q}_{\Delta} = \begin{bmatrix} 0 & & & & \\ k_1 & 0 & & & \\ k_2 & k_1 & 0 & & \\ \vdots & & & \ddots & \\ k_{\Delta-1} & k_{\Delta-2} & \cdots & k_1 & 0 \end{bmatrix}, \tag{7.10}$$

with

$$k_0 = \sum_{j\in\{m,r\}} \lambda_j (P_j B_j)^{-2/\alpha} \left\{ {}_2F_1 \left[\begin{matrix} S_j, \frac{-2}{\alpha} \\ 1-\frac{2}{\alpha} \end{matrix} \middle| \frac{-\hat{\gamma} S_m B_m}{S_j B_j} \right] - 1 \right\} \tag{7.11}$$

$$k_i = \sum_{j\in\{m,r\}} \lambda_j (P_j B_j)^{-2/\alpha} \frac{\Gamma(S_j+i)}{\Gamma(S_j)\Gamma(1+i)} \frac{(\frac{-\hat{\gamma} S_m B_m}{S_j B_j})^i}{1-\frac{\alpha}{2}i} \times {}_2F_1 \left[\begin{matrix} i+S_j, i-\frac{2}{\alpha} \\ i+1-\frac{2}{\alpha} \end{matrix} \middle| \frac{-\hat{\gamma} S_m B_m}{S_j B_j} \right], \tag{7.12}$$

and ${}_2F_1(\cdot|\cdot)$ is the ordinary or Gaussian hyper geometric function.

Proof; See appendix D.2. □

On the other hand, for a single-input single-output (SISO) environment in the RRH tier the following theorem provides the coverage equation.

Theorem 7.2 (RRH-tier SIR coverage)**.** *The success probability of a typical user served by a RRH cell is given by*

$$\mathcal{S}_{RRH}(\gamma) = \kappa \left[{}_2F_1 \left[\begin{matrix} 1, -\frac{2}{\alpha} \\ 1-\frac{2}{\alpha} \end{matrix} \middle| -\hat{\gamma} \right] + \kappa_o \, {}_2F_1 \left[\begin{matrix} S_j, -\frac{2}{\alpha} \\ 1-\frac{2}{\alpha} \end{matrix} \middle| -\hat{\gamma} \frac{B_r}{S_m B_m} \right] \right]^{-1} \tag{7.13}$$

where $\kappa_o = \frac{\lambda_m}{\lambda_r} (\frac{P_m B_m}{P_r B_r})^{2/\alpha}$

Proof; See appendix D.3. □

The total coverage for a typical user can be computed in the following corollary according to the total probability theory.

Corollary 7.2.1 (Entire Network SIR coverage)**.** The total success probability of a typical user in the H-CRAN network is given by

$$\mathcal{S}_{H-CRAN}(\hat{\gamma}) = \mathcal{A}_m \mathcal{S}_{MBS}(\hat{\gamma}) + \mathcal{A}_r \mathcal{S}_{RRH}(\hat{\gamma}) \tag{7.14}$$

where $\mathcal{S}_{MBS}(\hat{\gamma})$ and $\mathcal{S}_{RRH}(\hat{\gamma})$ are according to theorems (7.1) and (7.2), respectively. These theorems can be used to characterise the distribution of the data rate for the system as we will see in the next subsection.

7.3.2 The Rate Coverage Analysis

In this section, we derive the complementary cumulative distributive function (CCDF) of the downlink rate (also defined as the rate coverage) and then we analyse the achievable average downlink rate of a typical user associated to different tiers. A typical user in an open access scheme is said to be in rate coverage if its effective downlink-rate is higher than the corresponding target. If we denote the target-rate for a j-th tier BS as τ, then the rate distribution of a typical user u can be mathematically given as

$$\begin{aligned}
\mathcal{Q}_{\text{het}}(\tau) &= \mathbb{P}(\mathcal{Q}_{het} > \tau) \\
&\overset{(a)}{=} \mathbb{P}\left(\bigcup_{j\in\{m,r\}} \max_{x\in\Phi_j} \mathcal{A}_j \ \log_2(1+\text{SIR}(x_j)) > \tau \right) \\
&\overset{(b)}{=} \bigcup_{j\in\{m,r\}} \mathcal{A}_j \, \mathbb{P}\left(\text{SIR}(x_j)) > 2^{\tau} - 1\right) \\
&\overset{(c)}{=} \bigcup_{j\in\{m,r\}} \mathcal{A}_j \, \mathcal{S}_j(2^{\tau} - 1\,)
\end{aligned} \tag{7.15}$$

where, (a) is the total rate distribution of the typical user $u \in \mathbf{\Phi}_u^j$ and follows since the rate equation is $\mathcal{Q}_j = S_j W \log_2(1+\text{SIR}_j)$, $j \in \{m,r\}$ with $\mathcal{A}_j = \mathbb{P}(u \in \mathbf{\Phi}_u^j)$ is the tier association probability, (b) follows after rearranging the inequality term and (c) follows due to the definition of the success probability.

7.3.3 The Area Spectral Efficiency

The Area Spectral Efficiency (ASE) evaluates the overall data-rate (transmitted bits per second) of the network per unit-area normalized by the available bandwidth and therefore, it's a fundamental-metric to measure the capacity and spatial-reuse

efficiency of the network where more users can be served when the network has a higher-ASE. The ASE, mathematically, can be defined as [124]

$$\text{ASE} = \log_2(1 + \hat{\gamma}) \left[S\lambda_m \mathcal{S}_m + \lambda_r \mathcal{S}_r\right] \tag{7.16}$$

where the unit is $(bps/Hz/m^2)$. Note that the formula of ASE in (7.16) is a function of the success probability $\mathcal{S}_j,\ j \in \{m, r\}$, and the number of data streams S, i.e., the MBS spatial multiplexing gain. Since ASE depends on the density of BSs $\lambda_j,\ j \in \{m, r\}$, hence it can tell the capacity gain achieved by cell intensification.

7.3.4 The Rate Analysis

Beside the link-quality metric which characterized in term of SIR, the user average achievable-rate is another key metric of interest for the performance evaluation of H-CRANs, it also depends upon the effective resources-allocated to each user. Here, for tractability, we assume that all BSs within the same tier have an equal number of users and resource allocation. Therefore, in an interference-limited scenario, the downlink rate of a typical user u served by the jth tier BS located at $x_k \in \Phi_j$ (assuming adaptive transmission scheme such that the Shannon limit is supported), can be calculated as [123]

$$\begin{aligned} \mathcal{Q}_j &= \text{BW} S_j \log_2\left[1 + \text{SIR}(x_j)\right],\ j \in \{m, r\} \\ &\overset{(a)}{=} \frac{\text{BW}\,\text{S}_\text{j}}{\ln 2} \int_0^\infty \frac{\mathcal{S}_j(t)}{1+t}\, dt, \end{aligned} \tag{7.17}$$

Next, we can compute the downlink data rate of the overall H-CRAN network as

$$\mathcal{Q}_{het} = \mathcal{A}_m S\, \mathcal{Q}_m + \mathcal{A}_r \mathcal{Q}_r \tag{7.18}$$

As it's mentioned previously in section 7.1, the 5G systems should achieve about 10× energy/spectrum efficiencies increase compared to the 4G systems [105]. Therefore, the following subsection will consider the system performance in terms of SE and EE.

7.3.5 The Spectral and Energy Analysis

A. Spectrum Efficiency; Another principal performance metric in the heterogeneous network is the SE, where higher SE denotes lower spectrum-consumption. The Spectrum-efficiency for the overall system can be expressed as follows

$$SE_{H-CRAN} = \mathcal{A}_m SE_{MBS} \cdot S + \mathcal{A}_r SE_{RRH} \tag{7.19}$$

Obviously, in this equation, SE is directly proportional with the number of the multiplexed users in the MBS tier.

B. Energy Efficiency; The energy_efficiency (bits/Joules) is one of the key performance metrics in 5G emerged Het-Nets and the key point in the sense of green_ communications due to the increasing circuit power consumption especially with densely deployed BSs (higher EE denotes lower energy consumption). Therefore, this section focuses on the energy consumption aspect in the massive aided H-CRANs, where the energy_efficiency for the overall system can be defined as the ratio of the network throughput to the total consumed power, namely

$$EE_{H-CRAN} = \frac{Throughput}{P^{total}} \overset{(a)}{=} \mathcal{A}_m S\, EE_{MBS} + \mathcal{A}_r EE_{RRH} \tag{7.20}$$

where P^{total} accounts for the total power-consumption for both MBS and RRH tiers and can be given by $P^{total} = P_m^{total} + P_r^{total}$, (a) follows using EE of the individual tiers and the total probability theorem. The total power consumption at the RRH can be calculated as [128]

$$P_r^{total} = \frac{K\, P_r}{\eta_r} + P_r^o + P_{fh} \tag{7.21}$$

with, P_r^o is is the RRH's static hardware power-consumption, η_r is the RRH's power amplifier efficiency, K is the number of t/f RBs and P_{fh} is the fronthaul link's power consumption. The total power consumption at the macro-BS, based on [128], can be calculated by the following formula

$$P_m^{total} = \frac{K\, P_m}{\eta_m} + K \sum_{i=1}^{3} \{S^i\, C_{i,0} + S^{i-1} N_t\, C_{i,1}\} + P_m^o + P_{bh} \tag{7.22}$$

where, η_m is the MBS's power amplifier efficiency, P_m^o is the macro BS's static hardware power-consumption*, P_{bh} is the backhaul link's power consumption, $C_{i,0}, C_{i,1}$ are the coefficients of circuit power terms and depends on the number of users and/or number of MBS antenna, precoding, coding decoding, transceiver chains, etc.(Table 7.2 presents the coefficients values under Zero forcing precoding).

7.4 Numerical results

In this section, theoretical results obtained by Theorems 7.1, 7.2 and Corollary 7.2.1 are presented and validated via Monte Carlo trials † which conducted on a square window of $19 \times 19\,\mathrm{Km}^2$ with Gamma distributed desired/interfering channel power-gains. In addition, a numerical analysis is introduced to provide insights into impacts of key design parameters. Unless otherwise stated in figures caption, we set these parameters as given in Table 7.2. First, in Fig.7.2, we analyse the impact of deployment massive antennas array on the tiers association probability. This figure suggests that with a high number of antennas N_t, a typical user is much more likely to correspond with the macro tier than with the RRH tier, owning to the high array gain of the massive scheme.‡

The link reliability (SIR coverage) for both the MBS and RRH tiers are validated via Monte Carlo simulations for different configurations of the system in Fig.7.3 and the overall SIR-distribution of a typical user also is shown. We can observe that the theoretical and numerical simulation curves match well with each other. In addition, this figure highlights some important trends of SIR distribution, where SIR success probability decreases when we increase the number of active users per resource block in each MBS cell due to the increase in interference power and the decrease in direct channel gain (serving link), as discussed before in section 7.2 regarding the transmission strategies in MIMO system, and the variety is more explicit in medium SIR operating regimes. For example, when S increases from 5 to 15 users

* As the static power is a function of the number of MBSs, RRHs and antenna elements, therefore from an EE perspective, it makes sense to put inactive antenna elements and BSs into sleep mode. However, an adaptive sleep/active switching mode requires complicated techniques in the sense of user mobility and transient behaviour [131], which are outside the scope of our research. Instead, we will characterise EE versus densities of MBS, RRH, number of N_t, and S.

† It should be highlighted here, that the results obtained by stochastic geometry (SG) theory are proved to be worst case descriptions compared to those given by system level simulations that consider the overall transceiver processing chain (e.g., see [49] and the references therein).

‡ Consequently, we can reduce the number of RRHs deployed in the network as massive antenna arrays BSs have the potential to sport more number of users, i.e., achieve higher multiplexing gain due to the increase in the available spatial DoF.

per RB, the average-fraction of covered users drops from 98% to 80% if the target SIR value for a typical-user to be under coverage is -17dB, However, at higher SIR threshold levels, the users under coverage are essentially those in the cell interior, therefore increasing S may not significantly affect the SIR of RRH cell interior users. By contrast, at lower SIR threshold levels, it is preferred to multiplex fewer users to achieve better SIR coverage since it can mitigate the dominating interference to other MUEs and RUEs. It's worth mentioning that the validation of Theorems 7.1, 7.2 and Corollary 7.2.1 (for the MBS, RRH tiers and H-CRAN, respectively) naturally, validates the rate distributions derived in subsection 7.3.2.

Next, Fig.7.4 investigates the impact of RRHs density on the rate coverage probability $\mathcal{Q}_r$, i.e., the percentage number of users who are satisfied with their QoS. Here, some important trends can be extracted, where we can observe that $\mathcal{Q}_r$ increases with the increase in RRHs density λ_r (dense RRHs deployment provides the best user rate coverage), the reason is that the averaged distance between the typical user and its serving RRH is shortened, such that the received signal is stronger (lower path loss). For example, if we consider target rate of 0.5 bps-per-Hz, we see that a sparse macro BSs and dense RRHs system achieves almost 20.0% percentage coverage gain (from 35.0% to 55.0%) for the system setting indicated in the figure. To gain a clear understanding of the rate distribution of the RRHs tier and the impact of the number of multiplexed users in MBS tier on the rate coverage of the RRH cells, next plot focuses on the rate coverage of RRHs users.

Fig.7.5, presents the RRHs 5-th percentile rate coverage, i.e., when 95% of RRHs users fulfil data rate higher than the predefined target($\mathcal{Q}_r = 0.95$). Clearly, the plot reveals that the cell edge data rate degrades from 2×10^4 bits/sec to 0.5×10^4 bits/sec as the number of multiplexed MBS users S increased from 2 to 4. The degradation can be interpreted according to the traits of channel gain of serving/interfering links of different transmission strategies for MIMO system where multiplexing more users results in increasing of interference power and reducing the useful power, i.e., higher inter/intra tier interference from the macro BSs tier.

Fig.7.6, illustrates the throughput versus number of MBS antennas N_t for different number of multiplexed users S. The figure shows the following performance-trend: (i) We see that multiplexing more users in the macro-BS cell can significantly enhance the throughput of the H-CRAN. For example, the performance-gain

in throughput for the setting $N_t = 250, S = 15$ is almost $1.2\times$ higher than that for $N_t = 250, S = 5$; (ii) The throughput of the macro-tier increases logarithmically with higher number of transmit-antennas given higher array gain and more users can be supported simultaneously whilst intra-cell interference is mitigated through ZFBF; and (iii) Increasing the transmit antennas of the MBS-tier has negligible impact on the RRHs-tier throughput.

In Fig.7.7, clearly, we observe that the RRHs-tier presents higher gain than the MBSs-tier in terms of EE since they use smaller transmit power also they need lower power for baseband processing. In addition, EE of the RRHs-tier increases with deploying more RRHs in the network λ_r, where serving more users in the RRH-tier can significantly escalate the throughput and consequently increase linearly the EE of the RRHs tier.

Fig.7.8 illustrates the impacts of massive-MIMO on the energy efficiency. We see that EE of the MBSs-tier decreases with increasing the MBS antennas, which is attributed to the fact that more power is required for the precoding process. On the other hand, multiplexing more users in the macro cell can significantly enhance the EE, where higher throughput can be achieved. Also, results demonstrate that, deploying more MBS antennas has a negligible impact on the EE of the RRHs-tier.

Fig.7.9, presents the EE and SE for different degree of MBS-users multiplexing S. First, figure 7.9-(a), indicates that increasing S will increase the EE of MBS-cell, due to increasing SE while the power-consumption is the same. Fig.7.9-(b) indicates that MBS-tier's SE significantly increases as we increase the user's number of the MBS. Accordingly, the SE of the H-CRAN also improves with increasing S. Meanwhile, this increment has a negligible impact on the RRH's SE.

7.5 Conclusion

This chapter develops a tractable framework for two-tier heterogeneous CRAN, where massive MIMO enabled macro cells coexist with single antenna RRHs. The macro tier performs multi user zero forcing beamforming (ZFBF) scheme to serve it's associated users assuming perfect channel state information (CSI). Whereas, the RRH tier applies SISO strategy to serve a single user per each RB. We analyse the success probability and rate distribution of the entire system and address the effect of massive MIMO deployment and RRH-tier density on these metrics.

Table 7.2: Numerical parameters used in the simulation, otherwise specified in figures caption.

PARAMETERS	SETTING
Density of MBSs λ_m	$1/(500^2 \times \pi)$ per square m
The macro BS and RRH static hardware power consumption	$P_m^o = 10W$, $P_r^o = 0.1W$
Power amplifier efficiency coefficients	$\eta_m = 0.3$, $\eta_r = 0.3$
The fronthaul/backhaul links power consumption	$P_{FH} = 0.2W$, $P_{BH} = 0.2W$
The ZFBF precoding power consumption coefficients	$C_{i,0} = \{4.8, 0, 2.08 \times 10^{-8}\}$, $C_{i,1} = \{1, 9.5 \times 10^{-8}, 6.25 \times 10^{-8}\}$
Number of RBs	$K = 25$
Tiers Biasing	$B_m = 1\,dB_m$, $B_r = 10\,dB_m$
Path loss (dB)	$4.0 \log(r)$, r is distance in meter
Large scale shadowing	i.i.d. Log-normal $\sim$ Log_N(μ, σ^2)
multi path fading	i.i.d. Rayleigh distribution $\sim$ exp(1)
Log-normal shadowing parameters μ and σ_{dB}^2	0 and 8dB, respectively [134]
Transmit power	$P_m = 45\,dB_m$, $P_r = 30\,dB_m$
Channel bandwidth	1.0 MHz
Monte Carlo realizations	10^5 geometry-drops

According to the network configuration and the adopted performance metrics, the number of users S and RRHs density λ_r should be carefully designed to achieve the optimal performance otherwise a complex enter tier interference coordination is required. Results show that in a multi user MIMO HetNets scenario the spectral efficiency is always higher than the single user HetNets, whereas the success probability is always smaller due to a limited direct link gain as compared to single user HetNets.

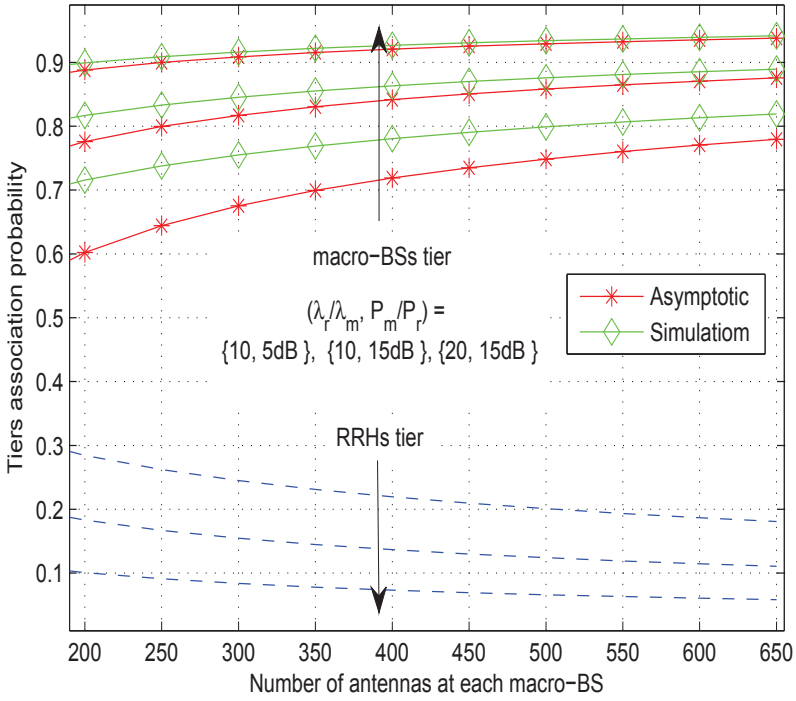

Figure 7.2: The macro/RRH tiers association probability for RRH transmit power $P_r = 30db_m$, and MBS's density $\lambda_m = (500^2 \times \pi)^{-1} m^{-2}$.

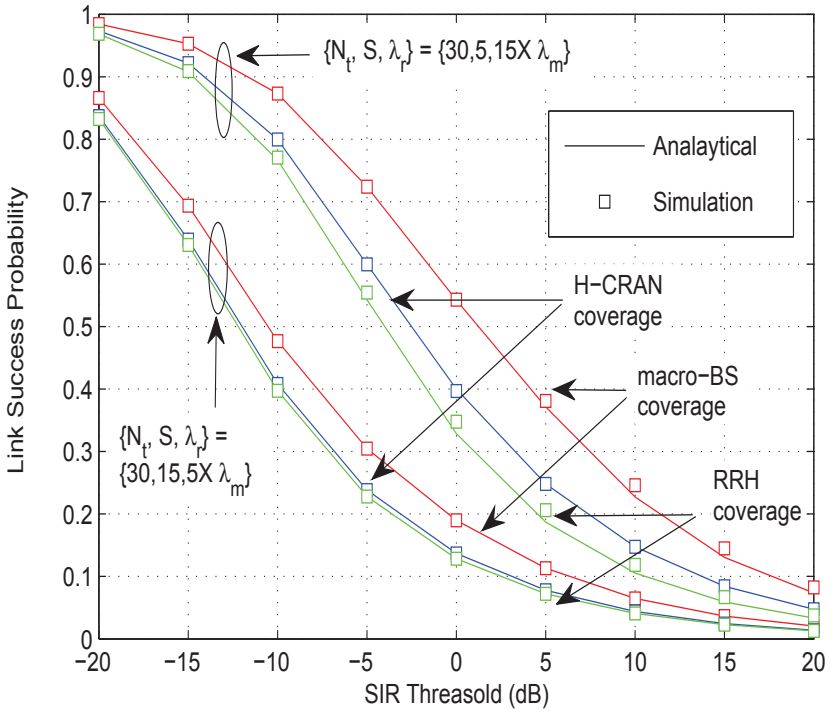

Figure 7.3: Validation of the SIR coverage probability based on Theorems 7.1, 7.2 and Corollary 7.2.1 for the Macro BS, RRH tier and H-CRAN, respectively: path loss $\alpha = 3.5$, and MBS's density $\lambda_m = (500^2 \times \pi)^{-1} m^{-2}$.

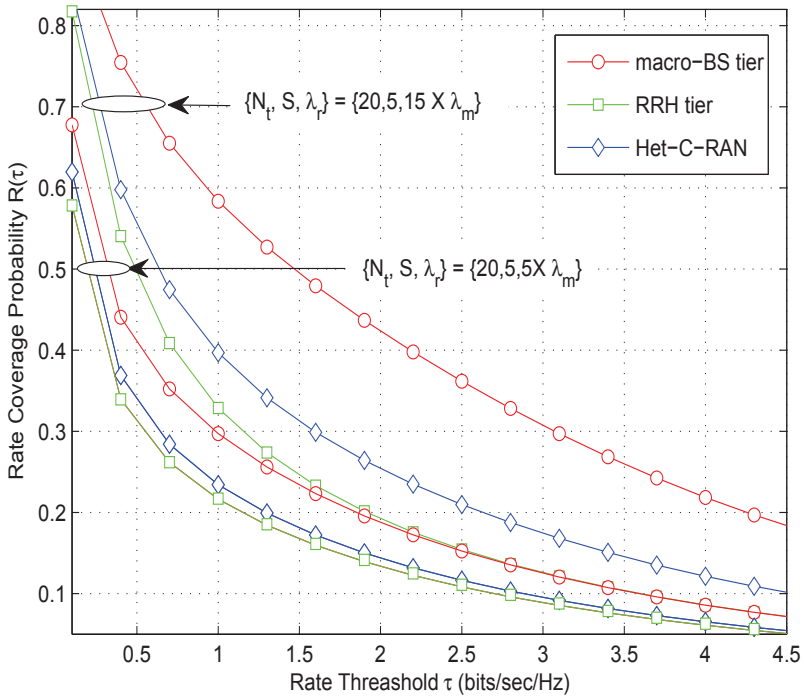

Figure 7.4: The rate coverage probability versus the target-rate for MBS's density of $\lambda_m = (500^2 \times \pi)^{-1} m^{-2}$.

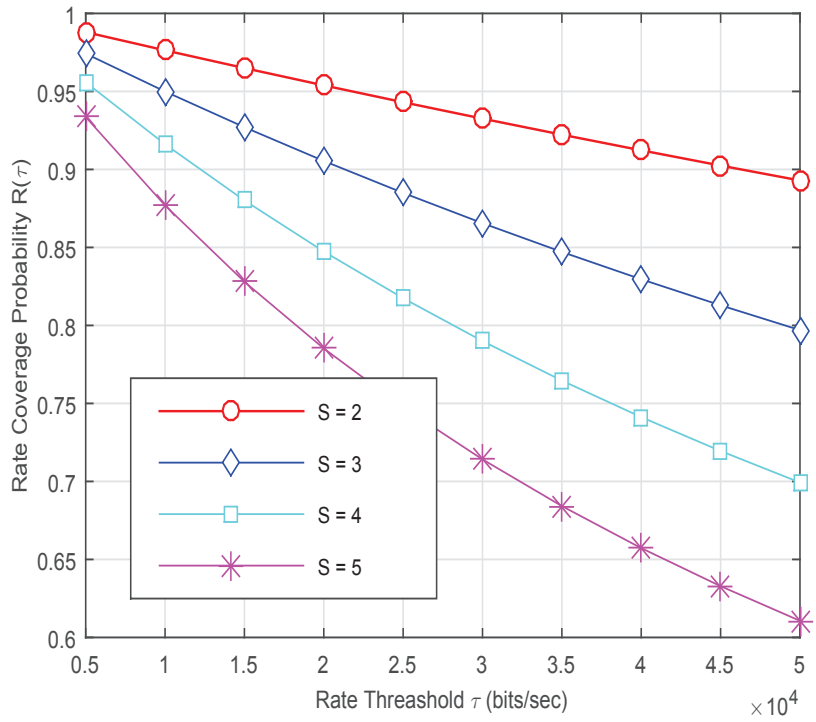

Figure 7.5: The rate coverage probability for the RRH tiers for different number of users S: with RRH's density of $\lambda_r = 20 \times \lambda_m$, path loss $\alpha = 3.5$, and MBS's density $\lambda_m = (500^2 \times \pi)^{-1} m^{-2}$.

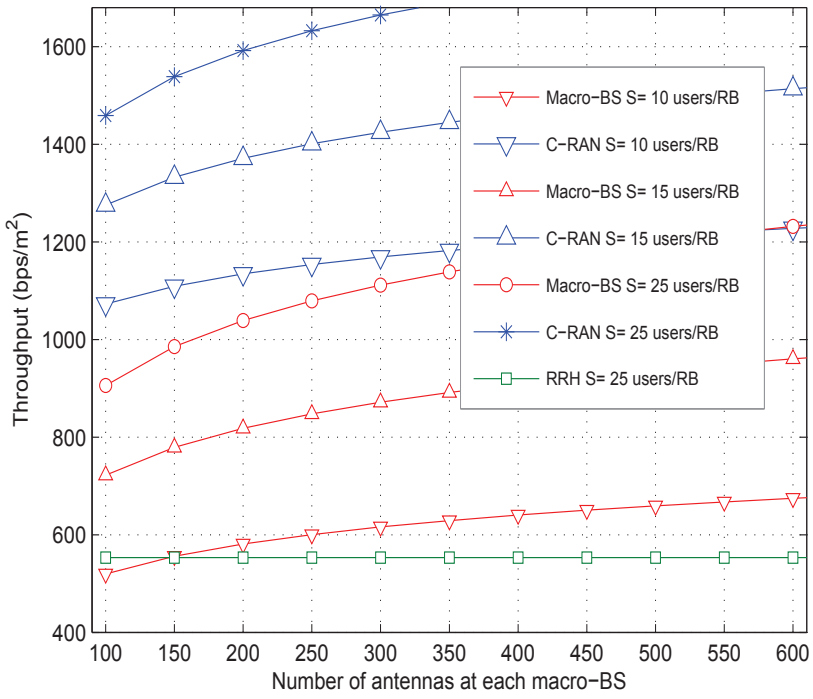

Figure 7.6: The throughput versus number of MBS antennas N_t for different number of multiplexed users S.

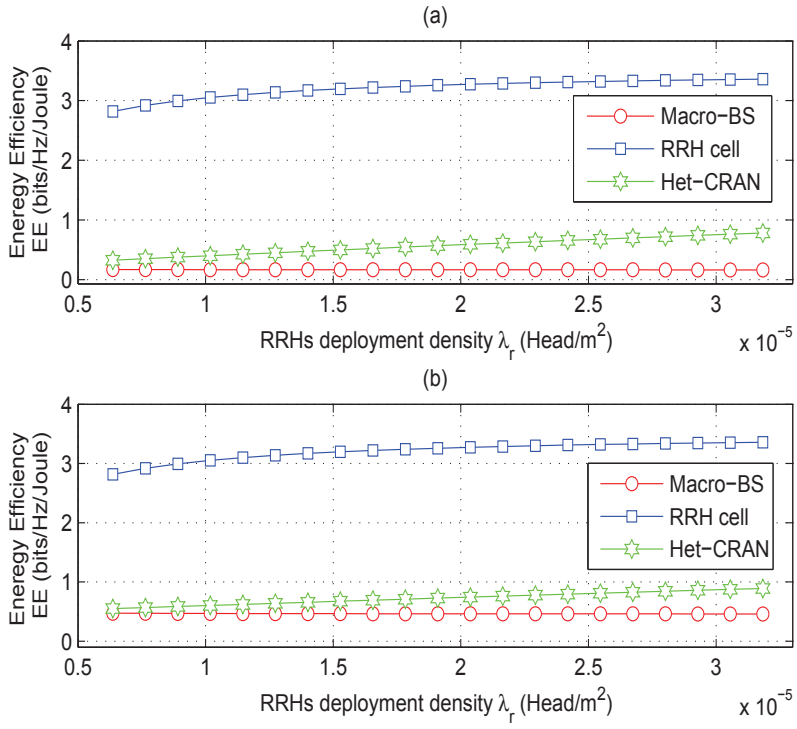

Figure 7.7: Energy efficiency (EE) with MBS antennas of $N_t = 200$; (a) for number of users served by the macro-BS, $S = 10$ and (b) for number of users served by the macro-BS $S = 25$.

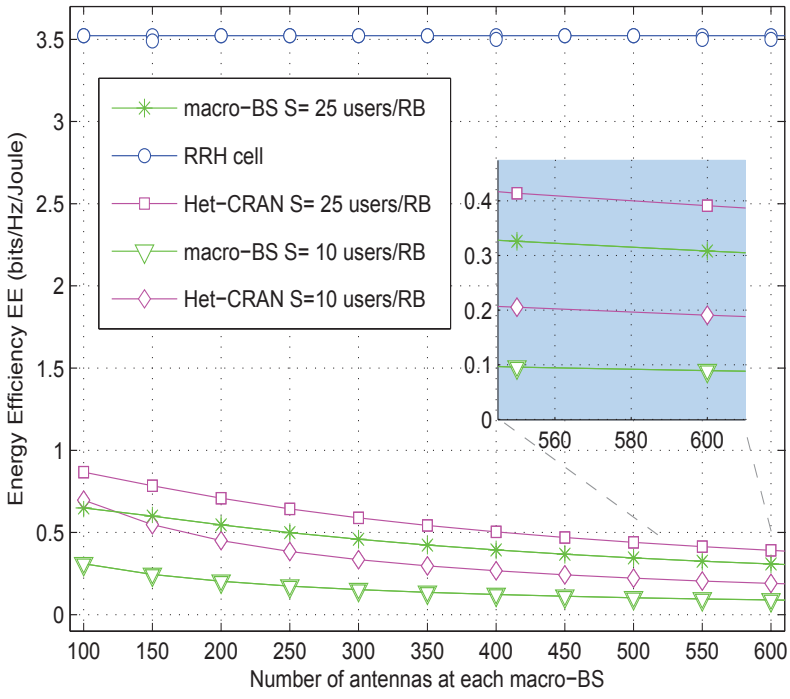

Figure 7.8: The EE versus number of antennas N_t for different number of users S served by the macro BS.

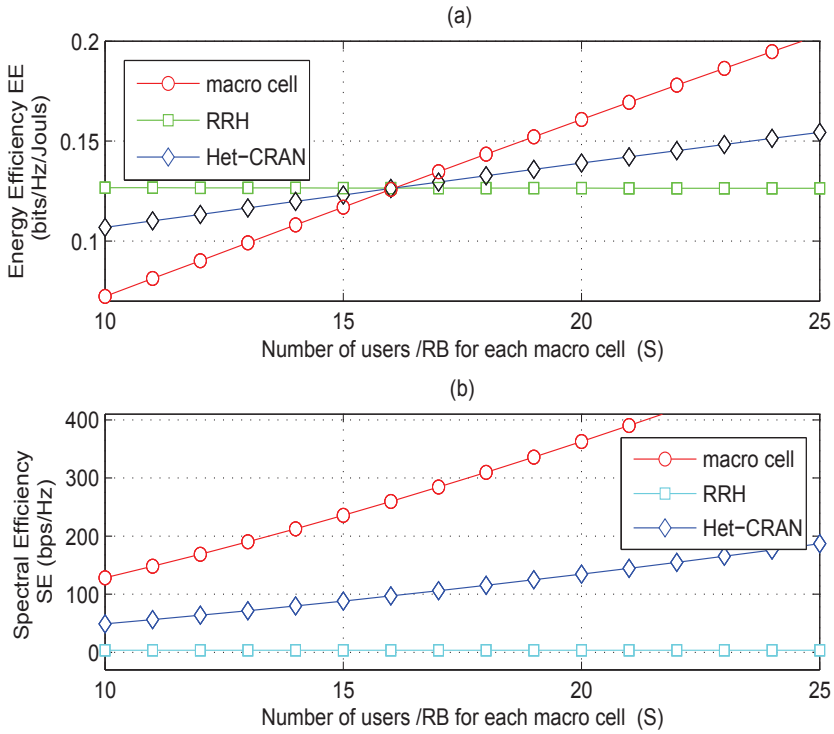

Figure 7.9: The SE and EE versus number of users S served by the macro BS for MBS's antennas of $N_t = 150$.

Chapter 8

Conclusion and future directions

The rapid growth in wireless communications has led to unprecedented demand for the radio frequency (RF) spectrum. This issue motivates the search for modern techniques that will use more efficiently the available radio resources. To this end, we need some alternative technologies to improve the spectral efficiency, either by suppression the co-channels interference or by providing more orthogonal channels within the same spectrum. A set of new technologies is proposed such as dense deployment of BSs and aggressive frequency reuse to efficiently manage the data-traffic demands. However, the proposed techniques create strong across cell interference that greatly degrades overall system performance. Therefore, it is important to consider multiple access strategies that can support a large number of users over same time/frequency resources while contributing less cross users interference. Massive multiple users MIMO is one of the promising technologies in this context due to its' appealing traits. In this thesis, the massive MU-MIMO has been analysed in different scenarios and system architectures. This concluding chapter summarises the principal findings of the thesis and proposes some possible directions for future research.

8.1 Conclusion

The main conclusions of this thesis can be summarised as follows: Chapter 3 has analysed the effective capacity in uplink transmission of an asymptotically large receive antennas system over generalised composed fading channels considering the QoS statistical exponent constraints. In the proposed approach, a location dependent and a location independent (averaged out) closed form expressions are derived

for the effective capacities in an asymptotically large receive antenna system with perfect and imperfect channel state information (CSI) scenarios. In addition, the analytical analysis considers the perfect and imperfect channel information CSI effects. Moreover, expressions for the asymptotically high signal-to-noise ratio regimes, also ,have been established. The conclusions from the obtained results of chapter 3 are twofold. First, proposed approach is a valid analysis approximation and the tractable analytical results of effective capacity can eliminate the need for time-intensive Monte Carlo simulations. Second, random shadowing degrades the QoS and stringent delay constraints can affect considerably the achieved effective capacity as the user's buffer delay constraints gets larger. Importantly, user location impacts on the effective capacity can be extended to different channel models. Chapter 4 has studied the asymptotic behaviour (error and outage probabilities) of a single cell multiple-input multiple-output (MIMO) system aided by a large scale antenna array. Specifically, the uplink transmission over composite fading channel with the power scaling scheme is considered. Where most reported studies in this respect discuss the case of downlink scenario for convenience MIMO systems. Two assumptions are addressed: perfect channel information (CSI) and imperfect- CSI. In both cases, closed form expressions for error and outage probabilities in asymptotically large receive antenna environments are derived. Moreover, users' location impact on system performance is investigated for different channel information scenarios. The findings of chapter 4 reveal that imperfect CSI degrades both the corresponding error probability and rate outage. However, results point out that increasing the number of received antennas at the BS can significantly compensate for this deterioration and improve error and outage probabilities performance. For instance, increasing the number of BS's antennas by 200 elements gives about 87% improvement in outage probability for rate threshold of 5 bps/Hz and certain system parameters.

Chapter 5 has investigated the statistical queueing constraints and pilot contamination phenomenon in random or irregular cellular massive MIMO system where base stations are Poisson distributed. Specifically, tractable analytical expressions are provided for the asymptotic SIR-coverage, rate coverage and the effective capacity under the quality of service (QoS) statistical exponent constraint in uplink transmission when each base station deploys a large number of antennas. Laplace transform of interference is derived with aid of mathematical tools from stochastic geometry. The presented results provide valuable insight into the impacts of key system features mentioned above on the statistical distributions of various system

metrics. Simulations clearly illustrate that the SIR-coverage performance improves as frequency reuse factor increases due to the increases of distances between the typical and interfering UEs. However, a trade off is required in selection FRF when a guaranteed minimum rate is required since increasing FRF will decrease the effective bandwidth. In addition, we show that the QoS constrained capacity is proportional to the path loss exponent and inversely proportional to the pilot reusing probability which in turn is a function of the cell load.

Chapter 6 has addressed the spatial average analysis of the uplink signal to interference ratio (SIR) and throughput in massive MIMO networks with maximum ratio combining (MRC). The analysis incorporates effects of fractional power control (FPC) and other cells interference (ICI) due to the estimation error in channel state information (CSI). Based on an asymptotic approach, tractable expressions are presented for SIR-distributions and specific performance metrics (coverage probability and average rate) in poisson topology model. Moreover, the considered approach is applicable both to random and deterministic network topologies. The impacts of key network features such as fractional power control, path loss exponent and BS density are characterised. More specific, numerical and analytical results draw several key network design insights regarding the SIR-coverage and the average rate in uplink massive MIMO systems. First, depending on network features, the coverage probability in lower 50 th percentile can be maximized by setting FPC compensation fraction between 0.2 and 0.5. Second, for SIR threshold of 0 dB, applying 25% of maximum uplink transmit power can achieve approximately 6% (from 0.78 to 0.84) improvement in coverage probability in cell edge area compared to constant-power policy, i.e., FPC = 0 and about 14% (from 0.70 to 0.84) improvement compared to full channel inversion policy, i.e., FPC = 1.

Chapter 7 has addressed the multiple-input multiple-output (MIMO) aided heterogeneous cloud radio access network (H-CRAN), where massive MIMO enabled macro cells coexist with remote radio heads (RRHs) to potentially achieve high spectral and energy efficiencies. Tractable formulas are established for the link reliability or signal-to-interference-ratio (SIR) distribution and rate coverage of a typical user in H-CRANs, employing a Toeplitz matrix tool from a linear algebra. The macro base station tier (MBS) is assumed to employ a multi user MIMO policy via space division multiple access technique (ZF beamforming with perfect CSI), whereas the second tier, i.e., RRH-tier employs a single user transmission via SISO strategy. According to the network configuration and the adopted performance metrics, the

number of served users and RRHs density should be carefully designed to achieve the optimal performance otherwise a complex enter tier interference coordination is required. Results show that in a multi user MIMO HetNets scenario the spectral efficiency is always higher than the single user HetNets, whereas the success probability is always smaller due to a limited direct link gain as compared to single user HetNets. To conclude, our obtained findings confirm the powerful gain of the massive MIMO for enhancing the throughput of the H-CRANs while small RRH cells are capable of achieving a higher energy efficiency. In addition, the number of the users served, simultaneously (with ZF beamforming) by an MBS can significantly affects the link reliability of the different tiers.

8.2 Future Work

We suggest, as possible future directions of this research, the following:
For the effective capacity in the uplink transmission of a multiuser massive environment, this research has only focused on the zero-forcing (ZF) detector to address the challenges of the QoS statistical exponent constraints. However, it is worth addressing different beamforming techniques, such as the minimum mean square error (MMSE) detector. In addition, the shadow fading has been modelled utilising gamma-distribution to approximate the fading profile. It's worth to quantify the log-normal distribution, where in a wide variety of propagation environments, the shadow fading has been observed, empirically, to obey a log-normal distribution.
For the error and outage probabilities of a single cell multiple-input multiple-output (MIMO) system aided by a large scale antenna array we study the uncorrelated gamma fading scenario. This study can motivate a future research toward addressing the scenario of correlated gamma-channel gain (i.e. non-i.i.d.) instead of i.i.d. gamma fading- environment only.
For the statistical queueing constraints and pilot contamination phenomenon in a random or irregular cellular massive MIMO system, an interesting research-direction is to consider the impact of equipping the user terminals with a different number of receive-antennas, where due to the great development in antenna technology, it is possible to equip the users' terminals with multiple antennas to conduct multiple streams transmission mode. It is also important to consider the impact of fractional power control on the system performance.
For the analysis that considers the impact of uplink fractional power control (FPC)

and other cells interference (ICI), a maximum ratio combining (MRC) strategy has been addressed in this study. It's interesting to address the uplink SIR and the throughput performance of massive MIMO cellular-networks over ZF and MMSE filters as well, while considering the estimation error in CSI acquiring.
For the MIMO aided heterogeneous cloud radio-access networks (H-CRANs), the rate and link reliability formulas are established for both massive MIMO enabled macro cells and remote radio heads (RRHs) in a non-cooperative environment. Since CRANs architectures have fully centralized baseband deployment, theretofore it's worth to think about different type of H-CRANs cooperation strategies such as coordinated multi point processing (CoMP) and multi point transmission (joint transmission (CoMP-JT)) schemes. The former scheme is a coordination mechanism which aims to achieve an optimal SE/EE balance while the latter scheme is a cellular networking cooperation mechanism that allows multiple BSs to jointly serve the same terminal. In addition, the study of optimal cell biasing under different settings of system parameters is an appealing research direction. Also, in this study, we assumed a fully loaded network (fixed number of users per cell), while, practically, each BS will randomly choose a certain number of users to serve at each time slot according to their channel conditions. Thereby, a promising future direction is to consider the analysis of the non fully loaded network (variable number of active users, typical in the realistic scenarios) together with more sophisticated mechanisms such as load balancing and interference coordination.

In the aforementioned analysis we assume that user terminals are uniformly distributed within the cell coverage area, however, it is an appealing trend to consider a scenario of highly non-homogeneous user density which is also referred to as "hot spots". In similar cases of dense irregularly deployed users, it will be important to adopt approaches for cell association that ensure efficient usage of the available wireless infrastructure, i.e., establish an optimal cell association mechanism. Besides, in our analysis, the considered power consumption model assumed that all the MBSs, RRHs and antenna elements are in active mode. However, it is worth addressing, from an EE perspective, a more practical scenario in which inactive MBSs, RRHs and antenna elements are put into sleep mode by adopting, e.g., adaptive sleep mode techniques.

Appendices

Appendix A

Proofs for Ch.3

A.1

Proof of Theorem 3.1.

First, we have to evaluate the following integral

$$\mathcal{I} = \int_0^\infty (1+\rho x)^\nu x^{-\alpha} e^{-\beta x} dx \tag{A.1}$$

Substitute for the first term, employing series representation with binomial coefficient [46, Eq.(1.110)] yields

$$\begin{aligned}(1+\rho x)^\nu &= \sum_{n=0}^{\infty} \rho^n x^n \binom{\nu}{n} \\ &= \sum_{n=0}^{\infty} \rho^n x^n \frac{\Gamma(\nu+1)}{\Gamma(n+1)\Gamma(\nu-n+1)}\end{aligned} \tag{A.2}$$

Substitute in (A.1), then with help of [46, eq.(3.326.2)] $\int_0^\infty x^m \exp -\beta^n dx = \frac{\Gamma(\frac{m+1}{n})}{n\,\beta^{\frac{m+1}{n}}}$, we arrive at the following

$$\mathcal{I} = \sum_{n=0}^{\infty} \frac{\rho^n}{\beta^{\alpha+n+1}} \frac{\Gamma(\nu+1)\Gamma(\alpha+n+1)}{\Gamma(n+1)\Gamma(\nu-n+1)} \tag{A.3}$$

Coefficients and parameters mapping from eq.(3.14) into eq.(A.3) yields

$$\mathcal{I} = \sum_{n=0}^{\infty} (p_u N_r \Omega)^n \frac{\Gamma(1-A)\Gamma(m+n)}{\Gamma(n+1)\Gamma(1-A-n)}, \tag{A.4}$$

with, ν is the geometric path loss attenuation, m is the channel shadowing factor, A is defined by $A \triangleq \theta_k TB/ln2$, T is the block length and B is system bandwidth. Now, using [46, eq.(3.326.2)] we obtain the following

$$\mathcal{I} = \sum_{n=0}^{\infty} (-\rho\Omega)^n \frac{\Gamma(m+n)}{n!\,\Gamma(m)} \frac{\Gamma(A+n)}{\Gamma(A)}, \tag{A.5}$$

In term of pochhammer symbol expression [39, eq.(06.10.02.0001.01)], i.e. using the definition $(\alpha)_n = \dfrac{\Gamma(\alpha+n)}{\Gamma(\alpha)}$, the integration becomes

$$\mathcal{I} = \sum_{n=0}^{\infty} \frac{(m)_n\ (A)_n}{n!} (-\rho\Omega)^n \tag{A.6}$$

One can evaluate $\mathcal{I}$, with aid of the primary definition of the generalized hyper geometric function [39, eq.(07.31.02.0001.01)], i.e.,

$${}_pF_q\left[\begin{matrix} a_1,\ \cdots,\ a_p \\ b_1,\ \cdots,\ b_q \end{matrix}\middle| z\right] = \sum_{n=0}^{\infty} \frac{(a_1)_n,\ \cdots,\ (a_p)_n}{(b_1)_n,\ \cdots,\ (b_q)_n} \frac{z_n}{n!}, \tag{A.7}$$

with, $(x)_n$ is the rising factorial or the Pochhammer polynomial, $(x)_n = \prod_{i=1}^{\infty}(x+i)$, p and q are non-negative integers. Substituting in eq.(3.14), we arrive at

$$C_{P,k}^{asy}(A, D_k, p_u, \Omega, m) = -\frac{1}{A} \log_2 \left\{ {}_2F_0\left[\begin{matrix} m, A \\ \cdots \end{matrix}\middle| \frac{-p_u N_r \Omega}{r_k^{\nu}}\right]\right\}, \tag{A.8}$$

which completes the proof. It is noteworthy that $\mathcal{I}$ can be expressed in term of Tricomi confluent hyper geometric function using the identity [39]

$$\int_0^{\infty} (1+\rho x)^{\nu} x^{-\alpha} e^{-\beta x} dx = \rho^{\alpha-1}\,\Gamma(1-\alpha)\ U(1-\alpha,\ 2+\alpha+\nu\,|\tfrac{\beta}{\rho}), \tag{A.9}$$

and the effective capacity will be

$$C_{P,k}^{asy}(A, D, p_u, \Omega, m) = -\frac{1}{A} \log_2((\frac{r_k^{\nu}}{p_u N_r \Omega})^m\ U(m,\ m+1-A\ |\frac{r_k^{\nu}}{p_u N_r \Omega})), \tag{A.10}$$

where the function $U(\cdot,\cdot|\cdot)$ represents the Tricomi confluent hyper geometric function [39, eq.(07.33.02.0001.01)], [43, eq.(13.2.20)] $U(a,b,z) = \frac{\Gamma(1-b)}{\Gamma(a-b+1)} + O\left(z^{1-\mathcal{R}b}\right)$, $\mathcal{R}b$ is the real part of the coefficient b.

A.2

Proof of Corollary 3.1.1.

Corollary 3.1.1 can be proved as follows. First, from the definition of effective capacity, we have

$$C_{P,k}^{asy}(A, D, p_u, \Omega, m) = -\frac{1}{A}\log_2 \mathbb{E}\Big\{(1+\beta_k p_u N_r)^{-A}\Big\} \tag{A.11}$$

Next, averaging eq.(A.11) over all users yields

$$C_{P,k}^{asy}(A, D, p_u, \Omega, m) = -\frac{1}{A}\log_2 \left\{\frac{1}{K}\sum_{k=1}^{K}\int_0^{\infty} \underbrace{(1+\beta_k p_u N)^{-A} f(x)}_{\mathcal{I}_2}\, dx\right\} \tag{A.12}$$

With the aid of eq.(3.6) $F_R(r) = \begin{cases} \dfrac{(r^2 - R_i^2)}{(R_o^2 - R_i^2)}, & \text{for } r \in (R_i, R_o] \\ 0, & \text{others,} \end{cases}$
that describes the random distribution of users, we get

$$C_{P,k}^{asy}(A, D, p_u, \Omega, m) = -\frac{1}{A}\log_2 \left\{\frac{2}{(R_o^2 - R_i^2)} \times \int_{R_i}^{R_o}\int_0^{\infty} \left(r\ \underbrace{(1+\beta_k p_u N)^{-A} f(x)}_{\mathcal{I}_2}\, dx\, dr\right)\right\} \tag{A.13}$$

Next, the integration $\mathcal{I}_2$ can be evaluated employing same approach used in the (A.8), then effective capacity equation becomes

$$C_{P,k}^{asy}(A, D, p_u, \Omega, m) = -\frac{1}{A}\log_2 \left\{\frac{2}{(R_o^2 - R_i^2)} \int_{R_i}^{R_o} \left(r\ {}_2F_0\left[\begin{matrix} m, A \\ \cdots \end{matrix}\middle| \frac{-p_u N_r \Omega}{r^{\nu}}\right] dr\right)\right\} \tag{A.14}$$

Changing of variables with $z = -\rho\,\Omega/r^{\nu}$, $(\cdots)$ denotes coefficients absence and using the integral identity that involve power and hypergeometric function [39, eq.(07.31.21.0002.01)] with some straightforward manipulation we conclude the proof.

A.3

Proof of Theorem 3.2.

The integral in eq.(3.19) can be re-written as

$$\mathcal{I}_{IP} = \int_0^\infty \left\{1 + \tau \frac{\Omega^2 p_u^2 N_r}{r_k^{2\nu}}\right\}^{-A} \frac{x^{m-1}}{\Gamma(m)\Omega} e^{-x/\Omega} dx \tag{A.15}$$

Employing similar approach used in Appendix-A, with help of [46, eq.(3.326.2)] $\int_0^\infty x^m \exp -\beta^n dx = \frac{\Gamma(\frac{m+1}{n})}{n\,\beta^{\frac{m+1}{n}}}$, we arrive at the following equation

$$\mathcal{I}_{IP} = \sum_{n=0}^{\infty} \left\{\frac{-\tau p_u^2 N_r \Omega^2}{r_k^{2\nu}}\right\}^n \frac{\Gamma(m+2n)}{\Gamma(n+1)} \frac{\Gamma(A+n)}{\Gamma(A)} \tag{A.16}$$

Using multiple argument property of gamma function [39, eq.(06.05.16.0006.01)]

$$\begin{aligned}\Gamma(m+2n) &= \Gamma(2(\tfrac{m}{2}+n)) \\ &= \frac{2^{m-1/2}}{\sqrt{2\pi}} 2^{2n}\, \Gamma(\tfrac{m}{2}+n)\, \Gamma(\tfrac{m+1}{2}+n)\end{aligned}$$

After some simple manipulation and employing pochhammer symbol definition, the expression in eq.(A.16) becomes

$$\mathcal{I}_{IP} = \sum_{n=0}^{\infty} \frac{(\frac{m}{2})_n\ (\frac{m+1}{2})_n\ (A)_n}{n!} \left\{\frac{-\tau p_u^2 N_r \Omega^2}{r_k^{2\nu}}\right\}^n \tag{A.17}$$

With aid of the primary definition of the generalized hyper geometric function [39, eq.(07.31.02.0001.01)], i.e., ${}_pF_q\left[\begin{matrix}a_1,\cdots,a_p\\ b_1,\cdots,b_q\end{matrix}\middle| z\right] = \sum_{n=0}^{\infty} \frac{(a_1)_n,\ \cdots,\ (a_p)_n}{(b_1)_n,\ \cdots,\ (b_q)_n} \frac{z_n}{n!}$, , we can evaluate $\mathcal{I}_{IP}$. Finally, plugging again into eq.3.14
$C_{P,k}^{asy}(A, D_k, p_u, \Omega, m) = -\frac{1}{A}\log_2 \int_0^\infty \underbrace{(1+\beta_k p_u N_r)^{-A} f(x) dx}_{\mathcal{I}}$,
we arrive at

$$C_{IP,k}^{asy}(A, D_k, p_u, \Omega, m) = -\frac{1}{A}\log_2 \left\{{}_3F_0\left[\begin{matrix}\frac{m}{2}, \frac{m+1}{2}, A\\ --\end{matrix}\middle| \frac{-4\tau p_u^2 N_r \Omega^2}{r_k^{2\nu}}\right]\right\}, \tag{A.18}$$

which concludes the proof.

A.4

Proof of Corollary 3.2.1.

Thanks to the analysis used in Appendix-A.2, employing similar methodology, we get the following

$$C_{P,k}^{asy}(A, D, p_u, \Omega, m) = -\frac{1}{A}\log_2\left\{\frac{2}{(R_o^2 - R_i^2)} \times \int_{R_i}^{R_o} r \; {}_3F_0\left[\begin{matrix}\frac{m}{2}, \frac{m+1}{2}, A \\ \cdots\end{matrix}\middle| \frac{-\tau p_u^2 N_r \Omega^2}{r_k^{2\nu}}\right] dr\right\} \quad \text{(A.19)}$$

Changing of variables by setting $z = -\tau p_u^2 N_r \Omega^2 / r_k^{2\nu}$, and using the integral identity that involve power and hyper geometric function [39, eq.(07.31.21.0002.01)]

$$\int z^{\alpha-1} \; {}_pF_q\left[\begin{matrix}a_1, \cdots, a_p \\ b_1, \cdots, b_q\end{matrix}\middle| z\right] dz = \frac{z^\alpha}{\alpha} \; {}_{p+1}F_{q+1}\left[\begin{matrix}\alpha, a_1, \cdots, a_p \\ \alpha+1, b_1, \cdots, b_q\end{matrix}\middle| z\right] \quad \text{(A.20)}$$

and after some basic algebra, we straightforwardly arrive at proof of eq.(3.21), i.e.,

$$C_{IP}^{asy}(A, D_k, p_u, \Omega, m) = -\frac{1}{A}\log_2\left\{\frac{R_o^2}{(R_o^2 - R_i^2)} \; {}_4F_1\left[\begin{matrix}\frac{-1}{\nu}, \frac{m}{2}, \frac{m+1}{2}, A \\ \frac{(\nu-1)}{\nu}\end{matrix}\middle| \frac{-4\tau p_u^2 N_r \Omega^2}{R_o^{2\nu}}\right] - \frac{R_i^2}{(R_o^2 - R_i^2)} \; {}_4F_1\left[\begin{matrix}\frac{-1}{\nu}, \frac{m}{2}, \frac{m+1}{2}, A \\ \frac{(\nu-1)}{\nu}\end{matrix}\middle| \frac{-4\tau p_u^2 N_r \Omega^2}{R_i^{2\nu}}\right]\right\} \quad \text{(A.21)}$$

Appendix B

Proofs for Ch.4

B.1

Proof of Proposition 4.1.

To obtain the unconditional average bit error probability (BEP), first we invoke the conditional error probability given by eq.(4.5)

$$\mathcal{P}_e(\gamma_k) = \frac{1}{2}\left\{1 - \frac{\gamma(b, a\gamma_k)}{\Gamma(b)}\right\}, \tag{B.1}$$

which then, can be averaged over the statistical distribution of the SNR (eq.(4.4)) $\gamma_k - \frac{p_u N_r}{D^\nu} \xrightarrow[N_r \to \infty]{a.s} 0$, that means finding the expectation over the shadowing distribution, [29, eq.26] as follows

$$\begin{aligned}\mathcal{P}_{e_k}^{(P)}(D, N_r, p_u, m) &= \mathbb{E}_{\mu_k}\left\{\frac{1}{2} - \frac{(a\gamma_k)^b}{2\Gamma(b+1)}\ {}_1F_1\left[\begin{matrix} b \\ b+1 \end{matrix}\middle| -a\gamma_k\right]\right\} \\ &= \int_0^\infty \left\{\frac{1}{2} - \frac{(axp_u N_r/D^\nu)^b}{2\Gamma(b+1)}\ {}_1F_1\left[\begin{matrix} b \\ b+1 \end{matrix}\middle| -\frac{axp_u N_r}{D^\nu}\right]\frac{x^{m-1}e^{-x/\Omega}}{\Omega^m\Gamma(m)}\right\}\mathrm{d}x \end{aligned} \tag{B.2}$$

where first line of eq.(B.2) follows by using hyper geometric identity of incomplete gamma function [46, eq.(8.351)]

$$\Gamma(\alpha,\, z) = \frac{(z)^\alpha}{\alpha}\ {}_1F_1\left[\begin{matrix} \alpha \\ \alpha+1 \end{matrix}\middle| -z\right], \tag{B.3}$$

and $\mathbb{E}(\cdot)$ is the expectation operator over the random variable μ_k, i.e., large scale shadowing In term of pochhammer symbol expression [39, eq.(06.10.02.0001.01)],

i.e. using the definition $(\alpha)_n = \dfrac{\Gamma(\alpha+n)}{\Gamma(\alpha)}$, the integration B.2 becomes

$$\mathcal{P}_{e_k}^{(P)}(D,N_r,p_u,m) = \int_0^\infty \left\{ \frac{1}{2} - \frac{(axp_uN_r/D^\nu)^b}{2\Gamma(b+1)} \times \sum_{n=0}^{\infty} \frac{(b)_n}{n!\ (b+1)_n} (-\frac{axp_uN_r}{D^\nu})^n \ \frac{x^{m-1}e^{-x/\Omega}}{\Omega^m\,\Gamma(m)} \right\} \mathrm{d}x \tag{B.4}$$

Interchanging summation symbol with integration and re-arranging terms yields

$$\mathcal{P}_{e_k}^{(P)}(D,N_r,p_u,m) = \frac{\Omega m}{2} - \frac{(ap_uN_r/D^\nu)^b}{2\Omega^m\Gamma(m)\,\Gamma(b+1)} \times \sum_{n=0}^{\infty} \frac{(b)_n}{n!\ (b+1)_n} \left(- \frac{ap_uN_r}{D^\nu} \right)^n \int_0^\infty \Big(\underbrace{x^{n+b+m-1}\, e^{-x/\Omega}}_{\mathcal{I}} \Big)\, \mathrm{d}x \tag{B.5}$$

Since we set $\Omega = 1/m$, so the mean Ωm is equal to one (a unit mean gamma r.v.) and henceforth, we will use this normalisation. Now, invoking the primary definition of gamma function [46, eq.(3.326.2)],
$\int_0^\infty x^m \exp -\beta^n dx = \dfrac{\Gamma(\frac{m+1}{n})}{n\,\beta^{\frac{m+1}{n}}}$, the integration $\mathcal{I}$ can be evaluated as

$$\begin{aligned} \mathcal{I} &= \Omega^{n+b+m}\Gamma(n+b+m) \\ &= \Omega^{n+b+m}\,\Gamma(b+m)\,(b+m)_n \end{aligned} \tag{B.6}$$

where the second line in (B.6) follows from the identity for gamma function given by [39, eq.(06.05.16.0003.01)] $\Gamma(\alpha+n) = \Gamma(\alpha)\,(\alpha)_n$

Next, substitution for $\mathcal{I}$ in eq.(B.5) gives

$$\mathcal{P}_{e_k}^{(P)}(D,N_r,p_u,m) = \frac{1}{2} - \frac{(ap_uN_r/D^\nu)^b\,\Gamma(b+m)}{2\Omega^m\,\Gamma(m)\,\Gamma(b+1)} \times \sum_{n=0}^{\infty} \frac{(b)_n, (b+m)_n}{n!\ (b+1)_n} \left(- \frac{ap_uN_r}{D^\nu} \right)^n \tag{B.7}$$

Now, by invoking [39, eq.(07.31.02.0001.01)], i.e., the definition of the generalized hyper geometric function ${}_pF_q\left[\begin{matrix}a_1,\cdots,a_p\\ b_1,\cdots,b_q\end{matrix}\middle| z\right] = \sum_{n=0}^{\infty} \dfrac{(a_1)_n,\ \cdots,\ (a_p)_n}{(b_1)_n,\ \cdots,\ (b_q)_n} \dfrac{z_n}{n!}$, the proof will

be straightforwardly completed and we arrive at

$$C_{IP,k}^{asy}(A, D_k, p_u, \Omega, m) = -\frac{1}{A}\log_2\left\{{}_3F_0\left[\begin{matrix}\frac{m}{2}, \frac{m+1}{2}, A \\ -- \end{matrix}\middle| \frac{-4\tau p_u^2 N_r \Omega^2}{r_k^{2\nu}}\right]\right\} \tag{B.8}$$

B.2

Proof of Theorem 4.1.

Assuming uniform distributed users given in eq.(3.6)

$$F_R(r) = \begin{cases} \dfrac{(r^2 - R_i^2)}{(R_o^2 - R_i^2)}, & \text{for } r \in (R_i, R_o] \\ 0, & \text{others,} \end{cases} \tag{B.9}$$

then the spatial averaging of asymptotical error probability eq.(B.4) can be expressed as

$$\mathcal{P}_e^{(P)}(D, N_r, p_u, m) = \frac{1}{2} - \frac{1}{(R_o^2 - R_i^2)}\int_{R_i}^{R_o}\left[r\left\{\frac{(ap_uN_r/r^\nu)^b\,\Gamma(b+m)}{\Omega^m\,\Gamma(m)\,\Gamma(b+1)} \times \sum_{n=0}^{\infty}\frac{(b)_n, (b+m)_n}{n!\;(b+1)_n}\left(-\frac{ap_uN_r}{r^\nu}\right)^n\right\}\right]dr \tag{B.10}$$

Using the basic definite integral identity $\int r^a dr = \frac{r^{a+1}}{a+1}$ result in

$$\mathcal{P}_e^{(P)}(D, N_r, p_u, m) = \frac{1}{2} - \frac{1}{(R_o^2 - R_i^2)}\left|\left[r^2\,\frac{(ap_uN_r/r^\nu)^b\,\Gamma(b+m)}{\Omega^m\,\Gamma(m)\,\Gamma(b+1)} \times \sum_{n=0}^{\infty}\frac{(b)_n, (b+m)_n}{n!\;(b+1)_n}\left(-\frac{ap_uN_r}{r^\nu}\right)^n\right]\right|_{R_i}^{R_o} \tag{B.11}$$

Then, after the substitution of integration limits we conclude the proof using the definition of the generalized hyper geometric function [39, eq.(07.31.02.0001.01)], i.e., ${}_pF_q\left[\begin{matrix}a_1,\cdots,a_p \\ b_1,\cdots,b_q\end{matrix}\middle| z\right] = \sum_{n=0}^{\infty}\frac{(a_1)_n,\,\cdots,\,(a_p)_n}{(b_1)_n,\,\cdots,\,(b_q)_n}\frac{z_n}{n!}$.

B.3

Proof of Proposition 4.2.

Invoking eq.(4.10) for the SNR

$$\gamma_k - \frac{\tau p_u^2 N_r}{D^{2\nu}} \xrightarrow[N_r \to \infty]{a.s} 0 \qquad \texttt{for fixed} \quad K \tag{B.12}$$

and eq.(3.5) for the channel distribution

$$f(x) = \frac{x_k^{m-1}}{\Gamma(m_k)\Omega_k^{m_k}} e^{-x/\Omega_k} U(0), \quad x, m_k, \Omega_k > 0, \tag{B.13}$$

and with help of eq.([46, eq.(3.351)])

$$\Gamma(\alpha,\, z) = \frac{(z)^\alpha}{\alpha}\ {}_1F_1\left[\begin{matrix}\alpha \\ \alpha+1\end{matrix}\middle| -z\right], \tag{B.14}$$

the average bit probability (BEP) in eq.(4.5) $\mathcal{P}_e(\gamma_k) = \frac{1}{2}\left\{1 - \frac{\gamma(b, a\gamma_k)}{\Gamma(b)}\right\}$, can be expressed as follows

$$\mathcal{P}_{e_k}^{(IP)}(D, N_r, p_u, m) = \int_0^\infty \left\{\frac{1}{2} - \frac{(a\tau x^2 p_u^2 N_r/D^{2\nu})^b}{2\Gamma(b+1)}\ {}_1F_1\left[\begin{matrix}b \\ b+1\end{matrix}\middle| -\frac{a\tau x^2 p_u^2 N_r}{D^{2\nu}}\right] \frac{x^{m-1}e^{-x/\Omega}}{\Omega^m \Gamma(m)}\right\} \mathrm{d}x \tag{B.15}$$

Similar to Appendix B.1, we have

$$\mathcal{P}_{e_k}^{(IP)}(D, N_r, p_u, m) = \frac{1}{2} - \frac{(a\tau p_u^2 N_r/D^{2\nu})^b}{2\Omega^m \Gamma(m)\Gamma(b+1} \sum_{n=0}^{\infty} \left\{\frac{(b)_n}{n!\ (b+1)_n} \times \left(-\frac{a\tau p_u^2 N_r}{D^{2\nu}}\right)^n \int_0^\infty \Big[\underbrace{x^{2n+2b+m-1} e^{-x/\Omega}}_{\mathcal{I}_2}\Big] \mathrm{d}x\right\} \tag{B.16}$$

With the aid of the identity [46, eq.(3.326.2)] $\int_0^\infty x^m \exp -\beta^n dx = \frac{\Gamma(\frac{m+1}{n})}{n\, \beta^{\frac{m+1}{n}}}$, the integration $\mathcal{I}_2$ can be evaluated as

$$\mathcal{I}_2 = \Omega^{2n+2b+m}\ \Gamma(2n+2b+m) \tag{B.17}$$

Now, using multiplication theorem of gamma function [39, eq.(06.05.16.0006.01)]

or [46, eq.(8.335)]

$$\begin{aligned}\Gamma(2n+2b+m) &= \Gamma(2(\frac{2b+m}{2}+n)) \\ &= \frac{2^{2b+m-1/2}}{\sqrt{2\pi}}\ 2^{2n}\,\Gamma(\tfrac{2b+m}{2}+n)\,\Gamma(\tfrac{2b+m+1}{2}+n)\end{aligned}$$

Plugging it again into eq.(B.16) yields

$$\begin{aligned}\mathcal{P}_{e_k}^{(IP)}(D,N_r,p_u,m) = \frac{1}{2} - \frac{(\frac{4a\tau p_u^2 N_r}{D^{2\nu}})^b\,\Gamma(\frac{2b+m}{2})}{\Omega^m\,\Gamma(m)\,\Gamma(b+1)}\,\frac{\Gamma(\frac{2b+m+1}{2})}{2^{2-m}\sqrt{\pi}} \\ \times\sum_{n=0}^{\infty}\frac{(b)_n\ (\frac{2b+m}{2})_n\ (\frac{2b+m+1}{2})_n}{n!\ (b+1)_n}\left[-\frac{4a\tau p_u^2 N_r}{D^{2\nu}}\right]^n\end{aligned} \tag{B.18}$$

Finally, with the aid of the generalized hypergeometric function definition [39, eq.(07.31.02.0001.01)], i.e., ${}_pF_q\left[\begin{matrix}a_1,\cdots,a_p\\ b_1,\cdots,b_q\end{matrix}\middle| z\right] = \sum_{n=0}^{\infty}\frac{(a_1)_n,\ \cdots,\ (a_p)_n}{(b_1)_n,\ \cdots,\ (b_q)_n}\frac{z_n}{n!}$, we straightforwardly conclude the proof.

B.4

Proof of Proposition 4.3.

Simple observation of equations (4.9) and (4.10), i.e., $R^{asy} \approx \log_2(1+\tau\beta_k^2 E_u^2)$, and $\gamma_k - \frac{\tau p_u^2 N_r}{D^{2\nu}} \xrightarrow[N_r\to\infty]{a.s} 0$, one may deduce the following expression for the rate outage probability

$$\mathcal{P}_{out_k}(D,N_r,p_u,m) = Pr\left[\frac{p_u N_r \mu_k}{D^\nu} < 2^{R_{th}} - 1\right] \tag{B.19}$$

Since μ_k is random variable (channel is random variable (r.v.) with gamma distribution), therefore, the probability of this inequality is simply the commutative distribution function (CDF) for this r.v.

$$\mathcal{P}_{out_k}(D,N_r,p_u,m) = \int_0^{\chi}\left\{\frac{x p_u N_r}{D^\nu}\,\frac{x^{m-1}e^{-x/\Omega}}{\Omega^m\Gamma(m)}\right\}\mathrm{d}x, \tag{B.20}$$

given that $\chi = (2^{R_{th}} - 1)$. Setting new variable $z = x/\Omega$, we obtain

$$\mathcal{P}_{out_k}(D, N_r, p_u, m) = \int_0^{\chi} \left\{ \frac{z\Omega p_u N_r}{D^{\nu}} \frac{z^{m-1} e^{-z}}{\Gamma(m)} \right\} \mathrm{d}z \tag{B.21}$$

Now, invoking the identity [39, eq.(06.06.02.0001.01)] for lower incomplete gamma function, i.e., $\Gamma(a,\, z) = \int_a^{\infty} t^{a-1} \exp(-t)\, dt$ and then express gamma function in term of confluent hyper geometric function [43, eq.(8.5.3)], [46, eq.(3.351)]

$$\gamma(a, z) = \frac{z^a}{a}\, {}_1F_1\left[\begin{matrix} a \\ a+1 \end{matrix} \middle| -z \right], \tag{B.22}$$

after simple parameters and coefficients mapping, we arrive at

$$\mathcal{P}^{(P)}_{out_k}(D, N_r, p_u, m) = \frac{(D^{\nu}\,(2^{R_{th}} - 1)/p_u N_r \Omega)^m}{m\,\Gamma(m)} \times {}_1F_1\left[\begin{matrix} m \\ m+1 \end{matrix} \middle| -\frac{D^{\nu}\,(2^{R_{th}} - 1)}{p_u N_r \Omega} \right],$$

and this concludes the proof.

B.5

Proof of Proposition 4.4.

From equations (4.8) and (4.11), i.e.,

$$\mathcal{P}^{(P)}_{e}(D, N_r, p_u, m) = \frac{1}{2} - \frac{\Gamma(m+b)}{(2-b\nu)\Gamma(b+1)\Gamma(m)} \left\{ \frac{a^b R_o^2 (p_u N_r \Omega / R_o^{\nu})^b}{(R_o^2 - R_i^2)}\, {}_3F_2\left[\begin{matrix} b, b+m, b-\frac{2}{\nu} \\ b+1, b-\frac{2}{\nu}+1 \end{matrix} \middle| \frac{-p_u N_r \Omega}{R_o^{\nu}} \right] - \frac{a^b R_i^2 (p_u N_r \Omega / R_i^{\nu})^b}{(R_o^2 - R_i^2)}\, {}_3F_2\left[\begin{matrix} b, b+m, b-\frac{2}{\nu} \\ b+1, b-\frac{2}{\nu}+1 \end{matrix} \middle| -\frac{a p_u N_r \Omega}{R_i^{\nu}} \right] \right\}$$

and

$$\mathcal{P}^{(IP)}_{e_k}(D, N_r, p_u, m) = \frac{1}{2} - \frac{(a\rho)^b \Gamma(b + \frac{m}{2}) \Gamma(b + \frac{(m+1)}{2})}{2^{2-m}\sqrt{\pi}\Gamma(b+1)\Gamma(m)}\, {}_3F_1\left[\begin{matrix} b, b+\frac{m}{2}, b+\frac{m+1}{2} \\ b+1 \end{matrix} \middle| -a\rho \right],$$

we obtain the following rate outage probability expression

$$\mathcal{P}_{out_k}(D, N_r, p_u, m) = Pr\left[\frac{\tau p_u^2 \mu_k^2 N_r}{D^{2\nu}} < 2^{R_{th}} - 1\right] \tag{B.23}$$

Employing similar procedure used in Appendix-B.4, we get the following

$$\mathcal{P}_{out_k}^{(IP)}(D, N_r, p_u, m) = \int_0^{\chi} \left\{ \frac{\tau(z\Omega p_u)^2 N_r}{D^{2\nu}} \; \frac{z^{m-1}e^{-z}}{\Gamma(m)} \right\} \mathrm{d}z \tag{B.24}$$

The proof can be completed by exploiting once more the identity given by [39, eq.(06.06.02.0001.01)], i.e., $\Gamma(a,\, z) = \int_a^{\infty} t^{a-1} \exp(-t)\, dt$ and then express gamma function in term of confluent hyper geometric function [43, eq.(8.5.3)], [46, eq.(3.351)]

$$\gamma(a, z) = \frac{z^a}{a} \; {}_1F_1\left[\begin{matrix} a \\ a+1 \end{matrix}\middle| -z\right], \tag{B.25}$$

with some straightforward algebraic manipulation, we arrive at the final equation

$$\mathcal{P}_{out_k}^{(IP)}(D, N_r, p_u, m) = \frac{(D^{2\nu}\,(2^{R_{th}} - 1)/\tau p_u^2 N_r \Omega)^{(m+2)}}{(m+2)\,\Gamma(m+2)} \quad {}_1F_1\left[\begin{matrix} m+2 \\ m+3 \end{matrix}\middle| -\frac{D^{2\nu}\,(2^{R_{th}} - 1)}{\tau p_u^2 N_r \Omega}\right] \tag{B.26}$$

.

Appendix C

Proofs for Ch.5

C.1

Proof of Theorem 5.1.

Starting with the formal definition of coverage probability, as the tail Probability of SIR, i.e., CCDF of SIR averaged over the distribution of the users, we have

$$\begin{aligned}\mathbf{P}_{cov}(T_1,\lambda_b,\nu) =& \mathbb{E}_r\Big[\mathbb{P}\Big\{SIR > T_1\Big\}\Big] \\ \overset{(a)}{=}& \int_0^{R_o} \mathbb{P}\Big\{SIR > T_1\Big\} f_{R_o}(r)dr \end{aligned} \tag{C.1}$$

Now, we are going to characterize the statistical distribution of SIR in (C.1) conditioned on user location r_{bbp} (where r_{bbp} denotes the distance between the user which employs pth pilot sequence, i.e., UE_{bp} and base station BS_b), namely

$$\begin{aligned}\mathbb{P}\Big\{SIR > T_1\Big\} \overset{(a)}{=}& \mathbb{P}\Bigg\{\beta_{bbp}^2 > T_1\, r_{bbp}^{2\nu} \sum_{l\in\mathcal{B}\setminus\{b\}} \frac{\alpha_{bl}\,\beta_{blp}^2\,\chi_{lp}}{r_{blp}^{2\nu}}\Bigg\} \\ \overset{(b)}{=}& \mathbb{E}_{I_{bp},\beta^2}\Bigg\{\exp\Bigg[-T_1\, r_{bbp}^{2\nu} \sum_{l\in\mathcal{B}\setminus\{b\}} \frac{\alpha_{bl}\,\beta_{blp}^2\,\chi_{lp}}{r_{blp}^{2\nu}}\Bigg]\Bigg\} \\ \overset{(c)}{=}& \mathbb{E}_{I_{bp},\beta^2,r}\Big\{e^{-T_1\, r_{bbp}^{2\nu}\, I_{bp}}\Big\} \\ \overset{(d)}{=}& \mathbb{E}_{I_{bp},\beta^2}\Big\{e^{-s\, I_{bp}}\Big\} \\ \overset{(e)}{=}& \mathscr{L}_{I_{bp}}(s), \end{aligned} \tag{C.2}$$

where, (a) is obtained by substituting for inter-cell interference I_{bp} which is the sum of the powers from all the interfering UEs placed farther than R_o (no intra-cell interference with orthogonal pilot sequences assumption) and re-arrange the inequality variables, (b) follows assuming $\{\beta_i\}_{i=0}^{\infty}$ is a set of i.i.d. unit-mean exponential random-variables, i.e. $\beta^2 \sim \exp(1)$, (c) follows assuming $s = T_1\, r_{bbp}^{2\nu}$ as a constant in Laplace equation and (d) is, by definition, the Laplacian of interference w.r.t to the constant s. Next, substitute for $\mathscr{L}_{I_{bp}}(s)$ from (5.15), we obtain expression for the probability

$$\mathbb{P}\Big\{SIR > T_1\Big\} = \exp\left[\frac{-\pi\,\lambda_b\,\bar{\chi}\,s^{1/\nu}}{\Omega\,\mathrm{sinc}(\frac{\pi}{\nu})}\right] \tag{C.3}$$

Re-setting $s = T_1\, r_{bbp}^{2\nu}$, averaging out the random variable $\mathrm{r_{bbp}}$ and then plugging again into (C.1) we obtain

$$\begin{aligned}\mathbf{P}_{cov}(T_1,\lambda_b,\nu) =& \mathbb{E}_{r_{bbp}}\left\{\exp\left[\frac{-\pi\,\lambda_b\,\bar{\chi}\,(T_1\, r_{bbp}^{2\nu})^{1/\nu}}{\Omega\,\mathrm{sinc}(\frac{\pi}{\nu})}\right]\right\}\\ &\overset{(a)}{=} \int_0^{R_o}\left\{e^{-C_1(T_1,\lambda_b,\nu)\, r_{bbp}^2}\right\} f_R(r)dr\\ &\overset{(b)}{=} \int_0^{R_o}\left\{\frac{2r_{bbp}}{R_o^2}e^{-C_1(T_1,\lambda_b,\nu)\, r_{bbp}^2}\right\}dr\end{aligned} \tag{C.4}$$

In (a), the expectation w.r.t the random variable r_{bbp} expressed in integral form, where $C_1(T_1,\lambda_b,\nu) = \dfrac{\pi\,\lambda_b\,\bar{\chi}\,T_1^{1/\nu}}{\Omega\,\mathrm{sinc}(\frac{\pi}{\nu})}$, (b) follows from substituting for $f_R(r)$, in our scenario, we have uniform user-distribution within disc of radius $\mathrm{R_o}$ such that $f_R(r) = (2r/R_o^2)$ for $r \in (0, R_o]$. Finally, setting $x = r^2$ and evaluating the integration we straightforwardly arrive at (5.16), i.e.,

$$\mathbf{P}_{cov}(T_1,\lambda_b,\nu) = \frac{1}{C_1(T_1,\lambda_b,\nu)\, R_o^2}\left[1 - \exp(-C_1(T_1,\lambda_b,\nu)\, R_o^2)\right],$$

with $C_1(T_1,\lambda,\nu) = \dfrac{\pi\,\lambda_b\,\bar{\chi}\,T_1^{1/\nu}}{\Omega\,\mathrm{sinc}(\frac{\pi}{\nu})}$, which completes the proof.

C.2

Proof of Theorem 5.2.

Starting from the definition of the normalized average-rate we have [7]

$$R_{cov}^{UL}(T_2, \lambda_b, \nu) = \mathbb{E}\Bigg\{ \frac{B\, T_{ov}\, T_u}{\Omega\, T_s}\ \log_2(1+SIR), \Bigg\} \tag{C.5}$$

given that B is the bandwidth, T_s is the orthogonal-frequency division-multiplexing (OFDM) symbol duration T_s = slot duration/# of symbole per slot, T_{ov} is the pilot overhead or training efficiency, $T_{ov} = \frac{(T_{slot} - T_{pilot})}{T_{slot}} = \frac{(T_{slot} - \tau\, T_s)}{T_{slot}}$, T_u is the useful symbol duration $T_u = 1/\text{subcarrier spacing} = 1/\Delta_f$, and Ω is the frequency reuse factor (FRF). It's worth pointing out that the pre-log percentage factor $(\frac{B\, T_{ov}\, T_u}{\Omega\, T_s})$ implies that the useful data transmission only occupies a fraction of the coherence-slot. The expectation in (C.5) can be expressed in term of integration as following (averaging over the SIR distribution)

$$\begin{aligned} R_{cov}^{UL}(T_2, \lambda_b, \nu) &= \int_{r=0}^{R_o}\int_{0}^{T_2} \mathbb{P}\Bigg\{ \Bigg[\frac{\vartheta\, B}{\Omega}\ \log_2(1+SIR)\ >\ t | r \Bigg] dt\, f_R(r) \Bigg\} dr \\ &\overset{(a)}{=} \int_{r=0}^{R_o}\int_{0}^{T_2} \mathbb{P}\Bigg\{ \underbrace{\Bigg[SIR\ >\ \Big(e^{\frac{\ln(2)\,\Omega\, t}{\vartheta\, B}}\ -\ 1 \Big) | r \Bigg]}_{\text{SIR-ccdf}}\ dt\, f_R(r) \Bigg\} dr \\ &\overset{(b)}{=} \frac{1}{C_2(T_2, \lambda_b, \nu)\, R_o^2} \Bigg[1 - \exp(-C_2(T_2, \lambda_b, \nu)\, R_o^2), \Bigg] \end{aligned} \tag{C.6}$$

where, $\vartheta = T_{ov} \cdot T_u/T_s$ accounts for both pilot and cyclic prefix (CP) overheads, the first equality follows exploiting the fact that power is non negative, so for a positive r.v. X, data rate in this case, we have $\mathbb{E}[X] = \int_{t>0} \mathbb{P}(X > t)\, dt$, (a) is obtained after re-arrange the inequality variables and (b) follows by substituting for ccdf of SIR from appendix-A, setting $T_1 = \exp(\frac{\ln(2)\,\Omega\, T_2}{\vartheta B}) - 1$, substitute for $f_R(r)$ and changing of variables with $x = r^2$, note that $C_2(T_2, \lambda_b, \nu)$ is given by (5.19) $C_2(T_2, \lambda_b, \nu) = \dfrac{\pi\, \lambda_b\, \bar{\chi}\, (e^{\frac{\ln(2)\,\Omega\, T_2}{\vartheta\, B}} - 1)^{1/\nu}}{\Omega\, \mathrm{sinc}(\frac{\pi}{\nu})}$, which concludes the proof.

C.3

Proof of Theorem 5.3.

The normalised effective capacity in (3.13) $C^{asy}_{P,k}(A, D_k, p_u, \Omega, m) = -\frac{1}{A}\log_2 \mathbb{E}\Big\{(1+\beta_k p_u N_r)^{-A}\Big\}$, can be expressed in term of the SIR distribution as follows

$$C^{UL}_{eff}(t, \lambda_b, \nu, \theta) = -\frac{1}{A}\log_2 \int_0^{R_o}\int_0^1 \mathbb{P}\Big\{\underbrace{\Big[(1+SIR)^{-A} > t|r\Big]dt}_{\mathcal{I}_2}\, f_R(r)\Big\}dr \tag{C.7}$$

Next, $\mathcal{I}_2$ after a simple manipulation will be

$$\begin{aligned}\mathcal{I}_2 &= \int_0^1 \mathbb{P}\Big\{\Big[SIR < \Big(t^{-1/A}-1\Big)\Big]dt\Big\} \\ &\overset{(a)}{=} 1 - \int_0^1 \underbrace{\mathbb{P}\Big\{\Big[SIR \geq \Big(t^{-1/A}-1\Big)|r\Big]}_{\text{CCDF of the SIR}}\, dt\Big\},\end{aligned} \tag{C.8}$$

where (a) follows since CDF = 1 − CCDF. Now, substituting for CCDF term from eq.(C.4) with $T_1 = \Big(t^{-1/A}-1\Big)$, we end-up with the following expression

$$C^{UL}_{eff}(t, \lambda_b, \nu, \theta) = -\frac{1}{A}\log_2\left[1 - \int_0^1 \Big(\frac{1}{C_3(t, \lambda_b, \nu, \theta)\, R_o^2}\Big[1 - e^{-C_3(t,\lambda_b,\nu,\theta)\, R_o^2}\Big]\Big)dt\right], \tag{C.9}$$

with $C_3(t, \lambda_b, \nu, \theta) = \dfrac{-\pi\, \lambda_b\, \bar{\chi}\, (t^{-1/A}-1)^{1/\nu}}{\Omega\, \mathrm{sinc}(\frac{\pi}{\nu})}$.

Finally, employing the Hermite approximation for the integral in (C.9), yields $C^{UL}_{eff}(t, \lambda_b, \nu, \theta) = -\frac{1}{A}\log_2\left[1 - \sum_{i=1}^{N} \omega_i\, V(x_i)\right] + \mathcal{O}_N$, which concludes the proof.

Appendix D

Proofs for Ch.7

D.1

PROOF OF LEMMA 7.1.

Tracking the same approach utilised in [124], * if we denote the tier associating the typical user using an index j, then we have macro-tier association, i.e., $j = m$ iff $P_m > P_r$. Consequently, $\mathcal{A}_m$ can be derived as follows

$$\begin{aligned}
\mathcal{A}_m &\triangleq \mathbb{P}[n = j] \\
&= \mathbb{P}(P_m\, Z_m^{-\alpha_m} \;>\; P_r\, \frac{B_r}{B_m}\, Z_r^{-\alpha_r}) \\
&\overset{(a)}{=} \mathbb{E}_{Z_m}\Big\{\, \mathbb{P}(Z_r \;>\; \left(\frac{P_r}{P_m}\frac{B_r}{B_m}\right)^{1/\alpha_r} \; z^{-\alpha_r/\alpha_m})\, \Big\} \\
&\overset{(b)}{=} \mathbb{E}_{Z_m}\Big\{\, \mathbb{P}(Z_r \;>\; (\hat{P}_r\, \hat{B}_r)^{1/\alpha_r}\, z^{-\tilde{\alpha}_r})\, \Big\} \\
&\overset{(c)}{=} \int_0^\infty \mathbb{P}(Z_r \;>\; (\hat{P}_r\, \hat{B}_r)^{1/\alpha_r}\, z^{-\tilde{\alpha}_r}\, f_{Z_m}(z)\, dz
\end{aligned} \tag{D.1}$$

where (a) follows after re-arranging the parameters in the inequality, in (b) we used the normalised expression of parameters ($\hat{P}_j \triangleq \frac{P_j}{P_k}$, $\hat{B}_j \triangleq \frac{B_j}{B_k}$, $\alpha = \alpha_r/\alpha_m$) and (c) follows from the definition of expectation operator over the distribution of the r.v. Z_m. For this probability to be solved we need to find the probability distribution functions (PDF) of Z_m and Z_r which in turn can be derived employing the null-probability of a Poisson-process with density of λ_j, which is $e^{-\lambda_j A)}$ for an area of A.

* According to Slivnyak's theorem this analysis is valid for any randomly chosen user since it's conducted on a typical-user located at the origin [124].

$$\mathbb{P}[\text{No BS closer than } (\hat{P}_j\hat{B}_j)^{1/\alpha_j} z^{\hat{\alpha}_j}] = \; e^{-\pi\lambda_j(\hat{P}_j\hat{B}_j)^{2/\alpha_j} z^{2/\hat{\alpha}_j}} \tag{D.2}$$

We know that for a circle of radius z, centred at the origin, the null probability, i.e, the probability that no points of ϕ_m or ϕ_r lie within this circle can be described using the complementary cumulative distribution function (CCDF) (the tail distribution)

$$\begin{aligned}\hat{F}_{Z_j}(z) = \mathbb{P}(Z_j \,>\, z) \;&= \mathbb{P}(\phi_j \cap b(0,z) \,=\, \{\emptyset\}) \\ &\overset{(a)}{=} \; \exp(-\pi\,\lambda_j\, z^2)\end{aligned} \tag{D.3}$$

where, $j \in \{m, r\}$, $b(0, z)$ is the Euclidean ball of radius z centered at origin and (a) stems since ϕ_m and ϕ_r are a PPP with densities of λ_m and λ_r, respectively. The cumulative distribution function (CDF) of Z_j is
$F_{Z_j}(z) = \mathbb{P}(Z_j \leqslant z) = 1 - \exp(-\pi\lambda_j z^2)$. The probability density function (PDF) of Z_ℓ can then be obtained as $f_{Z_j}(z) = \frac{d}{dz}(F_{Z_j}(z)) = 2\pi\lambda_j z \exp(-\pi\lambda_j z^2)$. Using (D.1) and (D.3) with $P_j = 1, B_j = 1$, and $\alpha_j = 1$ for $j = k$, we obtain

$$\begin{aligned}\mathcal{A}_m \;&= \; 2\pi\lambda_m \int_0^\infty z\, e^{-\pi\lambda_r(\hat{P}_r\hat{B}_r)^{2/\alpha_r} z^{2/\hat{\alpha}_r} - \pi\lambda_m z^2}\, \mathrm{d}z \\ &\overset{(a)}{=} \; 2\pi\lambda_m \int_0^\infty z \exp\left\{-\pi \sum_{j\in\{m,r\}} \lambda_j(\hat{P}_j\hat{B}_j)^{2/\alpha_j} z^{2/\hat{\alpha}_j}\right\} \mathrm{d}z \\ &\overset{(b)}{=} 2\pi\lambda_m \int_0^\infty z \, \exp\left\{-\pi \sum_{j\in\{m,r\}} \lambda_j(\hat{P}_j\hat{B}_j)^{2/\alpha} z^2\right\} \mathrm{d}z \\ &\overset{(c)}{=} \; \frac{\lambda_m}{\sum_{j\in\{m,r\}} \lambda_j(\hat{P}_j\hat{B}_j)^{2/\alpha}} \\ &\overset{(d)}{=} \; \frac{\lambda_m}{\lambda_m + \lambda_r(\hat{P}_r\hat{B}_r)^{2/\alpha}}\end{aligned} \tag{D.4}$$

where (b) follows assuming $\alpha_m = \alpha_r$. Similarly, by using these distributions, $\mathcal{A}_r$ can be obtained as

$$\begin{aligned}\mathcal{A}_r \;&= \; \mathbb{P}(P_r\, Z_r^{-\alpha_r} \,>\, P_m\, z^{-\tilde{\alpha}_m}) \\ &= \; \mathbb{E}_{Z_r}\Big\{\, \mathbb{P}(Z_m \,>\, (\hat{P}_m)^{1/\alpha_m}\, z^{-\tilde{\alpha}_m})\,\Big\}\end{aligned}$$

$$= \int_0^{\infty} \mathbb{P}\Big(Z_m \; > \; (\hat{P}_m)^{1/\alpha_m} \, z^{-\tilde{\alpha}_m}\Big) \, f_{Z_r}(z) \, dz \tag{D.5}$$

or according to the total probability theory, the RRH users probability is

$$\mathcal{A}_r = 1 \; - \; \mathcal{A}_m \tag{D.6}$$

Now, for asymptotic model (massive array antennas), from Lemma 3- [95] we have

$$\begin{aligned}
\mathcal{A}_m \; &\overset{N_t \to \infty}{\approx} \; 2\pi\lambda_m \int_0^{\infty} z \, \exp\Big\{ - \, \pi \, \lambda_m \, z^2 \Big\} \, dz \\
&\times \; 2\pi\lambda_m \int_0^{\infty} \exp\Big\{ - \; \pi \, \lambda_r \, (\rho \hat{B})^{\frac{2}{\alpha_r}} \, z^{1+\frac{\alpha_m}{\lambda_r}} \Big\} dz \\
&\overset{(a)}{=} \; \frac{(\pi\lambda_m)^{\frac{\alpha_m}{\alpha_r}} \; - \; \pi \, \lambda_r \, (\frac{\alpha_m}{\alpha_r})! \; \; (\rho \, \hat{B})^{\frac{2}{\alpha_r}}}{(\pi\lambda_m)^{\frac{\alpha_m}{\alpha_r}}} \\
&\overset{(b)}{=} \; \frac{\lambda_m \; - \; \lambda_r \, (\rho \, \hat{B})^{\frac{2}{\alpha}}}{\lambda_m}
\end{aligned} \tag{D.7}$$

where the first term of (a) stems with aid of the identity, $\int_0^{\infty} z e^{-bz^2} dz = \frac{1}{2b}, \quad Re(b) > 0$, the notation $(.)!$ stand for the factorial operation, the second term of (a) follows since for $N_t \to \infty$ we have $\frac{1}{\rho} \to \infty$ and invoking the approximation $e^{-\frac{1}{z}} \overset{z \to \infty}{\approx} 1 - z$, then with the aid of the following identity

$$\int_0^{\infty} z^{1+a} e^{-bz^2} dz = \; \frac{(\frac{a}{2})! \; \; b^{-1-\frac{a}{2}}}{2}, \quad Re(b) > 0, \tag{D.8}$$

we arrive at (a), and (b) stems assuming equal path loss exponents, i.e., $\alpha_m = \alpha_r = \alpha$, $\rho = \; (\frac{P_r B_r}{P_m B_m})^{-1/\alpha}$

D.2

Proof of Theorem 7.1.

By conditioning on the distance to the nearest macro-BS, the success probability for the macro-BS-tier can be written as follows

$$\begin{aligned}
\mathcal{S}_M(\hat{\gamma}) = \; &\mathbb{P}(SIR \geq \bar{\gamma} | u \in \mathcal{U}_m, X_m = x) \\
&\overset{(a)}{=} \mathbb{P}(\frac{P_m g_{x_0,m} z^{-\alpha} / S_m}{\sum_{j \in \{m,r\}} \sum_{x \in \Psi_j \setminus \{x_0\}} P_j g_{x,j} \, \|x\|^{-\alpha} / S_j} > \hat{\gamma})\} \\
&\overset{(b)}{=} \mathbb{P}(g_{x_0,m} \geq z_m^{\alpha} \hat{\gamma} \sum_{j \in \{m,r\}} I_{m,j})
\end{aligned}$$

$$\begin{aligned}
&\overset{(c)}{=} \mathbb{E}_s\left[\sum_{n=0}^{\Delta-1}\mathbb{E}_{I_M}\left[\frac{(sI_M)^n}{n!}e^{-sI_M}\right]\right]\\
&\overset{(d)}{=} \mathbb{E}_s\left[\sum_{n=0}^{\Delta-1}\frac{(-s)^n}{n!}\mathcal{L}_{I_M}^{(n)}(s)\right]\\
&\overset{(e)}{=} \mathbb{E}_s\left[\sum_{n=0}^{\Delta-1}\mathbb{E}_{z_m}[a_n]\right], \qquad \text{(D.9)}
\end{aligned}$$

where (a) results from substituting for SIR, (b) from re-arranging the inequality given that,

$I\overset{\Delta}{=}\sum_{x\in\Psi_j\setminus\{x_0\}}P_jS_mg_{x,j}\left\|x\right\|^{-\alpha}/P_mS_j$ and $I_M = I_{m,m} + I_{m,r}$, (b) stems since $g_{x_0,m}\sim\Gamma(\Delta,1)$, $\Delta = N_t - S_m + 1$ is array gain when ZF-beamforming is employed and S_m is the multiplexing gain for the MBS. Denote $s\overset{\Delta}{=}z_0^{\alpha}$ then (c)stems when using sequence representation of gamma lower incomplete function due the the fact that $g_{x_0,m}$ is gamma random variable and its cumulative-distribution function is the regularized gamma-function, which is $\mathbb{P}(Z < z) = \frac{\gamma(N,z)}{\Gamma(N)}$. Therefore, its CCDF is given as, $\mathbb{P}(Z > z) = \sum_{n=0}^{k-1}\frac{z^n}{n!}e^{-z}$, where the inner expectation is with respect to the r.v. I_M. Following the property of the Laplace transform, we have (d) in which $\mathcal{L}_I^{(n)}(s)$ is the $n-$th derivative of L.T., i.e., $\mathcal{L}_I^{(n)}(s) = \frac{d^n}{ds^n}\mathcal{L}_I(s)$ where Laplace derivative property states that $\mathbb{E}_I(e^{-s\,I}(sI)^n) = (-s)^n\frac{\mathrm{d}^n\mathcal{L}_I(s)}{\mathrm{d}s^n}$ we finally arrive at (d), (e) follows from denoting a sequence a_n as, $a_n = \frac{s^n(-1)^n}{n!}\mathcal{L}_{\mathcal{I}}^{(n)}(s)$. To derive $\mathcal{S}_M(\hat{\gamma})$ based on (D.9), we start from the expression of Laplace transform of I_M for a fixed s, as follows

$$\begin{aligned}
\mathcal{L}_{I_M}(s) =&\mathbb{E}_s\left[\exp\left(-s\sum_{j\in\{m,r\}}\sum_{x\in\Psi_j\setminus\{x_0\}}g_{x,j}\beta_j\left\|x\right\|^{-\alpha}\right)\right]\\
&\overset{(a)}{=}\prod_{j\in\{m,r\}}\mathbb{E}_{\Psi_j,g_x}\left[\prod_{x\in\Psi_j\setminus\{x_0\}}\left(\exp\left[-sg_{x,j}\beta_j\left\|x\right\|^{-\alpha}\right]\right)\right]\\
&\overset{(b)}{=}\prod_{j\in\{m,r\}}\mathbb{E}_{\Psi_j}\left[\prod_{x\in\Psi_j\setminus\{x_0\}}\frac{1}{\left(1+s\beta_j\left\|x\right\|^{-\alpha}\right)^{S_j}}\right]\\
&\overset{(c)}{=}\exp\left[-\pi\sum_{j\in\{m,r\}}\lambda_j\int_{r\geq z_j^2}\left\{1-\frac{1}{\left(1+s\beta_jr^{-\frac{\alpha}{2}}\right)^{S_j}}\right\}dr\right], \qquad \text{(D.10)}
\end{aligned}$$

where, $\beta_j = \frac{P_jS_m}{P_mS_j}$, $j\in\{m,r\}$, the equality (a) follows since $\{\Psi_j\}$ and $\{g_{x,j}\}$ are

independent, (b) follows due to gamma distribution of $g_{x,j} \sim \Gamma(S_j, 1)$, (c) is derived using the probability generating functional (PGFL) of PPP [74] with integration limit start from the minimal-distance between the interfering RRH or MBS and the typical-user, Then, the nth derivative of $\mathcal{L}_{I_M}(s)$ w.r.t, s can be expressed in the following formula that recursively defines the sequence $\mathcal{L}_I^{(n)}(s)$

$$\mathcal{L}_I^{(n)}(s) = \pi \sum_{i=0}^{n-1} \binom{n-1}{i} (-1)^{n-i} \sum_{j\in\{m,r\}} \lambda_j \frac{\Gamma(S_j+n-i)}{\Gamma(S_j)} \times \int_{r\geq z_j^2} \frac{\left(\beta_j r^{-\frac{\alpha}{2}}\right)^{n-i}}{\left(1+s\beta_j r^{-\frac{\alpha}{2}}\right)^{S_j+n-i}}\, dr\ \mathcal{L}_I^{(i)}(s), \quad \text{(D.11)}$$

By substituting $s = \hat{\gamma}\, z_m^{\alpha}$ into (D.11) and denoting $a_n = \frac{(-s)^n}{\Gamma(n+1)}\mathcal{L}_I^{(n)}(s)$, then we arrive at the following equation for $n = 0$,

$$\begin{aligned} a_0 &= \mathcal{L}_{I_M}(s)\,|_{s=\hat{\gamma}\, z_j^{\alpha}} \\ &\overset{(a)}{=} \exp\left[-\pi \sum_{j\in\{m,r\}} \lambda_j \int_{r\geq z_j^2} \left(1 - \frac{1}{\left(1+\hat{\gamma} z_m^{\alpha}\beta_j r^{-\frac{\alpha}{2}}\right)^{S_j}}\right) dr\right] \\ &\overset{(b)}{=} \exp\left[-\pi z_m^2 (P_m B_m)^{-2/\alpha} k_0\right], \end{aligned} \quad \text{(D.12)}$$

where the distance between the nearest interferer BS and the typical user is given by $z_j^2 \geq z_m^2 (\frac{P_j B_j}{P_m B_m})^{2/\alpha}$ due to the association criteria of $P_m B_m z_m^{-\alpha} \geq P_j B_j z_j^{-\alpha}$ and expression in (b) implies that , k_0 has the form of eq.(7.11). Now, for $n > 0$ we get the following sequence

$$\begin{aligned} a_n &= \pi \sum_{i=0}^{n-1} \frac{n-i}{n}\, a_i \sum_{j\in\{m,r\}} \lambda_j \frac{\Gamma(S_j+n-i)}{\Gamma(S_j)\Gamma(1+n-i)} \times \int_{r\geq z_j^2} \frac{\left(\beta_j r^{-\frac{\alpha}{2}}\right)^{n-i}}{\left(1+s\beta_j r^{-\frac{\alpha}{2}}\right)^{S_j+n-i}}\, dr \\ &\overset{(a)}{=} \pi z_m^2 (P_m B_m)^{-2/\alpha} \sum_{i=0}^{n-1} \frac{(n-i)\, k_{n-i}}{n}\, a_i \end{aligned} \quad \text{(D.13)}$$

given that

$$k_0 = \sum_{j\in\{m,r\}} \lambda_j (P_j B_j)^{-2/\alpha} \left\{ {}_2F_1 \left[\begin{matrix} S_j, \frac{-2}{\alpha} \\ 1-\frac{2}{\alpha} \end{matrix} \middle| \frac{-\hat{\gamma} S_m B_m}{S_j B_j} \right] - 1 \right\} \tag{D.14}$$

$$k_i = \sum_{j\in\{m,r\}} \lambda_j (P_j B_j)^{-2/\alpha} \frac{\Gamma(S_j+n-i)}{\Gamma(S_j)\Gamma(1+n-i)} \frac{(\frac{-\hat{\gamma} S_m B_m}{S_j B_j})^i}{1-\frac{\alpha}{2}i} \times {}_2F_1 \left[\begin{matrix} i+S_j, i-\frac{2}{\alpha} \\ i+1-\frac{2}{\alpha} \end{matrix} \middle| \frac{-\hat{\gamma} S_m B_m}{S_j B_j} \right], \tag{D.15}$$

The sequence a_n which is defined by a linear-recurrence equation (D.13), can be solved in explicit-expression via linear-algebra. Now, by introducing a $\Delta \times \Delta$ matrix:

$$\mathbf{G}_\Delta = \begin{bmatrix} 0 & & & & \\ \frac{1}{2}k_1 & 0 & & & \\ \frac{2}{3}k_2 & \frac{1}{3}k_1 & 0 & & \\ \vdots & & & \ddots & \\ 1-\frac{1}{\Delta}k_{\Delta-1} & 1-\frac{2}{\Delta}k_{\Delta-2} & \cdots & \frac{1}{\Delta}k_1 & 0 \end{bmatrix}, \tag{D.16}$$

and the following two vectors:

$\boldsymbol{a}_\Delta = [a_1, a_2, \ldots a_\Delta]^T$,

$\boldsymbol{k}_\Delta = [k_1, k_2, \ldots, k_\Delta]^T$,

consequently we can represent a_n (eq.D.13), in a matrix form as

$$\boldsymbol{a}_\Delta = c\, a_0 \boldsymbol{k}_\Delta + c\, \mathbf{G}_\Delta \boldsymbol{a}_\Delta, \tag{D.17}$$

with $c = \pi z_m^2 (P_m B_m)^{-2/\alpha}$.

This linear recursive equation of a_n can be expressed as a finite sequence formula since, for $n > \Delta$, we have $\mathbf{G}_\Delta^n = 0$ ($\mathbf{G}_\Delta$ is a lower triangular-matrix):

$$\begin{aligned} \boldsymbol{a}_\Delta &= a_0 \sum_{n=1}^{\Delta} c^n \mathbf{G}_\Delta^{n-1} \boldsymbol{k}_\Delta \\ &\overset{(a)}{=} a_0 \sum_{n=1}^{\Delta} \frac{c^n}{n!} \mathbf{Q}_{\Delta+1}^n (2:\Delta+1, 1) \end{aligned} \tag{D.18}$$

By the equation in first line, we have obtained a solution for (D.17), however, in (a) we progress further to obtain more explicit expression where we define the following

Toeplitz matrix (diagonal constant matrix, where each descending diagonal from left to right is constant):

$$\mathbf{Q}_{\Delta+1} = \begin{bmatrix} 0 & & & & \\ k_1 & 0 & & & \\ k_2 & k_1 & 0 & & \\ \vdots & & & \ddots & \\ k_{\Delta-1} & k_\Delta & \cdots & k_1 & 0 \end{bmatrix}, \tag{D.19}$$

and for $\Delta \geq 1$ we have the following equality $\mathbf{G}_\Delta^{n-1}\mathrm{k}_\Delta = \frac{1}{n!}\mathbf{Q}_{\Delta+1}^n(2:\Delta+1,1)$ for $n \in \mathbb{N}^+$. Now, $\boldsymbol{a}_\Delta$ can be substituted to (D.9) and using the matrix norm induced by the vector norm L_1 yields

$$\begin{aligned} \mathcal{S}_M(\hat{\gamma}) &= \mathbb{E}_s\left[\sum_{n=0}^{\Delta-1}\mathbb{E}_{z_m}[a_n]\right] \\ &\overset{(a)}{=} \mathbb{E}_s\left[\mathbb{E}_{z_m}[a_0 + \|\boldsymbol{a}_{\Delta-1}\|_1]\right] \\ &\overset{(b)}{=} \mathbb{E}_{z_m}\left[\left\|a_0\sum_{n=0}^{\Delta-1}\frac{c^n}{n!}\mathbf{Q}_\Delta^n\right\|_1\right] \\ &\overset{(c)}{=} \frac{\kappa}{\kappa+k_0}\sum_{n=0}^{\Delta-1}\left(\frac{1}{\kappa+k_0}\right)^n\|\mathbf{Q}_\Delta^n\|_1 \\ &\overset{(d)}{=} \frac{\kappa}{\kappa+k_0}\left\|\sum_{n=0}^{\Delta-1}\left[(\frac{1}{\kappa+k_0})\mathbf{Q}_\Delta\right]^n\right\|_1 \\ &\overset{(e)}{=} \frac{\kappa}{\kappa+k_0}\left\|\left[\mathbf{I}-\left(\frac{1}{\kappa+k_0}\right)\mathbf{Q}_\Delta\right]^{-1}\right\|_1 \\ &\overset{(f)}{=} \kappa\left\|\left[(k_0+\kappa)\mathbf{I}+\mathbf{Q}_\Delta\right]^{-1}\right\|_1, \end{aligned} \tag{D.20}$$

where (c) follows by averaging out the r.v. z_m which is the distance between a typical terminal to its closest MBS (the complementary CDF of z_m is obtained using the null probability of a PPP), $\kappa = \sum_{j\in\{m,r\}}\lambda_j(P_jB_j)^{-2/\alpha}$, (d) is equivalent to (c) due to the property of the L_1 induced matrix norm ($\|\mathrm{A}\|_1 = \max_{1\leq j\leq n}\sum_{i=1}^m|a_{ij}|$), (e) stems using the Taylor expansion and step (f) completes the proof via a simple algebraic manipulation.

D.3

Proof of Theorem 7.2

By conditioning on the distance to the nearest RRH, the success probability for the RRH-tier is given by

$$\begin{aligned}
\mathcal{S}_{RRH}(\hat{\gamma}) &= \mathbb{P}(SIR \geq \bar{\gamma} | u \in \mathcal{U}_r, X_r = x) \\
&\overset{(a)}{=} \mathbb{P}(\frac{P_r g_{x_0,r} z^{-\alpha}}{\sum_{j\in\{m,r\}} \sum_{x\in\Psi_j\setminus\{x_0\}} P_j g_{x,j} \left\|x\right\|^{-\alpha} / S_j} > \hat{\gamma})\} \\
&\overset{(b)}{=} \mathbb{P}(g_{x_0,r} \geq z_r^{\alpha}\hat{\gamma} \sum_{j\in\{m,r\}} I_{r,j}) \\
&\overset{(c)}{=} \mathbb{E}\Bigg[\exp(-P_r z^{-\alpha}\hat{\gamma}\{\sum_{j\in\{m,r\}} I_{r,j}\})\Bigg] \\
&\overset{(d)}{=} \prod_{j\in\{m,r\}} \mathbb{E}_{I_{r,j}}\Bigg[\exp(-P_r z^{-\alpha}\hat{\gamma} I_{r,j}\Bigg] \\
&\overset{(e)}{=} \prod_{j\in\{m,r\}} \mathcal{L}_{I_R}(s)\,,
\end{aligned} \tag{D.21}$$

where (a) results from substituting for SIR, (b) from re-arranging the inequality given that, $I_{r,j} \triangleq \sum_{x\in\Psi_j\setminus\{x_0\}} P_j g_{x,j} \left\|x\right\|^{-\alpha} / P_r S_j$ and $I_R = I_{r,m} + I_{r,r}$, (c) stems since $g_{x_0,r} \sim \Gamma(1,1)$ is the channel gain for the RRHs links,(d) follows from the independence of $I_{r,j}$ and (e) from the definition of L.T. Now, to derive $\mathcal{S}_{RRH}(\hat{\gamma})$ based on (D.21), we start from the expression of Laplace transform of I_R for a fixed s as follows

$$\begin{aligned}
\mathcal{L}_{I_R}(s) =& \mathbb{E}\left[e^{-sI_R}\right] \\
\overset{(a)}{=}& \mathbb{E}\left[\exp\left(-s \sum_{j\in\{m,r\}} \sum_{x\in\Psi_j\setminus\{x_0\}} g_{x,j}\beta_j \left\|x\right\|^{-\alpha}\right)\right] \\
\overset{(a)}{=}& \prod_{j\in\{m,r\}} \mathbb{E}_{\Psi_j, g_x}\left[\prod_{x\in\Psi_j\setminus\{x_0\}}\left(\exp\left[-s g_{x,j}\beta_j \left\|x\right\|^{-\alpha}\right]\right)\right] \\
\overset{(b)}{=}& \prod_{j\in\{m,r\}} \mathbb{E}_{\Psi_j}\left[\prod_{x\in\Psi_j\setminus\{x_0\}} \frac{1}{\left(1 + s\beta_j \left\|x\right\|^{-\alpha}\right)^{S_j}}\right]
\end{aligned}$$

$$\overset{(c)}{=}\exp\left[-\pi\sum_{j\in\{m,r\}}\lambda_j\int_{r\geq z_j^2}\left\{1-\frac{1}{\left(1+s\beta_j r^{-\frac{\alpha}{2}}\right)^{S_j}}\right\}dr\right]$$

$$\overset{(d)}{=}\exp(-\pi\sum_{j\in\{m,r\}}\lambda_j\sum_{n=1}^{S_j}\binom{S_j}{n}\int_{r\geq z_j^2}(\frac{\left(s\beta_j r^{-\frac{\alpha}{2}}\right)^n}{\left(1+s\beta_j r^{-\frac{\alpha}{2}}\right)^{S_j}})dr), \tag{D.22}$$

where, $\beta_j = \frac{P_j S_m}{P_m S_j}$, $j \in \{m, r\}$, the equality (a) follows since $\{\Psi_j\}$ and $\{g_{x,j}\}$ are independent, (b) follows from gamma distribution of $g_{x,j} \sim \Gamma(S_j, 1)$, (c) is derived utilising the probability generating-functional (PGFL) of PPP [74] with integration limit start from the minimal-distance between the interfering RRH or MBS and the typical-user, (d) follows due to binomial-expansion. Now perform the integration in (D.22) using change of variables, $1/\left(1+s\beta_j r^{-\frac{\alpha}{2}}\right) \longrightarrow v$, then substitute again in (D.21) gives the success probability of typical user served by RRH cell as

$$\mathcal{S}_{RRH}(\gamma) = \mathbb{E}_{Z_r}\left\{\exp\left[-\Upsilon_2(\frac{\hat{\gamma}Sz_r^{\alpha}}{P_r\mathcal{C}})\right]\right\}, \tag{D.23}$$

given that

$$\Upsilon_2(s) = 2\pi\lambda_m\sum_{i=1}^{S}\binom{S}{i}(s\frac{P_m}{S})^i(-s\frac{P_m}{S})^{\frac{2}{\alpha}-i}\frac{1}{\alpha}B(-s\frac{P_r\mathcal{C}}{Sz_r^{\alpha}};\, i-\frac{2}{\alpha},\, 1-S)$$
$$+\ 2\pi\lambda_r\frac{P_r\, z_r^{2-\alpha}\, s}{(\alpha-2)}\,{}_2F_1\left[\begin{matrix}1, 1-\frac{2}{\alpha}\\ 2-\frac{2}{\alpha}\end{matrix}\middle|-s\frac{P_r}{z_r^{\alpha}}\right], \tag{D.24}$$

and $B(x; a, b)$ is the incomplete Beta function which can be given by the following formula

$$B(z; a, b) = \frac{z^a}{a}\,{}_2F_1\left[\begin{matrix}a, 1-b\\ 1+a\end{matrix}\middle|z\right] \tag{D.25}$$

Finally, using the statistical distribution of z_r given by (7.6) to average out this r.v. will straightforwardly complete the proof of (7.13).

Bibliography

[1] I. Hwang, B. Song, and S. Soliman. "A Holistic View on Hyper-Dense Heterogeneous and Small Cell Networks," *IEEE Commun. Mag.,* vol.51, no.6, pp.20-27, 2013.

[2] Y. Niu, Y. Li, D. Jin, L. Su, and A. Vasilakos, "A Survey of Millimeter Wave Communications (mmWave) for 5G: Opportunities and Challenges," *Wireless Networks,* vol.21 no.8, pp.2657-2676, 2015.

[3] E. Larsson, O. Edfors, F. Tufvesson, and T. Marzetta, "Massive MIMO for Next Generation Wireless Systems," *IEEE Commun. Mag.,* vol.52 no.2, pp.186-195, 2014.

[4] J. Mietzner et al., "Multiple-antenna techniques for wireless communications-a comprehensive literature survey," *IEEE communications surveys & tutorials* 11, no. 2 (2009).

[5] S. Alamouti, "A simple transmit diversity technique for wireless communications," *IEEE J. Select. Areas Commun.*, vol. 16, no. 8, pp. 1451–1458, Oct. 1998.

[6] A. Paulraj, D. Gore, R. Nabar and H. Bolcskei, "An overview of MIMO communications - A key to gigabit wireless," *Proc. of the IEEE,* vol. 92, pp. 198-218. 2004.

[7] T. Marzetta, "Noncooperative cellular wireless with unlimited numbers of base station antennas," *IEEE Transactions on Wireless Communications* 9.11 (2010): 3590-3600.

[8] T. Rappaport, *Wireless Communications: Principles and Practice,* 2nd ed. Prentice Hall PTR, 2002.

[9] 3GPP, TS 36.201 V8.3.0, "Evolved universal terrestrial radio access (E-UTRA); LTE physical layer - general description," Rel. 8, Mar. 2009.

[10] 3GPP TR 36.913, "Requirements for further advancements for Evolved Universal Terrestrial Radio Access (E-UTRA)," V10.0.0,2011 [Online]. Available: http://www.3gpp.org/DynaReport/36913.htm.

[11] F. Boccardi, R. Heath, A. Lozano, T. Marzetta, and P. Popovski, "Five disruptive technology directions for 5G," *IEEE Communications Magazine,* 52(2):74-80, February 2014.

[12] G. Raleigh and J. Cio , "Spatio-temporal coding for wireless communication," *IEEE Transactions on Communications, vol.* 46, no. 3, pp. 357-366, March 1998.

[13] H. Ngo and E. Larsson, "Blind estimation of effective downlink channel gains in Massive MIMO," *in Proc. IEEE International Conference on Acoustics, Speed and Signal Processing* (ICASSP), Brisbane, Australia, April 2015.

[14] F. Fabio, A. Ashikhmin, and T. Marzetta, "Inter-cell interference in noncooperative TDD large scale antenna systems," *IEEE Journal on Selected Areas in Communications* 31.2 (2013): 192-201.

[15] Q. Zhang, S. Jin, K. Wong, H. Zhu, and M. Matthaiou, "Power scaling of uplink massive MIMO systems with arbitrary-rank channel means," *IEEE J. Sel. Topics Signal Process.*, vol. 8, no. 5, pp. 966–981, Oct. 2014.

[16] E. Björnson and E. Jorswieck, "Optimal resource allocation in coordinated multi-cell systems," *Found. Trends Commun. Inf. Theory,* vol. 9, nos. 2–3, pp. 113–381, 2013.

[17] M. Sadek, A. Tarighat, and A. Sayed, "A leakage-based precoding scheme for downlink multi-user MIMO channels," *IEEE Trans. Wireless Commun.,* vol. 6, no. 5, pp. 1711-1721, May 2007.

[18] A. Wyner, "Shannon-theoretic approach to a Gaussian cellular multiple-access channel," *IEEE Transactions on Information Theory,* vol. 40, no. 6, pp. 1713–1727, 1994.

[19] J. Xu, J. Zhang, and J. Andrews, "On the accuracy of the Wyner model in cellular networks," *IEEE Trans. Wireless Commun.,* vol. 10, no. 9, pp. 3098-3109, Sep. 2011.

[20] H. ElSawy, E. Hossain, and M. Haenggi, "Stochastic geometry for modeling, analysis, and design of multi-tier and cognitive cellular wireless networks: a Survey," *IEEE Commun. Surveys Tuts.,* vol. 15, no. 3, pp. 996-1019, third quarter 2013.

[21] J. Andrews, H. Claussen, M. Dohler, S. Rangan, and M. C. Reed, "Femtocells: Past, present, and future," *IEEE J. Sel. Areas Commun.,* vol. 30, no. 3, pp. 497-508, Apr. 2012.

[22] D. Stoyan, W. Kendall, and J. Mecke, *Stochastic Geometry and its Applications*, 2nd edition. Hoboken, NJ, USA: Wiley, 2008.

[23] D. Wu and R. Negi, "Effective capacity: a wireless link model for support of quality of service," *IEEE Trans. Wireless Commun.*, vol. 2, no. 4, pp. 630–643, July 2003

[24] J. Tang and X. Zhang, "Quality-of-service driven power and rate adaptation over wireless links," *IEEE Trans. Wireless Commun.*, vol.6, no. 8, pp. 3058–3068, Aug. 2007.

[25] L. Liu and J.-F. Chamberland, "On the effective capacity of multiantenna Gaussian channels," in *Proc. 2008 IEEE Int. Sym. Inf. Theory*,pp. 2583–2587.

[26] M. Gursoy, "MIMO wireless communications under statistical queueing constrains," *IEEE Trans. Inf. Theory*, vol. 57, no. 9, pp. 5897–5917, Sep. 2011.

[27] M. Ismail, A. Gamage, W. Zhuang, and X. Shen, "Energy efficient uplink resource allocation in a heterogeneous wireless medium," *Communications (ICC), 2014 IEEE International Conference, Sydney*, pp. 5275-5280.

[28] J. Zhang, Z. Tan, H. Wang, Q. Huang, and L. Hanzo, "The Effective Throughput of MISO Systems over $\kappa - \mu$ Fading Channels," *IEEE Transactions on Vehicular Technology*, vol. 63, no. 2, pp. 943-947, Feb. 2014.

[29] H. Ngo, E. Larsson, and T. Marzetta, "Energy and spectral efficiency of very large multiuser MIMO systems," *IEEE Trans. Commun.*, vol. 61, no. 4, pp. 1436-1449, Apr. 2013.

[30] H. Ngo, M. Matthaiou, T. Duong, and E. Larsson, "Uplink performance analysis of multicell MU-MIMO systems with ZF receivers," *IEEE Trans. Veh. Technol.*, vol. 62, no. 9, pp. 4471–4483, Nov. 2013.

[31] S. Jin, X. Wang, Z. Li, K. Wong, Y. Huang, and X. Tang, "On Massive MIMO Zero-Forcing Transceiver Using Time-Shifted Pilots," *IEEE Trans. Veh. Technol.*, vol. 65, no. 1, pp. 59-74, Jan. 2016.

[32] A. Laourine, M. Alouini, S. Affes, and A. Stephenne, "On the capacity of generalized-K fading channels," *IEEE Trans. Wireless Commun.*,vol. 7, no. 7, pp. 2441-2445, Jul. 2008.

[33] K. Baltzis, "Hexagonal vs circular cell shape: a comparative analysis and evaluation of the two popular modeling approximations," *in Cellular Networks–Positioning, Performance Analysis, Reliability,* Rijeka, Croatia: InTech, 2011, ch. 4, pp. 103–122.

[34] S. Jacobsson, G. Durisi, M. Coldrey, U. Gustavsson, and C. Studer, *Massive MIMO with low-resolution ADCs,* ArXiv E-Print, Feb. 2016.

[35] A. Guo and M. Haenggi, "Spatial stochastic models and metrics for the structure of base stations in cellular networks," *IEEE Trans. Wireless Commun.,* vol. 12, no. 11, pp. 5800–5812, Nov. 2013.

[36] A. Kammoun, A. Muller, E. Bjornson, and M. Debbah, "Linear precoding based on polynomial expansion: Large-scale multi-cell MIMO systems," *IEEE J. Sel. Topics Signal Process.,* vol. 8, no. 5, pp. 861–875, Jan. 2014.

[37] A. Kilbas and M. Saigo, *H-Transforms: Theory and Applications,* Boca Raton, FL: CRC Press LLC, 2004.

[38] S. Payami and F. Tufvesson, "Channel measurements and analysis for very large array systems at 2.6 GHz," in *Proc. 2012 Europ. Conf. Anten.Propag.*

[39] Wolfram, "The Wolfram-functions site," Available online: http://functions.wolfram.com

[40] V. Gopal, M. Matthaiou, and C. Zhong, "Performance analysis of distributed MIMO systems in Rayleigh/Inverse- Gaussian fading channels," *IEEE Global Communications Conference, GLOBECOM 2012, Anaheim, United States, 3-7 December*, pp. 2468- 2474.

[41] C. Lau and C. Leung, "Capture models for mobile packet radio networks," *IEEE Trans. Commun.*, vol. 40, no. 5, pp. 917–925, May 1992.

[42] J. Tang and X. Zhang, "Cross-layer-model based adaptive resource allocation for statistical QoS guarantees in mobile wireless networks," *IEEE Trans. Wireless Commun.*, vol. 7, no. 6, pp. 2318–2328, Jun. 2008.

[43] F. Olver, D. Lozier, R. Boisvert, and C. Clark,*NIST handbook of mathematical functions*, Cambridge University Press New York, NY, USA, 2010.

[44] S. Jin, J. Wang, Q. Sun, M. Matthaiou, and X. Gao "Cell Coverage Optimization for the Multicell Massive MIMO Uplink," *IEEE Trans. Veh. Technol.*, vol. 64, no. 12, pp. 5713–5727, Dec. 2015.

[45] M. Simon and M. Alouini,*Digital Communication over Fading Channels*, 2nd ed. John Wiley & Sons, Inc., 2005.

[46] I. Gradshteyn, I. Ryzhik. *Table of integrals, series and products*, Oxford, Academic, 2007.

[47] A. Mathai, R. Saxena, and H. Haubold,*The H-Function: Theory and Applications*, 1st ed. Dordrecht-Heidelberg-London-New York: Springer Science, 2009.

[48] P. Moschopoulos, "The distribution of the sum of independent gamma random variables," *Annals of the Institute of Statistical Mathematics*,37, 541–544,1985.

[49] M. Haenggi, *Stochastic Geometry for Wireless Networks,* Cambridge University Press, 2013.

[50] A. Prudnikov, Y. Brychkov, and O. Marichev, *Integrals and Series: More Special Functions*, Gordon and Breach Science, vol. 3, translated from the Russian by G. G. Gould., 1990.

[51] M. Abramowitz and I. Stegun, *Handbook of Mathematical Functions with Formulas, Graphs, and Mathematical Tables*, 9th ed. New York: Dover Publications, 1972.

[52] H. Ngo, E. Larsson, and T. Marzetta, "The multicell multiuser MIMO uplink with very large antenna and a finite dimensional channel," *IEEE Trans. Commun.*, vol. 61, no. 6, pp.2350–2361, 2013.

[53] J. Hoydis, S. Brink, and M. Debbah, "Massive MIMO in the UL/DL of cellular networks: how many antennas do we need?," *IEEE J. Sel. Areas Commun.*, vol. 31, no. 2, pp. 160–171, Feb. 2013.

[54] H. Ngo, M. Matthaiou, T. Duong, and E. Larsson, "Uplink performance analysis of multiuser MU-SIMO systems with ZF receivers," *IEEE Trans. Veh. Technol.*, vol. 62, no. 9, pp. 4471–4483, Nov. 2013.

[55] L. Zhao, K. Zheng, H. Long, and H. Zhao, "Performance analysis for downlink massive MIMO system with ZF precoding," in *Proc. Trans. Emerging Telecom. Technol., 2013.*

[56] A. Papazafeiropoulos, H. Ngo, M. Matthaiou, and T. Ratnarajah, "Uplink performance of conventional and massive MIMO cellular systems with delayed CSIT," in *Proc. IEEE Int. Symp. PIMRC, Washington, DC, USA, Sep. 2014*, pp. 574–579.

[57] C. Kong, C. Zhong, A. Papazafeiropoulos, H. Ngo, M. Matthaiou, and Z. Zhang, "Effect of channel aging on the sum rate of uplink massive MIMO systems," accepted in *IEEE International Symposium on Information Theory (ISIT), June 2015.*

[58] C. Kong, C. Zhong, A.Papazafeiropoulos, M. Matthaiou, and Z. Zhang, "Sum-Rate and Power Scaling of Massive MIMO Systems With Channel Aging," in *IEEE Transactions on Communications*, vol. 63, no. 12, pp. 4879-4893, Dec. 2015.

[59] Z. Muhammad, and S. Ali, "Outage Analysis of Multi-User Massive MIMO Systems Subject to Composite Fading," *Vehicular Technology Conference (VTC Spring), 2015 IEEE 81st.*

[60] Y. Li, M. Peng, A. Manzoor, and C. Wang, "Co-channel interference in two-tier heterogeneous networks: analytical model and ergodic capacity," *Trans. Emerging Tel. Tech.*, 27: 101–110, 2016.

[61] A. Pitarokoilis, S. Mohammed, and E. Larsson, "On the optimality of single-carrier transmission in large-scale antenna systems," *IEEE Wireless Commun. Lett.,* vol. 1, no. 4, pp. 276–279, Aug. 2012.

[62] F. Rusek, D. Persson, and B. Lau, "Scal1ing up MIMO: opportunities and challenges with very large arrays," *IEEE Signal Proces. Mag.,* Vol.30, no. 1, pp. 40–60, Jan. 2013.

[63] E. Larsson, F. Tufvesson, and O. Edfors, “Massive MIMO for next generation wireless systems,” *IEEE Commun. Mag.,* vol. 52, no. 2, pp. 186–195, Feb. 2014.

[64] B. Gopalakrishnan and N. Jindal, “An analysis of pilot contamination on multi-user MIMO cellular systems with many antennas,” *in Proc. of IEEE 12th International Workshop on Signal Processing Advances in Wireless Communications (SPAWC),* 2011, pp. 381–385.

[65] T. Bai and R. W. Heath, "Asymptotic coverage probability and rate in massive MIMO networks,” *arXiv preprint arXiv*:1305.2233 (2013).

[66] H. Ngo, M. Matthaiou, T. Duong, and E. Larsson, “Uplink performance analysis of multiuser MU-SIMO systems with ZF receivers,” *IEEE Trans. Veh. Technol.*, vol. 62, no. 9, pp. 4471–4483, Nov. 2013

[67] I. Atzeni, J. Arnau, and M.Debbah, “Fractional pilot reuse in massive MIMO systems,” *IEEE International Conference on Communication Workshop* (ICCW). IEEE, 2015.

[68] Z. Yuehao, C. Zhong, and Z. Zhang, “Performance comparison of different transmission schemes in uplink massive MIMO systems with dual-antenna users." *Wireless Communications & Signal Processing (WCSP), 2015 International Conference on.* IEEE, 2015.

[69] E. Björnson, G. Larsson, and M. Debbah, “Massive MIMO for maximal spectral efficiency: How many users and pilots should be allocated?,” *IEEE Transactions on Wireless Communications* 15.2 (2016): 1293-1308.

[70] P. Herath, C. Tellambura, and W. Krzymien, “Stochastic Geometry Modeling of Cellular Uplink Power Control under Composite Rayleigh-Lognormal Fading,” *Vehicular Technology Conference (VTC Fall)*, 2015 IEEE 82nd. IEEE, 2015.

[71] A. Goldsmith, *Wireless Communications,* Cambridge University Press, New York, 2005.

[72] B. Błaszczyszyn and H. Keeler, “Equivalence and comparison of heterogeneous cellular networks,” Personal, Indoor and Mobile Radio Communications (PIMRC Workshops), *2013 IEEE 24th International Symposium on. IEEE*, 2013.

[73] J. Kingman, *Poisson Processes (Oxford Studies in Probability)*, Oxford University Press, USA, January 1993. [Online]. Available: http://www.worldcat.org/isbn/0198536933

[74] J. Andrews, F. Baccelli, and R. Ganti, "A tractable approach to coverage and rate in cellular networks," *IEEE Trans. Commun.*, vol. 59, pp. 3122 – 3134, Nov. 2011.

[75] A. Ashikhmin and T. Marzetta, "Pilot contamination precoding in multicell large scale antenna systems," *in Proc. of IEEE International Symposium on Information Theory Proceedings (ISIT)*, 2012, pp. 1137–1141.

[76] N. Thomas, H. Dhillon, and J. Andrews, "Analytical modeling of uplink cellular networks," *IEEE Transactions on Wireless Communications 12.6* (2013): 2669-2679.

[77] F. Fernandez, A. Ashikhmin, and T. Marzetta, "Interference reduction on cellular networks with large antenna arrays," *in Proc. of IEEE International Conference on Communications (ICC),* 2012.

[78] X. Zhang and H. Martin, "A stochastic geometry analysis of inter-cell interference coordination and intra-cell diversity," *IEEE Transactions on Wireless Communications* 13.12 (2014): 6655-6669.

[79] J. Andrews, K. Abhishek, and S. Dhillon, "A primer on cellular network analysis using stochastic geometry," *arXiv preprint arXiv:1604.03183*(2016).

[80] X. Lin, R. Heath, and J. Andrews, "The interplay between massive MIMO and underlaid D2D networking." *IEEE Transactions on Wireless Communications* 14.6 (2015): 3337-3351.

[81] S. Kusaladharma and Ch. Tellambura, "Massive MIMO based underlay networks with power control," *Communications (ICC), 2016 IEEE International Conference, Kuala Lumpur.*

[82] J. Ferenc and Z. Neda, "On the size distribution of poisson voronoi cells," *Phisica A: Statistical Mechanics and its Applications,* vol. 385, no. 2, pp. 518–526, Nov 2007.

[83] S. Dhillon and J. Andrews, "Downlink rate distribution in heterogeneous cellular networks under generalized cell selection," *IEEE Wireless Communications Letters* 3.1 (2014): 42-45.

[84] F. Boccardi, R. Heath, A. Lozano, T. Marzetta, and P. Popovski, "Five disruptive technology directions for 5G," *IEEE Communications Magazine*, vol. 52, no. 2, pp. 74–80, February 2014.

[85] T. Bai, and R. Heath, "Uplink massive MIMO SIR analysis: How do antennas scale with users?," *2015 IEEE Global Communications Conference (GLOBECOM)*. IEEE, 2015.

[86] W. Xiao et al., "Uplink power control, interference coordination and resource allocation for 3GPP E-UTRA," in *Proc. of IEEE 64th Vehicular Technology Conference,* Sep. 2006, pp. 1–5.

[87] M. Peng and W. Wang, "Technologies and Standards for TD-SCDMA Evolutions to IMT-Advanced," *IEEE Commun. Mag.,* vol. 47, no. 12, pp. 50-58, Dec. 2009.

[88] I. Chih-Lin et al., "Toward green and soft: A 5g perspective," *IEEE Commun. Mag.,* vol. 52, no. 2, pp. 66–73, Feb. 2014

[89] A. Checko, H. Christiansen, Y. Yan, L. Scolari, G. Kardaras, M. Berger, and L. Dittmann, "Cloud ran for mobile networks–a technology overview," *IEEE Commun. Surveys & Tutorials,* vol. 17, no. 1, pp. 405–426, 2015.

[90] J. Andrews et al., "What will 5G be?," *IEEE J. Sel. Areas Commun.,*vol. 32, no. 6, pp. 1065–1082, Jun. 2014.

[91] J. Hoydis, S. Brink, and M. Debbah, "Massive MIMO in the UL/DL of cellular networks: How many antennas do we need?," *IEEE J. Sel. Areas Commun.,* vol. 31, no. 2, pp. 160–171, Jan. 2013.

[92] Y. Kim, H. Ji, J. Lee, Y. Nam, B. Ng, I. Tzanidis, Y. Li, and J. Zhang, "Full dimension MIMO (FD-MIMO): The next evolution of MIMO in LTE systems," *IEEE Wireless Commun. Mag.,* vol. 21, no. 3, pp. 92–100, Jun. 2014.

[93] D. Ying, H. Yang, T. Marzetta, and D. Love, "Heterogeneous massive mimo with small cells," in Proc. *IEEE Vehicular Technology Conference (VTC 2016-Spring),* Nanjing, China, May 2016.

[94] Q. Ye, O. Bursalioglu, H. Papadopoulos, C. Caramanis, and J. Andrews, "User association and interference management in massive MIMO HetNets," *IEEE Trans. Commun.,* vol. 64, no. 5, pp. 2049–2065, May 2016.

[95] A. Gupta, H. Dhillon, S. Vishwanath, and J. Andrews, "Downlink multi-antenna heterogeneous cellular network with load balancing," *IEEE Trans. Commun.,* vol. 62, no. 11, pp. 4052–4067, Nov. 2014.

[96] C. Li, J. Zhang, and K. B. Letaief, "Throughput and energy efficiency analysis of small cell networks with multi-antenna base stations," *IEEE Trans. Wireless Commun.,* vol. 13, no. 5, pp. 2505–2517, May 2014.

[97] F. Rusek et al., "Scaling up MIMO: Opportunities and challenges with very large arrays," *IEEE Signal Process. Mag.,* vol. 30, no. 1, pp. 40–60, Jan. 2013.

[98] D. Liu et al., "Distributed energy efficient fair user association in massive MIMO enabled hetnets," *IEEE Commun. Lett.,* vol. 19, no. 10, pp. 1770–1773, Oct. 2015.

[99] N. Wang, E.Hossain and K. Bhargava, "Joint downlink cell association and bandwidth allocation for wireless backhauling in two-tier HetNets with large-scale antenna arrays," *IEEE Transactions on Wireless Communications* 15.5 (2016): 3251-3268.

[100] A. Adhikary, H.Dhillon, and G. Caire, "Massive-MIMO meets HetNet: Interference coordination through spatial blanking," *IEEE J. Sel. Areas Commun.,* vol. 33, no. 6, pp. 1171–1186, Jun. 2015.

[101] Z. Ding and H. Poor, "The use of spatially random base stations in cloud radio access networks," *IEEE Signal Process. Lett.,* vol. 20, no. 11, pp.1138–1141, Nov. 2013.

[102] F. Khan, H. He, J. Xue, and T. Ratnarajah, "Performance analysis of cloud radio access networks with distributed multiple antenna remote radio heads," *IEEE Trans. Signal Process.,* vol. 63, no. 18, pp. 4784–4799, Sep. 2015.

[103] S. Zaidi, A. Imran, D. Mclernon, and M. Ghogho, "Characterising coverage and downlink throughput of cloud empowered hetnets," *IEEE Commun. Lett.,* vol. 19, no. 6, pp. 1013–1016, 2015.

[104] M. Peng, K. Zhang, J. Jiang, J. Wang, and W. Wang, "Energy-efficient resource assignment and power allocation in heterogeneous cloud radio access networks," *IEEE Trans. Veh. Technol.,* pp. 1–13, 2015.

[105] M. Peng, Y. Li, J. Jiang, J. Li, and C. Wang, "Heterogeneous cloud radioaccess networks: a new perspective for enhancing spectral and energy efficiencies," *IEEE Wireless Commun.,* vol. 21, no. 6, pp. 126–135, 2014.

[106] A. He, L. Wang, Y. Chen, K. Wong, and M. Elkashlan, "Throughput and Energy Efficiency for S-FFR in Massive MIMO Enabled Heterogeneous C-RAN," *IEEE Global Communications Conference (GLOBECOM),* Washington, DC, pp. 1-6, 2016.

[107] H. Dhillon, M. Kountouris, and J. Andrews, "Downlink MIMO HetNets: Modeling, ordering results and performance analysis," *IEEE Trans. Wireless Commun.,* vol. 12, no. 10, pp. 5208–5222, Oct. 2013.

[108] R. Heath, M. Kountouris, and T. Bai, "Modeling heterogeneous network interference using Poisson point processes," *IEEE Trans. Signal Process.,* vol. 61, no. 16, pp. 4114–4126, Aug. 2013.

[109] S. Veetil, K. Kuchi, and R. Ganti, "Performance of PZF and MMSE receivers in cellular networks with multi-user spatial multiplexing," *IEEE Trans. Wireless Commun.,* vol. 14, no. 9, pp. 4867–4878, Sep. 2015.

[110] M. Renzo and W. Lu, "Stochastic geometry modeling and performance evaluation of MIMO cellular networks using the Equivalent-in-Distribution (EiD)-based approach," *IEEE Trans. Commun.,* vol. 63, no. 3, pp. 977–996, Mar. 2015.

[111] M. Renzo and P. Guan, "Stochastic geometry modeling of coverage and rate of cellular networks using the Gil-Pelaez inversion theorem," *IEEE Wireless Commun. Lett.,* vol. 18, no. 9, pp. 1575–1578, Sep. 2014.

[112] Qualcomm Incorporated, "LTE Advanced: Heterogeneous networks," white paper, Jan. 2011.

[113] D. Gesbert, M. Kountouris, R. Heath, C. Chae, and T. Salzer, "From single user to multiuser communications: shifting the MIMO paradigm," *IEEE Signal Process. Mag.*, vol. 24, no. 5, pp. 36–46, Sep.2007.

[114] Gupta, A. K., Dhillon, H. S., Vishwanath, S. and Andrews, J. G. "Downlink MIMO HetNets with Load Balancing," *CoRR,* abs/1310.6795. 2013.

[115] H. Dhillon, S., Marios Kountouris, and J. Andrews, "Downlink MIMO HetNets: Modeling, ordering results and performance analysis," *IEEE Transactions on Wireless Communications* 12.10 (2013): 5208-5222.

[116] F. Zheng and T. Kaiser, "On the channel capacity of multiantenna systems with Nakagami fading," *EURASIP J. Advances Signal Process.,* vol. 2006, pp. 039 436–1–039 436–11, 2006.

[117] H. Huang, C. Papadias, and S. Venkatesan, *MIMO Communication for Cellular Networks,* Springer, 2012.

[118] M. Renzo and W. Lu, "Stochastic geometry modeling and performance evaluation of MIMO cellular networks using the equivalentin-distribution (EiD)-based approach," *IEEE Trans. Commun.,* vol. 63, no. 3, pp. 977–996, Mar. 2015.

[119] M. Renzo and P. Guan, "Stochastic geometry modeling of coverage and rate of cellular networks using the Gil-Pelaez inversion theorem," *IEEE Commun. Letter,* vol. 18, no. 9, pp. 1575–1578, Sep. 2014.

[120] L. Afify, H. ElSawy, T. Al-Naffouri, and M. Alouini, "Unified stochastic geometry model for MIMO cellular networks with retransmissions," *IEEE Trans. Wireless Commun.,* Oct. 2016.

[121] V. Chandrasekhar, M. Kountouris, and J. Andrews, "Coverage in multi-antenna two-tier networks," *IEEE Trans. Wireless Commun.,*no. 10, pp. 5314–5327, Oct. 2009.

[122] R. Heath, J. Kountouris, and T. Bai, "Modeling heterogeneous network interference with using poisson point processes," *IEEE Trans.on Signal Processing.,* vol. 61, no. 16, pp. 4114–4126, Aug. 2013.

[123] J. Andrews, F. Baccelli, and R. Ganti, "A tractable approach to coverage and rate in cellular networks," *IEEE Trans. Commun.*, vol. 59, no. 11, pp. 3122–3134, November 2011.

[124] S. Singh, H. Dhillon, and J. Andrews, "Offloading in heterogeneous networks:Modeling, analysis, and design insights," *IEEE Trans. Wireless Commun.*, vol. 12, no. 5, pp. 2484–2497, May 2013.

[125] H. Jo, Y. Sang, P. Xia, and J. Andrews, "Heterogeneous cellular networks with flexible cell association: A comprehensive downlink SINR analysis," *IEEE Trans. Wireless Commun.,* vol. 11, no. 10, pp. 3484–3495, Oct. 2012.

[126] S. Singh and J. Andrews, "Joint resource partitioning and offloading in heterogeneous cellular networks," *IEEE Trans. Wireless Commun.,* vol. 13, no. 2, pp. 888–901, Feb. 2014.

[127] A. Gupta et al., "Downlink coverage probability in MIMO HetNets with flexible cell selection," *Global Communications Conference (GLOBECOM),* 2014 IEEE. IEEE, 2014.

[128] E. Bjornson, L. Sanguinetti, J. Hoydis, and M. Debbah, "Designing multi-user MIMO for energy efficiency: When is massive MIMO the answer?," *in Proc. IEEE Int. Conf. Wireless Commun. Netw.,* Apr. 2014, pp. 242–247.

[129] S. Payami and F. Tufvesson, "Channel measurements and analysis for very large array systems at 2.6 GHz," in *Proc. 2012 Europ. Conf. Anten.Propag.*

[130] A. Kilbas and M. Saigo, *H-Transforms: Theory and Applications,* Boca Raton, FL: CRC Press LLC, 2004.

[131] S. Cui, A. Goldsmith, and A. Bahai, "Energy-constrained modulation optimization," *IEEE Trans. Wireless Commun.,* vol. 4, no. 5, pp. 2349–2360, 2005.

[132] A. Prudnikov, Y. Brychkov, and O. Marichev, *Integrals and Series: More Special Functions*, Gordon and Breach Science, vol. 3, translated from the Russian by G. G. Gould., 1990.

[133] M. Abramowitz and I. Stegun, *Handbook of Mathematical Functions with Formulas, Graphs, and Mathematical Tables*, 9th ed. New York: Dover Publications, 1972.

[134] 3GPP, TR 36.872, "Technical specification group radio-access network; small cell enhancements for evolved universal terrestrial radio-access (E-UTRA) and e-utran physical-layer aspects (release 12)," 3rd Generation Partnership Project, Sophia Antipolis, France, Sep. 2013. [Online]. Available: http://www.3gpp.org/dynareport/36872.htm